Stem Cells International

Promoting Tissue Repair by Micrograft Stem Cells Delivery

Lead Guest Editor: Letizia Trovato
Guest Editors: Fabio Naro, Francesco D'Aiuto, and Federico Moreno

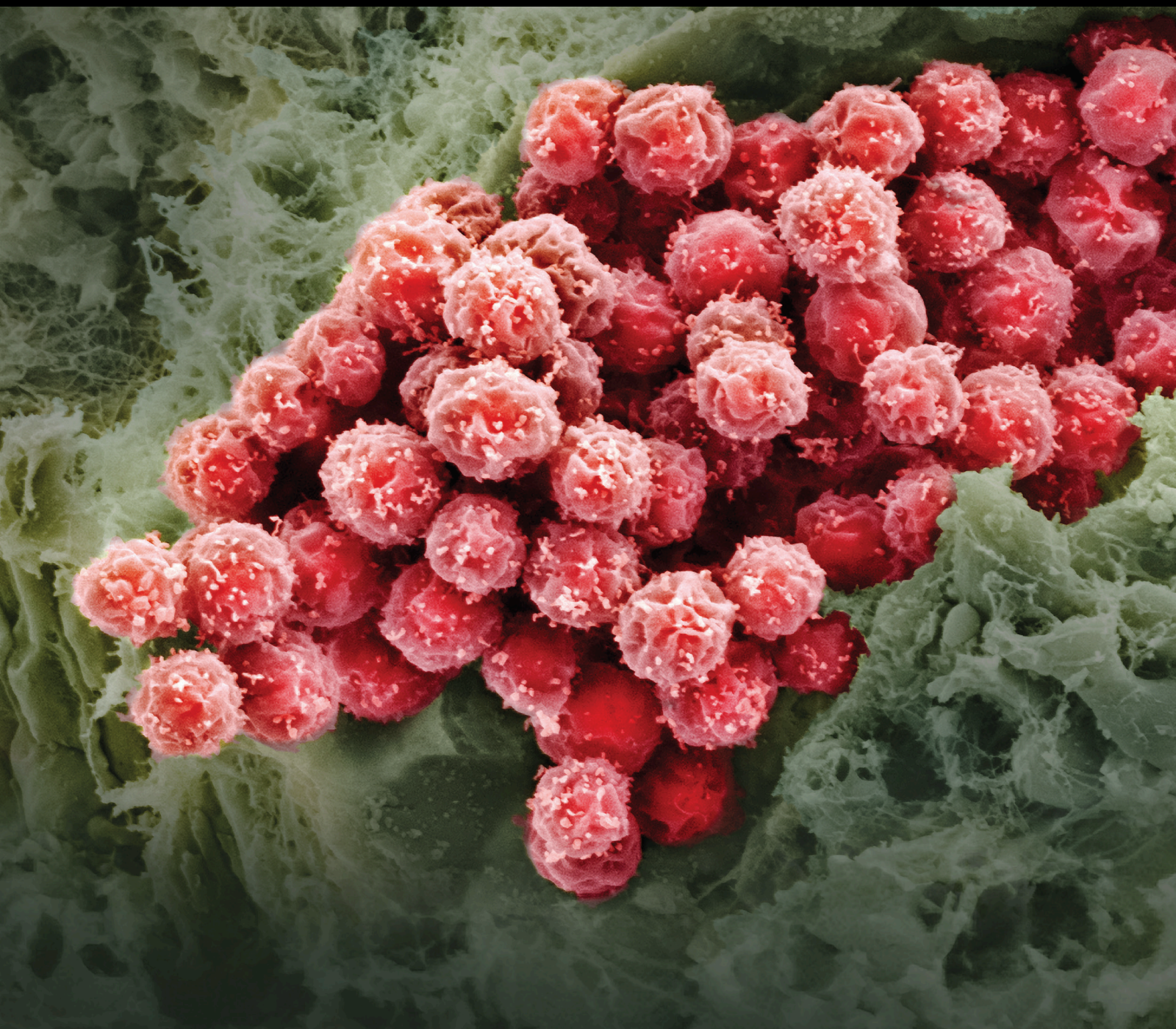

Promoting Tissue Repair by Micrograft Stem Cells Delivery

Stem Cells International

Promoting Tissue Repair by Micrograft Stem Cells Delivery

Lead Guest Editor: Letizia Trovato
Guest Editors: Fabio Naro, Francesco D'Aiuto, and Federico Moreno

Contents

The Role of Autologous Dermal Micrografts in Regenerative Surgery: A Clinical Experimental Study
Marco Mario Tresoldi, Antonio Graziano, Alberto Malovini, Angela Faga, and Giovanni Nicoletti
Clinical Study (8 pages), Article ID 9843407, Volume 2019 (2019)

Hindawi
Stem Cells International
Volume 2020, Article ID 2195318, 2 pages
https://doi.org/10.1155/2020/2195318

Editorial

Promoting Tissue Repair by Micrograft Stem Cells Delivery

Letizia Trovato,[1] **Fabio Naro**,[2] **Francesco D'Aiuto**,[3] **and Federico Moreno**[3]

[1]*University of Turin, Turin, Italy*
[2]*University of Sapienza, Rome, Italy*
[3]*UCL Eastman Dental Institute, London, UK*

Correspondence should be addressed to Letizia Trovato; letizia.trovato@unito.it

Received 7 January 2020; Accepted 7 January 2020; Published 28 January 2020

Stem cell therapy provides new insights for the treatment of diseases or disorders that cannot yet be successfully managed through conventional care. Current cell-based approaches are mainly focused on the use of Mesenchymal Stem Cells (MSCs) which are multipotent stem cells with unique biological properties and are readily available from almost every organ and tissue. MSCs are becoming widely used to improve outcomes for multiple clinical scenarios: heart failure, wound healing, bone regeneration, and many others. Despite promising in vitro and in vivo results, the need for extensive manipulation steps to obtain sufficient cell numbers for delivery significantly increases the regulatory, practical, and financial barriers for the routine use of these novel therapies. Helping to overcome some of these limitations, the use of micrografts represents a suitable approach for tissue regeneration. Micrografting can be used to deliver not only progenitor cells but also growth factors and matrix extracellular components naturally available in the tissues which further increase the regenerative potential.

Only few clinical trials have reported the efficacy of stem cell therapy; further research must be conducted to investigate also the safety of these techniques in the long term. Micrografting is attracting a growing interest from the research community since it involves easy/quick and simple procedures which reduce the amounts of donor tissues required while reducing morbidity.

In this special issue, new procedures able to promote repair or regeneration in areas such as plastic surgery and wound healing are reported, using both stem cells and micrografts. In the manuscript by M. M. Bashir et al., the authors evaluate the effect of adipose tissue grafts mixed with adipose tissue-derived stem cells (ASCs) to promote fat graft retention in patients with contour deformities of the face showing an improvement in clinical outcomes when compared to the control group. The papers from M. Riccio et al. and M. M. Tresoldi et al. report the results from two clinical trials investigating the use of dermal micrografts in the treatment of traumatic or complex wounds in different patient populations. M. Riccio et al. present the management of 70 patients affected by traumatic wounds of the lower and upper limbs characterized by an extensive loss of substance. The results showed complete wound healing after 35 to 84 days. On the other hand, M. M. Tresoldi et al. treated elderly patients with wither micrografts or another dermal skin substitute, aiming to compare the efficacy for wound repair of both tissue replacement therapies. All patients reached a good degree of reepithelialization, but the authors failed to demonstrate a statistically significant difference between both groups. Finally, the study from A. Andreone et al. proposes a new approach for the management of burns based on the combination of platelet-rich fibrin and micrografts as a spray-on skin, reporting a rapid reepithelialization and impressive resurfacing.

This special issue also introduces the reader to fine original basic research focused on the biological and cellular mechanisms involved in tissue repair in different conditions, helping to better elucidate some of the key players activated in these processes. The study conducted by C. Zhang et al. assessed the role of autophagy in cavernosal endothelial dysfunction of diabetic rats, explaining the therapeutic effect of urine-derived stem cells (USCs) which upregulated autophagic activity in the cavernosal endothelium, ameliorating

cavernosal endothelial dysfunction and improving erectile dysfunction. Another interesting study carried out by F. Wang et al. explored the potential of injectable hydrogels as cell-carrying scaffolds able to mimic the condition of the natural extracellular matrix (ECM) of nucleus pulposus (NP), providing binding sites for cells. The authors reported that, in rats, the transplantation of injectable hydrogel-loaded NP-derived MSCs can delay the level of intervertebral disc (IVD) degeneration while promoting its regeneration and restoring the structure and ECM content of degenerated NP eight weeks after treatment.

Skeletal muscle has a remarkable capacity to regenerate following injury due to the presence within the adult muscle of a tissue-resident stem cell population known as satellite cells (SC). These cells remain quiescent until physical exercise, or muscle damage induces their activation. In the manuscript by S. Aguanno et al., the researchers present a culture model of the myogenic C2C12 cell line in suspension, able to self-assemble in three-dimensional cultures and to form a system able to preserve the quiescence and the staminality of these cells. The findings from this study support the conclusion that this model could be used to investigate the pathways controlling SC quiescence entrance and maintenance.

Micrograft therapies are a promising and affordable alternative to improve skin regeneration through enhancement of the endogenous wound repair processes. In the publication from M. Balli et al., the authors provide new insights which might contribute to a better understanding of the molecular pathways involved in micrograft-induced wound repair. Remarkably, the authors identified new key players in the wound healing process such as the active protein-1 (AP-1) and member Fos-related antigen-1 (Fra-1) which enhanced cell migration in mouse adult fibroblasts and human keratinocytes treated with soluble. These results were confirmed when inhibition of both ERK and AP-1 completely reverted the in vitro wound closure otherwise induced by the soluble micrograft treatment. This outcome highlights the important role of ERK-dependent transcriptional activity of AP-1 in the promotion of micrograft-induced wound closure.

We sincerely hope that the articles published in this special issue can help researchers to better understand the potential roles of stem cell therapy and micrografting techniques for tissue regeneration, including the different advantages and disadvantages of both approaches. Further, the basic research manuscripts included in the issue provide new insights that improve the current understanding of the cellular and molecular mechanisms involved in the wound healing process, especially in pathological conditions such as diabetes or intervertebral disc degeneration.

Conflicts of Interest

Letizia Trovato, lead guest editor, declares that she works for the Scientific Division of Human Brain Wave SrL, a company that developed the Rigenera micrografting technology. Her role in the company is to collect clinical evidence about the application of this technology. Additionally, none of the other guest editors have a conflict of interest to declare.

Acknowledgments

We would like to thank all the authors and reviewers who contributed so greatly to the success of this special issue and to express our gratitude to the editorial board members of this journal for their support throughout the reviewing process.

Letizia Trovato
Fabio Naro
Francesco D'Aiuto
Federico Moreno

Hindawi
Stem Cells International
Volume 2019, Article ID 6461580, 19 pages
https://doi.org/10.1155/2019/6461580

Research Article

Activator Protein-1 Transcriptional Activity Drives Soluble Micrograft-Mediated Cell Migration and Promotes the Matrix Remodeling Machinery

Martina Balli, Jonathan Sai-Hong Chui, Paraskevi Athanasouli, Willy Antoni Abreu de Oliveira, Youssef El Laithy, Maurilio Sampaolesi, and Frederic Lluis

Department of Development and Regeneration, Stem Cell Institute, KU Leuven, B-3000 Leuven, Belgium

Correspondence should be addressed to Frederic Lluis; frederic.lluisvinas@kuleuven.be

Received 12 July 2019; Revised 23 October 2019; Accepted 16 November 2019; Published 31 December 2019

Guest Editor: Fabio Naro

Impaired wound healing and tissue regeneration have severe consequences on the patient's quality of life. Micrograft therapies are emerging as promising and affordable alternatives to improve skin regeneration by enhancing the endogenous wound repair processes. However, the molecular mechanisms underpinning the beneficial effects of the micrograft treatments remain largely unknown. In this study, we identified the active protein-1 (AP-1) member Fos-related antigen-1 (Fra-1) to play a central role in the extracellular signal-regulated kinase- (ERK-) mediated enhanced cell migratory capacity of soluble micrograft-treated mouse adult fibroblasts and in the human keratinocyte cell model. Accordingly, we show that increased micrograft-dependent *in vitro* cell migration and matrix metalloprotease activity is abolished upon inhibition of AP-1. Furthermore, soluble micrograft treatment leads to increased expression and posttranslational phosphorylation of Fra-1 and c-Jun, resulting in the upregulation of wound healing-associated genes mainly involved in the regulation of cell migration. Collectively, our work provides insights into the molecular mechanisms behind the cell-free micrograft treatment, which might contribute to future advances in wound repair therapies.

1. Introduction

The skin is the largest organ of the human body providing protection, immune defense, and sensation. Traumatic injuries and impaired wound healing greatly affect the quality of life of patients and eventually contribute to mortality. Therefore, optimal tissue regeneration and proper wound management are required to maintain skin integrity.

The process of wound healing emerges as a result of a complex interplay between transcription factors that regulate essential transcriptional networks. Their activation is tightly regulated by signaling cascades that translate the input of intrinsic and extrinsic factors into a transcriptional cellular response to such cellular changes. During wound healing, sequential cellular processes are actively coordinated by waves of growth factors and cytokines [1–3]. Upon injury, several transcription factors are triggered by the damaged tissue. Among those, TGF-β signaling and the classical transcription factor NF-κB have been described as regulators which elicit the immune response as the initial step of the wound healing process. This results in the immune cell and platelet-derived production of a plethora of growth factors including transforming growth factor-beta (TGF-β), epidermal growth factor (EGF), platelet-derived growth factor (PDGF), vascular endothelial growth factor (VEGF), and connective tissue growth factor (CTGF) at the site of injury [4–6]. These in turn establish key repair processes such as angiogenesis, matrix deposition, migration, proliferation, and fibroblast transdifferentiation through pivotal signaling cascades [4]. While TGF-β signaling is an essential regulator of wound contraction and matrix deposition by myofibroblasts, the MEK/ERK cascade has been reported to promote proliferation and migration in both keratinocytes and fibroblasts, the main cell types involved in wound healing [7–9]. Interestingly, the activator protein-1 (AP-1) family has been reported as a transcription factor downstream of the ERK

cascade [10, 11]. Upon injury, AP-1 activity has been shown to be induced in an MAPK-dependent manner in fetal mouse skin [12]. This protein family consists of homo- and heterodimers formed mainly between proteins of the Fos and Jun families [13]. Upon phosphorylation, AP-1 is known to regulate genes involved in wound healing, such as growth factors and matrix metalloproteases (MMPs) [14]. Collectively, successful wound repair strongly depends on the spatiotemporal activity of several cellular signaling pathways.

The gold standard treatment to promote wound repair remains skin graft methods involving skin transplantations and have been widely used for the treatment of extensive wounds, such as burns, skin trauma, and cancer. As these lack blood vessels, additional blood support underneath the wound bed is required to guarantee the success of the skin graft. Moreover, this technique is associated with distress, pain, and hypertrophic scar formation [15]. Over the past years, great advances have been made in micrograft (MG) treatments, of which many have shown promising results in the clinical setting [16]. Compared to the conventional skin graft methods, the micrograft technique comprises of viable microtissue fragments that are directly applied to the site of injury. This autologous treatment has been reported to allow a 100-fold expansion of the micrograft transplant and offers a fast and reliable procedure for the patients with minimal surgical risks [17]. Recently, a novel MG technique has emerged as an innovative and affordable wound treatment whereby skin tissues are ground into a resulting solution of 80 μm microtissue fragments containing tissue-residing progenitor cells and matrix components [18]. Moreover, a recent study has shown that skin injury treatment with the soluble MG fraction deprived of tissue-residing cells and highly enriched in growth factors (such as IGF-1 and bFGF) is sufficient to promote the endogenous regenerative capacity of the skin by accelerating wound closure, showing increased reepithelialization, and increasing granulation formation and increased $CD31^+$ vessel formation [19].

Recently, the extracellular signal-regulated kinase (ERK) signaling pathway has been identified as one of the main drivers of the molecular mechanism behind this technique [19]. Upon MG treatment, both fibroblasts and keratinocytes displayed high levels of phosphorylated ERK (p-ERK) and exhibited upregulated transcription of MMPs. In accordance with this, the beneficial effects induced by the MG were reverted upon ERK inhibition. Nevertheless, a detailed molecular roadmap of the transcriptional network connecting ERK activation and downstream target expression and increased migratory capacity upon soluble MG treatment still remains largely unknown.

In this work, we dissect the molecular regulatory network behind the accelerated cell migration obtained by the MG treatment. To unveil key transcriptional regulators involved in the ameliorating effects mediated by this therapy, we integrated differentially expressed genes (DEGs) obtained upon a 5 h treatment with the noncellular micrograft solution into a gene regulatory network analysis (GSE123829) [19]. Interestingly, MG-dependent DEGs appeared to be likely regulated by important members of the AP-1 transcription factors, such as Fra-1. Accordingly, MG-induced fibroblast and keratinocyte migration as well as enzymatic activity of MMPs are significantly impaired upon AP-1 inhibition. Finally, our findings provide evidence that AP-1 connects higher ERK activity with increased MMP activity, which in turn regulates cell migration in both fibroblasts and keratinocytes. Collectively, our study provides a deeper view into the molecular mechanism behind the MG treatment, revealing the significance of AP-1 and its vital role in current and future advances in wound healing therapies.

2. Methods

2.1. Cell Culture. Tail tips (0.5 cm) of the C57BL/6 mouse model under proper anesthesia (isoflurane) were used to extract primary fibroblasts. Tissues were digested with collagenase IV for 40 minutes at 37°C. Cells were then cultured in DMEM GlutaMax (Cat No. 61965-026, Gibco Life Science, Grand Island) supplemented with 10% of fetal bovine serum, 1% penicillin-streptomycin, 1% L-glutamine, 1% sodium pyruvate, and 1% nonessential amino acids. The immortalized keratinocyte (HaCaT) cell line was used as a human keratinocyte cell model and was grown in Dulbecco's modified Eagles' medium (DMEM) supplemented equally to the previous media. Cells were cultured at 37°C in a humidified incubator with 5% of CO_2.

2.2. Preparation of Micrografts. Micrografts were generated from murine skin biopsies (1 cm^2) employing the Rigenera® technique. Tissues were minced using the Rigeneracons® tissue disruptor [20]. Resulting micrografts were subsequently filtered through 70 μm filter membranes to obtain a protein concentration of 5 $\mu g/\mu L$, followed by a centrifugation step (10 min at 3000 rpm) to deplete the solution of residing cells and cellular debris. The extracted soluble micrograft was then stored at −80°C for later use. Subsequently, the soluble MGs were then diluted 1 : 10 in growth media and applied on fibroblast and keratinocytes cells. Signaling pathways and transcription factor AP-1 were altered by inhibitory drugs such as MEK inhibitor PD0325901 (1 μM; Cat No. PZ016, Sigma) and c-fos/AP-1 inhibitor T-5224 (60 μM; Cat No. 530141-72-1, MedChemExpress (MCE)), respectively.

2.3. Cell Scratch Assay. Fibroblasts and keratinocytes were plated at a density of 3500 cell/cm^2 and 10000 cell/cm^2, respectively. The scratch assay was performed on cell monolayers using a pipette tip, resembling an artificial *in vitro* wound [21]. Subsequently, dead cells were removed using sterile phosphate-buffered saline (PBS) and images were taken over a time course until full closure of the *in vitro* scratch was achieved. The comparison between images allowed quantification of the cell migration rate. MGs were added onto the cells for different treatment durations (1 h, 5 h, and 12 h).

2.4. Cell Cycle Assay and Cell Viability. Changes in the cell cycle were assessed using the 5-ethynyl-2′-deoxyuridine (EdU) assay (Thermo Fisher Scientific) [22]. MG-treated cells were incubated for 2 hours at 37°C with 10 μM EdU (ethynyl-2′-deoxyuridine) according to the manufacturer's

instructions (Cat. No 900584-50MG, Sigma-Aldrich). Samples were then examined by Flow Cytometry (BD Biosciences) and analyzed by FlowJo software. Viability of MG-treated cells was evaluated by flow cytometry (BD Biosciences) using the Fixable Viability Stain 660 (564405; BD Biosciences). Statistical analysis was performed using two-tailed unpaired *t*-tests and two-way analysis of variance (ANOVA). No significant differences were found ($n = 3$ biological replicates).

2.5. Immunohistochemistry, Immunofluorescence Staining, and Protein Analysis. Scratched cells and 60-70% confluent conditions were used for immunohistochemistry and immunofluorescence analysis. Cells were fixed with 4% PFA for 20 minutes at RT, permeabilized with 1% BSA, 0.2% Triton-X in PBS for 30 minutes at RT, washed repeatedly, and blocked with donkey serum 1 : 10 in PBS (blocking solution) for 40 minutes at RT. Cells were then incubated overnight at 4°C with the following primary antibodies: Rabbit mAb Phospho-Fra-1 (Ser265) (D22B1; CST5841T, Bioké-Cell Signaling) and Mouse mAb Fra-1 (D3; sc-376148, Santa Cruz Biotechnology) were used at a 1 : 200 dilution. Subsequently, cells were washed with PBS and incubated with secondary Alexa Fluor antibodies for 1 h at RT. Finally, cells were incubated in Hoechst 33342 at a 1 : 10000 dilution for nuclear counterstaining. Finally, cells were mounted using the DAKO™ mounting medium. Images were acquired using a Zeiss AxioImager Z1 Microscope and the AxioVision SE64 software. Images were analyzed using the ImageJ software (NIH).

Western blotting analyses were used to unveil the role of important proteins of the AP-1 complex in regulating the effects induced by the MG treatment. MG-treated cells were lysed in RIPA buffer containing 1 : 100 protease inhibitor and phosphatase inhibitor cocktails (Cat. No P8340-1 mL, P5726-1 mL, P0044-1 mL, respectively). Samples (30 μg of proteins) were heat-denatured in sample-loading buffer (50 mM of Tris-HCl, pH 6.8, 100 mM DTT, 2% SDS, 0.1% bromophenol blue, 10% glycerol), resolved by SDS-PAGE and transferred to PVDF membranes (Cat. No 1620177, Bio-Rad). Membranes were then stained with Ponceau S dye (Sigma-Aldrich) and blocked with 5% BSA (bovine serum albumin) in TBS (Tris-buffered saline) supplemented with Tween 0.05% for 1 hour at RT. Membranes were then incubated overnight at 4°C with the following primary antibodies: mouse p-ERK (1 : 1000, sc-7383, Santa Cruz), rabbit ERK (1 : 1000, sc-94, Santa Cruz), pFra-1 (Phospho-Fra-1 (Ser265) (D22B1) Rabbit mAb; 1 : 1000, Cat. No CST5841T, Bioké-Cell Signaling), Fra-1 (Fra-1 Antibody (D-3) Mouse monoclonal, 1 : 1000, Cat. No sc-376148, Santa Cruz Biotechnology), pJun (Phospho-c-Jun (Ser73) (D47G9) XP® Rabbit mAb; 1 : 1000, Cat. No 3270 T, Bioké-Cell Signaling), JUN (c-Jun (60A8) Rabbit mAb; 1 : 1000, Cat. No 9165T, Bioké-Cell Signaling), and mouse Tubulin-alpha (1 : 1000, T5168, Sigma-Aldrich). The following day, membranes were incubated with secondary horseradish peroxidase HRP-conjugated antibodies (1 : 5000, Santa Cruz Biotechnology, CA, USA), in TBS 0.05% Tween and 2.5% nonfat dry milk. Membranes were stripped and reblotted for the total forms of Erk, Fra-1, and c-Jun. Analyses were performed using the Clarity Western ECL Substrate (Cat. No 1705060, Bio-Rad).

2.6. Matrix Metalloproteinase (MMP) Enzymatic Activity. MMP activity was detected using the MMP activity Assay Kit (Cat No. ab112146, Abcam), according to the manufacturer's instructions. Data is presented as RFU (relative fluorescence units). Following MG treatment, conditioned medium was collected after 24 hours. Signals were evaluated 30 minutes after initiation of the enzymatic reaction using a microplate reader with a filter set of Ex/Em = 485/535 and normalized to the substrate control.

2.7. Transwell Migration Assay. Cells were dissociated using 0.25% trypsin-EDTA, washed with PBS (1x), and pelleted. Multiple well plates with permeable polycarbonate membrane transwell inserts (Cat No. 3422, Thermo Fisher Scientific) were used for this experiment. Fibroblasts or keratinocytes (10^5 cells) were plated on the upper compartment of the transwell in a total volume of 100 μL of growth media. 600 μL of 1 : 10 diluted MGs were applied to the lower chamber. 100,000 cells (fibroblast or keratinocytes) were submerged in 600 μL of complete GlutaMax medium as a control. After incubation, the transwell inserts were removed, cleaned of stationary cells, and fixed with 70% ethanol. Afterwards, membranes were stained with 0.1% of crystal violet. Finally, membranes were detached from the inserts, deposited on slides, and mounted using DPX. Images were acquired using the AxioVision SE64 software on a Zeiss AxioImager Z1 Microscope. Images were analyzed using the ImageJ software (NIH).

2.8. RNA Extraction and mRNA Gene Expression. Total RNA was purified using the PureLink® RNA Mini Kit (Cat No. 12183018A, Life Technologies™) according to the manufacturer's instructions. cDNA was generated from 0.5 μg of RNA and using the Superscript III Reverse Transcriptase First-Strand Synthesis SuperMix (Invitrogen). Quantitative real-time PCRs (qRT-PCR) were performed using the Platinum® SYBR® Green qRT-PCR SuperMix-UDG (Cat No. 11733038, Thermo Fisher Scientific) on a ViiA™ 7 Real-Time PCR System with 384-well plate (Cat No. 4453536, Applied Biosystems). Gene expression values were normalized to *GAPDH*, *Rpl13a*, and *β-actin* for mouse primary fibroblasts and *GAPDH*, *RPL13A*, and *β-actin* housekeeping genes for human keratinocytes. All primers used were purchased from IDT technologies, Leuven, Belgium, and are reported in Table S1.

2.9. RNA Sequencing and Bioinformatics Analyses. The data presented in this paper has been deposited in GEO Datasets under accession no. GSE134113. The integrity of the RNA was evaluated using the Bioanalyzer (Agilent 2100) combined with the Agilent RNA 6000 Nano Kit (Ca No. 5067-1511). Samples were processed by the Genomics Core Leuven (KU Leuven–UZ Leuven, Belgium). Library preparation was performed using the Illumina TruSeq Stranded mRNA Sample Preparation Kit, according to the manufacturer's protocol (Cat No. 20020594). RNA denaturation was performed at 65°C, followed by cool-down at 4°C. Subsequently, samples were indexed for multiplexing. Sequencing libraries were quantified using the Qubit fluorometer

(Thermo Fisher Scientific, Massachusetts, USA). Library quality and size range were assessed using the Bioanalyzer (Agilent Technologies) with the DNA 1000 kit (Agilent Technologies, California, USA). Libraries were sequenced using the Illumina HiSeq4000 platform. 50 bp single-end reads and average of 20 million reads were obtained. Quality control of raw reads was performed with the FastQC v0.11.5. Filtering of adapters was performed using ea-utils v1.2.2.18. The splice-aware alignment was performed with TopHat v2.0.13 against the mouse genome mm10. The number of allowed mismatches was set to two and only unique mapping reads with alignment score of 10 or more were included. Resulting SAM and BAM alignment files were handled with Samtools v0.1.19.24. Quantification of reads per gene was performed with HT-Seq count v0.5.3p3. Count-based differential expression analysis was done using the R-based (The R Foundation for Statistical Computing, Vienna, Austria) Bioconductor package DESeq. Reported P values were adjusted for multiple testing with the Benjamini-Hochberg procedure, which controls false discovery rate (FDR).

2.10. ChIP Sequencing Analysis. Publicly available ChIP-seq data on the binding of Fra-1 in mouse embryonic fibroblasts was processed using the pipeline from the Kundaje lab (Version 0.3.3) [23]. Reads were aligned to reference genome (mm10) using Bowtie2 (v2.2.6) using the "–local" parameter. Single-end reads that aligned to the genome with mapping quality ≥30 were kept as usable reads (reads aligned to the mitochondrial genome were removed) using SAMtools (v1.2). PCR duplicates were removed using Picard's MarkDuplicates (Picard v1.126). Coverage was calculated using bamCoverage function with bin size = 1 bp and normalized using RPKM.

2.11. Statistical Analysis. Statistical analysis of RNA sequencing data statistical analysis was performed by bioconductor package DESeq (R-based). Reported P values were adjusted for multiple testing with the Benjamini-Hochberg procedure, which controls false discovery rate (FDR). In all the experiments, significant differences were determined by one-way analysis of variance (ANOVA), two-way ANOVA, adjusted for multiple comparison, and two-tailed unpaired t-test. Data are presented as the mean ± standard error of mean (SEM) or as fold change (FC). Data are visualized using GraphPad Prism 6 software (San Diego, CA, USA).

3. Results

3.1. AP-1 as a Predicted Regulator of Wound Healing-Associated Gene Expression in Fibroblasts. Together with immune cells, fibroblasts release growth factors as an immediate response to tissue damage, causing surrounding fibroblasts and keratinocytes to migrate towards the site of injury. To reestablish skin homeostasis, these cells cooperate to restore the wounded area with the formation of new tissue. This is achieved by cellular proliferation and migration as well as their capacity to remodel the extracellular matrix through continuous synthesis and breakdown of collagens [3, 6].

A recent study indicated that increased autologous micrograft- (AMG-) mediated fibroblast migration requires activation of the ERK signaling pathway that has been shown to be induced by the growth factors present in the soluble fraction of the micrograft [19]. To identify the transcriptional regulators mediating this behavior, we made use of the DEGs of wounded adult murine fibroblasts treated with the noncellular fraction of the micrograft treatment [19]. These genes were subsequently integrated in a gene regulatory network analysis using the iRegulon analysis software [24] (Figure 1(a)). The initial transcriptome analysis showed 123 upregulated DEGs (logFC > 1 , adjusted P value < 0.05), including genes involved in cell migration (i.e., *Cxcl2*, *Ccl20*, *Mmp3*), angiogenesis (i.e., *Ets1*, *Vegfa*, *Flt1*), cell cycle (i.e., *Nos2*, *Ptgs2*, *Lif*), and epithelialization (i.e., *Dusp10*, *Ptgs2*, *Hmox1*) (Figures 1(b) and 1(c), Table S2).

The iRegulon analysis of AMG-dependent DEGs identified *Bcl3*, *Foxc2*, *Cebpg*, *Mms19*, *Foxo6*, *Crx*, *Fosl1*, *Otud4*, and *Plag1* as predicted transcription factors regulating DEG expression (Figure S1A). Interestingly, among these, we identified AP-1 family member *Fosl1*, encoding the Fra-1 protein. AP-1 transcription factors have been reported to regulate the expression of genes encoding growth factors and MMPs [14]. Additionally, it has been shown that AP-1 activity is regulated by the ERK pathway [10, 25]. Prompted by this evidence, we decided to focus our attention on the role of the transcription factor AP-1 in regulating MG-mediated wound healing. Explicitly, our findings obtained from transcriptome analysis and gene regulatory network analysis suggested that AP-1 family member Fra-1 might retain a potential role in the regulation of the molecular mechanisms behind the beneficial effects of the soluble MG treatment (Figure 1(d)).

To validate the predicted binding of AP-1 as a transcriptional regulator to the promoter of wound healing-associated genes, we used publicly available ChIP-seq data to investigate the ability of the Fra-1 protein to bind the promoter region of several upregulated DEGs (Figure S1B) [23]. Correspondingly, we confirmed binding of Fra-1 to the promoters of several genes, such as *Cxcl2*, *Ets1*, *Mmp13*, and *Fosl1* itself in mouse fibroblasts. Collectively, these findings provide strong evidence that the induced regenerative transcriptional profile in AMG-treated fibroblasts is likely regulated by the AP-1 family members.

3.2. Micrograft Treatment Induces AP-1 Activity via Increased Fosl1 Expression and Fra-1 Phosphorylation. Studies have reported that the lack of AP-1 function in both fibroblasts and keratinocytes resulted in impaired cell migration and cell proliferation, and, in turn, led to delayed wound closure [14]. Therefore, we aimed to determine whether the noncellular MG treatment induces transcriptional activity of AP-1 through changes at transcriptional level or through post-translational modifications in both cell types.

To determine the regulation of AP-1 activity upon soluble MG treatment, we assessed the transcript levels of its family members following 5 and 12 hours of MG treatment. In adult mouse fibroblasts as well as in the epithelial/keratinocyte (HaCaT) cell model, *Fosl1* and *FOSL1*, respectively,

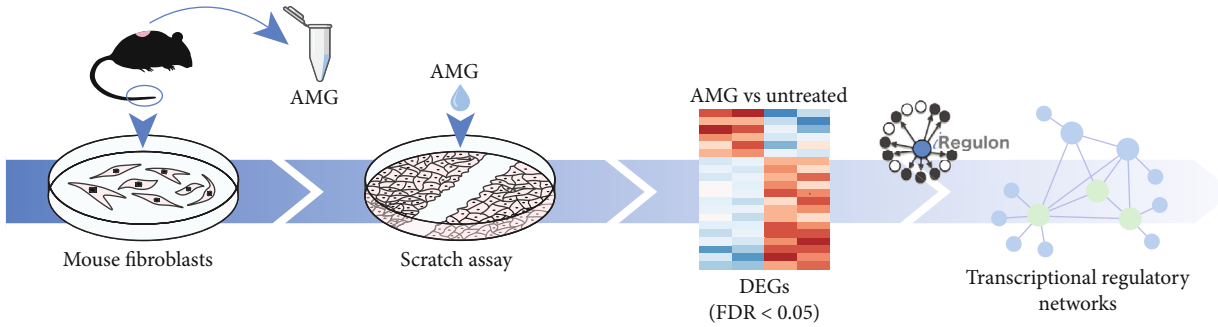

(a)

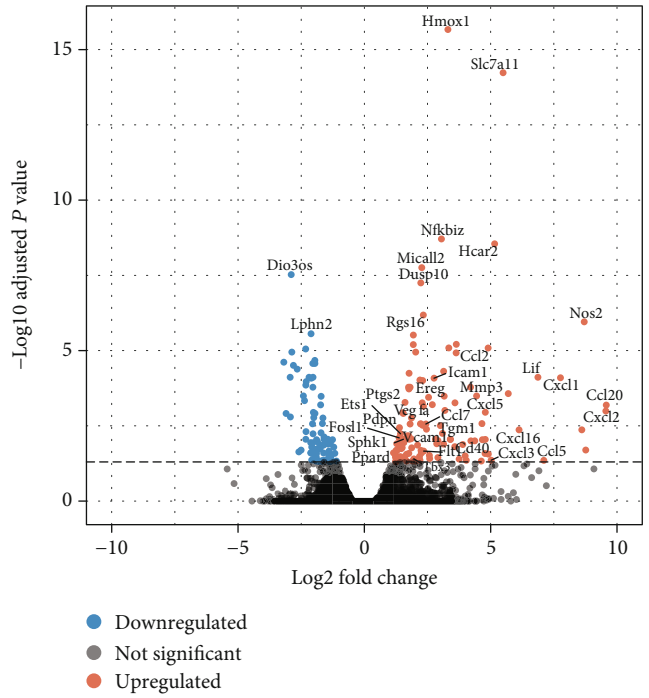

(b)

Figure 1: Continued.

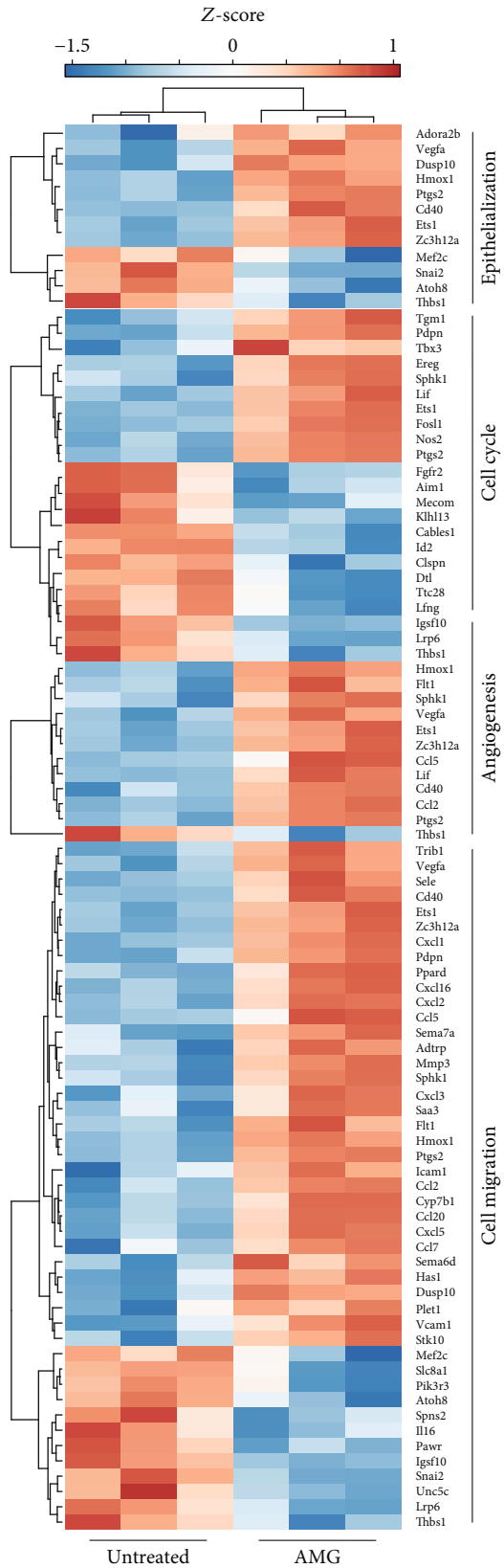

(c)

Figure 1: Continued.

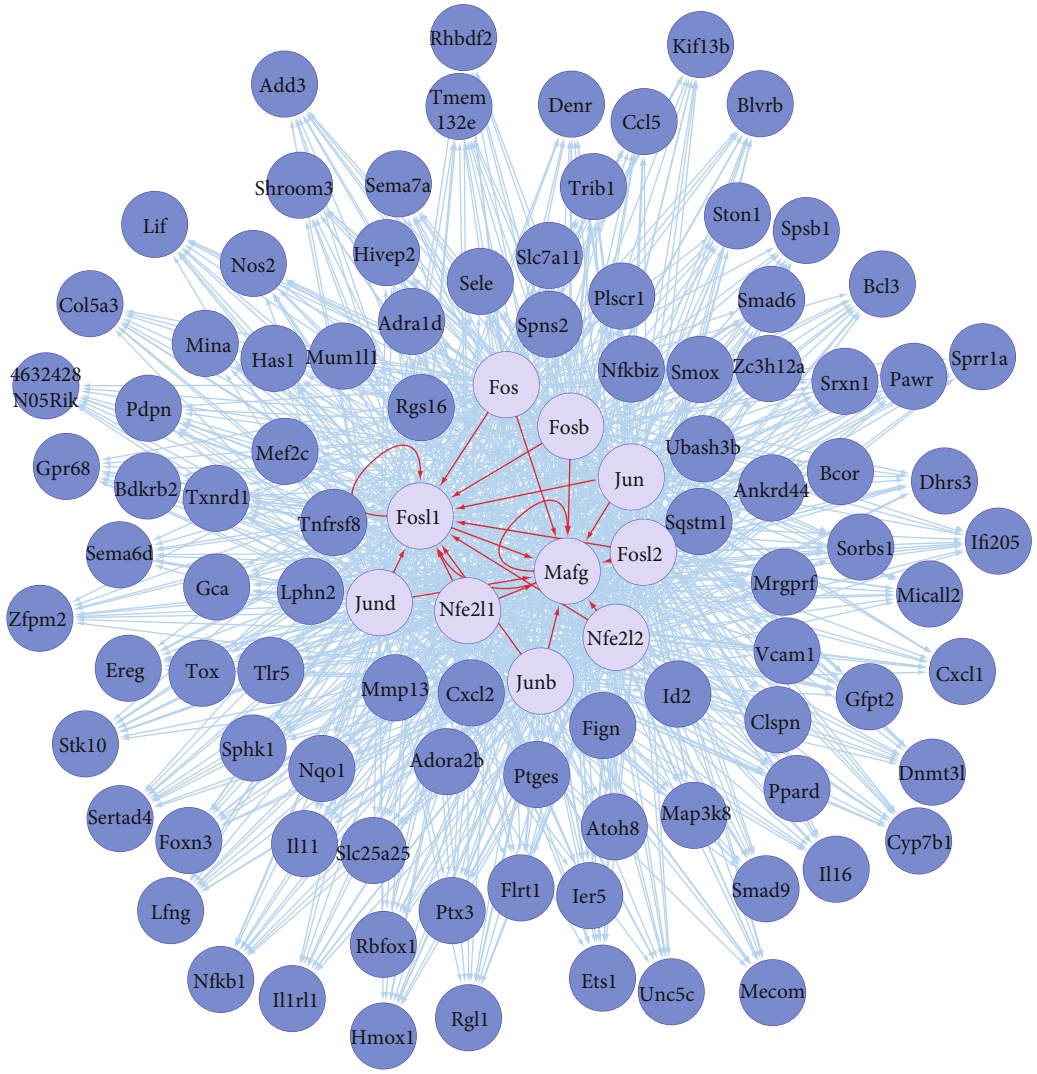

(d)

Figure 1: Predicted transcription factors and gene targets from a set of MG-induced DEGs. (a) Schematic representation of the transcriptional regulatory network analysis. Mouse primary fibroblasts isolated from tail's tip were used in the *in vitro* the scratch wound assay. MGs processed from a murine skin biopsy according to the Rigenera® protocol were processed to remove cellular remains and were subsequently applied to the *in vitro* scratch layers. Differentially expressed genes (DEGs) obtained via RNA-seq analysis ($N = 3$) were then used to identify the transcriptional regulatory networks using iRegulon. (b) Volcano plot showing up- (red) and downregulated (blue) genes upon 5 h of MG treatment. Black dots represent statistically insignificant genes. Gene values are reported as a $\log_2$ fold change (P value < 0.05). (c) Heatmap showing MG-dependent DEGs involved in essential wound healing process, such as epithelialization, cell cycle, angiogenesis, and cell migration. (d) Transcriptional regulatory network established around *Fosl1* using iRegulon, showing predicted transcription factors (light blue) to regulate their target genes (dark blue).

appeared as the sole AP-1 factor to be significantly upregulated upon treatment at the transcript level (Figure 2(a)). Although increased expression levels of Fos and Jun genes lead to higher activation of AP-1, posttranslational regulation of AP-1 family members also greatly contributes to its activity. As the DNA-binding properties of AP-1 member proteins and their transcriptional activity strongly depend on posttranslational phosphorylation, we evaluated the levels of phosphorylated Fra-1 (pFra-1) in mouse fibroblasts and FRA-1 (pFRA-1) in human keratinocytes after 1 and 5 h of MG treatment [11, 26]. As immunostaining and western blotting analysis revealed an increase in both total Fra-1 and phosphorylation of Fra-1 at serine 265 residues, this could indicate that newly formed Fra-1 proteins are immediately posttranslationally modified upon MG treatment (Figures 2(b), 2(c), and 2(d)).

Optimal transcriptional activity of Fra-1 is highly dependent of its binding to members of the Jun family. As the most potent transcriptional regulator of this family, *c-Jun* mRNA levels appear to be significantly increased upon 5 h of MG treatment in wounded murine adult fibroblasts (Figure 2(a)). Subsequently, we investigated whether c-Jun, as part of the AP-1 complex, was also posttranslationally regulated upon treatment with the micrograft solution. In both

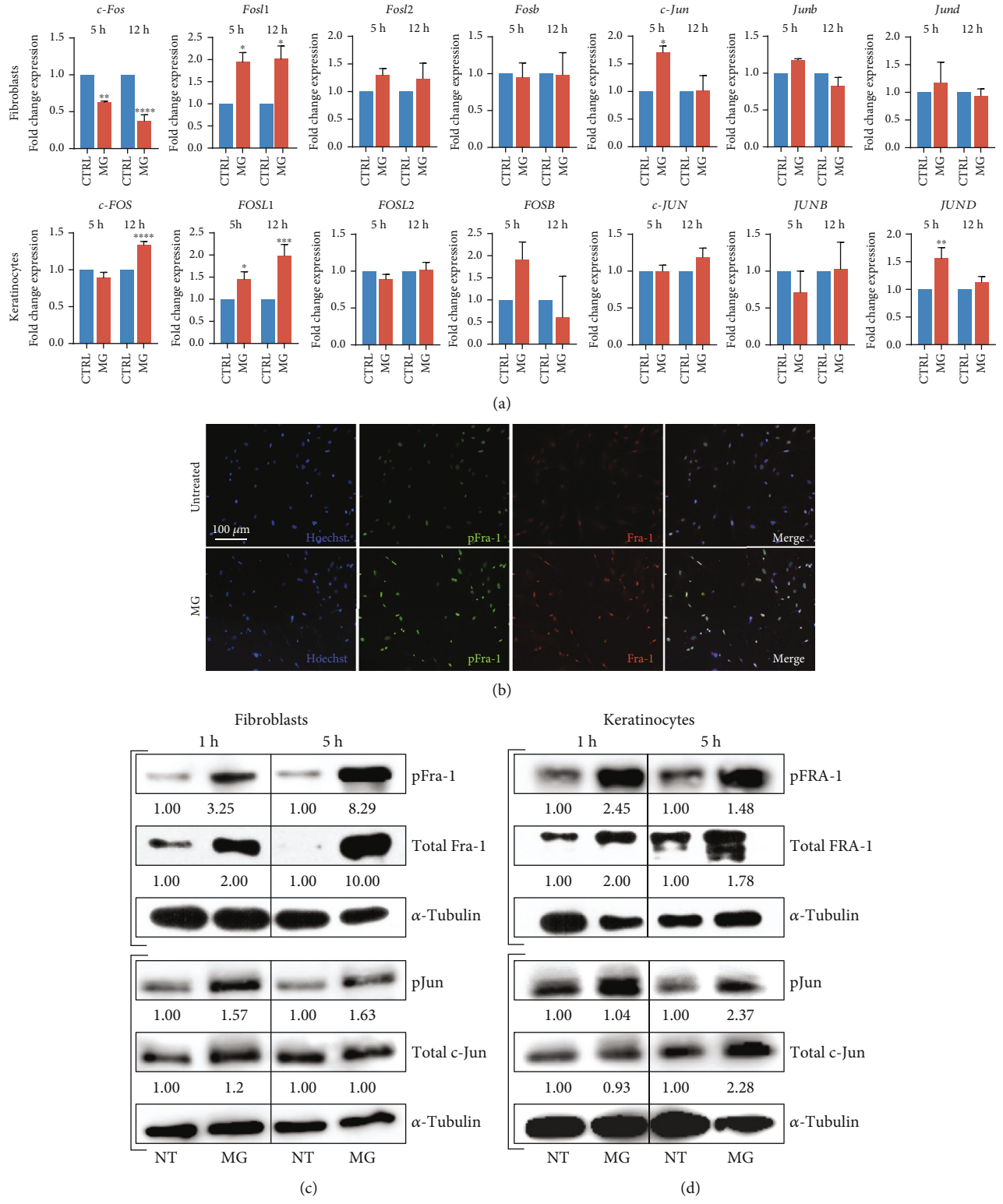

Figure 2: MG-dependent transcriptional and posttranscriptional regulation of AP-1 family members. (a) Transcript levels of AP-1 family members evaluated by RT-qPCR. Expression values are expressed as a fold change normalized to the expression of *Gapdh*, *β-actin*, and *Rpl13a* housekeeping genes. Differences are calculated with one-way ANOVA ($N = 3$) and indicated as $^{*}P < 0.05$, $^{**}P < 0.01$, $^{***}P < 0.001$, and $^{****}P < 0.0001$. (b) Representative immunofluorescence showing phosphorylation and total levels of Fra-1 protein in MG-treated and untreated primary adult fibroblasts. Nuclei were counterstained with Hoechst 33342 ($N = 3$). (c) Representative western blot membranes showing level of phosphorylated and total Fra-1 and c-Jun from wounded fibroblasts upon different time durations of MG treatment (1 h and 5 h). Untreated cells were used as a control. (d) Representative western blot membranes showing level of phosphorylated and total FRA-1 and c-JUN from MG-treated and MG-untreated human keratinocyte (HaCaT) cells exposed to 1 h and 5 h of MG treatment.

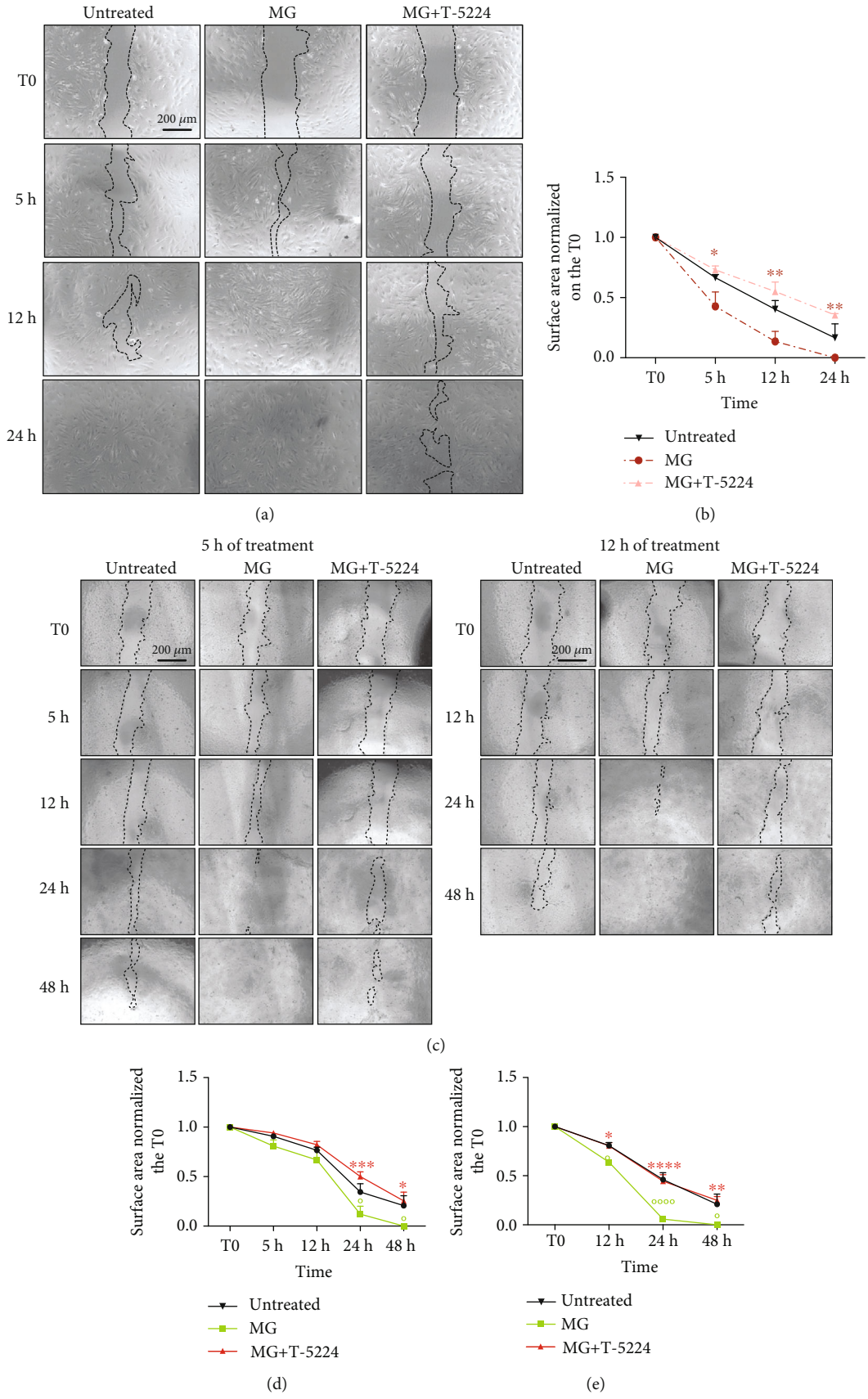

Figure 3: Continued.

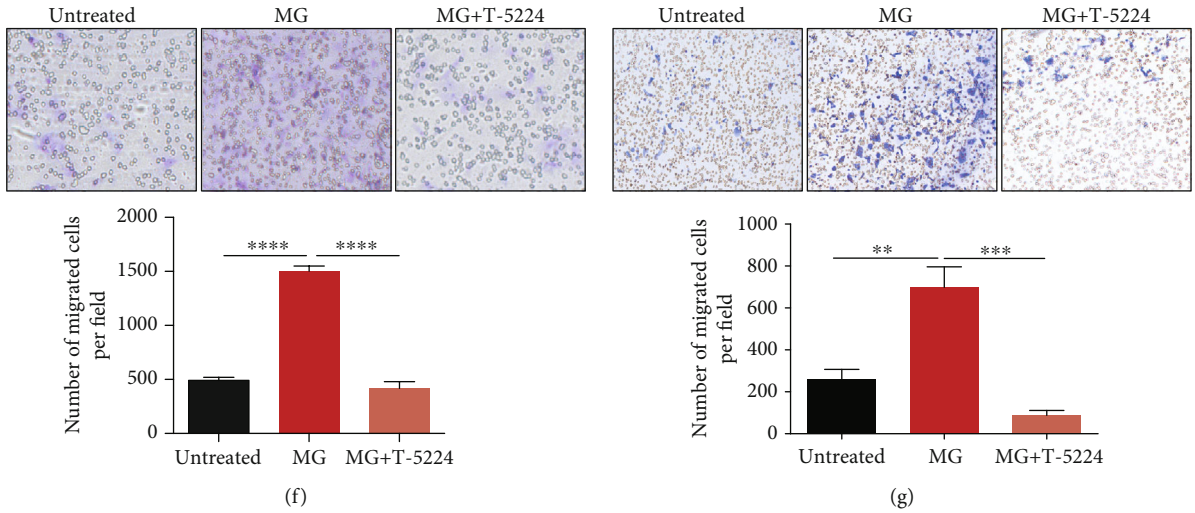

Figure 3: MG treatment accelerates scratch closure and cell migration through transcriptional activity of AP-1. (a) Representative images of wounded adult mouse fibroblasts exposed to 5 h of MG treatment in the presence or absence of the specific AP-1 inhibitor T-5224 (60 μM). (b) Quantification of scratch closure from 3 independent experiments as in Figure 3(a). Data is presented as the mean ± SEM ($N = 3$). The surface area was normalized to the T0 image, and significant differences are calculated with two-way ANOVA, followed by the Holm-Sidak test and indicated as $^{*}P < 0.05$; $^{**}P < 0.01$; $^{***}P < 0.001$. (c) Representative images of wounded human keratinocytes exposed to 5 h and 12 h of MG treatment in the presence or absence of AP-1 inhibitor T-5224 (60 μM). (d, e) Quantification of scratch closure from 3 independent experiments as in Figure 3(c). Data is shown as the mean ± SEM ($N = 3$). The surface area was normalized to the T0 image and significant differences are calculated by two-way ANOVA followed by the Tukey test and indicated as $^{*}P < 0.05$, $^{**}P < 0.01$, $^{***}P < 0.005$, and $^{****}P < 0.001$. (f, g) Pictures showing transwell migration assays chamber membranes. Adult murine fibroblasts (left panel) and human (HaCaT) keratinocytes (right panel) were exposed to MG treatment in the presence or absence of the AP-1 inhibitor T-5224 (60 μM). Data is presented as the mean ± SEM. P values were calculated using ordinary one-way ANOVA corrected by the Tukey test. $^{*}P < 0.05$, $^{**}P < 0.01$, $^{***}P < 0.001$, $^{****}P < 0.0001$.

keratinocytes and fibroblasts, increased phosphorylation levels of c-Jun/c-JUN were observed after 1 h and 5 h of treatment (Figures 2(c) and 2(d)).

Taken together, we demonstrate that posttranslational activity of both Fra-1 and c-Jun in fibroblasts and keratinocytes is increased upon soluble MG treatment. This suggests that these AP-1 members are involved in the molecular mechanism of MG treatment and in the previously shown accelerated AMG-dependent wound healing [19].

3.3. Micrograft-Induced Cell Migration Is Reverted upon AP-1 Inhibition. Recently, it has been shown that the soluble fraction of autologous micrograft (AMG) treatment on wounded murine adult fibroblasts resulted in increased *in vitro* cell migration and MMP activity, leading to an improved *in vitro* scratch closure capacity and an improved *in vivo* wound healing [19]. As the predicted transcription factor AP-1 is known to regulate cell migration, we assessed its involvement in the accelerated MG-mediated scratch closure by evaluating the migratory capacity of MG-treated murine primary adult fibroblasts and human HaCaT cells using the *in vitro* cell scratch assay in the presence or absence of the specific c-Fos/AP-1 inhibitor T-5224 (Figures 3(a)–3(e)) [27]. AP-1 inhibition significantly delayed the *in vitro* scratch closure in MG-treated fibroblasts (Figures 3(a) and 3(b)). Similarly, MG-treated keratinocytes showed a significant delay in scratch closure following 5 h and 12 h of treatment in the presence of the AP-1 inhibitor, suggesting the essential role of AP-1 in regulating the migratory capacity of this cell type (Figures 3(c)–3(e)).

Interestingly, transwell migration assay of both MG-treated fibroblasts and keratinocytes showed significantly reduced cell migration upon AP-1 inhibition (Figures 3(f) and 3(g), respectively). This could suggest that AP-1 inhibition results in downregulation of essential chemokine receptors, leading to impaired cell migration. Collectively, we showed that inhibition of AP-1 directly resulted in impaired cell migration, completely reverting the effects of MG treatment on the migratory capacities in both fibroblasts and keratinocytes.

3.4. Micrograft-Accelerated Scratch Closure through AP-1 Activity Does Not Depend on Fibroblast Cell Proliferation. As the AP-1 family has been described to regulate both migration and proliferation [14], we assessed possible changes in cell cycle regulation in order to investigate the contribution of cell proliferation to the *in vitro* scratch closure.

To determine the role of AP-1 in cell proliferation under cell-free MG-treated conditions, we performed a cell cycle assessment on soluble MG-treated proliferating fibroblasts and keratinocytes using the 5-ethynyl-2′-deoxyuridine (EdU) assay in the presence of the AP-1 inhibitor T-5224. Interestingly, no changes in cell cycle phases were observed in MG-treated fibroblasts and the overall proliferation rate remained unchanged (Figure 4(a)). In contrast, MG-treated keratinocytes showed a decreased number of cells in the S-phase, indicating reduced cell proliferation of keratinocytes upon MG treatment (Figure 4(b)). Furthermore, we showed that MG treatment upon AP-1 inhibition does not alter cell viability in both cell types (Figures 4(c) and 4(d)). Therefore,

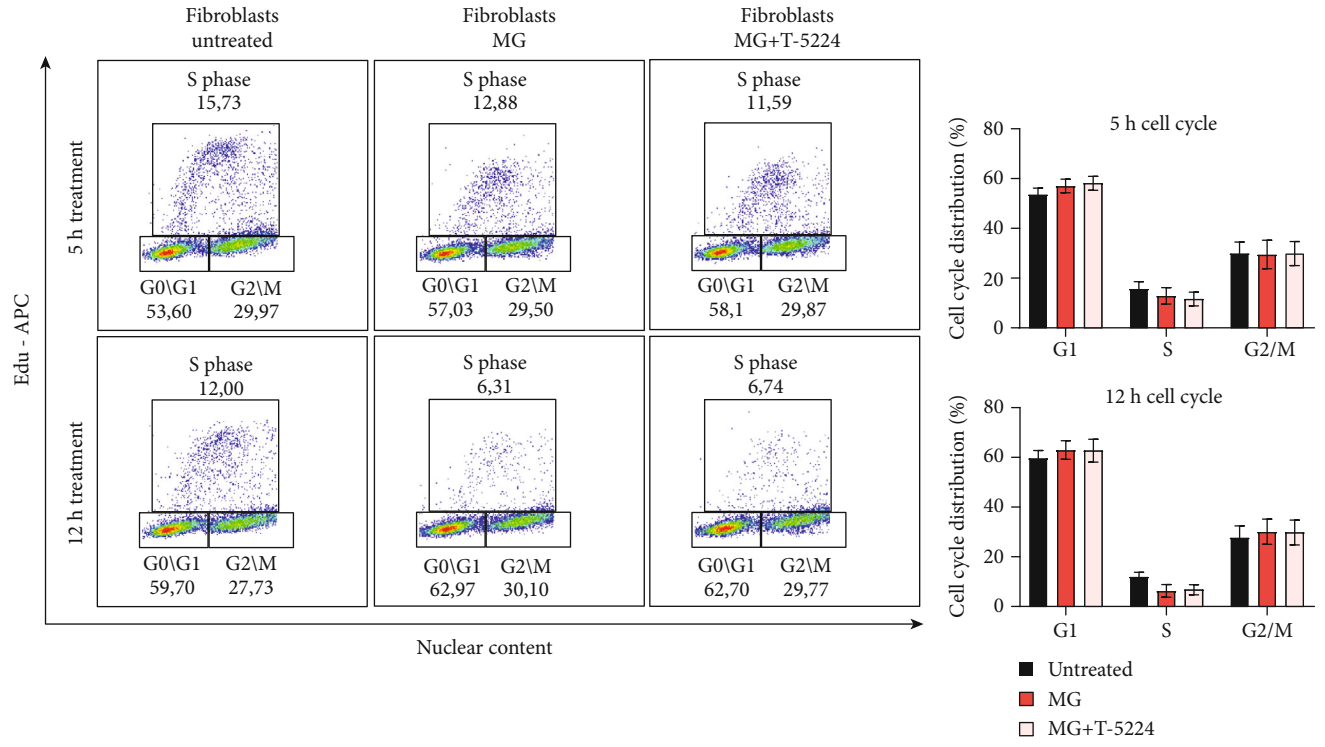

(a)

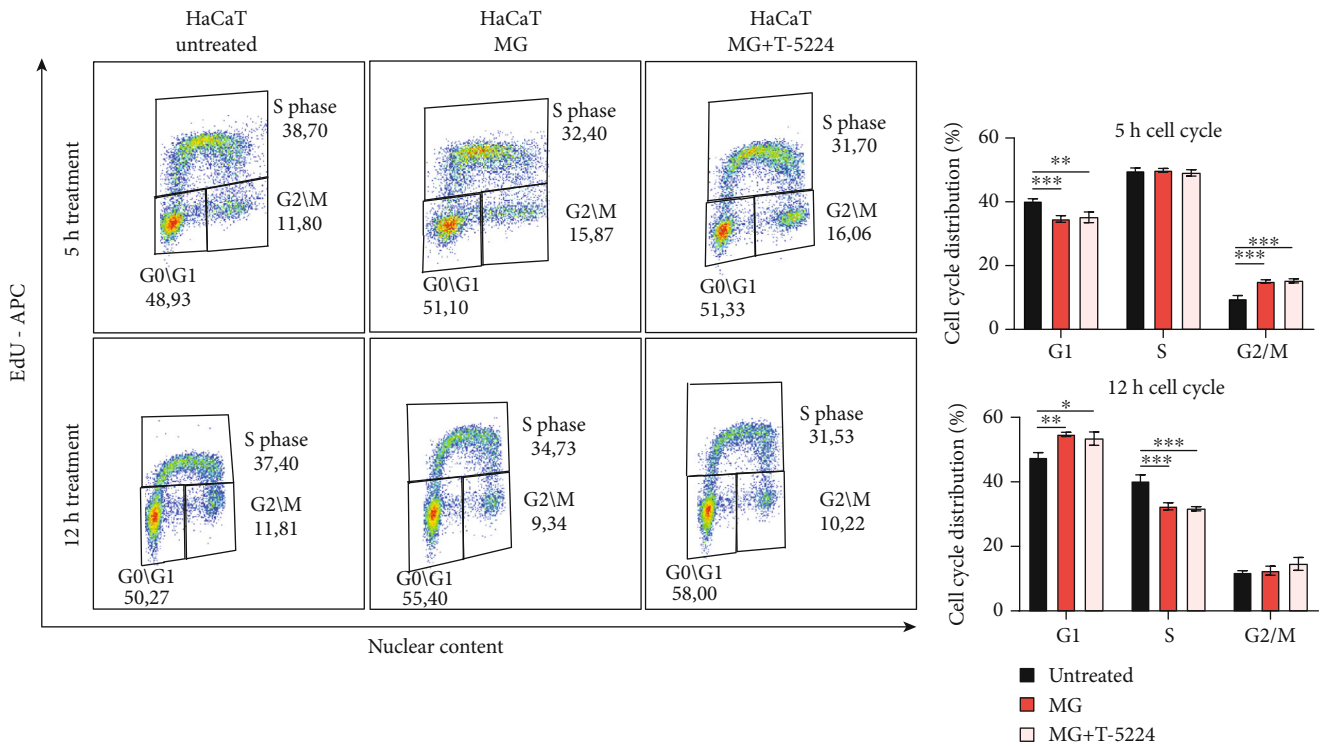

(b)

Figure 4: Continued.

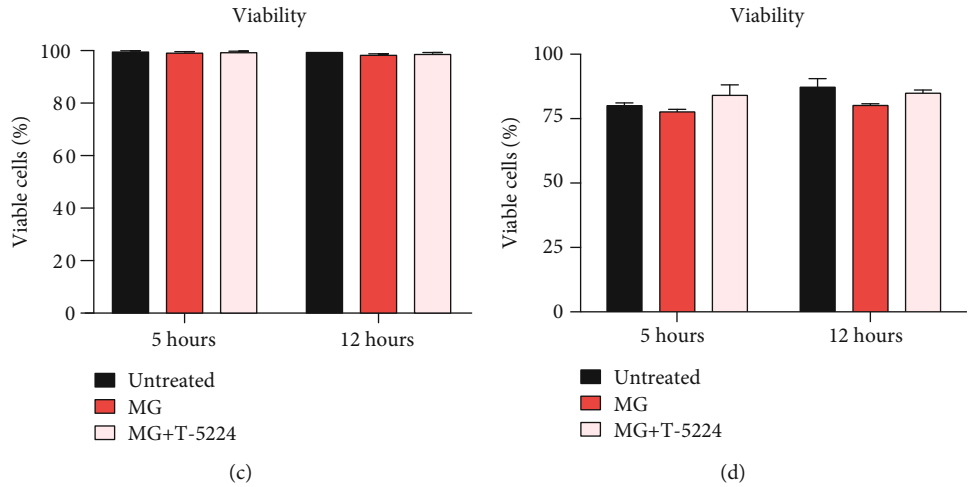

Figure 4: AP-1 in MG-treated cells does not affect fibroblast cell proliferation and viability. (a, b) Cell cycle changes were analyzed using the common 5-ethynyl-2′-deoxyuridine (EdU) assay (associated with DAPI staining to evaluate the nuclear content) on both MG-treated fibroblasts and human keratinocytes exposed to 5 and 12 h of MG treatment in the presence or absence of the AP-1 inhibitor T-5224. Quantification average of $N = 3$ is shown. Data is presented as the mean ± SEM. Two-way ANOVA was used to perform statistical analysis. $^{*}P < 0.05$; $^{**}P < 0.01$; $^{***}P < 0.001$. (c, d) MG-induced effects on cell viability were evaluated via FACS analysis using the Fixable Viability Stain 660. Percentage (%) of viable cells after exposure to 5 and 12 h of MG treatment is shown. No significant differences were found among the different conditions.

we exclude the involvement of AP-1 in promoting cell proliferation upon soluble MG treatment *in vitro*.

3.5. Micrograft Treatment Regulates the Matrix Remodeling Machinery in an AP-1-Dependent Manner. During the healing process, cell migration and active extracellular matrix (ECM) remodeling represent crucial events for successful wound healing. Therefore, we aimed to assess the impact of AP-1 activity on the enzymatic function of MMPs. Recently, it has been shown that essential wound healing-associated genes, such as cytokines and MMPs, were strongly upregulated upon AMG treatment [19]. Upon transcriptional analysis of this dataset, these in turn appeared to be targets of the AP-1 (Figures 1(b) and 1(d) and Figure S1B). Additionally, it has previously been shown that upon AMG treatment, MMP expression levels and their enzymatic activity were significantly increased [19]. As AP-1 has been reported to regulate the expression levels of several genes, including those encoding MMPs [14], we determined whether the soluble MG-induced activity of MMPs was AP-1 dependent. Cell-free MG-treated fibroblasts and keratinocytes were cocultured in the presence of the AP-1 inhibitor T-5224. Interestingly, we observed that AP-1 inhibition in MG-treated fibroblasts and keratinocytes expressed significantly lower transcript levels of several MMP members after 5 h and 12 h of treatment (Figures 5(a) and 5(c)). Subsequently, we exposed fibroblasts and keratinocytes in the *in vitro* scratch assay to the MG solution treatment with and without AP-1 inhibition. The conditioned medium collected from these conditions was then used to perform a fluorescence-based assay to determine the enzymatic activity of the MMPs. Remarkably, enzymatic activity was greatly hindered upon AP-1 inhibition in fibroblasts and keratinocytes (Figures 5(b) and 5(d)). These findings indicate that AP-1 might play a central role in MG-induced cell migration, and more importantly, this connection might explain the improved wound healing upon cell-free MG treatment.

3.6. AP-1 Transcriptional Activity Is Responsible for ERK-Mediated Wound Healing upon Micrograft Treatment. Wound healing processes enhanced by the soluble MG have been shown to be induced in an ERK-dependent manner [19]. To further unravel the downstream mechanism of this treatment at the transcriptional level, we showed the importance of the transcription factor AP-1 in regulating cell migration and MMP activity upon MG treatment. As it has been reported that AP-1 is regulated by ERK, we assessed whether this regulation takes place in both MG-treated fibroblasts and keratinocytes [11, 12]. Therefore, we determined posttranslational modification of important AP-1 family members, including phosphorylation of the mouse and human homologs of Fra-1 and c-Jun in the presence of the MEK inhibitor PD0325901.

Interestingly, upon ERK inhibition in MG-treated cells, reduced levels of pFra-1/pFRA-1 were observed while pJun/pJUN did not decrease (Figure 6(a)). This could suggest that heterodimers involving Fra-1 regulate the ERK-dependent effects of the MG treatment. To validate this, we performed RNA sequencing on MG-treated wounded fibroblasts in the presence or absence of the MEK inhibitor PD0325901 (Figure 6(b)). Using DEG-derived GO terms, expression values of genes involved in cell migration, angiogenesis, cell cycle, and epithelialization showed clear transcriptional changes upon MEK inhibition (Figure 6(c)). As these genes are known to be differentially expressed upon micrograft treatment [19], we assessed whether these genes were affected by MEK inhibition. Although a few crucial genes of angiogenesis (e.g., *Vegfa* and *Flt1*) were altered by

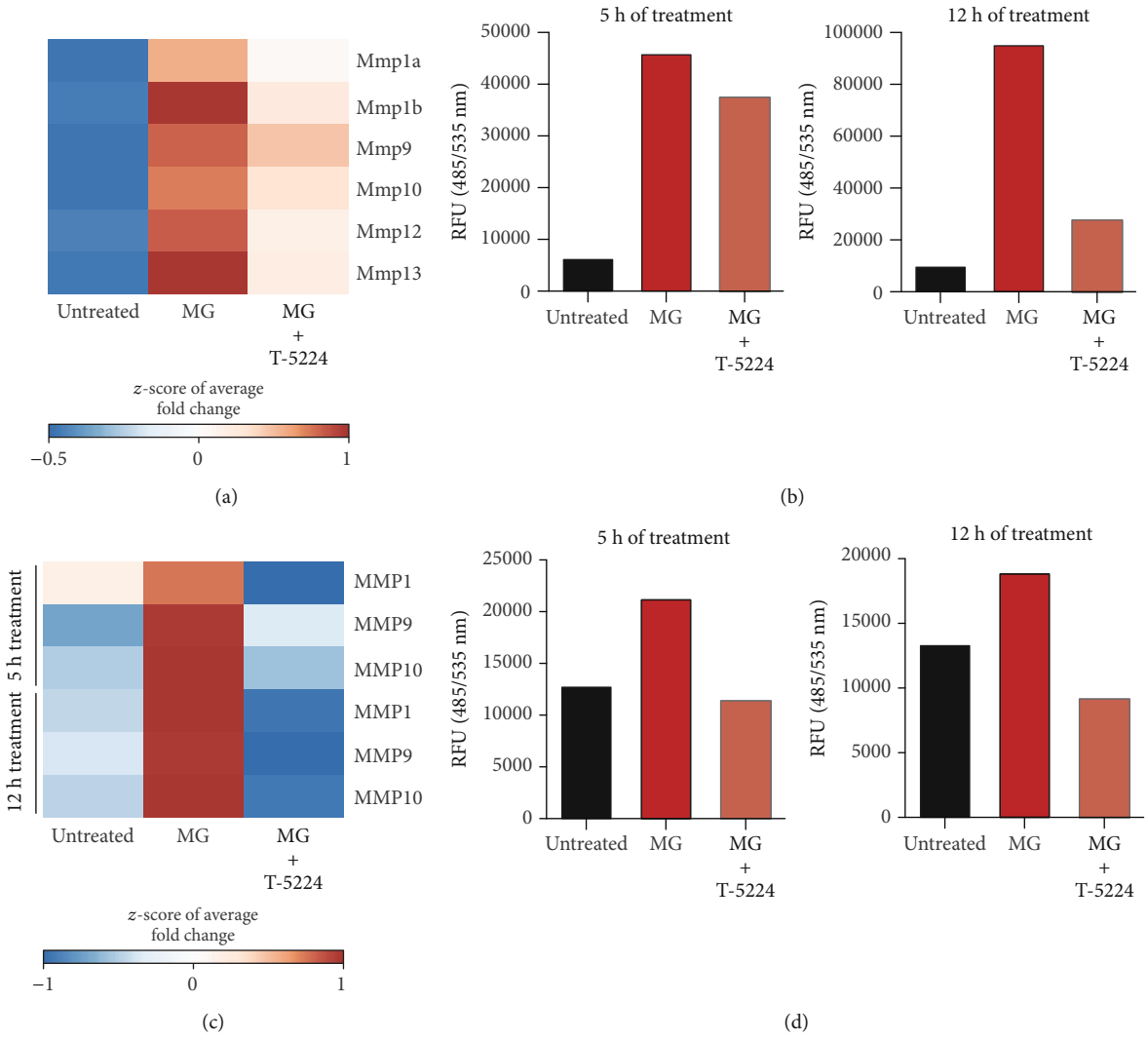

Figure 5: Transcriptional and posttranscriptional regulation of the matrix remodeling machinery via MG-dependent AP-1 activity. (a) Matrix metalloproteinase (MMP) gene expression levels were evaluated by RT-qPCR in 5 h MG-treated adult fibroblasts in the presence or absence of T-5224 (60 μM). Expression values are expressed as z-score of the average fold change (FC) normalized to the expression of *GAPDH*, *β-actin*, and *Rpl13a* genes ($N = 3$). (b) Enzymatic activity of MMPs in adult fibroblasts exposed to 5 and 12 h of MG treatment was evaluated via FRET (fluorescence resonance energy transfer). Signal intensities were normalized to the substrate control. Data is reported as relative fluorescence units (RFU). (c) MMP gene expression levels were evaluated by RT-qPCR in 5 h and 12 h MG-treated human keratinocytes in the presence or absence of T-5224 (60 μM). Expression values are expressed as z-score of the average FC normalized on the expression of *GAPDH*, *β-actin*, and *RPL13A* genes ($N = 3$). (d) Enzymatic activity of matrix metalloproteinases of conditioned media derived from human keratinocytes exposed to 5 and 12 h of MG treatment was evaluated via FRET (frequency resonance energy transfer). Signal intensity signals were normalized to the substrate control. Data is reported as relative fluorescence units (RFU).

this inhibition, a multitude of genes involved in cell migration were significantly affected upon treatment with PD0325901, confirming that the soluble MG treatment mainly increased cell migration. Additionally, high levels of *Fosl1* and *Junb* were downregulated after MEK inhibition, possibly linking this reduction to the changes in cell migration.

4. Discussion

As skin injuries and impaired tissue regeneration have drastic financial and medical consequences for patients, micrografts (MG) provide an affordable treatment to aid the endogenous wound healing. Although multiple MG systems have been shown to be successful in clinical trials, the molecular mechanisms behind these techniques remain unclear [16]. Previously, it has been demonstrated that cell-free autologous MG (AMG) treatment improves ERK-dependent cell migration and matrix remodeling, resulting in accelerated wound closure *in vitro* and *in vivo* [19]. However, the downstream mechanisms of the transcriptional regulation behind the soluble MG-induced cellular changes have not yet been explored.

In the present work, we identified AP-1 among other transcription factors responsible for establishing a regenerative transcriptional profile in both fibroblasts (Figure 1) and

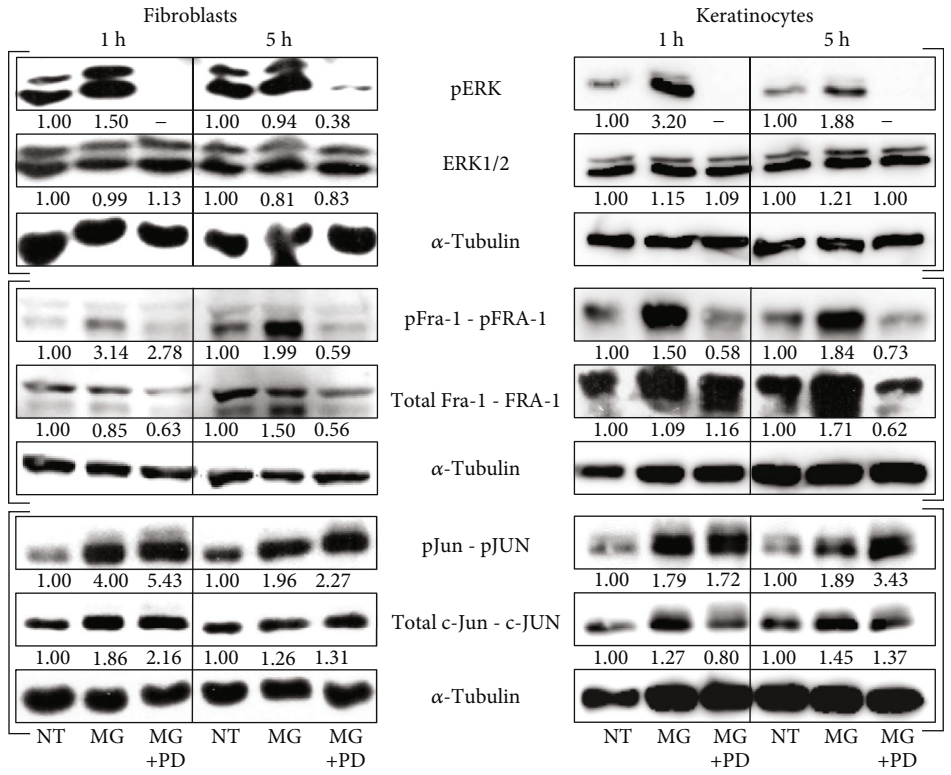

(a)

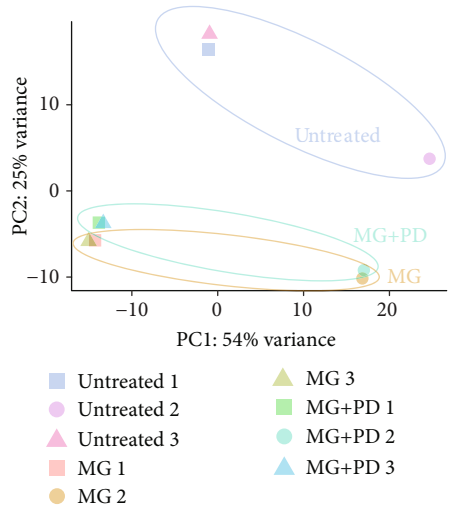

(b)

Figure 6: Continued.

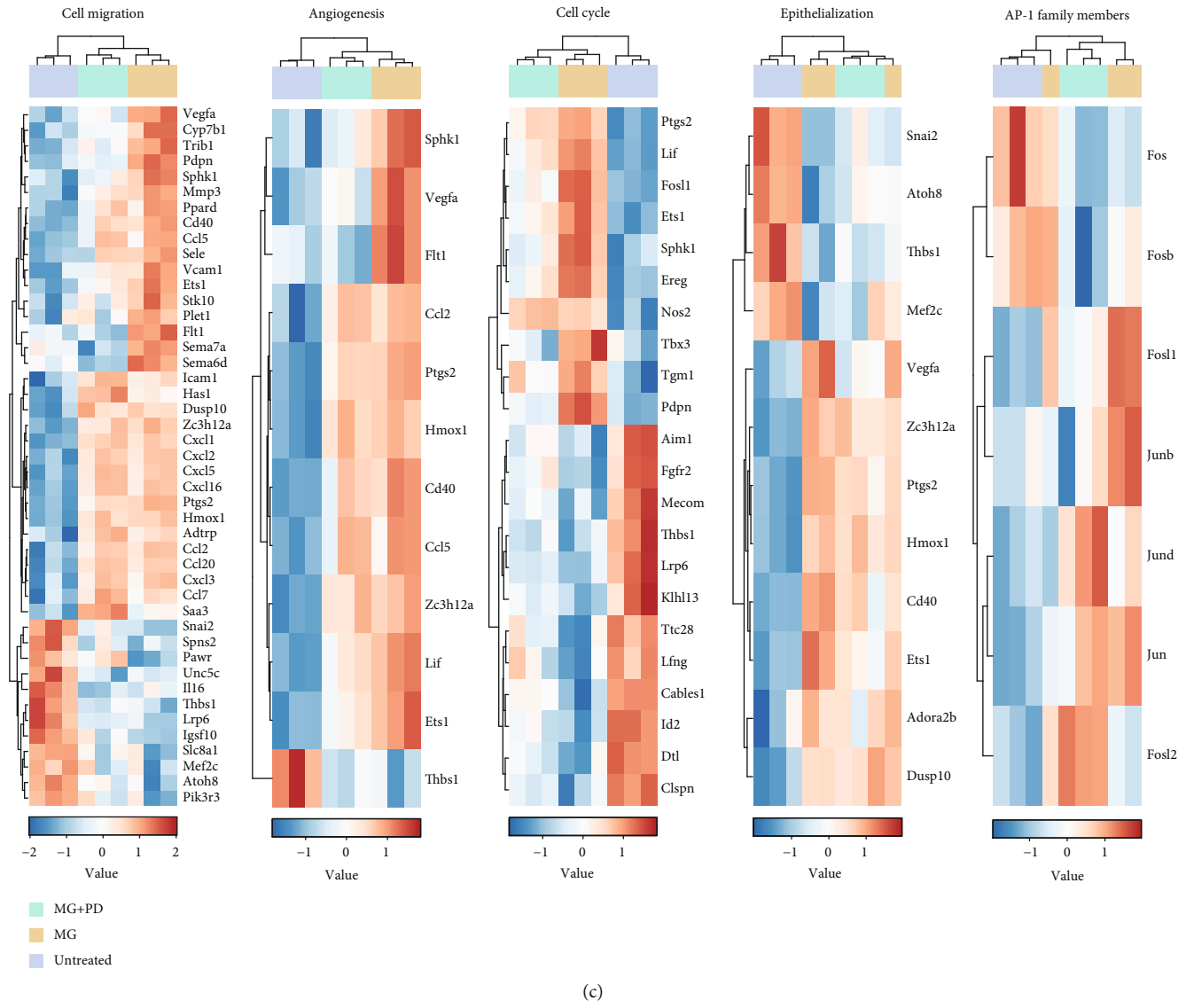

(c)

Figure 6: ERK signaling pathway activation regulates wound healing events through AP-1 transcription factor activity. (a) Representative western blot showing protein levels of phosphorylated and total ERK, Fra-1, and c-Jun from wounded murine adult fibroblasts and unwounded human keratinocytes (HaCaT cells) exposed to 1 h and 5 h of MG treatment in the presence or absence of the MEK inhibitor PD0325901 (1 μM). (b) Principal component analysis (PCA) plot obtained from RNA-seq data indicates clustering between untreated and MG-treated samples with or without MEK inhibition. (c) Heatmaps showing gene expression levels of DEGs discovered through RNA-seq analysis are shown to be involved in essential wound healing related events, including cell migration, angiogenesis, cell cycle, and epithelialization. Gene expression levels of AP-1 family members are presented as heatmap in all the conditions under study.

keratinocytes. Although inhibition of AP-1 activity leads to a drastic reduction in cell migration and loss of a transcriptional program favoring matrix remodeling, we do not exclude indirect effects triggered by AP-1 nor the contribution of other essential transcription factors to the improved soluble MG-induced wound healing. As another predicted regulator of the identified DEGs, B cell lymphoma 3 (Bcl3) has been shown to promote wound healing as its knockdown resulted in significantly reduced cell proliferation and migration in the human osteosarcoma U2OS line [28]. Additionally, keratinocyte migration has been demonstrated to be drastically impaired upon *CAAT enhancer-binding protein gamma* (*C/EBPγ*) silencing [29]. Aside from cell migration, dysregulated genes involved in other wound healing processes might be regulated by other predicted TFs. For example, *Forkhead box protein C2* (*Foxc2*) is a known regulator of angiogenesis in both wound healing and oral squamous cell carcinoma [30, 31]. However, as AP-1 is known to regulate both MMP activity and cell migration, and is additionally regulated by ERK signaling, we aimed our attention at the AP-1 complex member *Fosl1*.

Upon cell-free MG treatment, both *Fosl1*/*FOSL1* transcript levels and phosphorylated Fra-1 and FRA-1 contribute to an elevated AP-1 activity in both fibroblasts and keratinocytes (Figures 2(a), 2(c), and 2(d)). The activator protein-1 (AP-1) complex is composed of homo- and heterodimers of

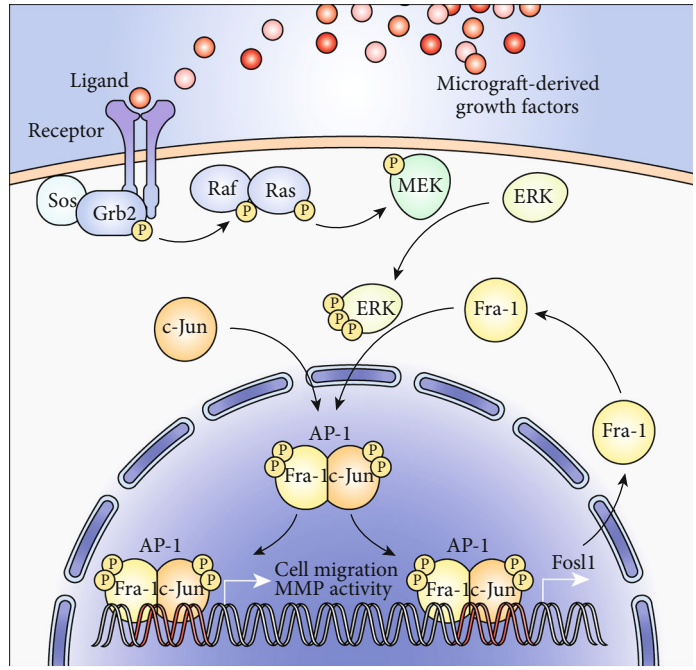

Figure 7: Schematic representation of the ERK-mediated mechanisms of MG treatment. Upon MG treatment, healing-associated growth factors present in the soluble fraction of the micrograft activate the MAPK signaling pathway, resulting in the phosphorylation of ERK. c-Jun and Fra-1 undergo dimerization to form the transcription factor AP-1. Once phosphorylated by ERK, AP-1 stabilizes in the nucleus to bind promoter regions of *Fosl1*, establishing a feedback loop. Additionally, AP-1 also binds the promoter regions of wound healing-associated genes, such as those involved in the regulation of cell migration.

leucine zipper proteins where a Fos family member binds to a protein of the Jun family [32]. While the Jun family is able to form homodimers, Fos proteins are restricted to dimerization with a Jun member [33]. Upon dimerization, AP-1 binds to 12-O-tetradecanoate-13-acetate (TPA) response elements (TRE) within the genome, although its transcriptional behavior strongly depends on the dimer composition and its phosphorylation [13]. As Fra-1 is likely to form the AP-1 complex by dimerization with the most potent Jun protein c-Jun, c-Jun phosphorylation (pJun) found to be increased upon soluble MG treatment. While it has been reported that *c-Jun* expression is minimally affected after *in vitro* wounding, elevated mRNA levels of Fos genes are found shortly after injury [34]. Among these Fos members, *c-Fos* and *Fosl1* have been reported to be briefly expressed as an immediate response to extracellular stimuli, favoring the wound recovery by initiating the expression of healing-associated genes, such as growth factors, MMPs, and integrins [14]. Accordingly, upon specific AP-1 inhibition, the soluble MG-induced scratch closure is completely reverted, and the cellular migratory capacity showed to be highly impaired (Figure 3). Of note, a slight MG-dependent reduction in proliferation was displayed in treated keratinocytes. However, as MG treatment as well as AP-1 induction did not increase cell proliferation, we affirm that changes in cell cycle did not contribute to accelerated *in vitro* wound closure in an AP-1-dependent way (Figure 4). In addition, the enzymatic activity of matrix remodeling enzymes (MMPs) was severely compromised in the presence of AP-1 inhibitor T-5224 (Figure 5). Interestingly, decreased Fra-1 expression has been reported to result in decreased MMP expression and cell migration [35, 36]. Moreover, overexpression of Fra-1 significantly improves cell motility and invasiveness in cancer [37, 38]. Taken together, these findings support the role of Fra-1/AP-1 in regulating cell migration in the context of wound healing as matrix remodeling and integrin expression facilitates cellular movement through the matrix.

Transcriptional regulation of Fos proteins occurs mainly through MAPK activity as a response to mitogenic cues. As a response to extracellular signals, ternary complex factor (TCF) phosphorylated by ERK enables its binding together with SRE-binding factor (SRF) to serum response elements (SRE) in the promoter region of *Fos* genes. Furthermore, it has been reported that AP-1 is able to autoregulate itself by binding to promoter regions of *Fos* genes and *c-Jun* [39–41]. In addition to transcriptional regulation, AP-1 members are posttranscriptionally phosphorylated by MAPK components, leading to reduced ubiquitination and increased transcriptional activity [42, 43]. Studies have shown that JNK-mediated phosphorylation of the serine 63 and 73 residues of c-Jun increases both stability and activity [42, 44]. Similarly, Fra-1 stability depends on phosphorylation on serine 252 and 265 by ERK1/2 signaling [45]. In addition, phosphorylation by ERK1/2 results in higher activity of Fos proteins [46, 47]. In this work, we confirm that MG-induced phosphorylation of Fra-1 is strongly dependent on ERK1/2 activity in both fibroblasts and keratinocytes (Figure 6(a)). Additionally, we report that both phosphorylated and total Fra-1 levels decrease in the presence of the ERK inhibitor, confirming the ERK-dependent

posttranscriptional regulation of this *Fosl1*-encoded protein. Noteworthy, cell-free MG-induced phosphorylation levels of c-Jun appear to be independent of ERK, suggesting its regulation through other mechanisms. As mentioned earlier, the JNK branch of the MAPK cascade could be responsible for this increase, as JNK contributes to AP-1 expression upon exposure to mechanical stress, in this case the *in vitro* wounding [48]. Finally, RNA-seq data indicate that ERK inhibition greatly impairs the migratory transcriptional profiles of MG-treated adult fibroblasts. As most of these DEGs are predicted to be regulated by AP-1 (Figure 1), this could suggest that soluble MG-enhanced cell migration arises as a result of the transcriptional activity of AP-1.

Collectively, we propose a mode of action behind the accelerated wound healing using the cell-free MG treatment (Figure 7). Our findings indicate that soluble MG-induced ERK signaling has a double mechanism to regulate matrix remodeling and cell migration through transcriptional activity of AP-1. As ERK signaling is activated upon MG solution treatment, this cascade leads to the increased gene expression of *Fosl1*, resulting in a higher amount of the transcription factor Fra-1/AP-1. This in turn becomes posttranscriptionally phosphorylated by the active ERK signaling. Phosphorylated AP-1 subsequently triggers a migratory phenotype in keratinocytes and fibroblasts through the activation of MMP activity and a transcription program favoring chemotaxis and cell motility. Although other signaling pathways and transcription factors are likely to contribute to this phenotype, we show that inhibition of both ERK and AP-1 is sufficient to completely revert *in vitro* wound closure by the soluble MG treatment. Altogether, our results highlight the crucial role of ERK-dependent transcriptional activity of AP-1 in coordinating the beneficial effects of the MG treatment, opening new opportunities for future wound healing studies.

Data Availability

The data presented in this paper has been deposited in GEO Datasets under accession no. GSE134113.

Conflicts of Interest

The authors declare no competing interests.

Authors' Contributions

M.B. designed the experiments and performed the scratch assays, immunofluorescence, transwell migration assay, and the enzymatic activity assays. J.S.H.C. analyzed RNA sequencing and ChIP sequencing and performed and analyzed qPCR data and prepared the manuscript. P.A. performed all western blotting analyses. W.A.A.d.O. conducted and analyzed the EdU assay and the viability assessment. Y.E.L. performed and quantified the transwell assay. F.L.L., M.S., J.S.H.C., and M.B. designed the experiments and edited and revised the manuscript. All authors provided input in the design of the experiments and cowriting of the manuscript and have edited it. Martina Balli and Jonathan Sai-Hong Chui are co-first authors. Frederic LLuis and Maurilio Sampaolesi are co-last authors.

Acknowledgments

We are grateful for the support from KU Leuven starting grant (STG), KU Leuven C1 funds (C14/16/078), and FWO (G097618N) funds to F.L.L.; FWO-SB fellowship (1S65319N) to J.S.H.C.; and FWO fellowship (1155619N) to W.A.A.d.O. M.S. is supported by the contribution of NATO grant "RAWINTS" project #G984961, FWO (#G088715N, #G060612N, and #G0A8813N), CARIPLO Foundation #2015, and C1 funds (C14/17/111).

Supplementary Materials

Supplementary 1. Table S1: primer sequences used to determine mRNA levels in mouse fibroblasts and human keratinocytes. Sequences are represented in the $5'$-$3'$ direction.

Supplementary 2. Table S2: list of differentially expressed genes (unregulated, downregulated, and nondifferentially expressed) upon 5 h of micrograft treatment (as represented in Figure 1).

Supplementary 3. Figure S1: (A) Predicted transcription factors identified by iRegulon as possible regulators of the DEGs discovered in MG-treated conditions. Transcription factor prediction is presented as network enrichment score (NES). (B) ChIP-seq showing the binding of Fra-1/AP-1 in the promoter regions of several upregulated DEGs involved in wound healing processes, predicted to be regulated by AP-1 in the iRegulon analysis.

References

[1] R. Richardson, K. Slanchev, C. Kraus, P. Knyphausen, S. Eming, and M. Hammerschmidt, "Adult zebrafish as a model system for cutaneous wound-healing research," *The Journal of Investigative Dermatology*, vol. 133, no. 6, pp. 1655–1665, 2013.

[2] R. A. F. Clark, "Overview and general considerations of wound repair," in *The Molecular and Cellular Biology of Wound Repair*, R. A. F. Clark and P. M. Henson, Eds., pp. 3–33, Springer US, Boston, MA, USA, 1998.

[3] P. Martin, "Wound healing–aiming for perfect skin regeneration," *Science*, vol. 276, no. 5309, pp. 75–81, 1997.

[4] N. Lian and T. Li, "Growth factor pathways in hypertrophic scars: molecular pathogenesis and therapeutic implications," *Biomedicine & Pharmacotherapy*, vol. 84, pp. 42–50, 2016.

[5] A. Oeckinghaus and S. Ghosh, "The NF-κB family of transcription factors and its regulation," *Cold Spring Harbor Perspectives in Biology*, vol. 1, no. 4, article a000034, 2009.

[6] R. A. F. Clark, "Wound repair," in *The Molecular and Cellular Biology of Wound Repair*, R. A. F. Clark, Ed., pp. 3–50, Springer US, Boston, MA, USA, 1988.

[7] K. W. Finnson, S. McLean, G. M. Di Guglielmo, and A. Philip, "Dynamics of transforming growth factor beta signaling in wound healing and scarring," *Advances in Wound Care*, vol. 2, no. 5, pp. 195–214, 2013.

[8] H. Escuin-Ordinas, S. Li, M. W. Xie et al., "Cutaneous wound healing through paradoxical MAPK activation by BRAF inhibitors," *Nature Communications*, vol. 7, no. 1, p. 12348, 2016.

[9] G.-D. Sharma, J. He, and H. E. P. Bazan, "p38 and ERK1/2 coordinate cellular migration and proliferation in epithelial wound healing: evidence of cross-talk activation between MAP kinase cascades," *Journal of Biological Chemistry*, vol. 278, no. 24, pp. 21989–21997, 2003.

[10] H. Gille, A. D. Sharrocks, and P. E. Shaw, "Phosphorylation of transcription factor p62 *TCF* by MAP kinase stimulates ternary complex formation at c-*fos* promoter," *Nature*, vol. 358, no. 6385, article BF358414a0, pp. 414–417, 1992.

[11] T. Deng and M. Karin, "c-Fos transcriptional activity stimulated by H-Ras-activated protein kinase distinct from JNK and ERK," *Nature*, vol. 371, no. 6493, pp. 171–175, 1994.

[12] S. Gangnuss, A. J. Cowin, I. S. Daehn et al., "Regulation of MAPK activation, AP-1 transcription factor expression and keratinocyte differentiation in wounded fetal skin," *The Journal of Investigative Dermatology*, vol. 122, no. 3, pp. 791–804, 2004.

[13] P. Angel, M. Imagawa, R. Chiu et al., "Phorbol ester-inducible genes contain a common cis element recognized by a TPA-modulated trans-acting factor," *Cell*, vol. 49, no. 6, pp. 729–739, 1987.

[14] S. Yates and T. E. Rayner, "Transcription factor activation in response to cutaneous injury: role of AP-1 in reepithelialization," *Wound Repair and Regeneration*, vol. 10, no. 1, pp. 5–15, 2002.

[15] H. J. You and S. K. Han, "Cell therapy for wound healing," *Journal of Korean Medical Science*, vol. 29, no. 3, pp. 311–319, 2014.

[16] A. Biswas, M. Bharara, C. Hurst, D. G. Armstrong, and H. Rilo, "The micrograft concept for wound healing: strategies and applications," *Journal of Diabetes Science and Technology*, vol. 4, no. 4, pp. 808–819, 2010.

[17] D. Kadam, "Novel expansion techniques for skin grafts," *Indian Journal of Plastic Surgery*, vol. 49, no. 1, pp. 5–15, 2016.

[18] L. Trovato, M. Monti, C. del Fante et al., "A new medical device Rigeneracons allows to obtain viable micro-grafts from mechanical disaggregation of human tissues," *Journal of Cellular Physiology*, vol. 230, no. 10, pp. 2299–2303, 2015.

[19] M. Balli, F. Vitali, A. Janiszewski et al., "Autologous micrograft accelerates endogenous wound healing response through ERK-induced cell migration," *Cell Death & Differentiation*, 2019.

[20] S. Jimi, M. Kimura, F. De Francesco, M. Riccio, S. Hara, and H. Ohjimi, "Acceleration mechanisms of skin wound healing by autologous micrograft in mice," *International Journal of Molecular Sciences*, vol. 18, no. 8, p. 1675, 2017.

[21] C.-C. Liang, A. Y. Park, and J.-L. Guan, "In vitro scratch assay: a convenient and inexpensive method for analysis of cell migration in vitro," *Nature Protocols*, vol. 2, no. 2, pp. 329–333, 2007.

[22] A. De Jaime-Soguero, F. Aulicino, G. Ertaylan et al., "Wnt/Tcf1 pathway restricts embryonic stem cell cycle through activation of the *Ink4/Arf* locus," *PLoS Genetics*, vol. 13, no. 3, article e1006682, 2017.

[23] C. Chronis, P. Fiziev, B. Papp et al., "Cooperative binding of transcription factors orchestrates reprogramming," *Cell*, vol. 168, no. 3, pp. 442–459.e20, 2017.

[24] R. Janky, A. Verfaillie, H. Imrichová et al., "iRegulon: from a gene list to a gene regulatory network using large motif and track collections," *PLoS Computational Biology*, vol. 10, no. 7, article no. e1003731, 2014.

[25] M. Kortenjann, O. Thomae, and P. E. Shaw, "Inhibition of v-raf-dependent c-fos expression and transformation by a kinase-defective mutant of the mitogen-activated protein kinase Erk2," *Molecular and Cellular Biology*, vol. 14, no. 7, pp. 4815–4824, 1994.

[26] W. J. Boyle, T. Smeal, L. H. Defize et al., "Activation of protein kinase C decreases phosphorylation of c-Jun at sites that negatively regulate its DNA-binding activity," *Cell*, vol. 64, no. 3, pp. 573–584, 1991.

[27] H. Makino, S. Seki, Y. Yahara et al., "A selective inhibition of c-Fos/activator protein-1 as a potential therapeutic target for intervertebral disc degeneration and associated pain," *Scientific Reports*, vol. 7, no. 1, p. 16983, 2017.

[28] A. Vivien Ya-Fan Wang, Y. Li, D. Kim et al., "Bcl3 phosphorylation by Akt, Erk2, and IKK is required for its transcriptional activity," *Molecular Cell*, vol. 67, pp. 484–497.e5, 2017.

[29] R. Melchionna, G. Bellavia, M. Romani et al., "C/EBPγ regulates wound repair and EGF receptor signaling," *The Journal of Investigative Dermatology*, vol. 132, no. 7, pp. 1908–1917, 2012.

[30] H. Hayashi and T. Kume, "Foxc2 transcription factor as a regulator of angiogenesis via induction of integrin β3 expression," *Journal of Biological Chemistry*, vol. 283, no. 35, pp. 23791–23800, 2009.

[31] T. Sasahira, N. Ueda, K. Yamamoto et al., "Prox1 and FOXC2 act as regulators of lymphangiogenesis and angiogenesis in oral squamous cell carcinoma," *PLoS One*, vol. 9, no. 3, article e92534, 2014.

[32] T. Curran and B. R. Franza, "Fos and Jun: the AP-1 connection," *Cell*, vol. 55, no. 3, pp. 395–397, 1988.

[33] J. N. M. Glover and S. C. Harrison, "Crystal structure of the heterodimeric bZIP transcription factor c-Fos–c-Jun bound to DNA," *Nature*, vol. 373, no. 6511, pp. 257–261, 1995.

[34] B. K. Dieckgraefe, D. M. Weems, S. A. Santoro, and D. H. Alpers, "ERK and p38 MAP kinase pathways are mediators of intestinal epithelial wound-induced signal transduction," *Biochemical and Biophysical Research Communications*, vol. 233, no. 2, pp. 389–394, 1997.

[35] A. Das, Q. Li, M. J. Laws, H. Kaya, M. K. Bagchi, and I. C. Bagchi, "Estrogen-induced expression of Fos-related antigen 1 (FRA-1) regulates uterine stromal differentiation and remodeling," *Journal of Biological Chemistry*, vol. 287, no. 23, pp. 19622–19630, 2012.

[36] R. L. Hanson, R. B. Brown, M. M. Steele, P. M. Grandgenett, J. A. Grunkemeyer, and M. A. Hollingsworth, "Identification of FRA-1 as a novel player in pancreatic cancer in cooperation with a MUC1: ERK signaling axis," *Oncotarget*, vol. 7, no. 26, pp. 39996–40011, 2016.

[37] H. Liu, G. Ren, T. Wang et al., "Aberrantly expressed Fra-1 by IL-6/STAT3 transactivation promotes colorectal cancer aggressiveness through epithelial–mesenchymal transition," *Carcinogenesis*, vol. 36, no. 4, pp. 459–468, 2015.

[38] P. Adiseshaiah, D. J. Lindner, D. V. Kalvakolanu, and S. P. Reddy, "FRA-1 proto-oncogene induces lung epithelial cell invasion and anchorage-independent growth *in vitro*, but is insufficient to promote tumor growth *in vivo*," *Cancer Research*, vol. 67, no. 13, pp. 6204–6211, 2007.

[39] P. Angel, K. Hattori, T. Smeal, and M. Karin, "The _jun_ proto-oncogene is positively autoregulated by its product, Jun/AP-1," *Cell*, vol. 55, no. 5, pp. 875–885, 1988.

[40] P. Sassone-Corsi, J. C. Sisson, and I. M. Verma, "Transcriptional autoregulation of the proto-oncogene *fos*," *Nature*, vol. 334, no. 6180, pp. 314–319, 1988.

[41] K. Matsuo, J. M. Owens, M. Tonko, C. Elliott, T. J. Chambers, and E. F. Wagner, "Fosl1 is a transcriptional target of c-Fos during osteoclast differentiation," *Nature Genetics*, vol. 24, no. 2, pp. 184–187, 2000.

[42] M. Treier, L. M. Staszewski, and D. Bohmann, "Ubiquitin-dependent c-Jun degradation in vivo is mediated by the delta domain," *Cell*, vol. 78, no. 5, pp. 787–798, 1994.

[43] C. Tsurumi, N. Ishida, T. Tamura et al., "Degradation of c-Fos by the 26S proteasome is accelerated by c-Jun and multiple protein kinases," *Molecular and Cellular Biology*, vol. 15, no. 10, pp. 5682–5687, 1995.

[44] T. Smeal, M. Hibi, and M. Karin, "Altering the specificity of signal transduction cascades: positive regulation of c-Jun transcriptional activity by protein kinase A," *The EMBO Journal*, vol. 13, no. 24, pp. 6006–6010, 1994.

[45] J. Basbous, D. Chalbos, R. Hipskind, I. Jariel-Encontre, and M. Piechaczyk, "Ubiquitin-independent proteasomal degradation of Fra-1 is antagonized by Erk1/2 pathway-mediated phosphorylation of a unique C-terminal destabilizer," *Molecular and Cellular Biology*, vol. 27, no. 11, pp. 3936–3950, 2007.

[46] L. O. Murphy and J. Blenis, "MAPK signal specificity: the right place at the right time," *Trends in Biochemical Sciences*, vol. 31, no. 5, pp. 268–275, 2006.

[47] M. R. Young and N. H. Colburn, "Fra-1 a target for cancer prevention or intervention," *Gene*, vol. 379, pp. 1–11, 2006.

[48] M. Göke, M. Kanai, K. Lynch-Devaney, and D. K. Podolsky, "Rapid mitogen-activated protein kinase activation by transforming growth factor alpha in wounded rat intestinal epithelial cells," *Gastroenterology*, vol. 114, no. 4, pp. 697–705, 1998.

Hindawi
Stem Cells International
Volume 2019, Article ID 5043518, 10 pages
https://doi.org/10.1155/2019/5043518

Clinical Study

A Multicentre Study: The Use of Micrografts in the Reconstruction of Full-Thickness Posttraumatic Skin Defects of the Limbs—A Whole Innovative Concept in Regenerative Surgery

Michele Riccio,[1] Andrea Marchesini,[1] Nicola Zingaretti,[2] Sara Carella,[3] Letizia Senesi,[1] Maria Giuseppina Onesti,[3] Pier Camillo Parodi,[2] Diego Ribuffo,[3] Luca Vaienti,[4] and Francesco De Francesco[1]

[1]*Department of Reconstructive Surgery and Hand Surgery, University Hospital (AOU Ospedali Riuniti di Ancona), via Conca 71, 60123 Torrette di Ancona, Ancona, Italy*
[2]*Department of Plastic and Reconstructive Surgery, Azienda Ospedaliero-Universitaria "Santa Maria della Misericordia", Piazzale S. Maria della Misericordia 15, 33100 Udine, Italy*
[3]*Department of Surgery "P.Valdoni", Unit of Plastic and Reconstructive Surgery, Sapienza University of Rome, Policlinico Umberto I, Rome, Italy*
[4]*Department of Plastic and Reconstructive Surgery, I.R.C.C.S. Policlinico San Donato, Università degli Studi di Milano, Via Morandi 30, 20097 San Donato Milanese, Milan, Italy*

Correspondence should be addressed to Francesco De Francesco; francesco.defrancesco@ospedaliriuniti.marche.it

Received 7 July 2019; Revised 6 September 2019; Accepted 3 October 2019; Published 1 December 2019

Guest Editor: Federico Moreno

The skin graft is a surgical technique commonly used in the reconstructive surgery of the limbs, in order to repair skin loss, as well as to repair the donor area of the flaps and cover the dermal substitutes after engraftment. The unavoidable side effect of this technique consists of unaesthetic scars. In order to achieve the healing of posttraumatic ulcers by means of tissue regeneration and to avoid excessive scarring, a new innovative technology based on the application of autologous micrografts, obtained by Rigenera technology, was reported. This technology was able to induce tissue repair by highly viable skin micrografts of 80 micron size achieved by a mechanical disaggregation method. The specific cell population of these micrografts includes progenitor cells, which in association with the fragment of the Extracellular Matrix (ECM) and growth factors derived by patients' own tissue initiate biological processes of regeneration enhancing the wound healing process. We have used this technique in 70 cases of traumatic wounds of the lower and upper limbs, characterized by extensive loss of skin substance and soft tissue. In all cases, we have applied the Rigenera protocol using skin micrografts, achieving in 69 cases the complete healing of wounds in a period between 35 and 84 days. For each patient, the reconstructive outcome was evaluated weekly to assess the efficacy of this technique and any arising complication. A visual analogue scale (VAS) was administered to assess the amount of pain felt after the micrografts' application, whereas we evaluated the scars according to the Vancouver scale and the wound prognosis according to Wound Bed Score. We have thus been able to demonstrate that Rigenera procedure is very effective in stimulating skin regeneration, while reducing the outcome scar.

1. Introduction

Complex injuries of the limbs, causing crushing and loss of skin and soft tissue, occur frequently due to common injuries, both domestic and at work. The aim of surgical treatment is the morphological and functional reconstruction, allowing the recovery of the shape of the injured limbs and, at the same time, the reconstruction of its normal protective well-padded and sensitive skin which has specific properties for giving the limbs their principal functions: gait ability and grasp ability. Unfortunately, the regeneration of a specialized tissue (*i.e.*, skin) requires the restoring of the entire

histological hierarchy. Usually, when the injury causes wide and deep loss of the skin and soft tissue, with bone fracture exposed, in order to achieve a functional reconstruction, using free flaps is preferable [1–3], while a useful option is covering the wound with a dermal template [4, 5]. However, in performing of all these techniques, skin grafts taken from the thighs/buttocks to directly repair the injury (or the donor site of the flap) are always essential, as well as the use of dermal substitute after its engraftment, often causing unsightly scars both at the donor and recipient site of skin grafts.

To avoid unaesthetic scars, considered an inevitable side effect of this technique, and to allow at the same time tissue regeneration of the injured site, a new innovative technology based on the application of autologous micrografts obtained by Rigenera® technology, able to induce tissue repair by highly viable skin micrografts achieved by a mechanical disaggregation method [6–8], was recently reported. A small piece of dermal/connective tissue may improve tissue repair of complex wounds [9–11] or hypertrophic scars [12]. At first, micrograft technology was applied in oral-maxillofacial surgery where micrografts derived from the human dental pulp or periosteum were used for periodontal regeneration, bone regeneration of atrophic maxilla, and alveolar socket preservation [13–16]. In the last few years, micrograft technology was applied in plastic and reconstructive surgery where micrografts derived from the cartilage were used for treatment of osteochondral lesion of the nose [17] and for enrichment of adipose tissue from human lipoaspirates [18].

Based on these considerations, the purpose of this observational study was to evaluate the efficacy of micrografts in the treatment of posttraumatic skin defects. For this reason, we have used this approach in the treatment of the posttraumatic wounds of the limbs, with excellent results in terms of clinical outcomes and demonstration of the regenerative capacity of this method by means of the tissue characterization [7].

2. Patients and Methods

2.1. Patients. From 2015 to February 2017 in four Italian Plastic and Reconstructive Units, we treated 70 patients, 38 females and 32 males with a mean age of 53 years (range 34-74 years), affected by chronic posttraumatic leg ulcer applying Rigenera protocol. All patients signed written consent to participate according to the Declaration of Helsinki. Ethics Committee approved the study (protocol N.2017-0274OR). Clinical Trial of the study is found inhttps://clinicaltrials.gov/ct2/show/NCT04030832. 24 patients suffer from bone exposure through chronic posttraumatic ulcer or surgical wound dehiscence with a mean bone exposed surface of 2 cm^2, and 12 patients suffer from tendon exposure through chronic posttraumatic ulcer or surgical wound dehiscence. In three cases, we combined the use of Rigenera procedure with the Integra® dermal regeneration template. In one of these three patients, the Rigenera protocol was used to treat the donor site of a free flap applying the Rigenera® biocomplex over the neoderma created by Integra®. The mean time between trauma and Rigenera treatment was 7 weeks (range 2-18 weeks) (Table 1). All patients provided informed consent at the study protocol conformed to the ethical guidelines of the 1975 Declaration of Helsinki. The primary diagnosis and initial operative procedures leading to wound dehiscence are listed in Table 1. We also reported the correlated diseases affecting the patients. After an average 1-year follow-up, the evaluation of wound closure was accomplished.

Table 1: Patients and wound description.

	n (%)	Mean value	Minimum-maximum
Patients			
Total	70 (100%)		
Sex			
Male	32 (23%)		
Female	38 (27%)		
Age		53 years	34-74 years
Underlying disease			
None	49 (70%)		
Diabetes type II	15 (22%)		
Arteriopathy	6 (8%)		
Wound description			
Wound location			
Thigh	6 (8%)		
Leg	30 (43%)		
Ankle	19 (28%)		
Foot	15 (21%)		
Type of injury			
Wound dehiscence	18 (26%)		
Posttraumatic ulcer	32 (45%)		
Metabolic ulcer	18 (26%)		
Burn	2 (3%)		
Surface area		14 cm^2	7-28 cm^2
Exposed structures			
None	34 (49%)		
Tendon	12 (17%)		
Bone	24 (34%)		
Rigenera procedure			
Infection			
Before procedure	8 (11%)		
After procedure	0 (0%)		
Rigenera treatment delay after trauma		7 weeks	2-18 weeks
Antibiotics postoperative	70 (100%)	6 days	6 days
Time of complete healing		48 days	35-84 days
None (S-J syndrome)	1 (1%)		
Complication/note			
None	66 (95%)		
Stevens-Johnson syndrome	1 (1%)		
Associate use (Rigenera+Integra®)	3 (4%)		

2.2. Surgical Procedure. All cases reported in this study were treated by means of the Rigenera protocol after surgical or enzymatic ulcer's debridement and after wound infection resolution probe by culture exam. The Rigenera® technology is based on the use of the Rigenera machine and Rigeneracons (Human Brain Wave, Turin, Italy), a biological disruptor able to disaggregate small pieces of human connective tissues and select a specific cell population including progenitor cells, on the basis of cellular size. These progenitor cells, in association with the fragment of the Extracellular Matrix (ECM) and growth factors derived by starting tissue, create autologous micrografts ready for use, which can be applied on the injured area alone or in combination with different biological scaffolds, such as collagen. This protocol consists of different steps: (1) collection of a skin tissue sample of 1 cm × 1 cm from a hide donor site with respect to the recipient site (expansion ratio 1 : 10) (Figure 1(a)) (each skin sample is divided into fragments of about 2 mm^2 each); (2) the fragments are positioned in two separated single-use capsules, below the rotating system of helical blades, resting on the filter placed on the bottom of the capsule (disaggregation of tissue for two minutes by Rigeneracons through the addition of 3 ml of sterile saline solution) (Figure 1(b)); (3) collection of 2.5 ml of autologous micrografts obtained after the disaggregation in a sterile solution (Figure 1(c)) from each capsule; (4) injection of 2.5 ml of micrograft solution on an equine collagen sponge to create a regenerative biocomplex (Figure 1(d)); (5) injection of 2.5 ml of micrograft solution into the site of injury by perilesional infiltrations and placement of the biocomplex over the ulcer taking care that the seeded surface of the sponges was in contact with the wound floor (Figures 1(e) and 1(f)); and (6) secondary medication by means of paraffin gauge tie over (Figure 1(g)).

In our patients, we collected small pieces of tissue by inguinal fold after local anaesthesia. Following the application of micrografts, all patients received for 6 days oral penicillin therapy. We performed the first dressing after 4 days without paraffin gauge removal and a second dressing after 3 days with paraffin gauge change and subjected the patients to weekly controls to evaluate the progression of wound healing. After complete healing on the treated site, moisture oil was gently applied, and after one month, the patient starts tissue massage and follow-up visit was delayed in a month's time.

2.3. Clinical, Pain, and Scar Evaluation. For each patient, the surface of the wounds at days 4 and 7 and every week up to complete healing has been measured and each wound was assessed for contraction. Surfaces were followed by tracing the wound edges on the computer with digital pictures. Wound contraction was measured by computer planimetry, expressed in percentage of reduction of the original wound area. At each follow-up visit, we record side effects and complications, and a visual analogue scale (VAS) was administered to assess the amount of pain felt after the micrografts' application. The pain VAS is in fact self-completed by the respondent who is asked to place a line perpendicular to the VAS line at the point representing its pain intensity. The number indicated by the respondent on the scale is recorded, and the scores range from 0 to 10, where 0 indicates pain absence and 10 severe pain [19]. Functional and aesthetic outcome was assessed using the Vancouver scale VSS [20] (height, pliability, vascularization, and pigmentation of scars) and Wound Bed Score [21] (healing time, eschar, granulation tissue, exudate, dermatitis, fibrosis, and wound bed) two months (T0) and 12 months (T1) after reepithelialisation.

2.4. Statistical Analysis. Application of the Shapiro-Wilk test showed data had no normal distribution; accordingly, all statistical analyses were carried out according to a nonparametric approach. To investigate the effectiveness of the Rigenera® technology, the total VSS and WBS score absolute variations between T0 and T1 were calculated, as well as the corresponding median values and their 95% Confidence Interval (95% CI). Median values were then compared using the Wilcoxon signed-rank test. Further, the percentage variation between T0 and T1 was calculated for each item of the VSS and WBS scale, and differences in each item of the two scales between T0 and T1 were investigated by means of Friedman's test.

All data were statistically analyzed using a one-way ANOVA test. The threshold for statistical significance was set at p values < 0.05. Repeatability is represented as a standard deviation to calculate the differences between measurements using SPSS 16.0 software (SPSS Inc., Chicago, IL, USA) for assessment.

3. Results

70 patients admitted to our Plastic and Reconstructive Unit were enrolled in this study. Follow-up of 90% was achieved at 1 year. Patient number 6 was removed from the study after developing Stevens-Johnson syndrome after administration of the second antibiotics. The mean age was 53 years (range 34-74 years), with 26 men (37%) and 44 women (63%). One hundred percent of wounds were located on the lower limb. Patients and wound descriptions are shown in Table 1. The origin of the soft tissue defect was open fracture in 24 patients (34%) and full-thickness skin wounds with tendon exposure in 12 patients (17%). In addition, Rigenera protocol was used in combination with Integra® dermal regeneration in 3 patients (4%). The mechanism of injury included trauma in the majority of cases (45%) and wound dehiscence (26%) and metabolic ulcer (26%) in the remaining cases. The mean time between trauma and the Rigenera treatment was 7 weeks (range 2-18 weeks). In all the other patients, we observed, on average, a complete healing of the ulcer with bone or tendon coverage in 48 days after the micrografts' application, with a range variable between 35 and 84 days. In all cases, the micrografts were applied only once; no side effect or complication was detected. In case numbers 7, 8, and 14, the micrografts were associated to Integra®. In cases 7 and 8, it was employed as secondary dressing; in these patients, the complete healing was achieved without a secondary surgical procedure of skin grafting. In case 14, the micrografts were put over the dermal substitute 30 days after its engraftments in order to achieve complete

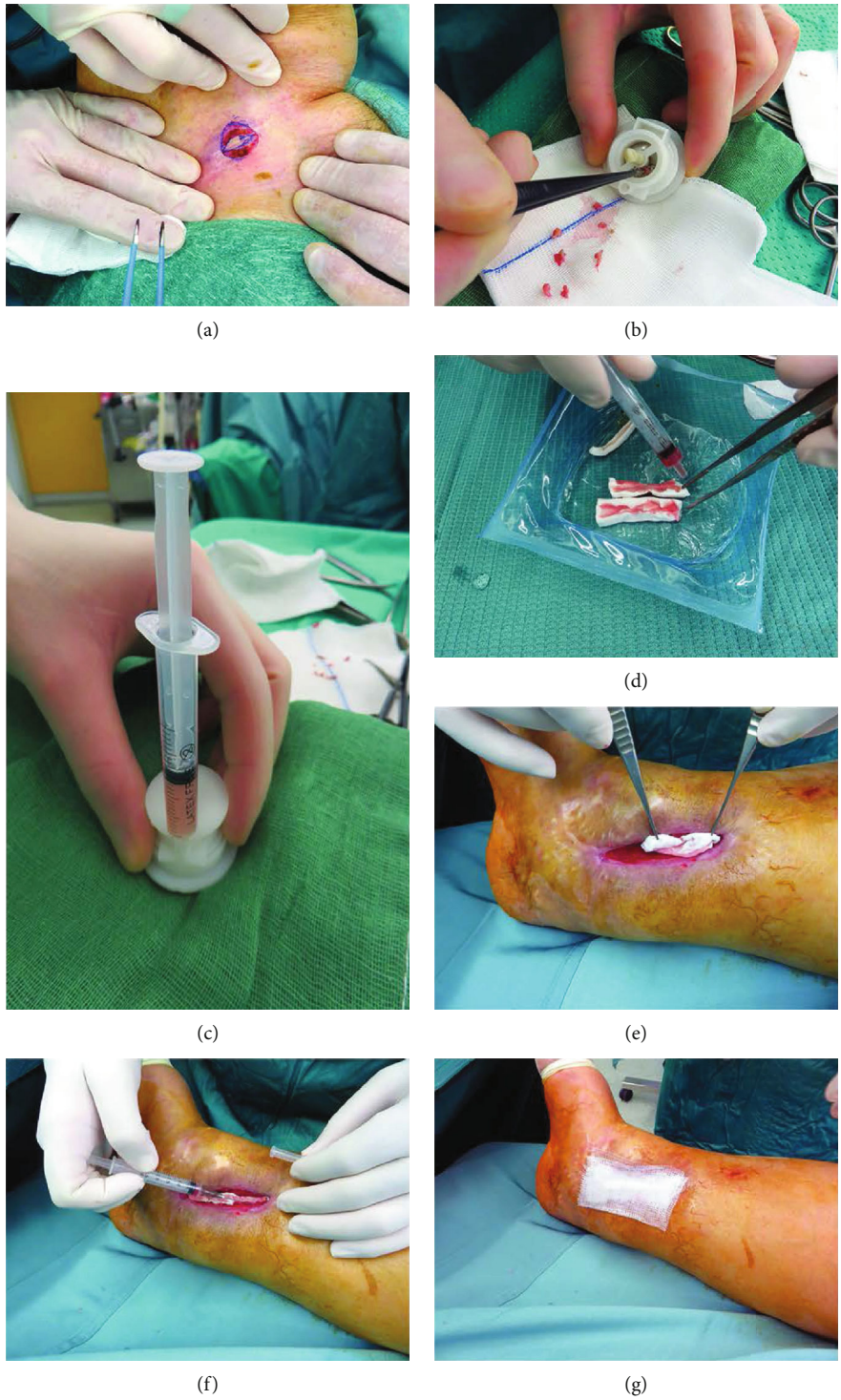

Figure 1: (a) Intraoperative view of skin tissue sample collection from the groin area. (b) Intraoperative view of Rigeneracons filling with 2 mm pieces obtained from the tissue sample. (c) Intraoperative view of collection of autologous micrografts obtained after the disaggregation in a sterile solution. (d) Injection of 1 ml of the micrograft solution on an equine collagen sponge. (e) Intraoperative view of Rigenera biocomplex, consisting of collagen sponge and disaggregated tissue solution, put in the wound's bed. (f) Intraoperative view of perilesional injection of 1 ml of micrograft solution. (g) Intraoperative view of tie over dressing over Rigenera biocomplex.

reepithelialisation without the secondary procedure of skin graft. In these three cases, wound healing was obtained after, respectively, 35, 42, and 35 days. At day 0, surfaces of every wound were about 14 cm^2 (range 7-28 cm^2). At day 7, mean surfaces were 11.6 cm^2 (standard error of the mean was ±2.3 cm^2). At day 14, mean surfaces were 9.3 cm^2 (standard error of the mean was ±1.6 cm^2). At day 21, mean surfaces were 4.5 cm^2 (standard error of

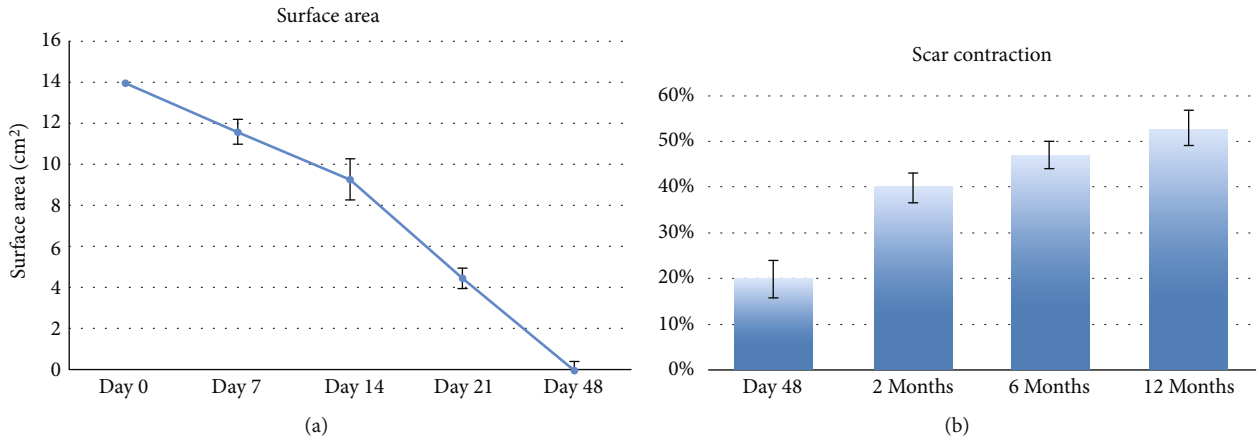

Figure 2: (a) Mean surfaces of the wound (cm^2). Error bars are the standard error of the means. (b) Scar contraction. We observe contraction of all wounds at 48 days, 2 months, 6 months, and 12 months. Error bars are the standard error of the means.

Table 2

	Pretreatment	T0 2-month follow-up	T1 12-month follow-up	p value
(a) **Results of VAS score**				
VAS score	6 (9-4)	3,4 (5-2)	1 (2-0)	$p < 0.05$
(b) **Results of Vancouver Scar Scale**				
Vascularity		2	0	$p = 0.003$
Pigmentation		0	0	$p = 0.5$
Pliability		1	1	$p = 0.5$
Height		2	1	$p = 0.016$
Total score		4,1 (6-2)	2,03 (4-0)	$p < 0.05$
(c) **Results of Wound Bed Score scale**				
Healing edges	0	1	2	$p < 0.05$
Black eschar	1	2	2	$p = 0.5$
Greatest wound	0	1	2	$p = 0.5$
Depth/granulation tissue	0	0	2	$p < 0.05$
Exudate amount	0	2	2	$p < 0.05$
Edema	1	1	2	$p = 0.5$
Periwound dermatitis	0	0	1	$p = 0.5$
Periwound callus/fibrosis	0	0	1	$p = 0.5$
Pink wound bed	0	0	1	$p = 0.5$
Total score	3	7	15	$p < 0.05$

the mean was $\pm 2.1\,cm^2$). At day 48, mean surfaces were $0\,cm^2$ (standard error of the mean was $\pm 1.3\,cm^2$) (Figure 2(a)). Moreover, we observed contraction of all wounds after the complete closure. Wound contraction percentage was significantly different from 20% at day 48 (standard error of the mean was 4%, $p < 0.001$) to 40% at day 60 (standard error of the mean was 3.4%, $p < 0.001$) (Figure 2(b)). The mean preoperative VAS score was 6 (ranging from 4 to 9); meanwhile, the mean VAS score at the first follow-up visit was 3 (ranging from 2 to 5) (Table 2(a)). The Vancouver Scar Scale (VSS) was used to evaluate functional and aesthetic characteristics of lesions after 2-month (T0) and 12-month (T1) follow-up as shown in Table 2(b). There was no statistical difference in sex, age, underlying disease, and size of the defect. The VSS mean value was 2 (ranging from 0 to 4). The VSS score showed a significant reduction at the T1 follow-up control visit ($p < 0.05$). The WBS mean value was 15.4. The WBS score showed a significant reduction at the T1 follow-up control visit ($p < 0.05$) (Table 2(c)). Results concerning the single items of VSS and WBS scale are summarized in Table 2. The scores showed a significant reduction at the T1 (12 months) follow-up control visit ($p < 0.05$): the median Vancouver total score

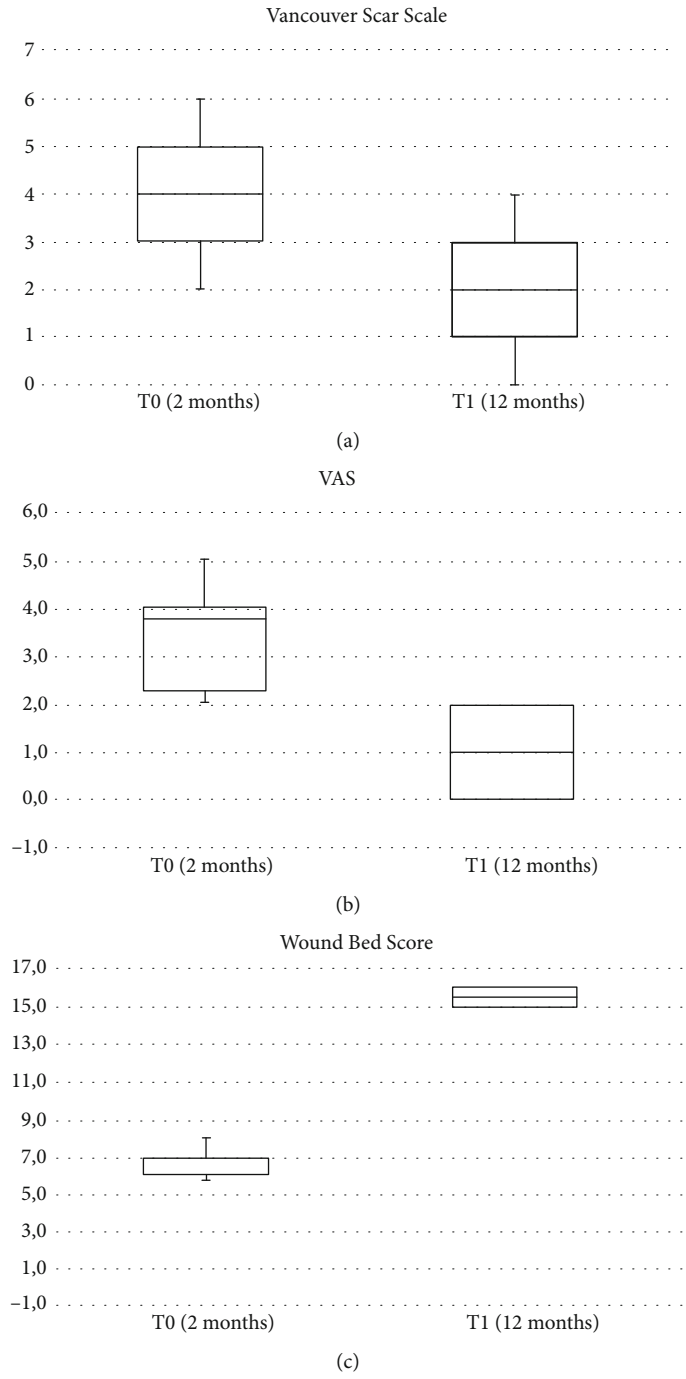

Figure 3: Variation of Vancouver (a), VAS (b), and WBS (c) total scores (squares, medians; bars, first and third quartiles). The reduction of the total score is significant ($p < 0.05$) in both cases.

decreased by 12 units (-85.7%) and the median VAS score decreased by 9 units (-90%) while the median WBS increased by 158% (Figures 3(a)–3(c)). The VSS and VAS scores decreased after the 12-month follow-up, the greatest reduction being observed in height, pliability, and pigmentation. All scars were supple, with a normal height and a normal pigmentation. The only difference between T0 and T1 was about the vascularization and height. The WBS score increased after the 12-month follow-up, the greatest increase being observed in healing edges, exudate amount, and depth/granulation tissue. We have used this technique in 70 cases of chronic wounds of the lower limbs, characterized by extensive loss of skin substance and soft tissue. In particular, a more fast and complete reepithelialisation with respect to the other advanced dressings that were previously utilized in the treatment of the traumatic wounds of the limbs has been observed, with excellent results (Figures 4–7).

(a) (b) (c)

Figure 4: (a) Preoperative view. Dorsal foot dehiscence without bone or tendon exposure. (b) Image of the initial skin regeneration at follow-up visit 7 days after treatment. (c) Image of the initial skin regeneration at follow-up visit 30 days after treatment.

(a) (b) (c)

Figure 5: (a) Preoperative view. Foot stump dehiscence with 2 cm^2 of bone exposure after forefoot amputation. (b) Intraoperative view of Rigenera biocomplex, consisting of collagen sponge and disaggregated tissue solution, put in the wound's bed and perilesional injection of 1 ml of micrograft solution. (c) Image of good skin regeneration at follow-up visit 6 months after complete reepithelialisation.

4. Discussion

The skin grafts are a surgical technique commonly used in the reconstructive surgery of the limbs, in order to directly repair skin loss, as well as to repair the donor area of the flaps and cover the dermal substitutes after engraftment. The inevitable side effect of this technique consists of unaesthetic scars. The autologous tissue grafts produce very evident scars and are unable to stimulate tissue regeneration, because the interruption of blood circulation leads to an extensive inner cell death. This issue is related to the prevalence of scarring on skin regeneration in the management of traumatic wounds and is even more evident in patients affected by chronic diseases who are highly exposed to the risk of delayed healing of the injured tissue leading to a pathological inflammatory state and chronic wounds [22]. Researchers are trying to find approaches able to reduce scarring after wound healing, stimulating at the same time tissue regeneration, by

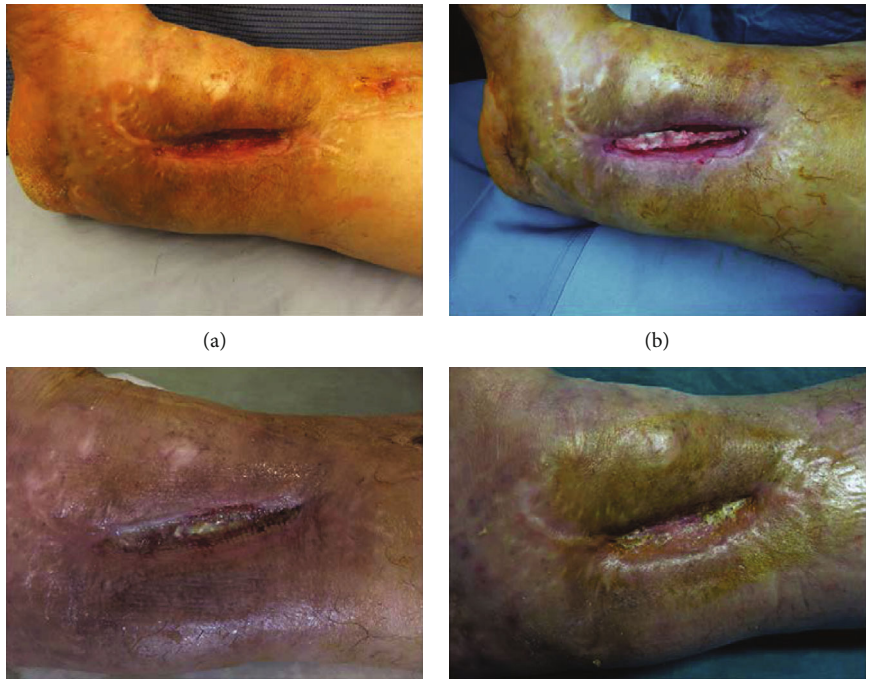

(a) (b) (c) (d)

Figure 6: (a) Preoperative view. Ankle dehiscence without bone or tendon exposure. (b) Intraoperative view of Rigenera biocomplex, consisting of collagen sponge and disaggregated tissue solution, put in the wound's bed and perilesional injection of 1 ml of micrograft solution. (c) Image of the initial skin regeneration at follow-up visit 7 days after treatment. (d) Image of good skin regeneration at follow-up visit 6 months after complete reepithelialisation.

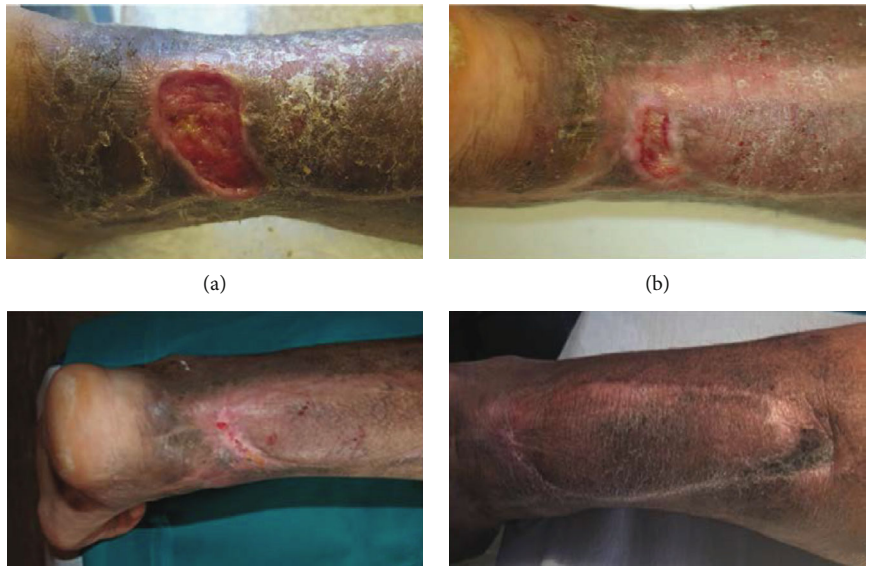

(a) (b) (c) (d)

Figure 7: (a) Preoperative view. Achilles tendon dehiscence without bone or tendon exposure. (b) Image of the initial skin regeneration at follow-up visit 7 days after treatment. (c) Image of skin regeneration at follow-up visit 21 days after treatment. (d) Image of good skin regeneration at follow-up visit 6 months after complete reepithelialisation.

means of tissue engineering methods. Tissue engineering aims to regenerate tissues through the combined use of biomaterials and biologic mediators such as stem cells and growth factors in order to provide new tools for regenerative medicine [23, 24]. The repair and regeneration of human tissues is particularly difficult in skeletal reconstruction of large bone defects caused by trauma, infection, or skeletal abnormalities, and given that regenerative ability of bone declines with increasing age, the dramatic rise in the ageing population worldwide determined an increasing need for innovative approaches [25]. Many approaches can be used when the normal process of tissue regeneration is impaired or simply

insufficient, such as grafting which includes autografts, allografts, xenografts, and biomaterial substitutes [26]. For the safety of grafting procedure, the autologous grafts are preferable to those homologous or heterologous grafts, and although it prevents immunoreactions and infections, this approach is limited due to additional surgical procedure on the donor site and discomfort for the patient. Furthermore, about the autologous grafts, the cell viability dramatically decreases after collection from the donor site for vessel interruption by surgery with reduced feeding for the cells. The Rigenera® technology represents a new approach for human injured tissue regeneration, and when using this technology, the patient is the donor and acceptor of calibrated and highly viable micrografts containing progenitor cells positive for mesenchymal stem cell markers able to induce tissue repair [7, 11]. In vitro data on their characterization have reported that micrografts display a mesenchymal phenotype and are positive for typical markers such as CD73, CD90, CD105, and CD117 and have showed their capability to differentiate in osteocytes, chondrocytes, or adipocytes in appropriate experimental conditions [13, 31]. Furthermore, the clinical efficacy of these micrografts has been demonstrated both in the healing of postoperative and posttraumatic wounds [9–11, 27] and pathological scars [12]. In particular, a more fast and complete reepithelialisation with respect to the other advanced dressings that were previously utilized in the treatment of the traumatic wounds of the limbs has been observed, with excellent results in terms of clinical efficacy and demonstration of the regenerative capacity of this method [7, 8]. The micrografting concept was conceived by Cicero Parker Meek and was based on the evidence that skin grafts expanded many times were able to heal a wound faster than the original-sized grafts [28]. Therefore, the best way to achieve a good grafting performance is by increasing the superficial area of the graft leading to a faster cellular migration onto the wound and reducing cellular death of the graft itself. Since then, the micrograft concept was applied to many procedures [29, 30].

Rigenera technology is different from any of them because it is able to generate a suspension of micron-sized grafts (micrografts) which are applied with the help of a syringe. The average size of the Rigenera-obtained micrografts is 80 μm, extremely smaller than any other technology available on the market or ever described in literature. Lastly, while performing the disaggregation, this technology allows for a collection of only the smaller cells which also express the mesenchymal stem cell markers, described as stem cell-like or progenitor cells, which are accounted for a strong regenerative effect [13, 31]. We have used this technology in 70 cases of chronic wounds of the lower limbs, characterized by extensive loss of skin substance and soft tissue. Some of these patients were affected by severe chronic diseases with poor vascularization of the skin. In all cases, we have applied the Rigenera protocol using skin micrografts, achieving in 69 cases the complete healing of wounds in a period between 35 and 84 days. Wound healing was characterized by complete reepithelialisation with clinical and histological evidence of a repair that occurred through a process of tissue regeneration and low presence of scar at the injured area [7, 8]. The regenerative efficacy of micrografts could arise from the presence of small particle-sized autografts characterized by a large grafting surface, leading to an optimal cellular viability and integrity, for minor nutritional needs of the cells. Particularly, the mechanical disaggregation of small pieces of human connective tissues produces a suspension of autologous micrografts of 80 μm size, ready for use, which can be applied on the injured area alone or in combination with different biological scaffolds, such as collagen and hyaluronic acid. The specific cell population of these micrografts includes progenitor cells, which in association with the fragment of the Extracellular Matrix (ECM) and growth factors derived by starting tissue initiate biological processes of cell proliferation and differentiation enhancing the wound healing process. This is the "micrograft theory" that may explain the excellent reconstructive outcomes in the treatment of the injured limbs applying autologous micrografts obtained by the Rigenera® technology.

5. Conclusions

The autologous micrografts obtained by the Rigenera® technology are an innovative protocol that introduces a whole new concept in regenerative surgery, allowing to repair severe traumatic wounds of the limbs by complete reepithelialisation. The impressive clinical outcomes combined with the laboratory tests on the tissue characterization demonstrate that this technology is really able to stimulate skin regeneration and probably it is the only one available today able to ensure the healing of traumatic injuries through a real regenerative procedure. In addition, the minimum amount of skin required to produce micrografts with the Rigeneracons in the repair of wide traumatic wounds prevents scarring usually produced by traditional techniques at the donor site.

Definitely, this innovative technology is not just a new technique but a whole new concept in regenerative surgery.

Data Availability

The data used to support the findings of this study are included within the article.

Conflicts of Interest

None of the authors have conflict of interest.

Acknowledgments

The authors wish to thank Dr. Marialuisa De Francesco, statistical expert, Statistical office of University of Milan, Milan, Italy, for providing excellent technical support.

References

[1] N. Fallico, F. Somma, E. Cigna, L. A. Dessy, M. Tarallo, and D. Ribuffo, "Coverage of exposed hardware after lower leg fractures with free flaps or pedicled flaps," *European Review for Medical and Pharmacological Sciences*, vol. 19, no. 24, pp. 4715–4721, 2015.

[2] A. Gupta, C. Lakhiani, B. H. Lim et al., "Free tissue transfer to the traumatized upper extremity: risk factors for postoperative complications in 282 cases," *Journal of Plastic, Reconstructive & Aesthetic Surgery*, vol. 68, no. 9, pp. 1184–1190, 2015.

[3] A. Soni, K. Tzafetta, S. Knight, and P. V. Giannoudis, "Gustilo IIIC fractures in the lower limb," *Journal of Bone and Joint Surgery. British Volume (London)*, vol. 94-B, no. 5, pp. 698–703, 2012.

[4] D. A. Milcheski, A. A. Chang, R. C. Lobato, H. A. Nakamoto, P. Tuma Jr., and M. C. Ferreira, "Coverage of deep cutaneous wounds using dermal template in combination with negative-pressure therapy and subsequent skin graft," *Plastic and Reconstructive Surgery. Global Open*, vol. 2, no. 6, p. e170, 2014.

[5] M. D. Helgeson, B. K. Potter, K. N. Evans, and S. B. Shawen, "Bioartificial dermal substitute: a preliminary report on its use for the management of complex combat-related soft tissue wounds," *Journal of Orthopaedic Trauma*, vol. 21, no. 6, pp. 394–399, 2007.

[6] L. Trovato, G. Failla, S. Serantoni, and F. P. Palumbo, "Regenerative surgery in the management of the leg ulcers," *Journal of Cell Science & Therapy*, vol. 07, no. 02, p. 2, 2016.

[7] V. Purpura, E. Bondioli, A. Graziano et al., "Tissue characterization after a new disaggregation method for skin micrografts generation," *Journal of Visualized Experiments*, vol. 109, no. 109, p. e53579, 2016.

[8] S. Jimi, M. Kimura, F. De Francesco, M. Riccio, S. Hara, and H. Ohjimi, "Acceleration mechanisms of skin wound healing by autologous micrograft in mice," *International Journal of Molecular Sciences*, vol. 18, no. 8, p. 1675, 2017.

[9] M. Marcarelli, L. Trovato, E. Novarese, M. Riccio, and A. Graziano, "Rigenera protocol in the treatment of surgical wound dehiscence," *International Wound Journal*, vol. 14, no. 1, pp. 277–281, 2017.

[10] E. Baglioni, L. Trovato, M. Marcarelli, A. Frenello, and M. A. Bocchiotti, "Treatment of oncological post-surgical wound dehiscence with autologous skin micrografts," *Anticancer Research*, vol. 36, no. 3, pp. 975–980, 2016.

[11] F. De Francesco, A. Graziano, L. Trovato et al., "A regenerative approach with dermal micrografts in the treatment of chronic ulcers," *Stem Cell Reviews*, vol. 13, no. 1, pp. 139–148, 2017.

[12] F. Svolacchia, F. De Francesco, L. Trovato, A. Graziano, and G. A. Ferraro, "An innovative regenerative treatment of scars with dermal micrografts," *Journal of Cosmetic Dermatology*, vol. 15, no. 3, pp. 245–253, 2016.

[13] M. Monti, A. Graziano, S. Rizzo et al., "In vitro and in vivo differentiation of progenitor stem cells obtained after mechanical digestion of human dental pulp," *Journal of Cellular Physiology*, vol. 232, no. 3, pp. 548–555, 2017.

[14] A. Graziano, F. Carinci, S. Scolaro, and R. D'Aquino, "Periodontal tissue generation using autologous dental ligament micro-grafts: case report with 6 months follow-up," *Annals of Oral and Maxillofacial Surgery*, vol. 1, no. 2, p. 20, 2013.

[15] R. d'Aquino, L. Trovato, A. Graziano et al., "Periosteum-derived micro-grafts for tissue regeneration of human maxillary bone," *Journal of Translational Science*, vol. 2, no. 2, pp. 125–129, 2016.

[16] R. R. y Baena, R. D'Aquino, A. Graziano et al., "Autologous periosteum-derived micrografts and PLGA/HA enhance the bone formation in sinus lift augmentation," *Frontiers in Cell and Development Biology*, vol. 5, p. 87, 2017.

[17] G. Ceccarelli, P. Gentile, M. Marcarelli et al., "In vitro and in vivo studies of Alar-Nasal cartilage using autologous micro-grafts: the use of the Rigenera® protocol in the treatment of an osteochondral lesion of the nose," *Pharmaceuticals (Basel)*, vol. 10, no. 4, p. 53, 2017.

[18] F. De Francesco, S. Mannucci, G. Conti, E. D. Prè, A. Sbarbati, and M. Riccio, "A non-enzymatic method to obtain a fat tissue derivative highly enriched in adipose stem cells (ASCs) from human lipoaspirates: preliminary results," *International Journal of Molecular Sciences*, vol. 19, no. 7, p. 2061, 2018.

[19] G. A. Hawker, S. Mian, T. Kendzerska, and M. French, "Measures of adult pain: Visual Analog Scale for Pain (VAS Pain), Numeric Rating Scale for Pain (NRS Pain), McGill Pain Questionnaire (MPQ), Short-Form McGill Pain Questionnaire (SF-MPQ), Chronic Pain Grade Scale (CPGS), Short Form-36 Bodily Pain Scale (SF-36 BPS), and Measure of Intermittent and Constant Osteoarthritis Pain (ICOAP)," *Arthritis Care and Research*, vol. 63, no. S11, pp. S240–S252, 2011.

[20] M. J. Baryza and G. A. Baryza, "The Vancouver Scar Scale: an administration tool and its interrater reliability," *Journal of Burn Care & Research*, vol. 16, no. 5, pp. 535–538, 1995.

[21] V. Falanga, L. J. Saap, and A. Ozonoff, "Wound bed score and its correlation with healing of chronic wounds," *Dermatologic Therapy*, vol. 19, no. 6, pp. 383–390, 2006.

[22] M. S. Hu, Z. N. Maan, J. C. Wu et al., "Tissue engineering and regenerative repair in wound healing," *Annals of Biomedical Engineering*, vol. 42, no. 7, pp. 1494–1507, 2014.

[23] R. S. Mahla, "Stem cells applications in regenerative medicine and disease therapeutics," *International Journal of Cell Biology*, vol. 2016, Article ID 6940283, 24 pages, 2016.

[24] F. de Francesco, G. Ricci, F. D'Andrea, G. F. Nicoletti, and G. A. Ferraro, "Human adipose stem cells: from bench to bedside," *Tissue Engineering. Part B, Reviews*, vol. 21, no. 6, pp. 572–584, 2015.

[25] C. Gardin, L. Ferroni, L. Favero et al., "Nanostructured biomaterials for tissue engineered bone tissue reconstruction," *International Journal of Molecular Sciences*, vol. 13, no. 1, pp. 737–757, 2012.

[26] M. Singh, K. Nuutila, C. Kruse, M. C. Robson, E. Caterson, and E. Eriksson, "Challenging the conventional therapy: emerging skin graft techniques for wound healing," *Plast Reconstr Surg*, vol. 136, no. 4, pp. 524e–530e, 2015.

[27] M. Giaccone, M. Brunetti, M. Camandona, L. Trovato, and A. Graziano, "A new medical device, based on Rigenera protocol, in the management of complex wounds," *Journal of Stem Cells Research, Reviews & Reports*, vol. 1, no. 3, p. 3, 2014.

[28] C. P. Meek, "Successful microdermagrafting using the Meek-Wall microdermatome," *American Journal of Surgery*, vol. 96, no. 4, pp. 557-558, 1958.

[29] T. Svensjö, B. Pomahac, F. Yao, J. Slama, N. Wasif, and E. Eriksson, "Autologous skin transplantation: comparison of minced skin to other techniques," *The Journal of Surgical Research*, vol. 103, no. 1, pp. 19–29, 2002.

[30] A. M. Klapper, S. Moradian, and P. Pack, "New technique: acute minced expansion graft of traumatic wound tissue," *Advances in Skin & Wound Care*, vol. 29, no. 12, pp. 540–545, 2016.

[31] L. Trovato, M. Monti, C. del Fante et al., "A new medical device Rigeneracons allows to obtain viable micro-grafts from mechanical disaggregation of human tissues," *Journal of Cellular Physiology*, vol. 230, no. 10, pp. 2299–2303, 2015.

Hindawi
Stem Cells International
Volume 2019, Article ID 5146594, 9 pages
https://doi.org/10.1155/2019/5146594

Clinical Study

Preenrichment with Adipose Tissue-Derived Stem Cells Improves Fat Graft Retention in Patients with Contour Deformities of the Face

Muhammad M. Bashir,[1] Muhammad Sohail,[1] Fridoon J. Ahmad,[2] and Mahmood S. Choudhery[2]

[1]*Plastic Surgery Department, King Edward Medical University/Mayo Hospital, Lahore, Pakistan*
[2]*Tissue Engineering and Regenerative Medicine Laboratory, Department of Biomedical Sciences, King Edward Medical University, Lahore, Pakistan*

Correspondence should be addressed to Mahmood S. Choudhery; ms20031@yahoo.com

Received 28 May 2019; Revised 8 August 2019; Accepted 30 August 2019; Published 20 November 2019

Guest Editor: Letizia Trovato

Quick absorption of adipose tissue grafts makes the outcomes less satisfactory for clinical applications. In the current study, adipose tissue grafts were mixed with adipose tissue-derived stem cells (ASCs) to improve retention of adipose tissue grafts and to make the clinical outcomes of fat grafting more reliable. Adipose tissue was either injected alone (conventional group) or mixed with ASCs (stem cell group) before injection. In both groups, adipose tissue was injected at the site of contour throughout layers of tissues till visual clinical symmetry with the opposite side was achieved. The volume of injected fat graft was measured after 72 hours and 6 months using a B-mode ultrasound device connected with a 12 MH frequency probe. The percentage reduction in the volume of injected fat, physician satisfaction scores (Ph-SCs), and patient satisfaction scores (P-SCs) were also recorded. After 6 months, there was significantly lower fat absorption in the stem cell group as compared to the conventional group. Mean physician and patient satisfaction scores were significantly improved in the stem cell group. No significant adverse effects were noted in any patient. Significantly lower absorption of graft due to the use of ASCs improves the clinical outcomes of conventional fat grafting for contour deformities of the face. The current preenrichment strategy is noninvasive, safe and can be applied to other diseases that require major tissue augmentation such as breast surgery. This trial is registered with NCT02494752.

1. Introduction

Autologous fat grafting is a frequently employed procedure in cosmetic and reconstructive surgery. Fat is a versatile filler for treating contour irregularities of the face brought about by congenital disorders, acquired diseases, and traumatic and developmental deformities. Unlike many other fillers of synthetic origin, fat is easy to procure with minimal donor site morbidity. Additionally, it is frequently available as autologous and thus without immunogenicity issue. Moreover, its soft and dynamic nature makes it useful especially for cosmetic and reconstructive surgery [1]. Although adipose tissue grafting is a well-known technique to correct contour irregularities, quick absorption of fat at the site of application is a major concern for patients as well as clinicians [2]. The rate of fat absorption may reach up to 90% due to hypoxic and ischemic environment after transplantation. Clinically, this unreliability produces unsatisfactory and suboptimal final clinical outcomes, and therefore, multiple sessions of fat grafts are required, making this procedure expensive and lengthy [2, 3]. In order to improve survival of transplanted adipose tissue graft, alternative approaches are required. In the current study, autologous fat graft was preenriched with culture-expanded adipose tissue-derived stem cells (ASCs) to enhance retention of transplanted graft and to make clinical outcomes more reliable.

Stromal vascular fraction (SVF) of adipose tissue is a heterogeneous cell population containing blood cells, fibroblasts, pericytes, endothelial cells, and ASCs. Studies indicate that ASCs have angiogenic, antiapoptotic, immunosuppressive, and immunomodulatory properties that make them ideal candidates for clinical use [4]. Recent animal studies have demonstrated improved survival and retention of grafted fat when adipose tissue grafts were preenriched with ASCs [5]. If enrichment of fat graft with ASCs can decrease its absorption rate, this innovative strategy can make fat transfer a more reliable option for soft tissue augmentation. This can definitely improve final clinical outcomes at lesser cost and reduce donor site morbidity.

The current study is aimed at evaluating the effect of ASCs on survival and retention of adipose tissue grafts in patients of contour deformities of the face. Autologous adipose tissue was harvested, processed, and either injected alone or mixed with ex vivo expanded ASCs at the site of face contour. Reduction in the volume of injected graft, physician satisfaction scores (Ph-SCs), and patient satisfaction scores (P-SCs) were recorded. Results indicated that preenrichment with ASCs significantly reduces fat absorption at the site of application and improves the clinical outcomes of conventional fat grafting as indicated by Ph-SCs and P-SCs. To the best of our knowledge, this is the first study that was performed on actual patients of contour deformities of the face to show the effect of preenrichment of adipose tissue grafts with ASCs. This technique will open a new avenue not only for the augmentation of contour deformities of the face but also for other conditions that require large tissue augmentation procedures such as breast reconstruction.

2. Material and Methods

It was a quasi-experimental study conducted at "Department of Plastic & Reconstructive Surgery" and "Tissue Engineering and Regenerative Medicine Laboratory" Department of Biomedical Sciences, King Edward Medical University/Mayo Hospital, Lahore. Thirty-seven patients with congenital or acquired contour deformities of the face were enrolled consecutively from September 2015 to September 2017. The patients with contour deformities in skin-grafted areas and where the skin was adherent to the facial skeleton were excluded [6]. Demographic and clinical data of patients was collected after obtaining informed written consent. One week before the surgery, patients in each group were advised to stop taking aspirin, alcohol, or any other herbal medications. The protocols used in the study were approved by the IRB (Institutional Review Board) of King Edward Medical University, Lahore, Pakistan (letter # 229/RC/KEMU). The study was performed according to "The Code of Ethics of the World Medical Association (Declaration of Helsinki)," and the trial was registered at ClinicalTrials.gov (NCT02494752). Both methods (fat graft only or stem cells mixed with fat graft) were offered to patients. Patients giving consent for traditional fat grafting (conventional group) underwent fat harvest, preparation, and transplantation on the same day, while patients giving consent for ASC-enriched fat grafting (stem cell group) underwent fat harvest two times, first to isolate and expand ASCs in vitro and second (after 2-3 weeks) to preenrich fat grafts with culture-expanded ASCs. The full overview of the study is given in Figure 1.

2.1. Fat Harvest and Processing. Depending on patient desire and accessibility, fat was harvested from either the abdomen or the lateral side of the thigh as described previously by our group [6]. Briefly, under local or general anesthesia, fat harvest area was infiltrated with tumescent solution consisting of 0.4% lidocaine and 1 : 1000.000 epinephrine. Fat was harvested using a 3 mm, two-hole, blunt cannula attached to a 10 ml Luer-Lok syringe. The plunger of a 10 cc syringe was pulled back only a few milliliters during suctioning to evade unnecessary negative pressure and to avoid fat cell rupturing. The required amount to fill the contour deformity was harvested accordingly on the basis of clinical judgment.

2.2. Preparation of Fat for Transplantation. The fat tissue for transplantation was prepared by using the methods of Bashir et al. [6]. Briefly, to separate the fat from liquid portion, 10 ml Luer-Lok syringes were kept vertically for 5-10 minutes (Figure 2(a)). The tumescent fluid and blood were drained out from the bottom. To further purify fat from debris and oil, the remaining fat in the syringes was passed through a common strainer (Figure 2(b)). The residue was then washed with 0.9% saline solution. After washing, purified fat was collected in 10 cc Luer-Lok syringes and was transferred to 1 cc syringes for transplantation (Figure 2(c)).

2.3. Isolation of Adipose Tissue-Derived Stem Cells (ASCs). For ASC isolation, fat tissue was harvested under local anesthesia and processed as described previously by us [6, 7]. Fat tissue (20 ml-30 ml) was harvested under sterilized conditions and transferred to a certified laboratory approved by the Human Organ Transplantation Authority (HOTA) for processing and isolation of ASCs. ASCs were isolated and culture expanded by enzymatic digestion using Good Manufacturing Practice- (GMP-) grade reagents. After 2 weeks, the ASCs were isolated by enzymatic digestion as described previously by Choudhery et al. [7]. Briefly, lipoaspirate was treated for 30 minutes with 0.2% collagenase type IV (Sigma, USA) to digest the tissue slurry. The patient serum was used to neutralize collagenase activity. The cell suspension was passed through a 70 μm strainer to remove undigested tissue pieces and debris. The filtered solution was centrifuged at 1000 rpm for 10 minutes at 4°C to obtain cells in a pellet. The pellet was washed with phosphate-buffered saline (PBS), and cell suspension was again centrifuged at 1000 rpm for 10 minutes. The cells were cultured in complete growth medium, i.e., MEM-alpha (Thermo Scientific, USA), supplemented with 1% each of nonessential amino acids, streptomycin/penicillin solution, and 5% autologous serum. The cells were resuspended in complete medium and were plated in 25 cm^2 culture flasks at 37°C/5% CO_2 with humidity. After 24 hours, the nonadherent cells were discarded and fresh medium was added. Medium was changed twice a week thereafter until the cells became confluent. The cells were trypsinized and cultured

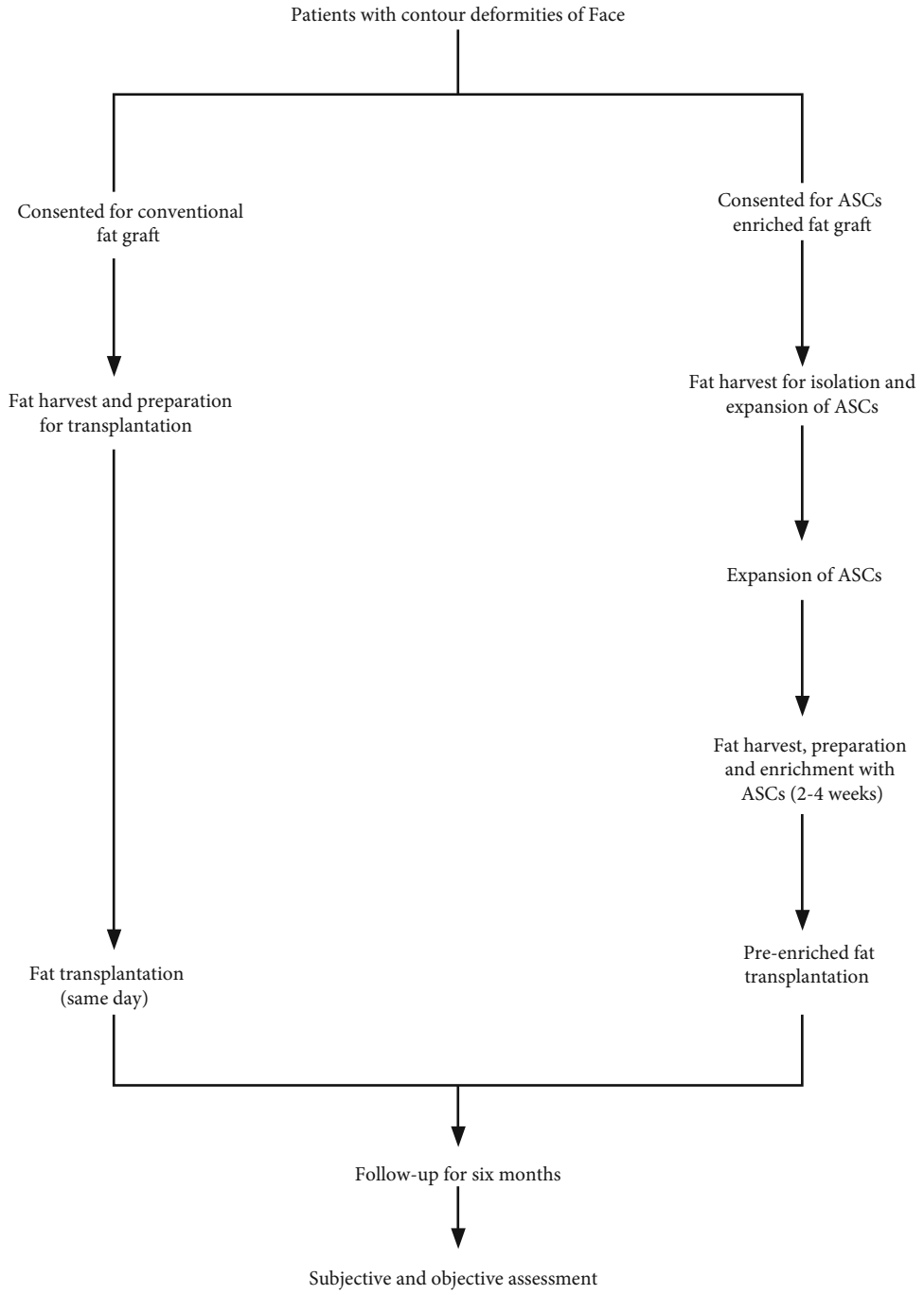

Figure 1: Flow chart showing the management plan of patients with contour deformities of the face.

in 75 cm^2 culture flasks. At 80%-90% confluence, cells were dissociated using trypsin-EDTA and counted using a hemocytometer. The cells at passage one were used for preenrichment of adipose tissue graft. During this period, the cells were regularly monitored under a microscope for any type of contamination or morphological changes.

2.4. Fat Grafting at Contour Deformities of the Face. In patients of the conventional group, purified fat collected in 10 cc syringes was transferred to 1 cc syringes (using a two-way connector) for transplantation to the recipient area. In patients of the stem cell group, on the day of fat transplantation, fat was again harvested, prepared, and purified as described above for the conventional group. The ex vivo expanded ASCs (10^6 cells per ml of fat) were mixed with the purified fat and transferred to 1 cc syringes (Figure 2(c)). In both groups, the fat was injected through a 1.5 mm blunt-tip cannula, with a lateral opening using small stab incisions. Fat was placed gently during the withdrawal of the cannula. Fat was placed in small fractions at different depths of soft tissue starting from just above the periosteum and moving superficially [8]. End point

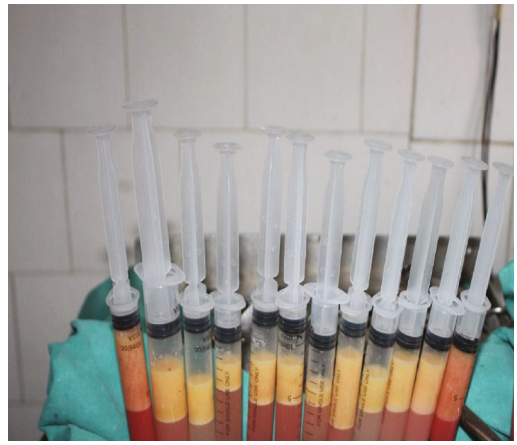

(a)

(b)

(c)

Figure 2: (a) Syringes standing vertically to allow gravity sedimentation. (b) The filtration of fat through the common strainer to concentrate the fat and to separate it from oil and debris. (c) The transfer of fat from 10 cc syringes to 1 cc syringes for transplantation.

of lipofilling was achieved by visual clinical symmetry with the opposite side. Quantity of fat transferred was noted in milliliters. Patients were given intravenous first-generation cephalosporin for 72 hours and discharged on oral antibiotic within a week. The patients were followed up at monthly intervals for six months.

2.5. Assessment. Both subjective and object assessments were performed to compare the outcomes of transplantation in both groups. Mean ± SD volume of injected fat per procedure was measured in milliliters (ml) as described [6]. The number of fat grafting sessions and total volume of fat injected to achieve clinical symmetry per case were also noted.

2.6. Surgeon Satisfaction and Patient Satisfaction Assessment. It was performed for clinical symmetry (comparing the affected side to the unaffected side) and overall appearance. It was done by clinical examination and comparing the preoperative and six-month postoperative (after the first and final fat graft sessions) photographs [6]. Two plastic surgeons (blinded to group allocation) independently rated postoperative appearance using a five-point scale as (1) very unsatisfied (gross asymmetry and severe deformity), (2) unsatisfied (significant asymmetry and deformity), (3) neither satisfied nor unsatisfied (perceptible asymmetry and deformity), (4) satisfied (hardly perceptible asymmetry and deformity), and (5) extremely satisfied (no asymmetry and normal appearance). The same surgeons rated each patient at both intervals. Similarly, using the same five-point scale, the patients were asked to comment about symmetry (comparing the affected side to the unaffected side) and overall appearance by comparing the preoperative and six-month postoperative (after the first and final fat graft sessions) photographs.

2.7. Objective Assessment. For objective assessment, we performed ultrasonography as described previously [6] using a B-mode ultrasound device and a 12 MH high-frequency probe (Sonoace X4, Medison). Each patient was placed in upright position, and a thick layer of water-based gel was put on the treated area for transmission of ultrasound waves. The transducer probe was placed on the assessment site perpendicular to the skin surface. The correct transducer position was determined to differentiate noise from proper ultrasound reflections. Linear measurements of soft tissue thickness of the treated area were performed. The thickness of the subcutaneous tissue was measured in millimeters in

Table 1

	Conventional group ($n = 21$)	Stem cell group ($n = 16$)	P value
Patient characteristics			
Males	4	7	0.151[a]
Females	17	9	
Age (years) (mean ± SD)	21 ± 5	30 ± 11	0.004[b]
Number of sessions and volume injected			
Number of fat graft sessions (mean ± SD)	2 ± 1	1 ± 0	<0.001[c]
Volume of fat transferred per session (ml) (mean ± SD)	26 ± 14	29 ± 14	0.524[b]
Assessment			
Soft tissue thickness (mm)			
(i) Preoperative (mean ± SD)	5 ± 2	5 ± 4	0.602[b]
(ii) Postoperative 72 hours after the first fat graft session (mean ± SD)	19 ± 8	24 ± 8	0.072[b]
(iii) Postoperative 6 months after the first fat graft session (mean ± SD)	13 ± 6	23 ± 9	<0.001[b]

[a]Chi-square test, [b]independent sample t-test, and [c]Mann–Whitney U test.

triplicate, and the mean of three readings was used for analysis. The first measurement of soft tissue thickness was done 72 hours after transplantation in both groups. In order to have a reproducible measurement in subsequent examinations, the operator noted down and marked precise anatomical landmark points with an indelible marker, saving a digital image for future reference. Ultrasonography was repeated after six months by the same operator who measured the subcutaneous thickness of the treated area. The difference in measurements taken at 72 hours postoperatively and at six months after the first fat graft session was noted down as percentage reduction in fat graft volume.

2.8. Regrafting. The need for regrafting the affected area was assessed based on patient and physician satisfaction. Fat grafting session was repeated following the same protocol in cases where symmetry was distorted. Patients were photographed on each follow-up under standard conditions of light, distance, views, and camera make.

2.9. Complications. All the patients were observed for possible complications such as infection (swelling and redness of the skin that feels hot and tender), bruising (skin discoloration due to rupture of small blood vessels), swelling (localized enlargement of the treated area due to inflammatory fluid accumulation), skin necrosis (loss of skin and subcutaneous tissue), hematoma (abnormal collection of blood), seroma (abnormal collection of fluid), and uneven skin texture (irregular, pebbly, and rough skin surface) [6].

2.10. Statistical Analysis. Data were analyzed using SPSS version 16. Qualitative variables like gender, etiology, fat harvesting site, and complications of procedure were expressed as proportions. Quantitative variables like age, patient and physician assessment scores, volume of fat injected in one procedure, total volume of fat injected per case, and percentage reduction in fat graft volume were expressed as mean (SD). In order to compare quantitative data, normality was tested using the one-sample Kolmogorov-Smirnov test. We applied the independent sample t-test (mean ± SD was compared) for variables with normal distribution and the Mann–Whitney U test for variables which did not have normal distribution (median ± IQR was compared). P value ≤ 0.05 was considered significant.

3. Results

The total number of patients in two groups was 37. The mean age of patients was 21 ± 5 and 30 ± 11 years with 17 (81%) and 9 (56%) females in the conventional and stem cell groups, respectively. The most common indication for fat grafting was idiopathic hemifacial atrophy in 10 (48%) and 9 (56%) patients followed by congenital craniofacial microsomia in 5 (24%) and 4 (25%), posttraumatic deformity in 5 (24%) and 2 (13%), and postinfective deformity in 1 (4%) and 1 (6%) patients in the conventional and stem cell groups, respectively. Patients underwent a total of 67 fat grafting sessions (51 sessions for 21 patients in the conventional group) and 16 sessions (one each for 16 patients in the stem cell group) over a period of 24 months.

There was no statistically significant difference in distribution of patients according to gender, preoperative soft tissue thickness, and mean volume of fat transferred per session (Table 1). However, there was a statistically significant difference in mean age of the patients and number of fat graft sessions in two groups (Table 1). After 6 months, there was a significantly lower fat absorption as evident by percentage reduction of 5 ± 4.4 in the stem cell group as compared to 31 ± 13 in the conventional group (P value < 0.001). Figure 3(a) shows ultrasonic measurement of soft tissue thickness after 72 hours, and Figure 3(b) shows measurements 6 months after injections. Comparison of mean

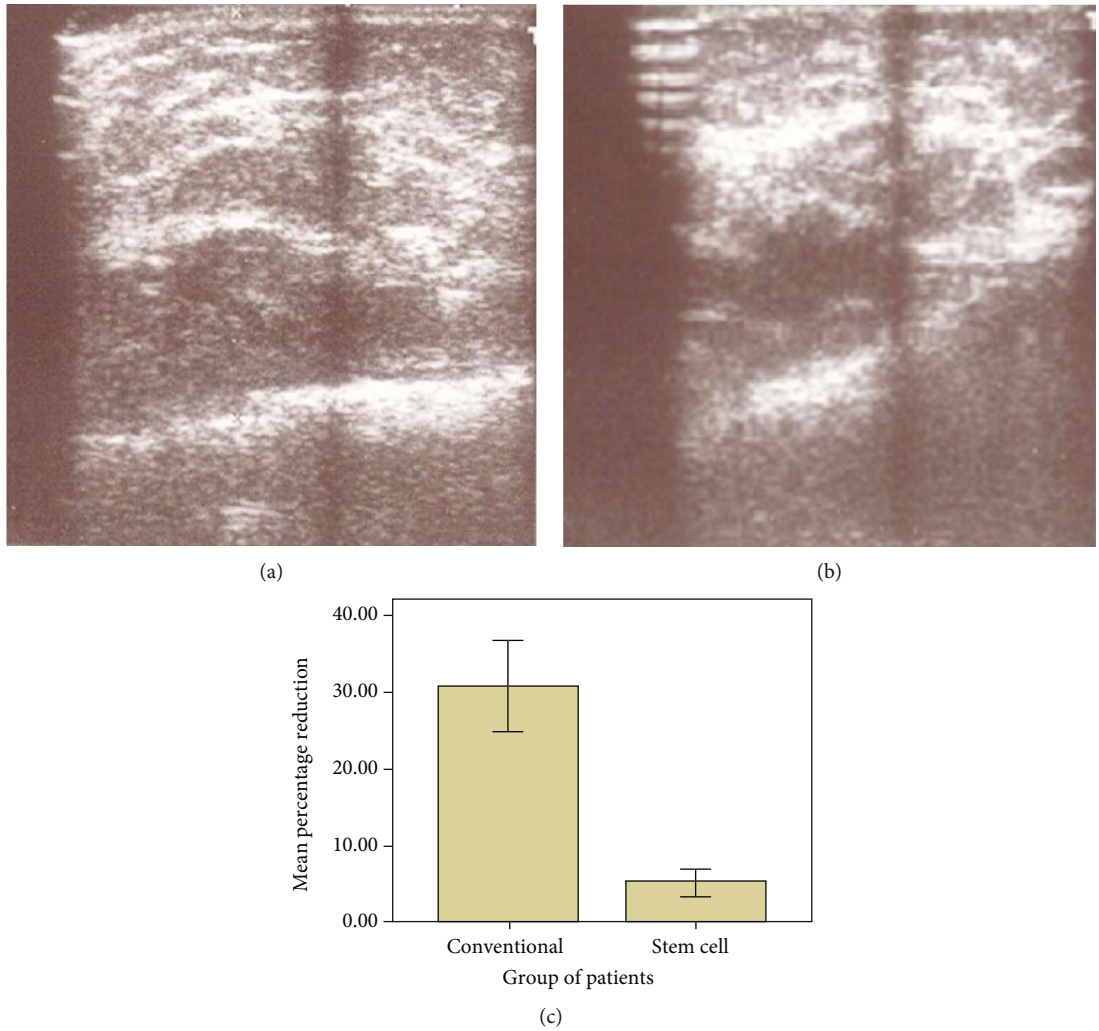

Figure 3: Representative ultrasonic measurement of soft tissue thickness (a) after 72 hours and (b) 6 months after transplantation. (c) Comparison of mean percentage reduction of fat absorption in both groups six months after the 1st fat graft session.

percentage reduction of fat absorption in both groups six months after the 1st fat graft session has been shown in Figure 3(c).

Mean patient and physician satisfaction scores have been depicted in Figure 4. Mean physician satisfaction score was 2.14 ± 0.36 in the conventional group and 3.69 ± 0.79 in the stem cell group. Similarly, mean patient satisfaction score (2.52 ± 0.521) in the conventional group was lower as compared to that in the stem cell group (4.25 ± 0.68). Overall, as shown in Figures 4(a)–4(c), there were significantly high patient and physician satisfaction scores in patients transplanted with ASC-enriched fat. Representative pictures of patients in both groups clearly show less absorption of fat when adipose tissue graft was enriched with culture-expanded ASCs (Figure 5).

None of the patients had serious complications during or after procedure; however, minor complications noted were comparable in both groups. For example, postoperative swelling was observed after in all procedures which settled on its own, and bruising was observed after 36 (71%) sessions which resolved in 2-3 weeks. Recipient site cellulitis developed in three (6%) cases which settled at two weeks with oral antibiotics in two cases, and in one case, it progressed to discharge of pus from the injection site that required IV clarithromycine for one month based on culture report. In the stem cell group also, the most common complication was postoperative swelling observed in all (100%) patients that also resolved in 2-3 weeks. Only one (6%) patient had recipient site cellulitis that settled at two weeks with oral antibiotics. Bruising was observed in 11 (69%) patients. None of the patients had seroma, hematoma, or skin necrosis in both groups.

4. Discussion

In the present study, clinical outcomes of treatment of contour deformities of the face with conventional fat grafting were compared with ex vivo expanded ASC-enriched fat grafting prospectively. To the best of our knowledge, it is the first study that was performed on patients of facial contour deformities using enriched ASCs. The results indicate that preenrichment of adipose tissue graft with ASCs

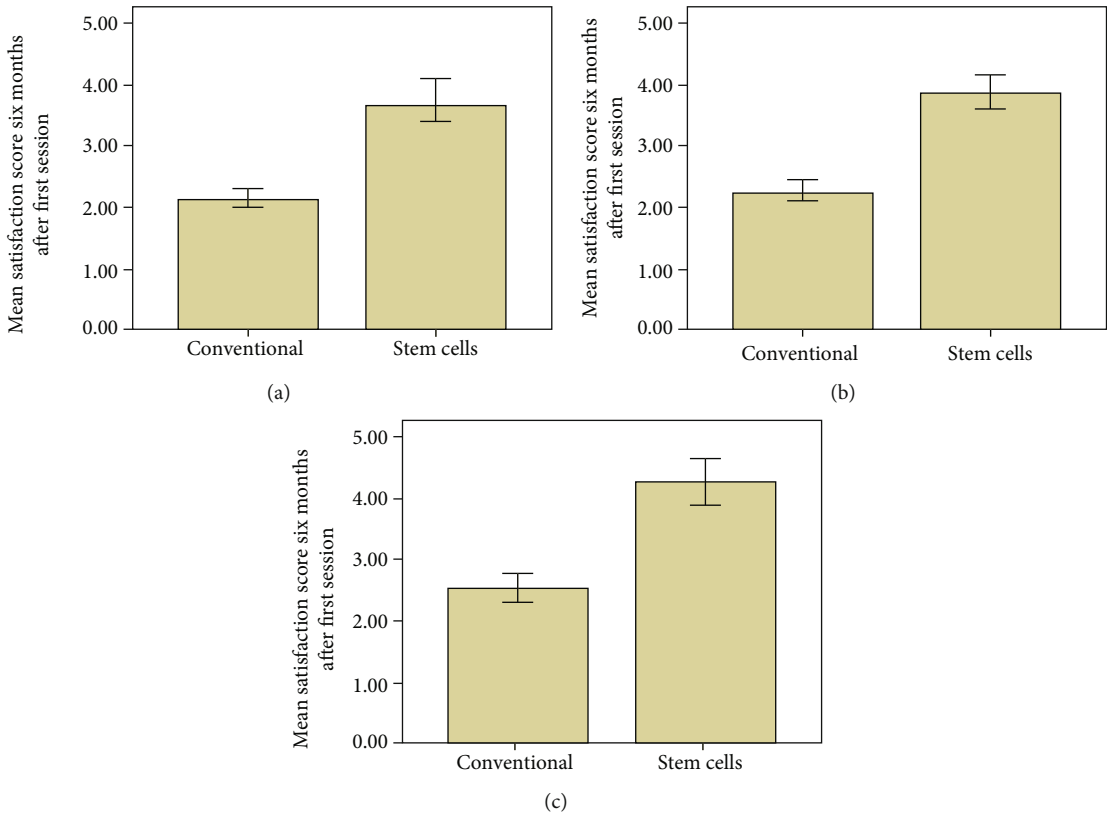

Figure 4: Comparison of mean (a) physician 1 and (b) physician 2 satisfaction score in both groups six months after the 1st fat graft session. (c) Comparison of mean of patient satisfaction score in both groups six months after the 1st fat graft session.

significantly reduces fat resorption and thus makes better the clinical outcomes in patients of contour deformities of the face. Although autologous fat grafting is a safe and effective technique for restoring volume in contour deformities of the face, significant resorption is observed in several studies including the current study (Table 1). This finding is noteworthy owing to the fact that mean preoperative soft tissue thickness, volume of transferred fat, and soft tissue thickness 72 hours after the first fat graft session were similar in both groups (Table 1). Patient and physician satisfaction has a pivotal role especially in facial plastic surgery. In our study, patient and surgeon satisfaction 6 months after the first fat graft session was significantly higher in the stem cell group as compared to the conventional group (Figure 4). Majority of the patients in the conventional group underwent more than one fat graft session due to high volume of fat absorbed over time; however, none of the patients in the stem cell group required a second session (Table 1).

Autologous fat grafting reported by Neuber in 1893 has now become the most widely accepted plastic surgery procedure for soft tissue augmentation, reconstruction, and rejuvenation [9, 10]. A large number of technical details of autologous fat grafting had been described claiming superiority of one over the other [4, 11]. Majority of studies found no difference in the number of adipocytes in fat harvested from the abdomen, thigh, flank, or around knee [12]. Different studies comparing harvesting methods have found a greater number of viable adipocytes with better cellular function in syringe-aspirated fat graft. Similarly, many studies comparing processing of fat graft by gravity and filtration followed by washing versus centrifugation showed no effect on cellular viability [13]. In the current study, adipose tissue was harvested with less traumatic syringe aspiration method to gain the maximum number of viable cells. Harvested adipose tissue was minimally handled and quickly processed with gravity and filtration (Figure 2). Small aliquots were injected throughout layers of tissue to improve long-term cell survival. Additionally, mean and total volume of injected fat in a single session were comparable to those delineated in the literature [14]. In recent reviews, outcomes of fat grafting determined by a multifactorial process showed highly variable retention rates (20% to 95%) [2, 3, 14]. We also found highly variable reduction in soft tissue thickness (12%-66%) in the conventional group at 6 months. Interestingly, however, in the stem cell group, reduction in soft tissue thickness was far less (1.06% to 12.62%) than that in the conventional group (Figure 3). This difference in outcome can be attributed to the addition of ex vivo expanded ASCs to the fat grafts in the stem cell group (Figures 3(c) and 5). In another study, fat samples enriched with SVF exhibited better survival and retention [15]. The considerable difference in resorption rates highlights the fact that SVF contain heterogenous cell population including ASCs [16]. Furthermore, the exact number of ASCs present in SVF varies between both individual patients and the body sites from which lipoaspirate is obtained [17]. The rationale for use of ASCs is to obtain a potentially larger number of more regenerative cells (ASCs) [18]. The ASC-enriched fat grafts displayed higher

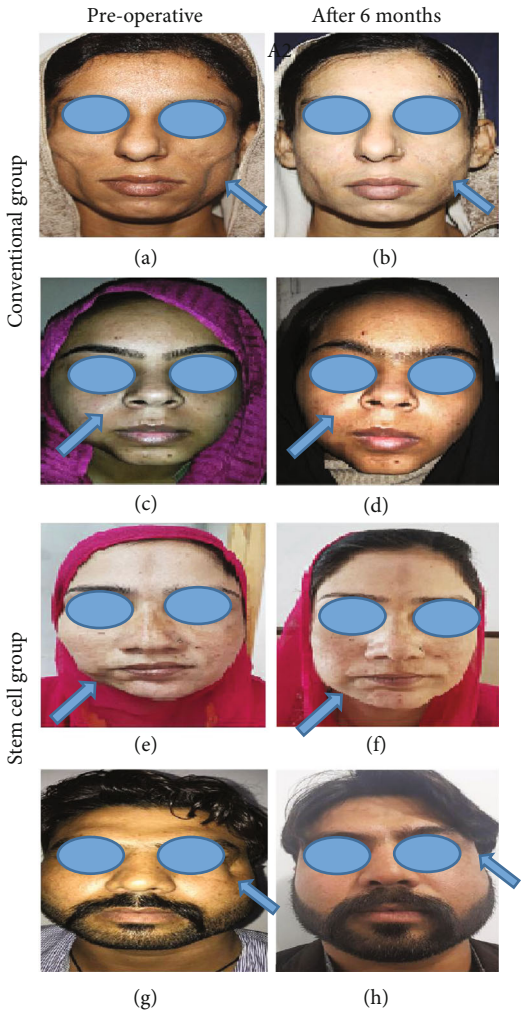

Figure 5: Representative picture showing preoperative and postoperative view of patients in (a–d) the conventional group and (e–h) the stem cell group. (a, c) Preoperative view of patient 1 (with facial contour deformity involving bilateral cheeks) and patient 2 (with facial contour deformity involving right mandibular area), respectively. (b, d) Fat absorption six months after the 1st session of conventional lipofilling. (e, g) Preoperative view and (f, h) postoperative view of patients in the stem cell group. (e) exhibits preoperative view of a patient with contour deformity of the right mandibular area, and (f) shows postoperative view six months after a single session of ex vivo expanded ASC-enriched lipofilling. (g) represents preoperative view of a patient with contour deformity of the face near the eye, and (f) shows postoperative view six months after a single session of ex vivo expanded ASC-enriched lipofilling in some patients.

amounts of transplanted adipose tissue and newly formed connective tissue and less necrotic tissue after 121 days [19]. Although previous studies have used different numbers of cells to preenrich adipose tissue graft [18, 19], in the current study, favorable results were obtained by adding 10^6 ASCs per ml of fat. This number of cells can easily be obtained in the initial passages of cells.

ASCs have the capacity to differentiate into multiple cell lines including chondrocytes, adipocytes, myocytes, and osteoblasts [20, 21]. ASCs also produce different secretomes ("vascular endothelial growth factor," "basic fibroblast growth factor," and "hepatocyte growth factor") having provasculogenic and immune modulatory properties [20]. Various in vivo models have analyzed the beneficial effects of ASCs in diabetic wounds, ischemic flaps, and replicas of cardiac ischemia [22, 23]. Recent studies have identified ASC-induced neovasculogenesis as a main contributor to survival of fat grafts [14, 24]. We propose that transferred fat may act as a natural scaffold and temporary filler to restore the volume immediately while ASCs will start participating in multiple parameters of tissue regeneration. This model supports the "host replacement theory" that has been put forward to describe how fat grafts survive after they are transplanted [18]. In this study, both photometric evaluation and volumetric assessment (soft tissue thickness of treated areas) were performed using B-mode ultrasonography [6], which is noninvasive, cost-effective, and easily available at the institution and avoids radiation exposure [10]. In the current study, frequencies of postoperative complications were comparable to those described in the literature. Swelling was observed in all patients which settled in 3-4 weeks. Infection was managed conservatively. The present study has few limitations. This is a single-center study limiting its generalizability. Furthermore, patients were not selected randomly with possibility of selection bias. Another limitation was small sample size of our study and short follow-up of six months. Although it was not possible to determine the long-term fate of transferred fat, previous studies have shown progressive reduction of the soft tissue thickness within the first 3 months after initial operations with stabilization of these rates from 3 to 6 months postoperatively. The suggested superiority of ex vivo expanded ASC-enriched lipotransfer over traditional lipofilling should be investigated further.

Abbreviations

ASCs: Adipose tissue-derived stem cells
SVF: Stromal vascular fraction
IRB: Institutional Review Board
GMP: Good Manufacturing Practice
HOTA: Human Organ Transplantation Authority
PBS: Phosphate-buffered saline
MEM: Minimum essential medium
Ph-SCs: Physician satisfaction scores
P-SCs: Patient satisfaction scores.

Data Availability

The data used to support the findings of this study are included within the article.

Conflicts of Interest

The authors declare that they have no conflicts of interest.

Acknowledgments

The work in this study was funded and supported by grant from King Edward Medical University, Lahore, Pakistan.

The authors are thankful to their colleagues for critical review of this manuscript. We are also thankful to Ms Faiza Aziz for her day-to-day help in the laboratory. The authors are grateful to Mr Asif Hanif for help in analysis of data.

References

[1] P. Pasquale, M. Gaetano, D.'. A. O. Giovanni, C. Luigi, and S. Gilberto, "Autologous fat grafting in facial volumetric restoration," *The Journal of Craniofacial Surgery*, vol. 26, no. 3, pp. 756–759, 2015.

[2] F. Simonacci, N. Bertozzi, M. P. Grieco, E. Grignaffini, and E. Raposio, "Procedure, applications, and outcomes of autologous fat grafting," *Annals of Medicine and Surgery*, vol. 20, pp. 49–60, 2017.

[3] A. Sterodimas, J. de Faria, B. Nicaretta, and F. Boriani, "Autologous fat transplantation versus adipose-derived stem cell–enriched lipografts: a study," *Aesthetic Surgery Journal*, vol. 31, no. 6, pp. 682–693, 2011.

[4] K. Yoshimura, H. Suga, and H. Eto, "Adipose-derived stem/-progenitor cells: roles in adipose tissue remodeling and potential use for soft tissue augmentation," *Regenerative Medicine*, vol. 4, no. 2, pp. 265–273, 2009.

[5] M. Zhu, Z. Zhou, Y. Chen et al., "Supplementation of fat grafts with adipose-derived regenerative cells improves long-term graft retention," *Annals of Plastic Surgery*, vol. 64, no. 2, pp. 222–228, 2010.

[6] M. M. Bashir, M. Sohail, A. Bashir et al., "Outcome of conventional adipose tissue grafting for contour deformities of face and role of ex vivo expanded adipose tissue-derived stem cells in treatment of such deformities," *Journal of Craniofacial Surgery*, vol. 29, no. 5, 2018.

[7] M. S. Choudhery, M. Badowski, A. Muise, and D. T. Harris, "Comparison of human mesenchymal stem cells derived from adipose and cord tissue," *Cytotherapy*, vol. 15, no. 3, pp. 330–343, 2013.

[8] S. R. Coleman, "Facial augmentation with structural fat grafting," *Clinics in Plastic Surgery*, vol. 33, no. 4, pp. 567–577, 2006.

[9] S. Metzinger, J. Parrish, A. Guerra, and R. Zeph, "Autologous fat grafting to the lower one-third of the face," *Facial Plastic Surgery*, vol. 28, no. 1, pp. 21–33, 2012.

[10] T. L. Tzikas, "Autologous fat grafting for midface rejuvenation," *Facial Plastic Surgery Clinics of North America*, vol. 14, no. 3, pp. 229–240, 2006.

[11] A. Condé-Green, I. Wu, I. Graham et al., "Comparison of 3 techniques of fat grafting and cell-supplemented lipotransfer in athymic rats: a pilot study," *Aesthetic Surgery Journal*, vol. 33, no. 5, pp. 713–721, 2013.

[12] M. S. Choudhery, M. Badowski, A. Muise, J. Pierce, and D. T. Harris, "Subcutaneous adipose tissue-derived stem cell utility is independent of anatomical harvest site," *Biores Open Access*, vol. 4, no. 1, pp. 131–145, 2015.

[13] R. Gupta, M. Brace, S. M. Taylor, M. Bezuhly, and P. Hong, "In search of the optimal processing technique for fat grafting," *The Journal of Craniofacial Surgery*, vol. 26, no. 1, pp. 94–99, 2015.

[14] N. Z. Yu, J. Z. Huang, H. Zhang et al., "A systemic review of autologous fat grafting survival rate and related severe complications," *Chinese Medical Journal*, vol. 128, no. 9, pp. 1245–1251, 2015.

[15] D. Matsumoto, K. Sato, K. Gonda et al., "Cell-assisted lipotransfer: supportive use of human adipose-derived cells for soft tissue augmentation with lipoinjection," *Tissue Engineering*, vol. 12, no. 12, pp. 3375–3382, 2006.

[16] N. M. Toyserkani, M. L. Quaade, and J. A. Sørensen, "Cell-assisted lipotransfer: a systematic review of its efficacy," *Aesthetic Plastic Surgery*, vol. 40, no. 2, pp. 309–318, 2016.

[17] V. M. Ramakrishnan and N. L. Boyd, "The adipose stromal vascular fraction as a complex cellular source for tissue engineering applications," *Tissue Engineering Part B: Reviews*, vol. 24, no. 4, pp. 289–299, 2018.

[18] K. Li, F. Li, J. Li et al., "Increased survival of human free fat grafts with varying densities of human adipose-derived stem cells and platelet-rich plasma," *Journal of Tissue Engineering and Regenerative Medicine*, vol. 11, no. 1, pp. 209–219, 2017.

[19] S.-F. T. Kølle, A. Fischer-Nielsen, A. B. Mathiasen et al., "Enrichment of autologous fat grafts with ex-vivo expanded adipose tissue- derived stem cells for graft survival: a randomised placebo-controlled trial," *The Lancet*, vol. 382, no. 9898, pp. 1113–1120, 2013.

[20] P. C. Baer and H. Geiger, "Adipose-derived mesenchymal stromal/stem cells: tissue localization, characterization, and heterogeneity," *Stem Cells International*, vol. 2012, Article ID 812693, 11 pages, 2012.

[21] M. S. Choudhery, M. Badowski, A. Muise, and D. T. Harris, "Effect of mild heat stress on the proliferative and differentiative ability of human mesenchymal stromal cells," *Cytotherapy*, vol. 17, no. 4, pp. 359–368, 2015.

[22] Y. Qin, P. Zhou, C. Zhou, J. Li, and W. Q. Gao, "The adipose-derived lineage-negative cells are enriched mesenchymal stem cells and promote limb ischemia recovery in mice," *Stem Cells and Development*, vol. 23, no. 4, pp. 363–371, 2014.

[23] S. J. Hong, P. I. Rogers, J. Kihlken et al., "Intravenous xenogeneic transplantation of human adipose-derived stem cells improves left ventricular function and microvascular integrity in swine myocardial infarction model," *Catheterization and Cardiovascular Interventions*, vol. 86, no. 2, pp. E38–E48, 2015.

[24] K. Y. Hong, I. I.-K. Kim, S. O. Park, U. S. Jin, and H. Chang, "Systemic administration of adipose-derived stromal cells concurrent with fat grafting," *Plastic and Reconstructive Surgery*, vol. 143, no. 5, pp. 973e–982e, 2019.

Hindawi
Stem Cells International
Volume 2019, Article ID 7548160, 12 pages
https://doi.org/10.1155/2019/7548160

Research Article

A Three-Dimensional Culture Model of Reversibly Quiescent Myogenic Cells

Salvatore Aguanno,[1] **Claudia Petrelli**,[1] **Sara Di Siena**,[1] **Luciana De Angelis**,[1] **Manuela Pellegrini**,[2] **and Fabio Naro**[1]

[1]*Department of Anatomical, Histological, Forensic and Orthopedic Sciences, Sapienza University, Rome, Italy*
[2]*Institute of Cell Biology and Neurobiology, CNR, Monterotondo, Rome, Italy*

Correspondence should be addressed to Salvatore Aguanno; salvatore.aguanno@uniroma1.it

Received 24 July 2019; Revised 24 September 2019; Accepted 3 October 2019; Published 11 November 2019

Academic Editor: Valeria Sorrenti

Satellite cells (SC) are the stem cells of skeletal muscles. They are quiescent in adult animals but resume proliferation to allow muscle hypertrophy or regeneration after injury. The mechanisms balancing quiescence, self-renewal, and differentiation of SC are difficult to analyze *in vivo* owing to their complexity and *in vitro* because the staminal character of SC is lost when they are removed from the niche and is not adequately reproduced in the culture models currently available. To overcome these difficulties, we set up a culture model of the myogenic C2C12 cell line in suspension. When C2C12 cells are cultured in suspension, they enter a state of quiescence and form three-dimensional aggregates (myospheres) that produce the extracellular matrix and express markers of quiescent SC. In the initial phase of culture, a portion of the cells fuses in syncytia and abandons the myospheres. The remaining cells are mononucleated and quiescent but resume proliferation and differentiation when plated in a monolayer. The notch pathway controls the quiescent state of the cells as shown by the fact that its inhibition leads to the resumption of differentiation. Within this context, notch3 appears to play a central role in the activity of this pathway since the expression of notch1 declines soon after aggregation. In summary, the culture model of C2C12 in suspension may be used to study the cellular interactions of muscle stem cells and the pathways controlling SC quiescence entrance and maintenance.

1. Introduction

Satellite cells (SC) lie between the basal lamina and the sarcolemma of skeletal muscle fibers. In adult muscle, they are quiescent until physical exercise or muscle damage induces their activation. SC proliferate and produce myoblasts that fuse either together or with existing myofibers, thereby allowing growth and repair of skeletal muscle [1]. A central question in adult stem cell biology regards the elucidation of the molecular mechanisms that preserve the regenerative potential of the tissues by maintaining a population of reversibly quiescent stem cells. Several findings suggest that reversible quiescence is not a state of cell inactivity but is the result of specific molecular programs [2, 3].

The study of SC biology *in vivo* is difficult owing to the complexity of the environment, the relatively low density of SC, and the absence of specific markers to recognize them [4]. It is not possible to maintain the quiescent state of SC *in vitro* because any isolation procedure triggers their activation and converts them into cycling myoblasts that undergo differentiation. SC lose their staminality because their return to quiescence is precluded in the monolayer culture by the lack of an appropriate niche.

The system of choice to characterize quiescent SC is to sort them by FACS from collagenase digested muscle. This procedure presents several problems since SC are heterogeneous and the antibodies chosen for FACS isolation select subsets of cells [5]. Furthermore, the isolation procedure

activates SC, and their activation continues during FACS purification, altering the pattern of gene expression [6, 7]; for example, the mere detachment of the monolayer for routine subculture rapidly alters the expression of notch1, which plays a pivotal role in determining SC behaviour [7].

For all of these reasons, the development of culture systems that allow undisturbed reversibly quiescent myogenic cells to be studied is very appealing [4, 5].

Three-dimensional (3D) cultures of myogenic cells have already been employed to grow SC from primary cultures. When isolated cells are seeded in nonadherent dishes, they spontaneously form floating myospheres. Such cultures are performed in growth factor-rich synthetic media that induce the expansion of satellite stem cells and conserve their staminality. The comparison of published data suggests that different combinations of cells resulting from different isolation procedures and different culture media give rise to myospheres containing stem cells with different characteristics in terms of proliferation, marker expression, and differentiation capacity [8–15].

An important advantage of myospheres is that they retain cellular interaction, which allows the involvement of the notch pathway in satellite cell biology to be studied *in vitro*. In skeletal muscle, notch is a key regulator engaged in embryonic myogenesis in myoblast proliferation [16]. Around birth, it locates myogenic progenitors in the SC compartment under the basal lamina on muscle fiber [17], whereas in adult muscle, it maintains the reversibly quiescent state of SC [18, 19]. A reduced activity of the notch pathway determines the reduced ability of muscles in old animals to regenerate [20, 21]. Notch signalling is activated when a cell displaying a notch ligand (jagged1-2, dll1-3-4) on its membrane binds a neighbouring cell exposing a notch receptor (notch1-4).

The members of the hes/hey family of transcription factors mediate most of the notch response by forming heterodimers with MyoD that inactivate this factor, thereby blocking myogenic differentiation [22, 23]. In SC, different members of the notch family appear to cover different roles, although it is not clear how they elicit different cellular responses while sharing the same pathway. For example, notch1 is involved to a greater extent in proliferation during regeneration [24] while notch3 expression is highest in self-renewing SC [19, 25, 26].

To investigate whether 3D cultures may be used to maintain SC in a quiescent status and eventually use them in skeletal muscle regeneration, we adopted the murine C2C12 myoblast cell line.

We found that C2C12 cells in myospheres spontaneously downregulate notch1 and maintain the expression of notch3. The expression of hes/hey genes accompanying this pattern of activation is lower than that of C2C12 cells proliferating in a monolayer, but it is critical for the cells to remain quiescent and undifferentiated. Indeed, when notch signalling is chemically inhibited, the cells of myospheres exit quiescence and differentiate. These data on the level of activation of hes/hey genes in myospheres differ from those obtained in freshly isolated SC, whose hes/hey expression is higher during quiescence but declines when the cells proliferate. The possibility that the isolation of satellite cells alters notch activity highlights the advantage of using a culture system with cells readily available for analysis.

Within a wider context, we believe that the ductility of the niche that arises in the C2C12 model may shed light on how the addition of other cell types, such as fibroblasts and circulating immune cells, or of exogenous soluble factors and ECM components affects specific aspects of stem cell behaviour.

2. Results

2.1. Generation and Evolution of C2C12 Myospheres. Mouse C2C12 myoblasts seeded in nonadhesive conditions form aggregates that appear within 3-4 h. Initially, the cells join together in loose networks, which subsequently compact in spherical myospheres (Figure 1).

At 6 h, flow cytometric analysis shows that the percentage of cells in G_1, S, and G_2/M in the aggregates is still the same as in the monolayer (Figure 2(a)). At 24 h, roughly 90% of the cells in the aggregates are in G0/G1; beyond 48 h, the percentage rises to 95-96%, remaining stable thereafter (Figures 2(a) and 2(b)). Evaluation of proliferation by the Ki67 expression (Figure 2(c), 6-day myospheres) confirmed the absence of proliferating cells in myospheres after 48 h of culture.

Between the 3rd and the 4th day of culture, some cells begin to fuse in syncytia. Sections of myospheres stained by haematoxylin and eosin or by immunofluorescence with an anti-sarcomeric myosin antibody display multinucleated syncytia located mainly in the periphery and often partially detached (Figure 2(e), C). At this stage, a halo that retains detached syncytia and degenerating cells appears around the myospheres (Figure 2(e), D). The halo can be easily removed by pipetting or by short DNase treatment, but it forms again in less than 24 h because the syncytia continue to leave the myospheres accompanied by mononuclear cells that form apoptotic bodies and release DNA once they are isolated in the culture medium (supplementary Fig. 1).

The halo spontaneously disappears between the 18^{th} and the 25^{th} day of culture. The surface of myospheres becomes smooth and clean although histological sections occasionally display the presence of remaining syncytia that do not detach (mature myospheres, Figure 1, 22 d).

Mature myospheres have a diameter of 80-200 μm and are formed by quiescent cells and an extracellular matrix, as shown by the presence of laminin which can already be detected by immunofluorescence 72-96 h after seeding and accumulates over time (Figure 2(f)). Mature myospheres kept in culture until 60 days do not display any further evolution except for a higher resistance to dissociation by proteases, which is evident at 33-35 days and makes it more difficult to isolate the cells. When differentiation terminates, the number of cells enclosed in the myospheres is $25.7 \pm 3.7\%$ of those initially seeded, as assessed in myospheres of 25 and 33 days after trypsinization and the cell count ($n = 7$). Besides the expulsion of syncytia, at least two other causes account for the loss of cells (Figure 2(e)). The first is that during the genesis of myospheres, a fraction of the cells does not aggregate and dies in the medium as a result

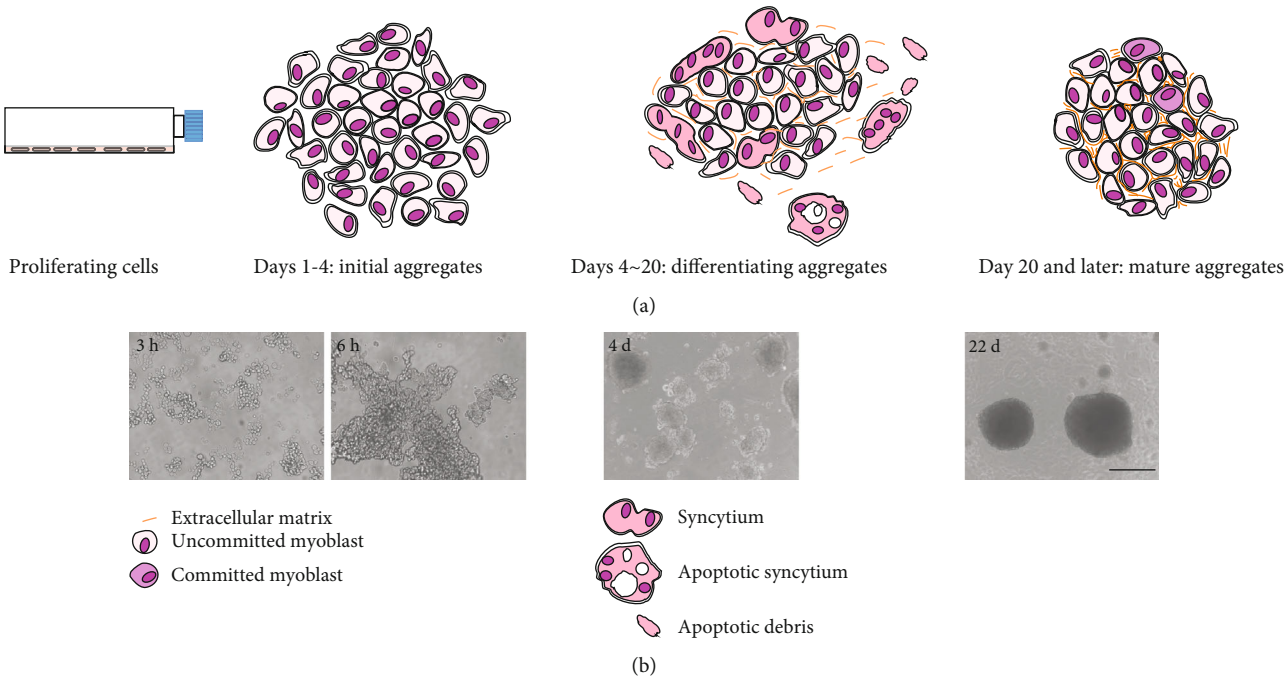

Figure 1: Scheme of myosphere evolution shown according to (a) culture time and (b) contrast phase microscopy.

of apoptosis (anoikis). The second is that when syncytia leave the myospheres, they frequently induce the disassembly of nearby mononuclear cells, which also degenerate (Figure 2(e), B and C; myospheres marked by (iv)). The cells in the myospheres are protected from apoptotic death, as demonstrated by the results of the TUNEL assay performed in the first 4 days of culture (not shown).

These data indicate that C2C12 cells aggregate when cultured in nonadherent conditions and that some of them differentiate, forming multinucleated syncytia that are lost.

2.2. Characterization of C2C12 Myospheres. To investigate the rate of differentiation, we assessed the expression of myosin by western blot during the maturation phase of myospheres (Figure 3(a)). Myosin expression starts on the 3rd day and peaks on the 9th-10th day of culture. Thereafter, it gradually decreases until it becomes undetectable at 18-20 days in parallel with the loss of syncytia. If these mature myospheres are dissociated and the cells are plated in monolayer, they proliferate and then fuse, though to a lesser extent than the original C2C12 cells (Figures 3(b) and 3(c)). Indeed, the fusion index is $55.5 \pm 2.6\%$ in the original C2C12 cells and $16.7 \pm 5.4\%$ in myoblasts derived from mature myospheres ($n = 6$). Assuming that both cell types proliferate at the same rate after plating, this indicates that the ratio between C2C12 cells that conserve their differentiation capacity (stem cells) and those that cannot differentiate ranges from 1 : 1 at the beginning of the 3D culture to 1 : 5-1 : 9 in mature myospheres.

Cells dissociated from mature myospheres are smaller than proliferating cells cultured in a monolayer (Figure 4(a)), which is in keeping with evidence showing that quiescent SC in vivo have few organelles in a little cytoplasm and a large nucleus-cytoplasmic ratio if compared with activated and proliferating cells [27, 28]. To assess the hypothesis that they might represent a model of quiescent SC cells, we evaluated the expression of different markers of SC. In particular, we estimated the expression of Sca1 because it is expressed in proliferating myogenic cells but not in quiescent cells [29]. Figure 4(b) compares the expression of Sca1 in C2C12 cells in myospheres with that of C2C12 cells in a monolayer as measured by flow cytometry. In agreement with previous results [29], C2C12 cells in myospheres are 1.3% Sca1$^+$ whereas C2C12 cells proliferating in a monolayer are 30% Sca1$^+$ positive.

Pax7 is a key marker widely used to recognize SC in skeletal muscle [30], though the fact that expression continues after myoblasts start proliferating limits the value of this factor for assessing quiescence. Figure 4(c) shows that Pax7 is expressed in C2C12 cells in a monolayer and in myospheres at two different ages, thus suggesting that cells in the myosphere retain SC characteristics.

CD34 is a surface marker of various progenitor cells. It has been reported that a full-length transcript of CD34 is expressed in quiescent SC cells and that a truncated form is expressed in proliferating SC [31]. In myospheres, we only find the full-length form of CD34 mRNA which is expressed in quiescent SC *in vivo*, whereas proliferating C2C12 cells display both the truncated and the full-length forms of CD34 mRNA (Figure 4(c)), which give rise to the mature protein form (Figure 4(d)).

Caveolin-1 is expressed in satellite cells *in vivo* and is downregulated in activated satellite cells [32]. WB analysis of caveolin-1 expression in myospheres shows that it is upregulated in mature myospheres that contain quiescent cells (Figure 4(e)).

Figure 4(f) shows the expression of MyoD, myogenin, and myosin, which discloses the presence of activated cells (MyoD), cells committed to myogenesis (myogenin), and differentiated cells (myosin).

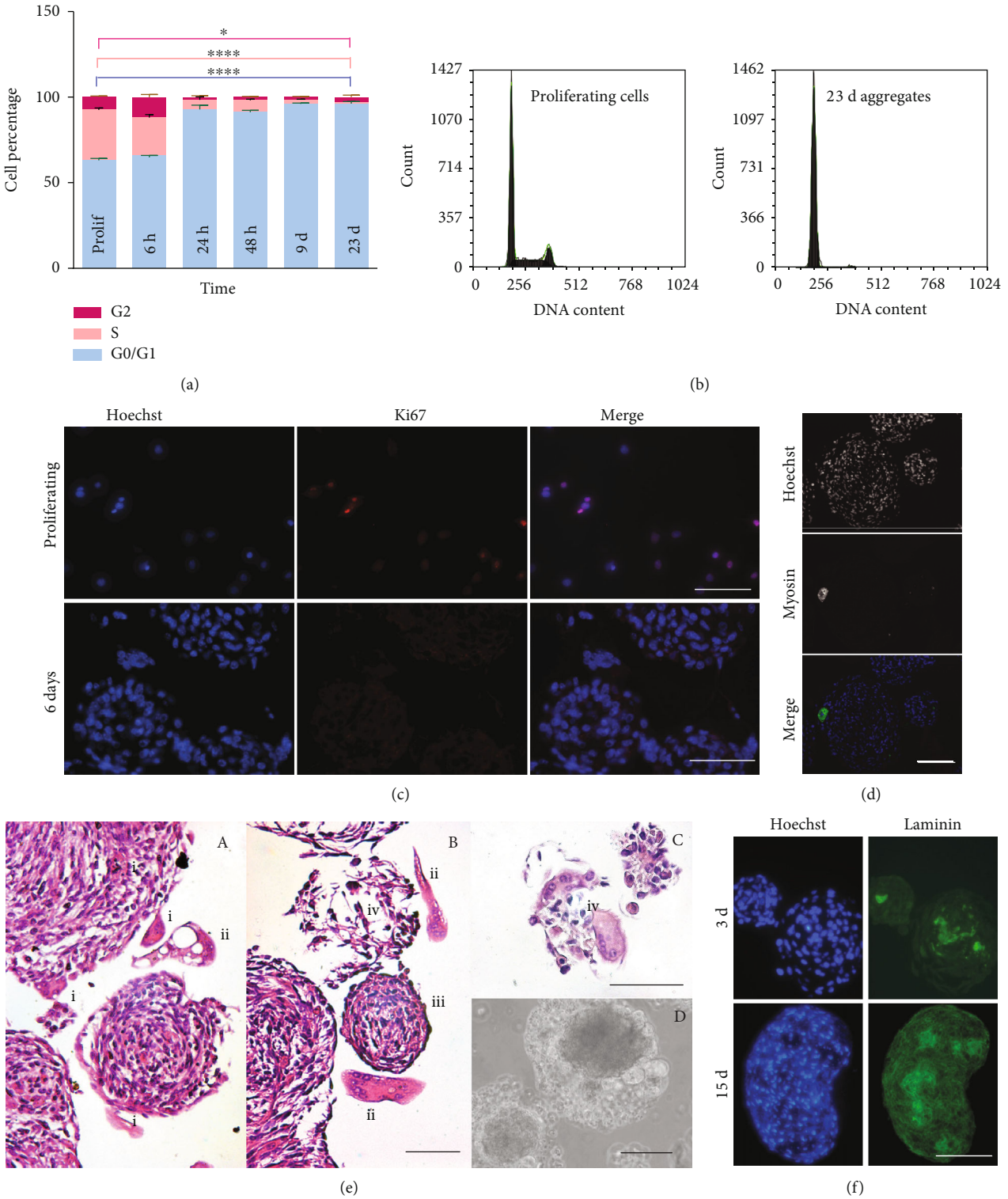

Figure 2: Characterization of C2C12 myospheres. (a) Bar chart from cytofluorometer data showing the proportion of cells (±SD) in different phases of the cycle, in a monolayer and in myospheres of different ages. $^{*}0.01 < p < 0.05$ and $^{****}p < 0.0001$. (b) Cytofluorometer plot comparing the cell cycle in cells proliferating in a monolayer and in 23-day myospheres. (c) Ki67 expression in a monolayer and 6-day myospheres. (d) Myosin expression evaluated by immunofluorescence. A labelled syncytium is at the periphery of a 9-day myosphere. (e) H&E staining of 9-day myospheres containing differentiating cells. Syncytia leaving the myospheres or internally located are indicated with (i), syncytia isolated in the medium after exit from a myosphere with (ii). (iii) indicates a mature myosphere that does not appear to contain syncytia. (e) in B and C, the symbol (iv) labels small myospheres dissolving after the detachment of syncytia. (f) Accumulation of extracellular matrix proteins in myospheres over time. Laminin expression in 3-day and 12-day myospheres. Scale bar: 50 μm in (c), (d), and (f) and 100 μm in (e).

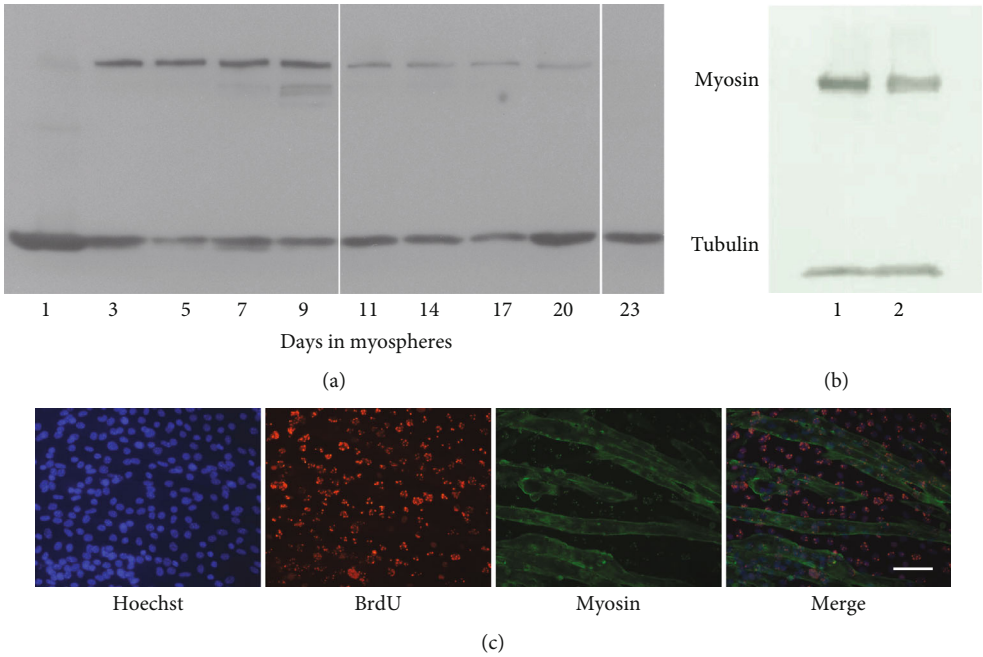

Figure 3: Trend of myogenic differentiation during myosphere maturation and differentiation potential retained in quiescent cells of mature myospheres. (a) Time course of myosin expression in myospheres by western blot from the 1st to 23rd day of culture. (b) The cells of mature myospheres retain the capacity to proliferate and differentiate. The western blot quantitatively compares myosin expression in a monolayer: (1) original C2C12 cells that were never grown as myospheres and (2) cells derived from the dissociation of 23-day myospheres plated in a monolayer and allowed to differentiate. (c) C2C12 cells dissociated from 23-day myospheres (mature); replated in a monolayer, the cells incorporate BrdU while proliferating before differentiating and expressing myosin. Scale bar: 50 μm.

In summary, the generation of mature myospheres requires approximately 20 days, by which time one-third of the C2C12 cells initially plated retain their stem cell characteristics. Such cells express SC markers, are quiescent, and retain their differentiation capacity.

2.3. Hypoxia Is Not Involved in the Quiescence of Cells in Myospheres. Three-dimensional cultures are commonly used as a model of the solid tumour microenvironment and angiogenesis thanks also to the state of hypoxia harbouring in their internal layers. The hypoxic environment favours quiescence of various stem and precursor cell types, as shown by the viability of stem cells in post-mortem muscle [33]. Moreover, it has been shown that hif-1α and the notch intracellular domain (NICD) synergize to activate the expression of notch target genes, which inhibit the expression of myogenic factors in myogenic cells and maintain the stem cell state [34].

Based on these data and on the observation that in myospheres syncytia localize mostly in the more oxygenated external layers [35], we hypothesized a role of hif-1α in maintaining cell quiescence in the cells at the centre of mature aggregates. hif-1α was found in myospheres at 8 days of culture, when differentiating cells are present but was absent in later mature aggregates (Figure 4(f)).

This result is in keeping with a report by Ono et al., who found that myogenic cells express hif-1α during differentiation in normoxic conditions, in which hif 1 α plays an essential role as its silencing inhibits the differentiation of C2C12 cells [36].

This result indicates that the expression of hif-1α in myospheres is linked to myogenic differentiation and not to hypoxia and quiescence.

2.4. Notch Signalling Is Active in Myospheres and Is Required to Maintain the Quiescence of the Cells. Notch activity plays a central role in controlling the quiescence of SC [18, 19]. Figure 5 shows an RT-PCR profile of factors related to the notch pathway in myospheres at different stages of maturation and in proliferating C2C12 cells. It shows that the cells in myospheres display all the factors required for an operative notch pathway. Indeed, in a 3D culture environment that is ideally suited to the promotion of cell-cell contacts, the coexpression of the notch ligands, dll1 and jag1, with their receptors, notch1 and notch3, ensures that the notch pathway can be activated. The constant presence of the Rbpj mediator guarantees the intracellular prosecution of the signal that switches on hes/hey downstream genes, which in turn inhibit myogenic factor expression and differentiation of the cells [22, 23].

According to their expression level, notch pathway factors in myospheres can be divided into two groups. In the first, which includes notch3, hey1, hes1, hes6, and Rbpj as well as the activators dll1 and jag1, the level of transcription remains approximately constant throughout culture time. The second group, which includes notch1, hey2, heyL, and Nrarp, shows a downregulated expression which reaches its minimum when differentiation terminates.

To investigate whether cell isolation affects the expression of notch genes in SC [6, 7], we checked their level of

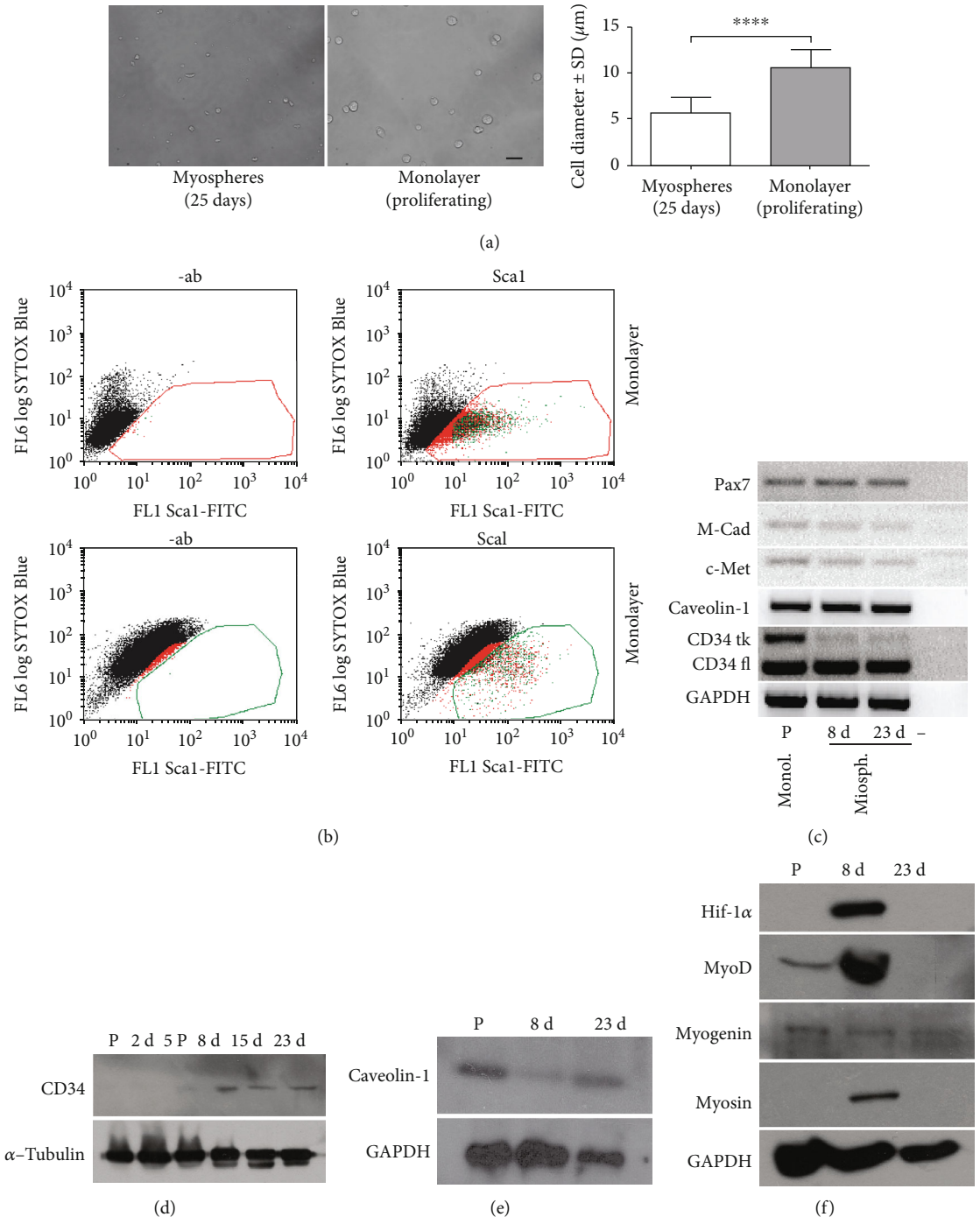

FIGURE 4: Cell size and marker expression. (a) Representative image comparing C2C12 cells shortly after dissociation of 25-day myospheres and detachment from the monolayer. The graph on the side shows the range of cell diameters. $^{****}p < 0.0001$. (b) Flow cytometric profile of Sca1 expression in cells from myospheres (25 days) and from a monolayer. (c) Semiquantitative RT-PCR profile of common quiescent satellite cell markers in differentiating and mature myospheres. Myogenin and myosin indicate the presence of differentiating cells. P: proliferating cells in monolayer. (d) Time course of CD34 expression in myospheres by western blot. (e) Caveolin-1 expression in proliferating cells and in differentiating and mature myospheres by western blot. (f) Western blot comparing hif-1α expression in proliferating cells and myospheres, with the expression of myogenic markers.

expression before and after enzymatic dissociation of mature myospheres.

Figure 6 shows that notch1 expression resumes after dissociation and accompanies that of notch3.

Since mature myospheres express only notch3 and display a low level of notch activation, we asked ourselves whether this level of hes/hey gene expression controlled the quiescent state of the cells.

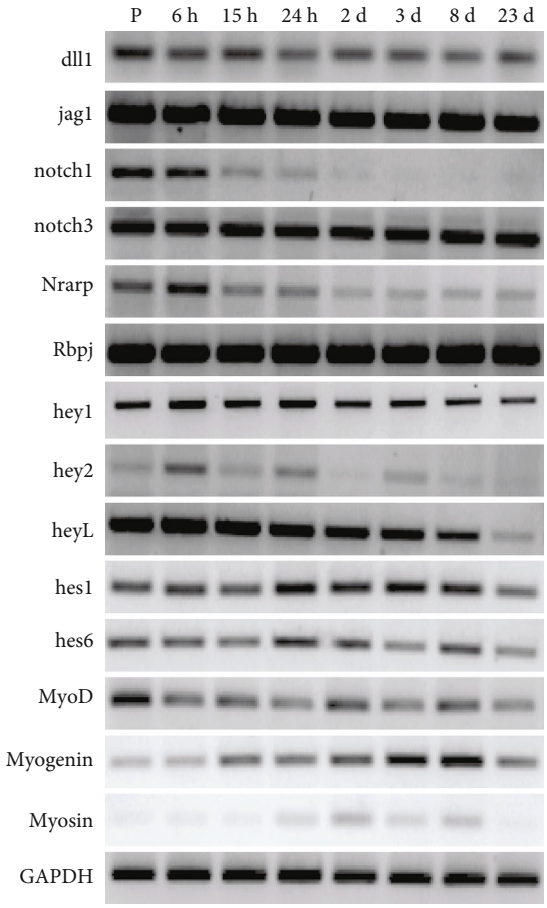

Figure 5: Expression of notch pathway genes in proliferating cells and in myospheres at different stages by RT-PCR. The figure summarizes experiments performed more than three times.

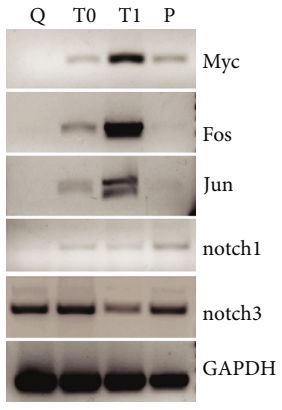

Figure 6: Dissociation of myospheres induces changes in the transcription pattern of the cells. Q: RNA extraction performed from mature myospheres; T0: cells processed for RNA extraction after myosphere dissociation was completed; T1: cells maintained in suspension in the culture medium at 37°C for 1 h after myosphere dissociation; P: cells from a monolayer.

For this purpose, we used the γ-secretase inhibitor DAPT, which inhibits notch signalling by blocking the generation of NICD from all notch paralogs. In preliminary experiments, we treated mature myospheres for 5 days with 5 μM DAPT and evaluated the expression levels of hes1 and heyL by RT-PCR. Compared with control DMSO-treated aggregates, DAPT reduced the expression of hes1 and heyL, respectively, by 75% and 79% (Figure 7).

The cells of mature myospheres treated with DAPT exit quiescence and differentiate. Indeed, whole-mount immunofluorescences performed with MF20 anti-myosin antibody on DAPT and control DMSO-treated mature myospheres demonstrated that the generation of new syncytia resumed following inhibition of notch signalling, (Figure 7(a)) with confocal microscopy also revealing the presence of elongated myotubes.

3. Discussion

Our work complements that published in other studies that used myosphere cultures maintained within a chemically defined media reach of growth factors. Such myospheres promote the proliferation of myogenic stem cells that conserve their differentiation potential [8–15].

The data collected in these studies, together with our finding showing that myospheres grown in a medium with 10% FCS contain cells that are in a state of reversible quiescence having the morphology of cells whose metabolic activity is reduced, show that stem cells can be directed towards proliferation or reversible quiescence while preserving their staminality merely by manipulating the growth factor component of the niche. Furthermore, this highlights the ductility of the niche that emerges in 3D cultures. This observation may be further exploited experimentally to investigate how the addition of different cell types, matrix components, or soluble factors in the culture affects the niche as well as the behaviour of SC. Another advantage is that the high cellular density allows the cells to be analyzed as they are in the intact niche, without the need for the isolation or concentration procedures required when dealing with SC in vivo, which are dispersed on muscle fibers. Quiescent stem cells react to the loss of interactions with the niche that accompanies any isolation procedure by changing their metabolic and gene expression pattern [37]. Quiescence of the cells within the myospheres is proved by the G0/G1 DNA content and Ki67 expression. Differentiating cells are lost during the maturation of myospheres and the remaining cells express markers widely used to recognize SC in vivo. Individually, none of these markers indicates the quiescent or proliferating state of the cells, but when combined, their expression is indicative of quiescence.

CD34 is the factor that we analyzed in most detail. Although this factor is not a specific marker of myogenic cells *in vivo*, it is useful within the context of C2C12 myospheres because it is expressed in quiescent cells alone and rapidly disappears after activation. In particular, quiescent and activated SC *in vivo* produce differently spliced isoforms of CD34 mRNA, i.e., full-length (fl) and truncated (tk) [31, 38, 39], a pattern of expression that is reproduced in myospheres and the monolayer of C2C12 cells. The detection of the CD34 protein, which does not start before the 7th–9th day of culture, may indicate that the cells reach a

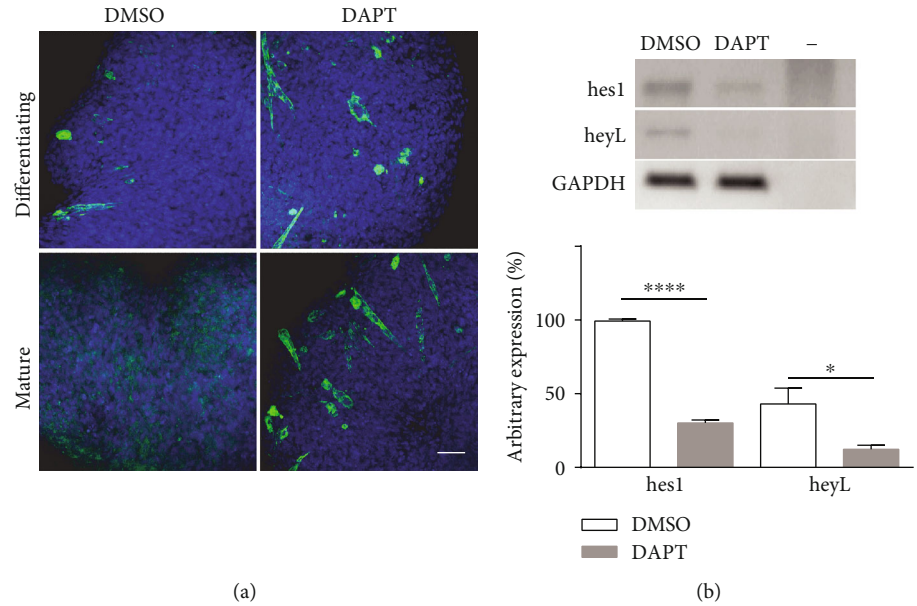

Figure 7: Differentiation resumes in mature myospheres following inhibition of the notch pathway. (a) Confocal image of whole-mount myosin immunofluorescence on differentiating (9 days) and mature (25 days) myospheres treated for 5 days with DAPT and respective DMSO controls. The effect of notch pathway inhibition is not particularly evident in differentiating myospheres because syncytia continue to leave the myospheres as they are formed. By contrast, DAPT resumes differentiation in mature myospheres, which retain the syncytia. Scale bar: 50 μm (b) RT-PCR showing the change of hes1 and heyL expression in mature myospheres in response to 5 μM DAPT treatment. Below the densitometric analysis of hes1 and heyL bands. $^{*}0.01 < p < 0.05$ and $^{****}p < 0.0001$.

state of complete quiescence only at this point. In this regard, Coller et al. reported that the transcriptional signature of fibroblasts induced to enter quiescence initially differs depending on how this state is induced, i.e., by mitogen withdrawal, loss of adhesion, or contact inhibition. Fibroblasts converge on a more common pattern of quiescent gene expression only many days later [2]. The expression of CD34 may mark a similar achievement for the cells in myospheres. The fact that the size of C2C12 cells in myospheres is smaller than that of those that proliferate in a monolayer points to a deeper state of quiescence, which is in agreement with the smaller size and lower mitochondrial and metabolic activity demonstrated in deeply quiescent satellite cells in skeletal muscle (G_0 cells) [28]. The ease with which exchanges with the environment occur may also influence the activity of the niche and affect differentiation. The exchange of substances with the environment is less efficient in myospheres than in monolayer cultures, although the lack of hif-1α accumulation in our cells indicates that at least oxygen diffusion is correct (Figure 4). When Marquette et al. cultured, in the same medium as those used by us, C2C12 aggregates in the rotating cell culture system, which is known to induce a higher mass transfer of nutrients, they reported better differentiation rates in the absence of proliferation in their stationary control cultures corresponding to those that we used [35].

Furthermore, in keeping with our results, Marquette et al. [35] found that C2C12 myoblasts in such cultures fuse without proliferating beforehand, a behaviour that was more recently shown not to be abnormal even *in vivo*, as SC have been found to fuse more frequently than was previously believed with uninjured fiber without previous proliferation [40].

Notch signalling plays a primary role in directing SC toward proliferation, differentiation, or quiescence, and its expression and activity displays a high degree of sensitivity to manipulation of the niche [7]. When aggregation is completed, notch1 expression is downregulated and myogenic cells express only the notch3 isoform. If a dissociation procedure activates the cells, the expression of notch1 soon resumes and accompanies that of notch3. The pattern of hes/hey expression in mature aggregates diverges from that reported in SC that have been freshly sorted from muscle, which appear to express higher levels of hes/hey genes in the quiescent state than when proliferating [18, 19]. The absence of notch1 signalling in myospheres may explain such differences. Indeed, notch3 alone is considered a weak activator of hes/hey genes [41], whose expression in mature myospheres is consequently lower than that of proliferating C2C12 cells. The pattern of expression of notch3 and of notch1 in myospheres is also consistent with studies that report a role of notch3 in maintaining the homeostasis of stem cells by guarding cell cycle access [42, 43].

In conclusion, our data suggest that myogenic cells that self-assemble in three-dimensional cultures in 10% FCS form a system that preserves the quiescence and the staminality of the cells. Taking the opportunity to examine these cells without any previous manipulation, we show that in this system, the cells express notch3 mRNA and fail to express notch1. Consequently, in contrast to previous findings [18, 19], we show that the activity of notch downstream factors in quiescent C2C12 cells is lower than that in proliferating cells.

We believe that C2C12 3D sphere cultures may be effectively used as a model to address unresolved questions in stem cell biology, such as how cell composition, matrix components, or diffusible factors affect the biological activity of the niche. Notably, C2C12 3D sphere cultures may be a good tool to promote skeletal muscle repair by delivering such cells to the damaged tissue.

4. Materials and Methods

C2C12 cells between the 4th and the 20th passage were maintained in a monolayer in DMEM glutamax (EuroClone, Pero (MI), Italy) supplemented with 10% FCS (EuroClone) and 50 μg/ml gentamicin in a humidified atmosphere of 5% CO_2 at 37°C and passaged at 70-80% confluence.

To generate aggregates, cells were grown to 80-85% confluence, detached enzymatically, and seeded at a density of $3 - 4 \times 10^5$/ml on 90 mm bacterial dishes in the same culture medium as that used to grow them in a monolayer with the addition of 0.3% methylcellulose (Sigma-Aldrich, St. Louis, MO, USA, Cat. 09967). In these conditions, cells do not adhere to plastic and join together in aggregates of various sizes (http://spherogenex.de) [44]. The medium was changed every 2-3 days.

4.1. Cell Count. 3D cultures contain aggregates of different sizes that do not disperse homogeneously in the plate. Consequently, sampling problems arise when aliquots of the medium are being collected. For this reason, in order to evaluate the number of cells remaining in aggregates after differentiation, we counted the cells obtained after trypsin dissociation of entire dishes.

4.2. Inhibition of the Notch Pathway. The γ-secretase inhibitor DAPT (Sigma Aldrich) was dissolved in DMSO and used at a concentration of 5 μM. The drug was added for 5 days on the 4th day of culture (differentiating aggregates) or on the 20th day (mature aggregates). In the latter case, the drug was added after the end of differentiation as indicated by the disappearance of a halo of dying cells surrounding the aggregates while cells differentiate. Culture medium with DAPT or DMSO was replaced every 2 days.

4.3. Frozen and Paraffin Section Preparation. Aggregates were fixed for 2 h with 4% paraformaldehyde (Sigma-Aldrich), at 4°C, washed with PBS, and stored at 4°C. Frozen sections (7 μm) were prepared after embedding of aggregates in OCT (Tissue-Tek, Sakura Finetek USA). Sections were incubated with primary antibodies directed against Ki67 (Santa Cruz Biotechnology, Inc., Heidelberg, Germany, SC7846, 1 : 100), laminin (Sigma L939, 1 : 100), CD34 (Santa Cruz Cat. SC9095, 1 : 100), and MF20 anti-sarcomeric myosin heavy chain (1 : 5 diluted hybridoma medium). Fluorescent images were acquired using an epifluorescence Zeiss Axioskop 2 Plus microscope (Carl Zeiss, Oberkochen, Germany) or a Leica Leitz DMRB microscope fitted with a DFC300FX camera (Leica, Wetzlar, Germany). For haematoxylin and eosin (H&E) staining, fixed aggregates were dehydrated, embedded in paraffin wax, and cut into 5 μm sections. Images were assembled using Adobe Illustrator or ImageJ.

4.4. Whole-Mount Immunofluorescence. Aggregates were fixed in cold (-20°C) methanol-acetone 1 : 1 (v/v) for 20 minutes and washed with PBS. They were then incubated, by shaking with MF20 anti-myosin antibody, (from hybridoma culture medium, diluted 1 : 5) at 4°C for 20 h. Washed aggregates were incubated with fluorescein-labelled secondary antibodies for 2 h at room temperature. Nuclei were stained with TO-PRO-3 (0.2 mg/ml, Molecular Probes, Molecular Probes Europe, Rijnsburgerweg, The Netherlands). Samples were observed by confocal microscopy with a Leica TCS SP2 (Leica, Wetzlar, Germany).

4.5. Fusion Index Quantification. The fusion index was measured in cells grown for 72 h in DM after reaching confluence and stained with MF20 anti-myosin antibody. This index was calculated as the ratio of the number of nuclei in myotubes with 3 or more nuclei versus the total number of nuclei in the field.

In detail, the comparison of the fusion index between cells from mature aggregates and original cells was performed as follows: fresh C2C12 cells were grown to 70-80% confluence in 6 different 150 mm dishes. The cells from such dishes were then dissociated and transferred each to a different 90 mm dish in nonadherent conditions to generate the myospheres, which were then left to mature. Three days after the disappearance of the halo, the myospheres (not counted) from each of the 90 mm dishes were dissociated and a portion of the cells obtained was plated in three 35 mm dishes (30000 cells/dish) and compared for their capacity of differentiation with fresh control cells plated in the same conditions in parallel in five 35 mm dishes.

4.6. Cell Cycle Analysis. Cells derived from trypsin dissociation of the aggregates were fixed in cold 80% ethanol, washed, and incubated at 37°C for 3 h in PBS containing 1% Triton X-100, 50 μg/ml propidium iodide, and 100 μg/ml DNase-free RNase A (Sigma-Aldrich). Flow cytometric analysis was performed on an Epics XL (Beckman Coulter, Fullerton, CA, USA) using Expo 32 software for acquisition and FCS Express 4 for analysis. Doublets were discriminated by means of gating.

4.7. BrdU Labelling. Cells obtained by the trypsinization of mature aggregates were plated at a density of $8 - 10 \times 10^3$/ml in 35 mm dishes. After 24 h, the cells were pulse-labelled with 10 μM BrdU (Sigma-Aldrich) in growth medium for 4 h. At 90-100% confluence, the growth medium was changed to DMEM + 2%HS for 4-5 days with daily changes. After fixation, cells were stained with anti-BrdU (Sigma B2531) and MF20 anti-myosin antibody.

4.8. Halo Characterization. To characterize the fate of the cells lost by myospheres during the maturation process and their subsequent fate, we examined the material released from myospheres by day 9 after 2 days of culture. Myospheres with their medium were transferred to a tube and left to settle by gravity. The spent medium was then removed and

centrifuged at 1000 rpm, and the pellet containing released cells and cellular fragments was resuspended without fixation in PBS for microscopical examination after staining with 1 μM Hoechst 33342, 2.5 μg/ml propidium iodide and annexin V, and Alexa Fluor™ 488 conjugate (Thermo Fisher Scientific A13201), all from 100x solutions. Samples were stained in ice for 5 min and discarded after a further 10 min because propidium iodide is no longer specific for dead cells after this time.

4.9. Semiquantitative RT-PCR. Total RNA was extracted by using TRI Reagent (Sigma T9424) according to the manufacturer's protocol. A 1 μg aliquot of total RNA was treated with DNase-I (New England Biolabs, EuroClone, Pero (MI), Italy) and reverse transcribed into first-strand cDNA using M-MLV reverse transcriptase (M-1705, Promega, Madison, WI, USA) and random hexamer primers (Invitrogen, Thermo Fisher Scientific Inc., Waltham, MA USA). Cycling parameters were 94°C/20 s, 58°C/20 s, and 72°C/20 s for 31 cycles. PCR products were run on 2% agarose gels. PCR was performed with the following primers: caveolin-1 (5′-GCACACCAAGGAGATTGACC-3′; 5′-GAATGGCAAAGTAAATGCCC-3'), jag1 (5′-*CCC CCTGAGTCTTCTGCTC-3′*; 5′-*GTGACGCGGGACTGATA CTC-3′*, M-Cad (5′-ATGATGGCTCTGTACCAGC-3′; 5′-AAGACTACGACCCAGAAGAC-3′), c-Met (5′-TCCTGA CATCCATCTCCACC-3′; 5′-GCATGAAGCGACCTTC TGAC-3′), Pax7 (5′-CCGTGTTTCTCATGGTTGTG-3′; 5′-GAGCACTCGGCTAATCGAAC-3′), MyoD (5′-AGC ACTACAGTGGCG ACTCA-3′; 5′-GCTCCACTATGCT GGACAGG-3′), myosin (5′-ACAAGCTGCGGGTGAAG AGC-3′; 5′-CAGGACAGTGACA AAGAACG-3′), myogenin (5′-CTACAGGCCTTGCTCAGCTC-3′; 5′-AGAT TGTGGGCGTCTGTAGG-3′), c-Myc (5′-CGGACACAC AACGTCTTGGAA-3′; 5′-AGGATGTAGGCGGTGGCT TTT-3′), c-Jun (5′-CTGCATGGACCTAACATTCG-3′; 5′-GCTTTCACCCTAGTATATTGGG-3′), c-Fos (5′-TGT TGTTCCTAGTGACACC-3′; 5′-ACATTCAGACCACCT CG-3′), notch1 (5′-TGCC TGTGCACACCATTCTGC-3′; 5′-CAATCAGAGATGTTGGAATGC-3′), notch3 (5′-TG CCAGAGTTCAGTGGTGG-3′; 5′-CACAGGCAAATCG GCCATC-3′), dll1 (5′-CCCTGGCAGACAGATTGG-3′; 5′-ACAGAGGGGAGAAGATGTGC-3′), hes1 (5′-GCCA ATTTGCCTTTCTCATC-3′; 5′-GAGAGGTGGGCTAG GGACTT-3′), hes6 (5′-CCCTAGAGCTCTGGATGGTG-3′; 5′-GCGCAACTGTGTTACAAACG-3′), hey1 (5′-TCA GCGTGGGGAATCTTAAC-3′; 5′-GATTCAGGGCACAG ACACCT-3′), hey2 (5′-TGGAAAAGGAAACGCCAT A-3′; 5′-ATCTGCAGCCTGACACATTG-3′), heyL (5′-GCGATT GAAGTCCCCAG ATA-3′; 5′-ACTGGGGTCACCAGAC TG AG-3′), Rbpj (5′-GGTCCCAGACATTTCTGCAT-3′; 5′-GGAGTTGGCTCTGAGAATCG-3′), GAPDH (5′-TCC TGACATCCATCTCCACC-3′; 5′-GCATGAAGCGACCTT CTGAC-3′). Primers used to distinguish full-length and truncated forms of CD34 transcripts were 5′-AGCACAGAACT TCCCAGCAA-3′ in exons 5/6 and 5′-CCTCCACCATT CTCCGTGTA-3′ in exon 8 (Beauchamp et al., 2000), which amplify, respectively, a fragment of 260 and 416 bp, as the truncated form includes an extra exon with a stop codon that arrests translation.

4.10. Immunoblot Analysis. Cells were lysed by sonication in ice-cold RIPA buffer (20 mM Tris-HCl pH 7.6 containing 150 mM NaCl, 2 mM EDTA, 1% NP40, 0.5% Na-deoxycholate) supplemented with protease inhibitor cocktail (Sigma-Aldrich P2714). Equal amounts of proteins were resolved on 8-10% SDS polyacrylamide gel. After being transferred onto PVDF membranes (Amersham GE Healthcare, Buckinghamshire, UK), proteins of interest were detected by using anti-CD34 (sc-9095 Santa Cruz, 1 : 500), anti-myosin (MF20 1 : 50), anti-MyoD (sc-377460 Santa Cruz, 1 : 1000), anti-myogenin (sc-12732 Santa Cruz, 1 : 300), anti-hif-1α (NB100-105 Novus Biologicals, Segrate, Italy, 1 : 1000), and anti-caveolin-1 (ab17052 Abcam, Cambridge, UK 1 : 1000) antibodies and anti-α-tubulin (T5168, Sigma, 1 : 2000) or anti-GAPDH (Santa Cruz, sc-25778, 1 : 1000) antibodies as a normalization control.

4.11. Statistical Analysis. Quantitative data of at least three independent experiments are presented as means ± SEM. Statistical analysis was performed by means of Graphpad Prism Software (La Jolla, CA, USA) using paired Student's t-tests to determine significance ($^{*}0.01 < p < 0.05$; $^{**}0.001 < p < 0.01$; $^{***}0.0001 < p < 0.001$; $^{****}p < 0.0001$).

Data Availability

All data used to support the findings of this study are included within the article.

Conflicts of Interest

The authors declare no competing or financial interests.

Authors' Contributions

S.A. planned the research, performed experiments, analyzed the data, and wrote the manuscript. C.P. and S.DS. performed experiments and analyzed the data. L.DA., M.P., and F.N. critically revised the manuscript. All the authors read and approved the final manuscript.

Acknowledgments

We thank A. D'Alessio and A. Filippini for the hif-1α and caveolin-1 antibodies and S. De Grossi and F. Padula for the confocal microscopy and cytofluorometric analysis. This work was funded by Sapienza University "Ateneo 2016" through a grant to FN.

Supplementary Materials

Supplementary Fig. 1: genesis of the halo. Cells released from the myospheres between the seventh and ninth days of culture. Once the cells are isolated in the medium, they enter

apoptosis. The sample shown in the figure contains cells at all stages of apoptosis since new cells are continuously released from myospheres. The new cells join those previously released and their debris, trapped by the released DNA that also induces their attachment to the microspheres. In fact, these aggregates are rapidly dissolved by treatment with DNase. (a) phase-contrast image; (b) Hoechst 33342 staining, labeling all nuclei; (c) propidium iodide staining, labeling dead cell nuclei; (d) annexin V staining. Annexin V binds to phosphatidylserine residues translocated to the external face of the plasma membrane. This is an early event in apoptosis. Bar = 50 μm. *(Supplementary Materials)*

References

[1] S. B. Charge and M. A. Rudnicki, "Cellular and molecular regulation of muscle regeneration," *Physiological Reviews*, vol. 84, no. 1, pp. 209–238, 2004.

[2] H. A. Coller, L. Sang, and J. M. Roberts, "A new description of cellular quiescence," *PLoS Biology*, vol. 4, no. 3, article e83, 2006.

[3] L. Liu, T. H. Cheung, G. W. Charville et al., "Chromatin modifications as determinants of muscle stem cell quiescence and chronological aging," *Cell Reports*, vol. 4, no. 1, pp. 189–204, 2013.

[4] J. Dhawan and T. A. Rando, "Stem cells in postnatal myogenesis: molecular mechanisms of satellite cell quiescence, activation and replenishment," *Trends in Cell Biology*, vol. 15, no. 12, pp. 666–673, 2005.

[5] B. D. Cosgrove, A. Sacco, P. M. Gilbert, and H. M. Blau, "A home away from home: challenges and opportunities in engineering in vitro muscle satellite cell niches," *Differentiation*, vol. 78, no. 2-3, pp. 185–194, 2009.

[6] S. C. van den Brink, F. Sage, Á. Vértesy et al., "Single-cell sequencing reveals dissociation-induced gene expression in tissue subpopulations," *Nature Methods*, vol. 14, no. 10, pp. 935-936, 2017.

[7] W. Liu, K. M. Morgan, and S. R. Pine, "Activation of the Notch1 stem cell signaling pathway during routine cell line subculture," *Frontiers in Oncology*, vol. 4, p. 211, 2014.

[8] K. A. Westerman, A. Penvose, Z. Yang, P. D. Allen, and C. A. Vacanti, "Adult muscle 'stem' cells can be sustained in culture as free-floating myospheres," *Experimental Cell Research*, vol. 316, no. 12, pp. 1966–1976, 2010.

[9] A. Penvose and K. A. Westerman, "Sca-1 is involved in the adhesion of myosphere cells to $\alpha V\beta 3$ integrin," *Biology Open*, vol. 1, no. 9, pp. 839–847, 2012.

[10] K. A. Westerman, "Myospheres are composed of two cell types: one that is myogenic and a second that is mesenchymal," *PLoS One*, vol. 10, no. 2, article e0116956, 2015.

[11] R. Sarig, Z. Baruchi, O. Fuchs, U. Nudel, and D. Yaffe, "Regeneration and transdifferentiation potential of muscle-derived stem cells propagated as myospheres," *Stem Cells*, vol. 24, no. 7, pp. 1769–1778, 2006.

[12] T. Hosoyama, J. V. McGivern, J. M. Van Dyke, A. D. Ebert, and M. Suzuki, "Derivation of Myogenic Progenitors Directly From Human Pluripotent Stem Cells Using a Sphere-Based Culture," *STEM CELLS Translational Medicine*, vol. 3, no. 5, pp. 564–574, 2014.

[13] N. Arsic, D. Mamaeva, N. J. Lamb, and A. Fernandez, "Muscle-derived stem cells isolated as non-adherent population give rise to cardiac, skeletal muscle and neural lineages," *Experimental Cell Research*, vol. 314, no. 6, pp. 1266–1280, 2008.

[14] Y. Wei, Y. Li, C. Chen, K. Stoelzel, A. M. Kaufmann, and A. E. Albers, "Human skeletal muscle-derived stem cells retain stem cell properties after expansion in myosphere culture," *Experimental Cell Research*, vol. 317, no. 7, pp. 1016–1027, 2011.

[15] C. Poulet, E. Wettwer, T. Christ, and U. Ravens, "Skeletal muscle stem cells propagated as myospheres display electrophysiological properties modulated by culture conditions," *Journal of Molecular and Cellular Cardiology*, vol. 50, no. 2, pp. 357–366, 2011.

[16] E. Vasyutina, D. C. Lenhard, H. Wende, B. Erdmann, J. A. Epstein, and C. Birchmeier, "RBP-J (Rbpsuh) is essential to maintain muscle progenitor cells and to generate satellite cells," *Proceedings of the National Academy of Sciences of the United States of America*, vol. 104, no. 11, pp. 4443–4448, 2007.

[17] D. Brohl, E. Vasyutina, M. T. Czajkowski et al., "Colonization of the satellite cell niche by skeletal muscle progenitor cells depends on notch signals," *Developmental Cell*, vol. 23, no. 3, pp. 469–481, 2012.

[18] C. R. R. Bjornson, T. H. Cheung, L. Liu, P. V. Tripathi, K. M. Steeper, and T. A. Rando, "Notch signaling is necessary to maintain quiescence in adult muscle stem cells," *Stem Cells*, vol. 30, no. 2, pp. 232–242, 2012.

[19] P. Mourikis, R. Sambasivan, D. Castel, P. Rocheteau, V. Bizzarro, and S. Tajbakhsh, "A critical requirement for notch signaling in maintenance of the quiescent skeletal muscle stem cell state," *Stem Cells*, vol. 30, no. 2, pp. 243–252, 2012.

[20] I. M. Conboy, M. J. Conboy, G. M. Smythe, and T. A. Rando, "Notch-mediated restoration of regenerative potential to aged muscle," *Science*, vol. 302, no. 5650, pp. 1575–1577, 2003.

[21] S. Fukada, A. Uezumi, M. Ikemoto et al., "Molecular signature of quiescent satellite cells in adult skeletal muscle," *Stem Cells*, vol. 25, no. 10, pp. 2448–2459, 2007.

[22] Y. Sasai, R. Kageyama, Y. Tagawa, R. Shigemoto, and S. Nakanishi, "Two mammalian helix-loop-helix factors structurally related to Drosophila hairy and enhancer of split," *Genes & Development*, vol. 6, no. 12B, pp. 2620–2634, 1992.

[23] J. Sun, C. N. Kamei, M. D. Layne et al., "Regulation of myogenic terminal differentiation by the hairy-related transcription factor CHF2," *The Journal of Biological Chemistry*, vol. 276, no. 21, pp. 18591–18596, 2001.

[24] I. M. Conboy and T. A. Rando, "The regulation of notch signaling controls satellite cell activation and cell fate determination in postnatal myogenesis," *Developmental Cell*, vol. 3, no. 3, pp. 397–409, 2002.

[25] S. Kuang, M. A. Gillespie, and M. A. Rudnicki, "Niche regulation of muscle satellite cell self-renewal and differentiation," *Cell Stem Cell*, vol. 2, no. 1, pp. 22–31, 2008.

[26] S. Fukada, M. Yamaguchi, H. Kokubo et al., "Hesr1 and Hesr3 are essential to generate undifferentiated quiescent satellite cells and to maintain satellite cell numbers," *Development*, vol. 138, no. 21, pp. 4609–4619, 2011.

[27] A. C. Wozniak, J. Kong, E. Bock, O. Pilipowicz, and J. E. Anderson, "Signaling satellite-cell activation in skeletal muscle: markers, models, stretch, and potential alternate pathways," *Muscle and Nerve*, vol. 31, no. 3, pp. 283–300, 2005.

[28] J. T. Rodgers, K. Y. King, J. O. Brett et al., "mTORC1 controls the adaptive transition of quiescent stem cells from G_0 to G_{Alert}," *Nature*, vol. 510, no. 7505, pp. 393–396, 2014.

[29] P. O. Mitchell, T. Mills, R. S. O'Connor et al., "Sca-1 negatively regulates proliferation and differentiation of muscle cells," *Developmental Biology*, vol. 283, no. 1, pp. 240–252, 2005.

[30] P. S. Zammit, F. Relaix, Y. Nagata et al., "Pax7 and myogenic progression in skeletal muscle satellite cells," *Journal of Cell Science*, vol. 119, pp. 1824–1832, 2006.

[31] L. A. Alfaro, S. A. Dick, A. L. Siegel et al., "CD34 promotes satellite cell motility and entry into proliferation to facilitate efficient skeletal muscle regeneration," *Stem Cells*, vol. 29, no. 12, pp. 2030–2041, 2011.

[32] D. Volonte, Y. Liu, and F. Galbiati, "The modulation of caveolin-1 expression controls satellite cell activation during muscle repair," *The FASEB Journal*, vol. 19, no. 2, pp. 237–239, 2005.

[33] M. Latil, P. Rocheteau, L. Châtre et al., "Skeletal muscle stem cells adopt a dormant cell state post mortem and retain regenerative capacity," *Nature Communications*, vol. 3, p. 903, 2012.

[34] M. V. Gustafsson, X. Zheng, T. Pereira et al., "Hypoxia requires notch signaling to maintain the undifferentiated cell state," *Developmental Cell*, vol. 9, pp. 617–628, 2005.

[35] M. L. Marquette, D. Byerly, and M. Sognier, "A novel in vitro three-dimensional skeletal muscle model," *In Vitro Cellular & Developmental Biology - Animal*, vol. 43, no. 7, pp. 255–263, 2007.

[36] Y. Ono, H. Sensui, Y. Sakamoto, and R. Nagatomi, "Knock-down of hypoxia-inducible factor-1α by siRNA inhibits C2C12 myoblast differentiation," *Journal of Cellular Biochemistry*, vol. 98, no. 3, pp. 642–649, 2006.

[37] S. R. Neves, P. Tsokas, A. Sarkar et al., "Cell shape and negative links in regulatory motifs together control spatial information flow in signaling networks," *Cell*, vol. 133, no. 4, pp. 666–680, 2008.

[38] J. R. Beauchamp, L. Heslop, D. S. Yu et al., "Expression of CD34 and Myf5 defines the majority of quiescent adult skeletal muscle satellite cells," *The Journal of Cell Biology*, vol. 151, no. 6, pp. 1221–1234, 2000.

[39] P. S. Zammit, T. A. Partridge, and Z. Yablonka-Reuveni, "The skeletal muscle satellite cell: the stem cell that came in from the cold," *The Journal of Histochemistry and Cytochemistry*, vol. 54, no. 11, pp. 1177–1191, 2006.

[40] B. Pawlikowski, C. Pulliam, N. D. Betta, G. Kardon, and B. B. Olwin, "Pervasive satellite cell contribution to uninjured adult muscle fibers," *Skeletal Muscle*, vol. 5, p. 42, 2015.

[41] P. Beatus, J. Lundkvist, C. Oberg, and U. Lendahl, "The notch 3 intracellular domain represses notch 1-mediated activation through hairy/enhancer of split (HES) promoters," *Development*, vol. 126, no. 17, pp. 3925–3935, 1999.

[42] A. Alunni, M. Krecsmarik, A. Bosco et al., "Notch3 signaling gates cell cycle entry and limits neural stem cell amplification in the adult pallium," *Development*, vol. 140, no. 16, pp. 3335–3347, 2013.

[43] T. Kitamoto and K. Hanaoka, "Notch3 null mutation in mice causes muscle hyperplasia by repetitive muscle regeneration," *Stem Cells*, vol. 28, no. 12, pp. 2205–2216, 2010.

[44] T. Korff and H. G. Augustin, "Integration of Endothelial Cells in Multicellular Spheroids Prevents Apoptosis and Induces Differentiation," *The Journal of Cell Biology*, vol. 143, no. 5, pp. 1341–1352, 1998.

Hindawi
Stem Cells International
Volume 2019, Article ID 8496025, 17 pages
https://doi.org/10.1155/2019/8496025

Research Article

Injectable Hydrogel Combined with Nucleus Pulposus-Derived Mesenchymal Stem Cells for the Treatment of Degenerative Intervertebral Disc in Rats

Feng Wang,[1,2] **Li-ping Nan**,[1,2] **Shi-feng Zhou**,[2] **Yang Liu**,[1,2] **Ze-yu Wang**,[2] **Jing-cheng Wang**,[2] **Xin-min Feng**,[2] **and Liang Zhang**[2]

[1]*Department of Orthopedics, Dalian Medical University, Dalian, 116000 Liaoning, China*
[2]*Department of Orthopedics, Clinical Medical College of Yangzhou University, Yangzhou, 225001 Jiangsu, China*

Correspondence should be addressed to Xin-min Feng; fxmspine@sina.com and Liang Zhang; zhangliang6320@sina.com

Received 20 June 2019; Accepted 17 August 2019; Published 15 October 2019

Guest Editor: Letizia Trovato

Stem cell-based tissue engineering in treating intervertebral disc (IVD) degeneration is promising. An appropriate cell scaffold can maintain the viability and function of transplanted cells. Injectable hydrogel has the potential to be an appropriate cell scaffold as it can mimic the condition of the natural extracellular matrix (ECM) of nucleus pulposus (NP) and provide binding sites for cells. This study was aimed at investigating the effect of injectable hydrogel-loaded NP-derived mesenchymal stem cells (NPMSC) for the treatment of IVD degeneration (IDD) in rats. In this study, we selected injectable 3D-RGD peptide-modified polysaccharide hydrogel as a cell transplantation scaffold. In vitro, the biocompatibility, microstructure, and induced differentiation effect on NPMSC of the hydrogel were studied. In vivo, the regenerative effect of hydrogel-loaded NPMSC on degenerated NP in a rat model was evaluated. The results showed that NPMSC was biocompatible and able to induce differentiation in hydrogel in vivo. The disc height index (almost 87%) and MRI index (3313.83 ± 227.79) of the hydrogel-loaded NPMSC group were significantly higher than those of other groups at 8 weeks after injection. Histological staining and immunofluorescence showed that the hydrogel-loaded NPMSC also partly restored the structure and ECM content of degenerated NP after 8 weeks. Moreover, the hydrogel could support long-term NPMSC survival and decrease cell apoptosis rate of the rat IVD. In conclusion, injectable hydrogel-loaded NPMSC transplantation can delay the level of IDD and promote the regeneration of the degenerative IVD in the rat model.

1. Introduction

Lower back pain (LBP) is a common disease with high incidence [1] and imposes an enormous economic burden on the society and family [2]. The prevalence of LBP is increasing due to the aging of population [3], and intervertebral disc degeneration (IDD) is considered associated with LBP [4]. Unfortunately, none of the common therapy can effectively repair or regenerate the structure and function of the degenerative intervertebral disc (IVD) [5, 6]. Thus, it is necessary to develop a new approach for IDD.

IVD is composed of three parts: the central gelatinous NP, the outer multilaminate annulus fibrosus (AF), and the cartilage endplate [7]. NP is one of the most critical parts of IVD, which can provide a suitable extracellular environment for the growth and secretion function of NP cells [8]. Therefore, it is believed that restoration of a degenerated NP may be of great importance to the treatment of IDD. The function and numbers of the endogenous IVD cells are decreasing during the IDD procedure, which results in failure of cell-based endogenous repair [9]. Mesenchymal stem cell-(MSC-) based therapy has broad application prospects for the treatment of IDD. Bone marrow-derived MSC [10], adipose-derived MSC [11], human umbilical cord-derived MSC [12], and other types of stem cells [13] have been used to treat IDD. Unfortunately, the local microenvironment of the degenerative IVD, which is characterized by hypertonicity, acidic pH, limited nutrition, and oxygen [2, 14, 15],

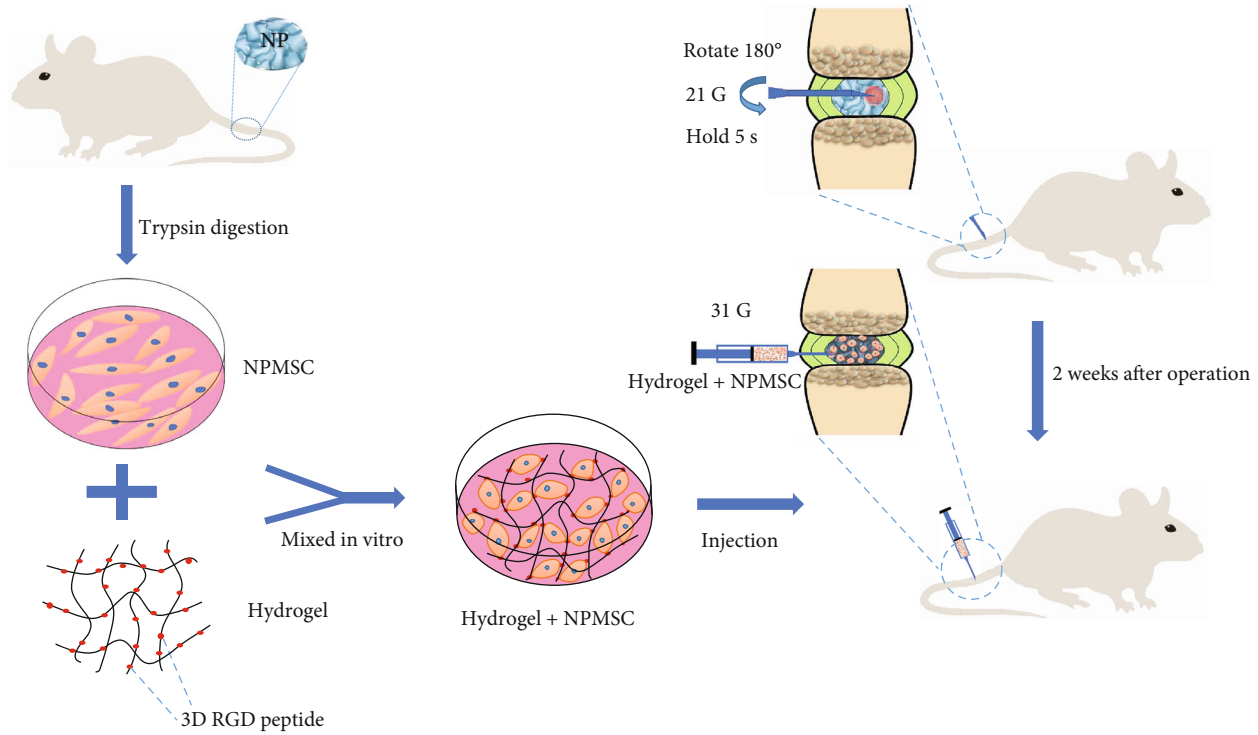

Figure 1: Schematic of the basic process of the present study. NPMSC were isolated from the coccygeal IVD of SD rats, and amplification was performed in vitro. After IDD model induction by a 21G needle, injectable hydrogel-loaded NPMSC was transplanted into the degenerated NP by a microsyringe.

impaired cell viability, cell proliferation ability, and biosynthesis ability of ECM [16, 17]. In 2007, Risbud et al. [18] confirmed the existence of endogenous progenitor cells in human NP. Other studies further confirmed that these kinds of endogenous NP-derived MSC (NPMSC) show a stronger tolerance to the harsh microenvironment compared with other types of MSC [19, 20]. NPMSC have got increasing attention and show remarkable prospects for the regeneration of degenerative IVD [21].

The survival of transplanted MSC is a major obstacle for MSC transplantation therapy [2]. MSC transplantation alone cannot improve the local adverse microenvironment [15]. The scaffold-loaded cell transplantation can not only transplant cells into the target locations but also create a suitable microenvironment for the better survival of transplanted MSC [22]. Due to the rheological and mechanical properties of hydrogel similar to those of the native NP [23, 24], injectable hydrogel has become the preferred material for NP repair. In this study, we aimed to investigate the regenerative effects of injectable hydrogel combined with NPMSC in a rat model of IDD. A schematic outline of the study is depicted in Figure 1.

2. Materials and Methods

2.1. Animal Care and Use. Seventy healthy Sprague-Dawley (SD) rats (weight, 180-220 g; age, 3-4 months) were provided by the Laboratory Animal Center of Jiangsu University (License no. SCXK (Su) 2018-0012). Animal care and use followed the guidelines of Laboratory Animals published by the US National Institutes of Health. All experiments were approved by the Institutional Animal Care and Use Committee of Yangzhou University. Animals were bred in a rat box at a controlled environment (26 ± 3°C, 12 : 12 h light/dark) with a relative humidity of 70-85%. Experimental animals were not restricted to get water and standard diet.

2.2. Isolation and Culture of NPMSC. Primary NPMSC were isolated from the coccygeal IVD tissues of twenty SD rats. The rats were killed by an overdose of pentobarbital, and their tails were taken. Coccygeal IVD were harvested under aseptic and light microscope conditions. The gel-like NP tissue sample was washed three times with phosphate-buffered saline (PBS) containing 1% penicillin-streptomycin (Gibco, MD, USA) and digested with 0.2% collagenase type II (Gibco, MD, USA) solution at 37°C for 2 h. After centrifugation at 800 g for 5 min, the cell pellets were cultured in MSC culture medium (Cyagen Biosciences, Guangzhou, China) supplemented with 20% fetal bovine serum (HyClone, UT, USA) and 1% penicillin/streptomycin at 37°C with 5% CO_2 of humidified atmosphere. The medium with suspension cells was removed after 1 day; then, the medium was completely changed twice a week. The cells were passaged at a 1 : 3 ratio at 80-90% confluence. After three passages, the NPMSC were used.

2.3. Immunophenotypic Characterization. In accordance with the appraisal standards of stem cells proposed by the International Society for Cellular Therapy (ISCT), the NP-progenitor cell surface marker Tie2 and the MSC surface

markers CD73, CD90, CD105, CD34, and CD45 were measured. Isotype controls (BD Biosciences, NJ, USA) were used in each case as the negative control. To put it simply, 2×10^5 NPMSC were incubated with monoclonal primary antibodies (CD105-phycoerythrin (PE), CD90-fluorescein isothiocyanate (FITC), CD73-PE, CD45-FITC, CD34-PE, and Tie2-FITC (BD Biosciences, NJ, USA)) for 30 min at room temperature in the dark. Then, cells were washed twice with cold PBS and resuspended in 500 μL PBS to produce a single cell solution, and specific surface marker expression was detected using flow cytometry (FACSCalibur, BD Biosciences).

2.4. Multipotent Differentiation. The multilineage differentiation potentials of NPMSC were characterized by osteogenic, adipogenic, and chondrogenic differentiation. Briefly, NPMSC were resuspended at a density of 5×10^5/mL and seeded in 6-well plates. When cultured cells reached 80% confluence, the cells were cultured with osteogenic, adipogenic, and chondrogenic differentiation kits (Cyagen Biosciences, Guangzhou, China). According to the manufacturer's instructions, after washing with PBS and fixing with 4% paraformaldehyde for 20 min, Alizarin red, Oil Red O, and Alcian blue were used when the differentiation reached the required days. Stained areas were observed under a fluorescence microscope (Leica, Wetzlar, Germany).

2.5. The Optimum Concentration of Hydrogels. VitroGel 3D-RGD hydrogel was purchased from TheWell Bioscience (NJ, USA). Cell Counting Kit-8 (CCK-8, Dojindo, Japan) and lactate dehydrogenase (LDH) assay kit (Beyotime Biotechnology, Haimen, China) were used to detect the optimum concentration of the hydrogel. The hydrogel solution was mixed directly with Hank's (HyClone, UT, USA) at 1 : 0, 1 : 1, 1 : 2, and 1 : 3 (hydrogel : Hank's, *v*/*v*) ratios at room temperature. NPMSC were resuspended at a density of 5×10^5/mL and mixed with different concentrations of hydrogels at the ratio of 1 : 4. Hydrogel-loaded NPMSC were cultured for 3, 7, and 14 days before determination. At each time point, CCK-8 solution (10% CCK-8 in fresh DMEM) was added and incubated at 37°C under 5% CO_2 for 3 h. The supernatant (100 μL) was collected and measured for the absorbance values at 450 nm. The cytotoxicity of different concentrations of hydrogel on NPMSC was detected using the LDH assay kit. The supernatant was collected at 3, 7, and 14 days and tested for the absorbance values at 450 nm by a microplate reader (Bio-Rad, Hercules, CA, USA).

2.6. Microstructure. As referred to the results above, the hydrogel was mixed with Hank's in the optimal concentration of hydrogel ratio; then, liquid medium was mingled with diluted hydrogels at the ratio of 1 : 4 at 37°C for 30 min. The specimens were lyophilized under vacuum and cut into small pieces with a thickness of 1 mm. Then, the samples were coated with gold and analyzed by a scanning electron microscope (SEM) at an accelerating voltage of 5 kV (SUPPA 55, ZEISS, Germany).

2.7. Cell Proliferation. For cell proliferation, 4′,6-diamidino-2-phenylindole (DAPI) and 5-ethynyl-2′-deoxyuridine (Edu) (Beyotime, Haimen, China) staining was used in in vitro 3D culture (hydrogel group) or 2D well plate culture (control group). Briefly, the cell suspension and hydrogel-loaded NPMSC were inoculated in 96-well plates (100 μL/well). After 1, 4, and 8 days after culture, cells were fixed with 4% paraformaldehyde for 10 min and washed, and then, cells were incubated with 100 μL DAPI at ambient temperature for 5 min. In addition, at 8 days after culture, cells of the two groups were incubated with Edu working solution as described by the manufacturer's protocol after being digested or released. The stained samples were photographed under a fluorescence microscope (Olympus Europe, Hamburg, Germany). ImageJ software (Wayne Rasband, National Institute of Health, USA) was used for image analysis. Three randomly selected fields from three samples were utilized for calculation.

2.8. Western Blot. NPMSC mixed with optimum concentration of hydrogel and inoculated (2.4 mL/well) in a 6-well plate was considered a hydrogel group, and NPMSC suspension cultured in the 6-well plate was considered a control group. Both groups were cultured in MSC differentiation kits (Cyagen Biosciences, Guangzhou, China) for 2 weeks. When the scheduled time reached, the cells were obtained and the total protein were extracted in RIPA buffer containing 1% PMSF on ice for 30 min. Protein supernatant was obtained by centrifugation for 20 min at 4°C, and protein concentration was measured using a bicinchoninic acid protein assay kit (Beyotime Institute of Biotechnology, Haimen, China). Following electrophoresis in 10% sodium dodecyl sulfate-polyacrylamide gel, the separated proteins were transferred onto polyvinylidene fluoride membranes (EMD Millipore, MA, USA). The membranes were blocked with 5% nonfat milk for 2 h at room temperature, then incubated with primary antibodies 12 h at 4°C. The primary antibodies were as follows: collagen type II (1 : 5000; Abcam, Cambridge, UK), aggrecan (1 : 1000; Abcam), and β-actin (1 : 10000; ABclonal, Wuhan, China). After washing three times with Tris-buffered saline and 0.1% Tween 20, the membranes were incubated with horseradish peroxidase- (HRP-) labeled secondary antibodies (Sanying, Wuhan, China) for 2 h on a shaker at room temperature. Bands were visualized using an enhanced chemiluminescence system. The relative amount of protein was analyzed using ImageJ software. β-Actin was used as the loading control.

2.9. IDD Model Induction and NPMSC Implantation. An SD rat IDD model was established according to the method reported in our previous study [25]. Briefly, the rats were anesthetized using intraperitoneal injection of 50-80 mg/kg pentobarbital. After sterilization with povidone iodine, coccygeal (Co) 5-6, Co6-7, Co7-8, and Co8-9 were percutaneously punctured by a 21G needle to a depth of 5 mm. Two weeks later, those different levels were divided into four groups: hydrogel+cell group (Co5-6, hydrogel-loaded NPMSC injection), hydrogel group (Co6-7, hydrogel injection only), PBS group (Co7-8, PBS injection only), and cell group (Co8-9, NPMSC injection only), while the Co4-5 level was designated as the control group.

To visualize the survival situation of transplanted NPMSC, the injected NPMSC expressing mCherry were generated. Following the manufacturer's protocol, when 50% confluence was reached, the cells were transfected with GV326 lentivirus vector-mCherry (GeneChem, Shanghai, China) at a multiplicity of infection (MOI) of 10, 20, 50, or 100. The fluorescence microscope was used to detect the expression of mCherry fluorescent protein 72 h later. Considering the transfection efficiency and cell damage, MOI = 100 was selected for succeeding infection. The NPMSC were transferred to a complete medium after 18 h of transfection. After 2 g/mL puromycin (Sigma-Aldrich, MO, USA) screening, the stably transfected NPMSC were used for transplantation. The 31G needle of a microsyringe was carefully inserted in the middle of the disc, and the volume of injection of each segment was 2 μL. The injection process was delayed for approximately 5 min to minimize leakage [26].

2.10. In Vivo Tracking. At 1 day and 30 days after injection, rats were anesthetized with the method as described above. After precooling the camera, anesthetized rats were sequentially placed in the in vivo imaging system (IVIS) chamber and the tail was placed in the center of panel. The IVIS Lumina III (Xenogen, CA, USA) was used to detect the signal intensity of mCherry fluorescent protein in the injected level (excitation wavelength: 587 nm; emission wavelength: 610 nm). The fluorescent signals were overlaid on a gray-scale of the rat and quantified as mean total radiant efficiency ([photons/s]/[mW/cm^2]) ± s.e.m. in a region of interest (ROI) via the Living Image software (PerkinElmer). The assured ROI was labeled at Co5-6 and Co8-9 where the NPMSC is transplanted. The total luminescence within ROI was procured from the overlaying luminescent images in the IVIS directory.

2.11. Radiographic Analysis. To assess the disc height, lateral radiographs of the coccygeal discs were taken preoperation, preinjection, and 1, 2, 4, and 8 weeks after injection under anesthesia as described above. Two independent imaging technologists who were blinded to the study design assessed the disc height index (DHI). According to the method of Han et al. [27], DHI% was calculated using the following formula: DHI% = (postpunctured DHI/prepunctured DHI) × 100%. The change of DHI expressed as DHI% (postinjection DHI/preinjection DHI) was used to describe disc height change.

MRI (3.0T, GE, CT, and US) taken preoperation, preinjection, and 1, 2, 4, and 8 weeks after injection was used to evaluate the signal and structural change. Shortly, the rats were anesthetized by intraperitoneal injection of 50-80 mg/kg pentobarbital and maintained by inhalation of 2% anesthetic isoflurane. Sagittal T2-weighted images were obtained in the following settings: (a) fast spin echo sequence with a time to repetition (TR) of 3000 ms and time to echo (TE) of 45 ms, (b) 9 excitations and 5 cm field of view, and (c) segment thickness of 0.5 mm with a 0 mm gap. The MRI images were evaluated by two radiologists who were blinded to the study design using the MRI index to evaluate the rehydration of NP tissue [28].

Table 1: Primers used for reverse transcription quantitative polymerase chain reaction.

Gene	Primer/probe sequence
Collagen type II	5′-CATCCCACCCTCTCACAGTT-3′
	5′-ACCAGTTAGTTTCCTGCCTCTG-3′
Aggrecan	5′-TCCACAAGGGAGAGAGGGTA-3′
	5′-GTAGGTGGTGGCTAGGACGA-3′
β-Actin	5′-GGACTTCGAGCAAGAGATGG-3′
	5′-GATGGAGTTGAAGGTAGTTTCG-3′

2.12. Histological Analysis. After MRI examination, the rats were killed by an intraperitoneal overdosage injection of pentobarbital and the tails were harvested at 4 weeks and 8 weeks after injection. The specimens were fixed with formaldehyde, decalcified with 10% ethylenediaminetetraacetic acid solution, and embedded in paraffin. Sections were stained with HE, safranin O (SO), and toluidine blue staining and then captured under a microscope. The degeneration score was evaluated by two independent observers as previously reported [11, 28].

2.13. Macroscopic Observation of IVD. At 8 weeks after injection, the rats were killed as described above and tails were obtained. After being washed with PBS, the surgical blade was used to separate the adjacent vertebrae along the middle of the disc under fluoroscopic guidance. The NP tissue was photographed, and the area in the cross section was analyzed by ImageJ software, which roughly represents the repair and regeneration of NP.

2.14. Terminal Deoxynucleotidyl Transferase-Mediated dUTP Nick End Labeling (TUNEL) Assay. IVD sections were obtained by the above method at 3 days after operation and 4 weeks and 8 weeks after injection; apoptosis-related DNA damage was evaluated by TUNEL staining. In brief, after being fixed in 4% paraformaldehyde solution for 30 min at 37°C, permeabilized in a solution containing 0.5% Triton X-100 for 5 min, and washed twice with PBS, sections were stained with freshly prepared TUNEL working liquid (Beyotime, Haimen, China) at room temperature for 1 h in the dark. Afterward, the sections were washed and stained with Fluorochrome DAPI (Beyotime, Haimen, China) for 10 min. The results were photographed by a fluorescence microscope and analyzed by ImageJ software.

2.15. Immunofluorescent Staining. The rats were killed as described above and the tails were obtained. The specimens of the whole IVD with adjacent vertebral bodies were harvested and cut into 5 μm with a freezing microtome (Leica, Wetzlar, Germany) at 8 weeks after injection. After being fixed in 4% paraformaldehyde for 30 min, washed twice with PBS, and blocked in 5% bull serum albumin for 1 h, the tissue sections were incubated, respectively, overnight with primary antibodies at 4°C: rabbit polyclonal anti-collagen type II and anti-aggrecan (1 : 100, Abcam, Cambridge, UK). After washing with PBS, slides were incubated, respectively,

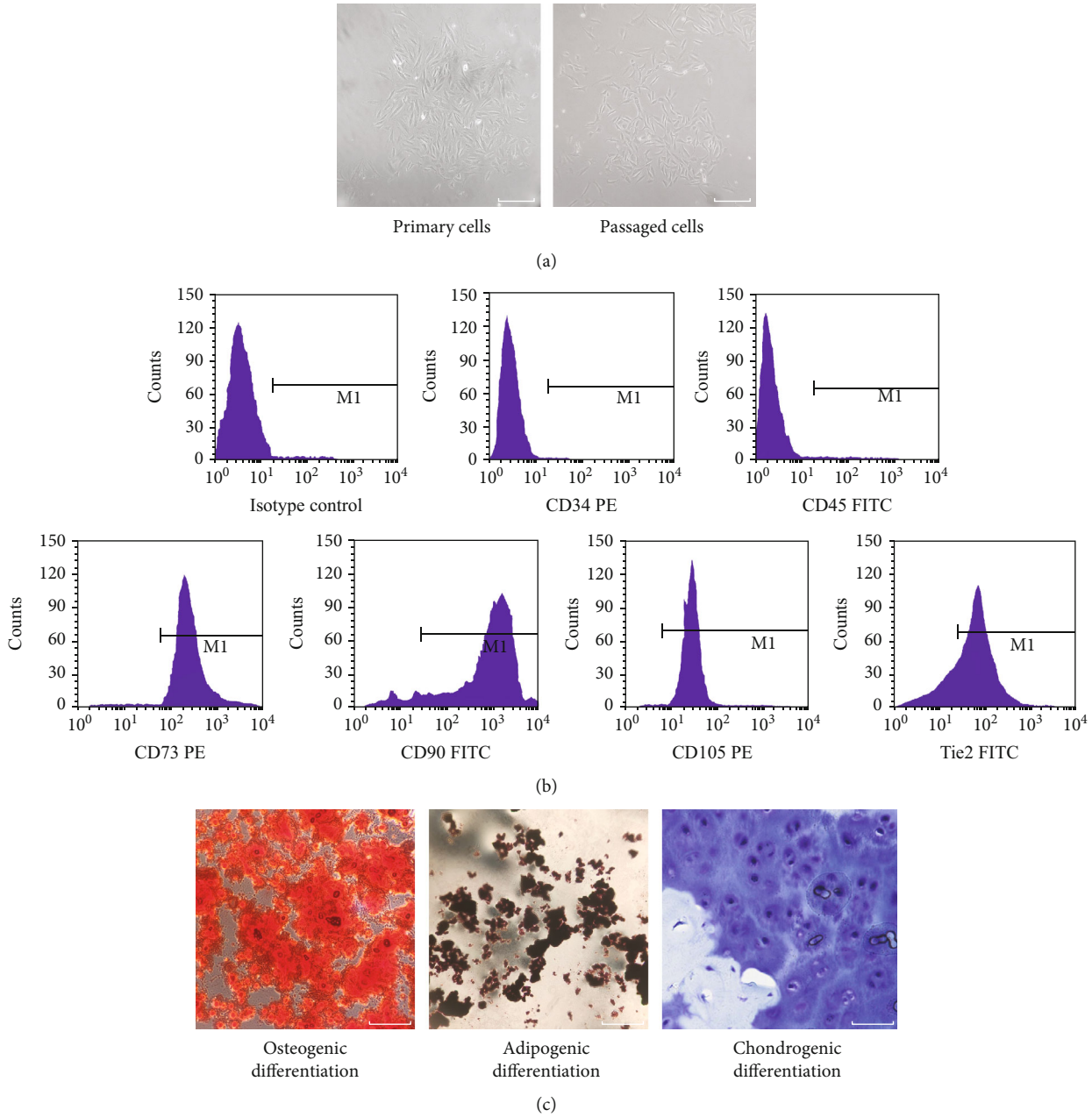

Figure 2: Identification of nucleus pulposus-derived mesenchymal stem cells (NPMSC). (a) Isolated primary cells presented with a long spindle shape and showed colony growth; the passaged cells were spindle-shaped. (b) NPMSC had higher expressions (>98%) of MSC surface markers CD73, CD90, and CD105 and lower expressions (<2%) of hematopoietic stem cell surface markers CD34 and CD45 and higher expressions (>80%) of Tie2. (c) NPMSC was positive for Alizarin red, Oil Red O, and Alcian blue staining after induced differentiation. White scale bar = 50 μm.

with FITC-conjugated and Cy3-conjugated goat anti-rabbit IgG (1 : 10000, ABclonal, Wuhan, China) secondary antibodies for 2 h at room temperature in the dark. The immunostaining results were photographed by a fluorescence microscope and analyzed by Image-Pro Plus 6.0 software.

2.16. Real-Time Polymerase Chain Reaction (RT-PCR). Quantification of collagen type II and aggrecan mRNA levels was conducted using RT-PCR at 8 weeks after injection. Total RNA was extracted using a TRIzol reagent (Invitrogen, Carlsbad, CA, USA). According to the instructions, the PrimeScript RT reagent kit and SYBR Premix Ex Taq (Vazyme Biotech, Nanjing, China) were used to transcribe reversely RNA to cDNA and amplify the cDNA. The mRNA expression levels of collagen type II and aggrecan were calculated by the comparative Ct method. Primer sequences are listed in Table 1.

2.17. Statistical Analysis. The quantitative data were expressed as the mean ± standard deviation (SD). The SPSS software (version 19.0 for Windows, SPSS, IL, US) was used to conduct statistical analysis. The data of multiple

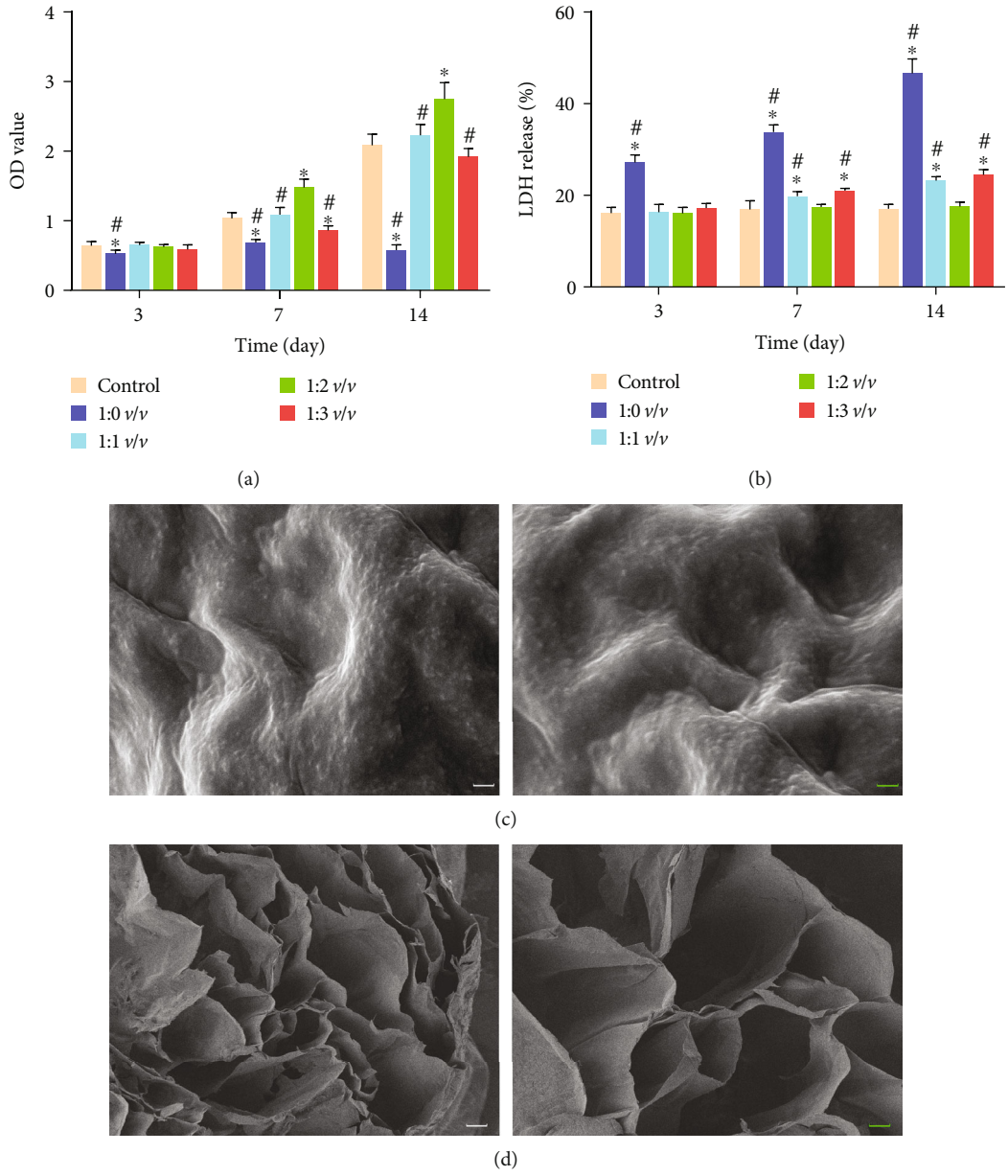

Figure 3: The proper concentration of hydrogel and microstructure of the hydrogel. (a) The proliferation of NPMSC cultured in different concentrations of hydrogels. (b) The cytotoxicity of different concentrations of hydrogel for NPMSC. (c) SEM image of the 1 : 2 *v*/*v* hydrogel surface. (d) Cross sections of 1 : 2 *v*/*v* hydrogel. Data represent mean ± SD; the error bars represent the standard deviation of measurements for 6 separate samples ($n = 6$); $^{*}p < 0.05$ compared with control group; $^{\#}p < 0.05$ compared with 1 : 2 *v*/*v* group. White scale bar = 100 μm, blue scale bar = 50 μm.

independent groups was analyzed by one-way ANOVA. The LSD *t*-test was used to analyze the data of two group parameters. When the *p* value is less than 0.05, the difference was considered significant.

3. Result

3.1. Evaluation of Isolated Cells. Cells isolated from rat coccygeal IVD tissues presented with a long spindle shape and showed colony growth, indicating the ability to adhere to plastic (Figure 2(a)). As shown in Figure 2(b), flow cytometry identified that the cells highly expressed CD105 (98.22%), CD90 (97.54%), and CD73 (97.55%) which are usually positive in MSC and inferiorly expressed CD34 (1.42%) and CD45 (0.95%) which are negative in MSC, while the cells highly expressed Tie2 (81.76%) which is positive in NP-progenitor cells. The multilineage differentiation was certified by induction into the osteogenic, chondrogenic, and adipogenic lineages in vitro (Figure 2(c)). All results showed that the cells corresponded to the evaluation criteria of MSC described by the ISCT.

3.2. Proper Concentration of the Hydrogel and Microstructure of the Hydrogel. As shown in Figure 3(a), the cell viability of

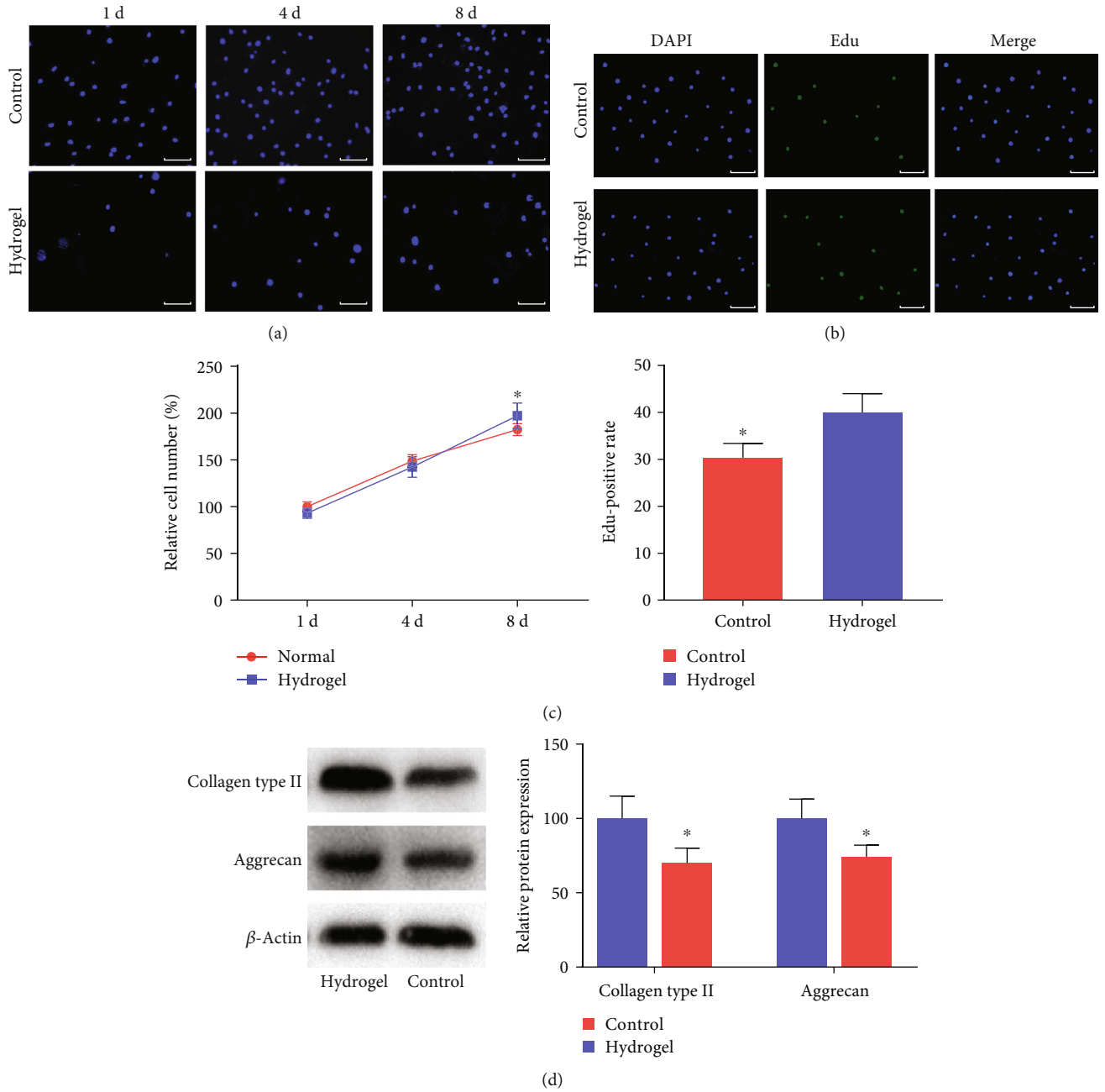

Figure 4: Cell proliferation and differentiation. (a) Representative images of DAPI staining for 2D (control group) and 3D (hydrogel group) cultured NPMSC at 1, 4, and 8 days after cultivation. (b) Representative images of Edu staining for 2D (control group) and 3D (hydrogel group) cultured NPMSC at 8 days after cultivation. (c) Investigation of growth rate and Edu-positive rate of NPMSC culture for 8 days in the control group and hydrogel group. (d) Relative protein levels of collagen type II and aggrecan in the control group and hydrogel group. Data represent mean ± SD; the error bars represent the standard deviation of measurements for 3 separate samples ($n = 3$); $^*p < 0.05$ compared with the hydrogel group. White scale bar = 50 μm.

all other groups was not significantly different from the control group except the 1 : 0 *v*/*v* group at day 3. Nonetheless, the cell viability of the 1 : 2 *v*/*v* group was significantly higher than those of other groups at days 7 and 14. In addition, the released LDH reflected the cytotoxicity of hydrogel. The LDH of the 1 : 0 *v*/*v* group was higher than those of the other groups, and the difference was statistically significant. The LDH of the 1 : 1 *v*/*v* group and 1 : 3 *v*/*v* group were higher than that of the control group at day 14. But there was no significant difference between the 1 : 2 *v*/*v* group and the control group at each time point of LDH (Figure 3(b)). As shown in Figures 3(c) and 3(d), the hydrogel at the concentration of 1 : 2 *v*/*v* displayed an irregular porous structure and the pores were well connected which would facilitate cell migration. Hence, the optimum concentration of hydrogel for NPMSC was identified as 1 : 2 *v*/*v*.

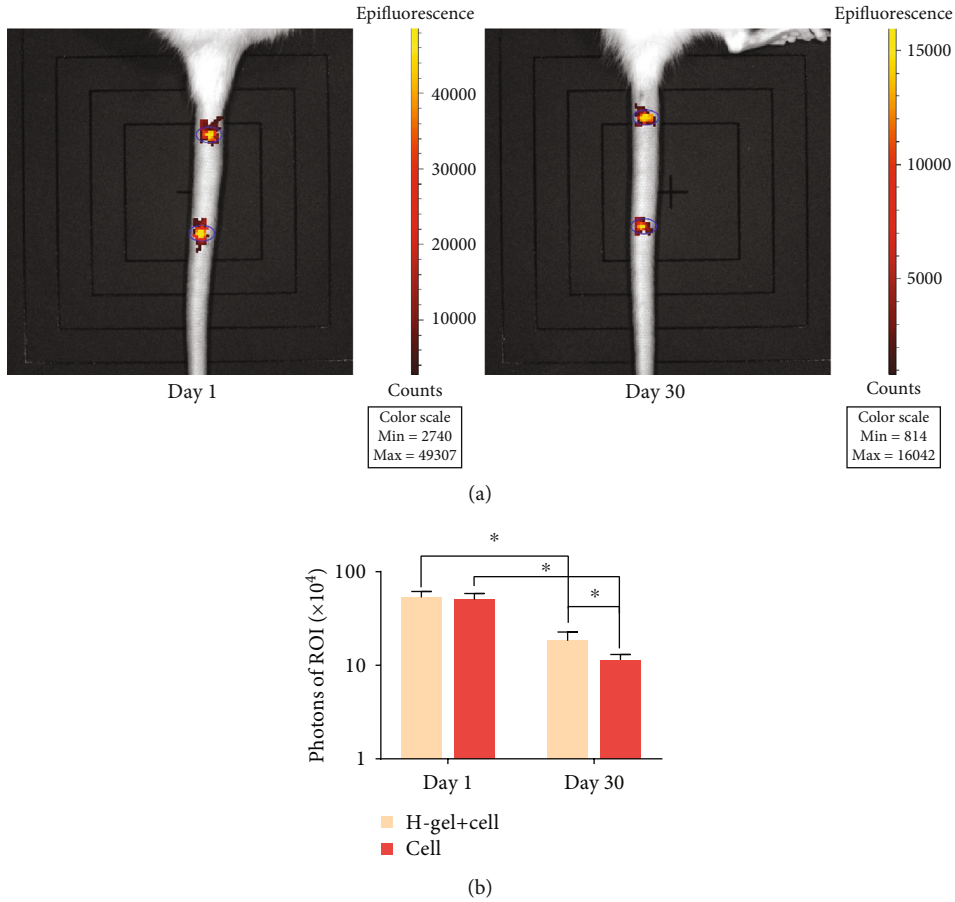

Figure 5: Cell retention in the IVD. (a) Representative images of IVIS at day 1 and day 30 after injection. (b) The histogram of luminescence of the hydrogel+cell group and cell group in the ROI in overlaying images. ROI was represented by a blue circle. The H-gel+cell group is the hydrogel+cell group. Data represent mean ± SD; the error bars represent the standard deviation of measurements for 3 separate samples ($n = 3$); $^*p < 0.05$ compared with the hydrogel+cell group.

3.3. Cell Proliferation and Differentiation. The proliferation of NPMSC cultured in the well plate and hydrogel was determined by cell number counting and the Edu method. The cell number of both groups increased gradually at each time point (Figure 4(a)). There was no significant difference between the two groups in terms of cell proliferation rate at day 4; however, the cell growth rate of the hydrogel group was significantly higher than that of the control group at day 8 (Figure 4(c)). At 8 days after culture, the rate of Edu-positive cells in the hydrogel group was significantly higher than that of the control group (Figures 4(b) and 4(c)). Collagen type II and aggrecan are specific extracellular matrices (ECM) of NP cells. The relative protein expressions of collagen type II and aggrecan in the hydrogel group were significantly higher than those of the control group (Figure 4(d)).

3.4. Cell Survival in the Transplanted IVD. To visualize the survival situation of transplanted NPMSC in vivo, the IVIS system was used to detect the luminescence of ROI after 1 day and 30 days after injection. As shown in Figures 5(a) and 5(b), there was no significant difference in the luminescence of defined ROI between the hydrogel+cell group and the cell group at 1 day after injection. The photons of both groups decreased significantly with time, and the luminescence of ROI in the hydrogel+cell group was significantly stronger than that of the cell group at 30 days after injection. Thus, it was indicated that hydrogel can be used as a carrier to support the long-term survival of NPMSC in vivo.

3.5. Radiographic and MRI Evaluation. To explore the degree of IDD after injection, the DHI% was calculated. As shown in Figures 6(a) and 6(b), the DHI% remained stable in the control group at each time point. The DHI% in all other groups were significantly lower than that of the control group after injection. There was no significant difference among different groups at 1 week and 2 weeks after injection. The DHI% of the hydrogel+cell and cell groups were significantly higher than those of the PBS group and hydrogel group at 4 weeks and 8 weeks after injection. In addition, there was no significant difference between the hydrogel+cell group and cell group at 2 weeks and 4 weeks after injection, but a significant difference at 8 weeks.

The MRI was used to evaluate the signal and structural change of NP tissue (Figures 7(a) and 7(b)). The MRI indexes of the PBS group and hydrogel group were lower than those of the hydrogel+cell group and cell group at 2, 4, and 8 weeks after injection. Additionally, there was no significant difference between the hydrogel+cell group and the cell group at

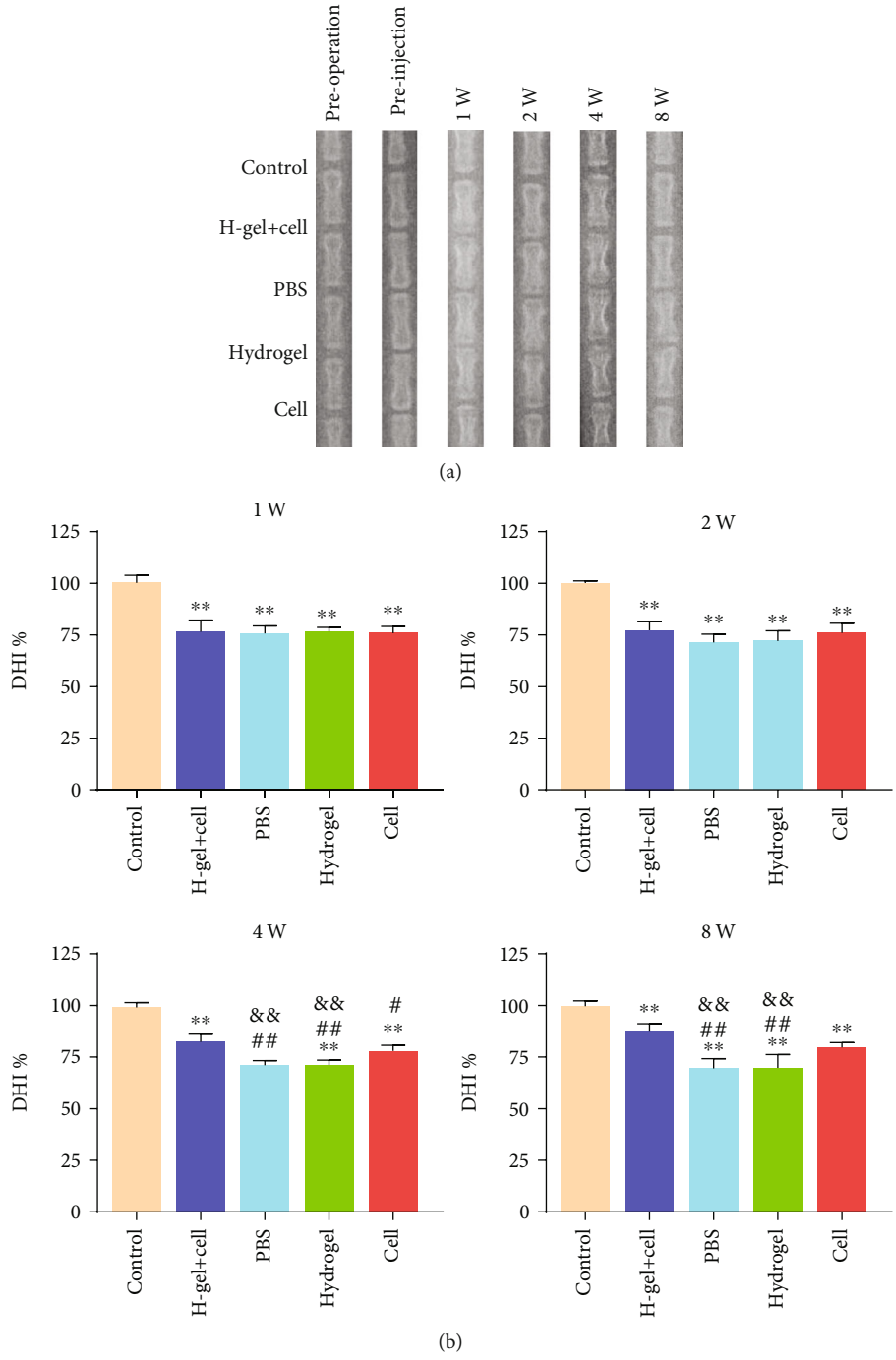

Figure 6: Typical radiographs and DHI% of different groups preoperation, preinjection, and 1, 2, 4, and 8 weeks after injection. (a) The radiographs of different groups. (b) DHI% was applied to quantitatively evaluate the changes of disc height. The H-gel+cell group is the hydrogel+cell group. All data are expressed as the mean ± SD; the error bars represent the standard deviation of measurements for 6 separate samples ($n = 6$); $^{*}p < 0.05$, $^{**}p < 0.01$ compared with control group; $^{\#}p < 0.05$, $^{\#\#}p < 0.01$ compared with hydrogel+cell group; $^{\&}p < 0.05$, $^{\&\&}p < 0.01$ compared with cell group.

1 and 2 weeks after injection, but a significant difference at 4 and 8 weeks after injection.

3.6. Histological Analysis and Macroscopic Observation of IVD. HE staining (Figure 8(a)) showed that NP tissue was well organized and homogeneous in the control group at each point after injection. In the contrary, NP tissue was destroyed or even disappeared, and AF tissue was disorganized and lost its concentric lamellar structure in the PBS group and hydrogel group. The NP tissue almost disappeared and was filled with fibrillar connective tissues in the PBS group and hydrogel group at 8 weeks after injection. The structure of NP and ECM distributions was clearly visible in the hydrogel+cell group and cell group, but the quantity and structure of the

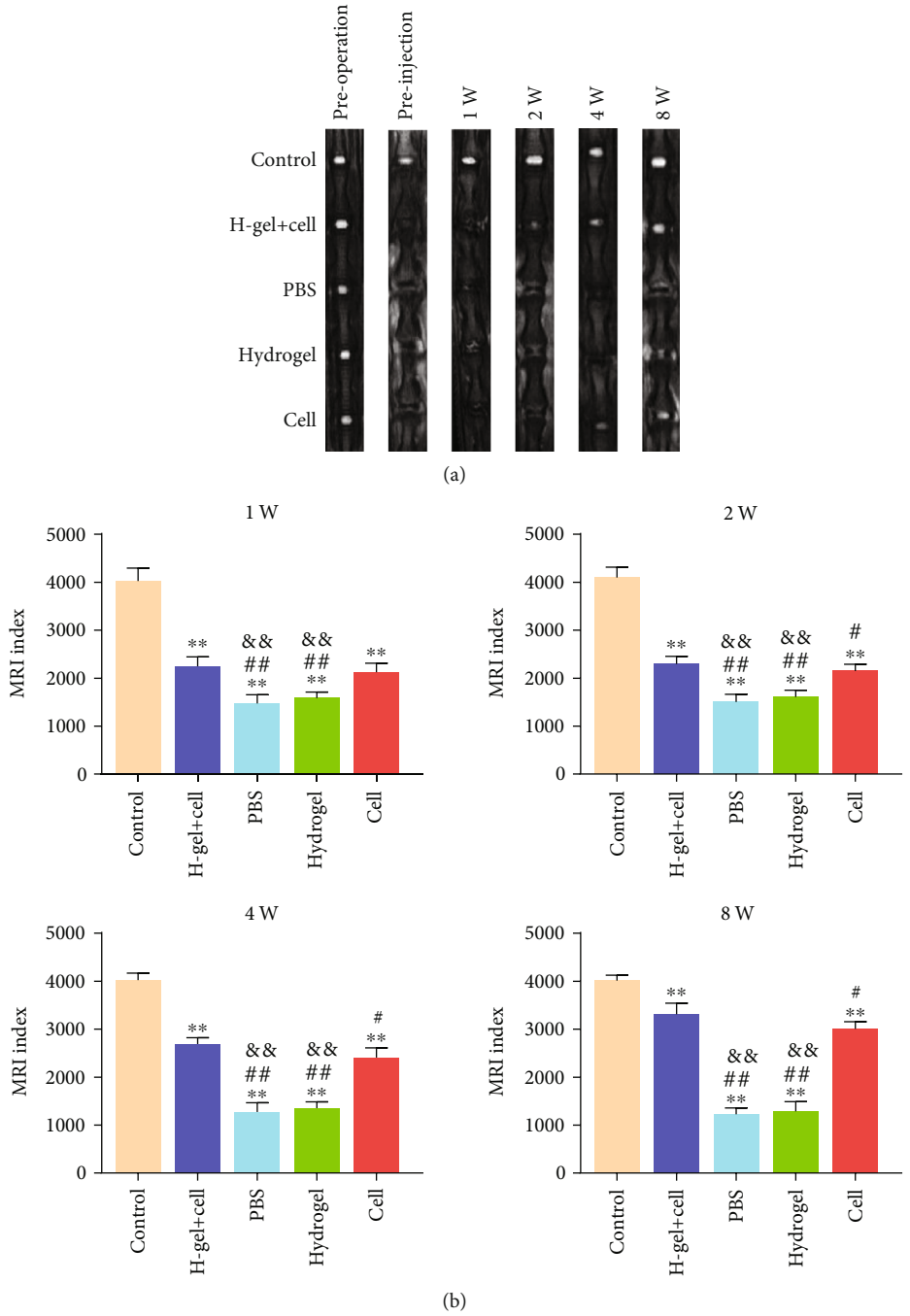

FIGURE 7: MRI images and MRI index of different groups. (a) Typical T2-weighted MRI images of different groups preoperation, preinjection, and 1, 2, 4, and 8 weeks after injection. (b) The MRI index was applied to quantitatively evaluate the rehydration and regeneration of degenerative disc. The H-gel+cell group is the hydrogel+cell group. All data are expressed as the mean ± SD; the error bars represent the standard deviation of measurements for 6 separate samples ($n = 6$); $^{*}p < 0.05$, $^{**}p < 0.01$ compared with control group; $^{\#}p < 0.05$, $^{\#\#}p < 0.01$ compared with hydrogel+cell group; $^{\&}p < 0.05$, $^{\&\&}p < 0.01$ compared with cell group.

ECM in the hydrogel+cell group were much better than those of the cell group. S-O staining (Figure 8(b)) showed that the proteoglycan levels decreased significantly in the PBS group and hydrogel group, but the hydrogel+cell group and cell group exhibited stronger staining than the PBS group and hydrogel group. Additionally, the hydrogel+cell group exhibited stronger staining than the cell group. Toluidine blue staining revealed that the hydrogel+cell group and cell group exhibited more NP chondrocytes and positive proteoglycan staining than the PBS group and hydrogel group (Figure 8(c)). In addition, the staining intensity of the hydrogel+cell group was better than that of the cell group. The histological scores of all other groups were significantly higher than that of the control group at 8 weeks after injection, but the histological score of the hydrogel+cell group was lower than that of the cell group (Figure 9(c)). Except for the

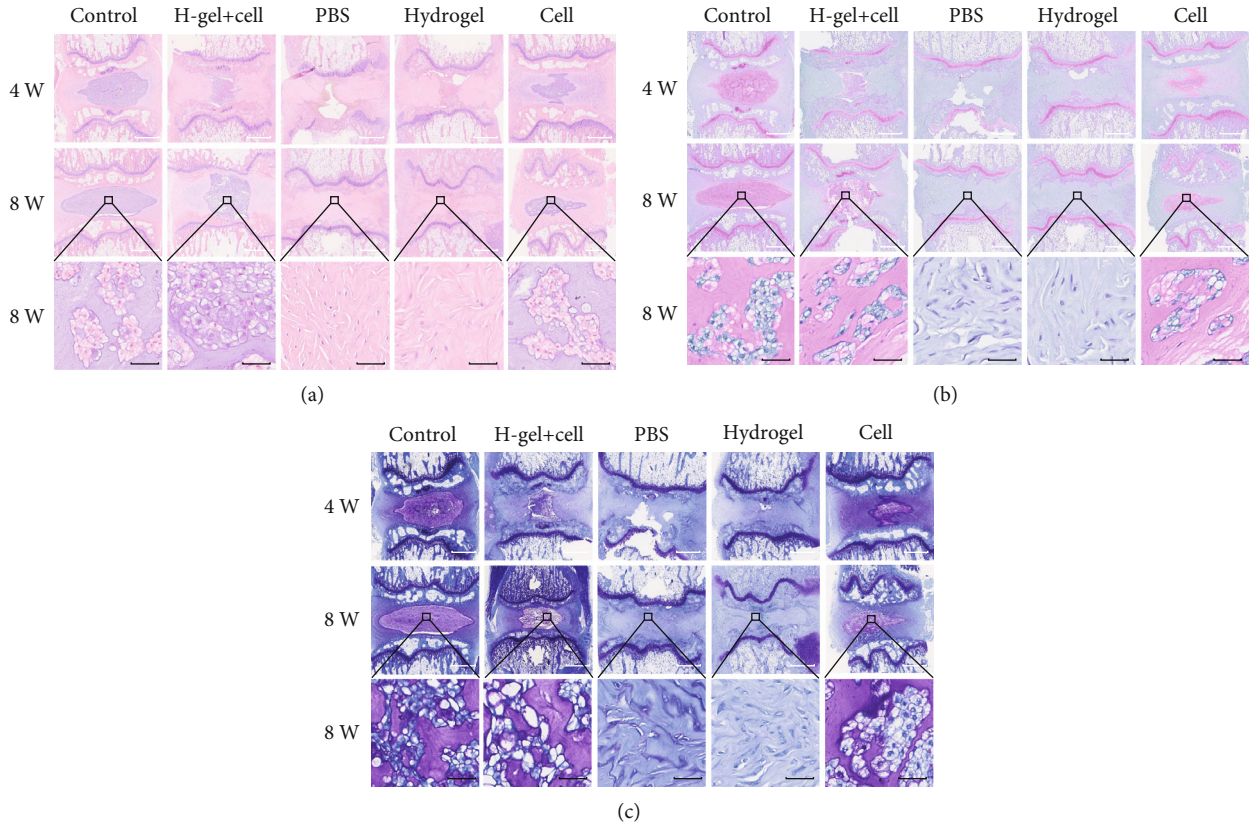

Figure 8: HE, S-O, and toluidine blue staining of different groups. (a) Representative HE staining at 4 and 8 weeks after injection. (b) Representative S-O staining at 4 and 8 weeks after injection. (c) Representative toluidine blue staining at 4 and 8 weeks after injection. The H-gel+cell group is the hydrogel+cell group. White scale bar = 1 mm, black scale bar = 50 μm.

hydrogel+cell group and control group, the histological score of the cell group was better than those of the other groups.

As shown in Figure 9(a), the shape of AF was regular and the NP tissue was abundant and rich in water in the control group at 8 weeks after injection. In the PBS group and hydrogel group, the structure of AF was disordered and the area of the NP was significantly reduced and replaced by fibrous tissue. Although the AF tissue was significantly thicker and the area of the NP was significantly reduced, the boundary between the AF and NP was clearer in the hydrogel+cell group and cell group than in the PBS group and hydrogel group. As shown in Figure 9(b), the relative areas of the NP tissue in the hydrogel+cell group and cell group were significantly larger than those of the PBS group and hydrogel group. Furthermore, the relative area of the NP tissue in the hydrogel+cell group was larger than those in the other groups except the control group.

3.7. The Cell Apoptosis Analysis. To elucidate the effect of needle puncture molding and hydrogel in a rat tail disc, we performed TUNEL staining for NP cells and NPMSC. At 3 days after operation, the rate of TUNEL-positive cells in other groups was significantly higher than that of the control group (Figure 10(a)). At 4 weeks after injection, the rate of TUNEL-positive cells decreased significantly and the TUNEL-positive cell rates in the hydrogel+cell group and cell group were lower than those of the hydrogel group and PBS group (Figure 10(b)). With the regeneration of NP tissue and the formation of scar tissue, the rate of TUNEL-positive cells in all groups was significantly lower than those before and there was no significant difference among the groups at 8 weeks after intervention (Figure 10(c)).

3.8. Immunofluorescence and RT-PCR Analysis. The protein and mRNA expressions of collagen type II and aggrecan were detected at 8 weeks after injection. There were expressions of collagen type II and aggrecan in the control group, hydrogel +cell group, and cell group (Figure 11(a)). Since the normal structure of NP disappeared in the PBS group and hydrogel group, only the smallest area of the NP tissue was found to be positive for collagen type II and aggrecan (Figure 11(a)). As shown in Figures 11(b) and 11(c), the quantitative analysis was significantly higher in both collagen type II and aggrecan in the hydrogel+cell group and cell group than in those in the PBS group and hydrogel group, but significantly lower than those in the control group. The quantitative analysis was higher in collagen type II and aggrecan in the hydrogel +cell group than in those in the other groups except the control group.

4. Discussion

Currently, conservation and surgical treatments are often used to treat IDD, but those methods can only relieve

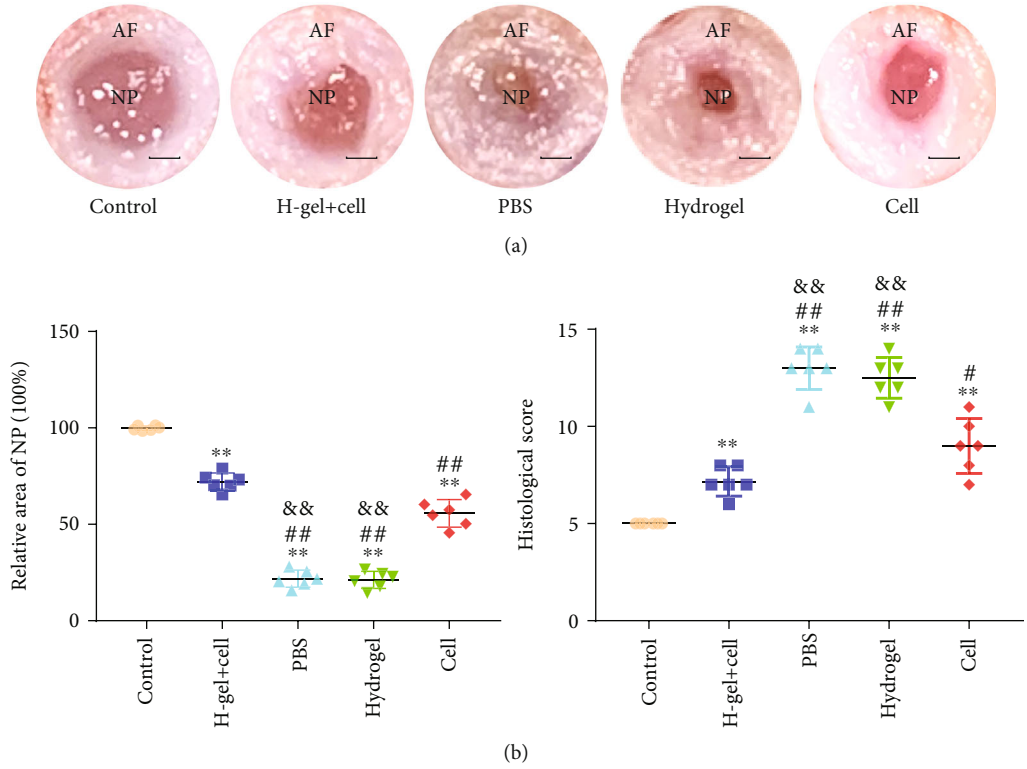

Figure 9: Macroscopic observation and histological score of different groups. (a) Macroscopic images of different groups at 8 weeks after injection. (b) The relative area of nucleus pulposus at 8 weeks after injection. (c) Histological scores obtained at 8 weeks after injection. The H-gel+cell group is the hydrogel+cell group. Data represent mean ± SD; the error bars represent the standard deviation of measurements for 6 separate samples ($n = 6$); $^{*}p < 0.05$, $^{**}p < 0.01$ compared with control group; $^{\#}p < 0.05$, $^{\#\#}p < 0.01$ compared with hydrogel+cell group; $^{\&}p < 0.05$, $^{\&\&}p < 0.01$ compared with cell group. Scale bar = 1 mm.

symptoms and may even aggravate the possibility of adjacent IDD [6, 29, 30]. Cell transplantation-based biological therapy may be more beneficial to repair and restore the biomechanical function of IVD. Although implanted, autologous NP cells could remain viable, produce ECM, and retain disc height in the degenerative human IVD in an ex vivo study [31]. However, several studies showed that the NP cell lost its ability to differentiate and synthesize ECM [32] and thus has limited application.

MSC have the ability to self-renew and multilineage differentiation; some types of MSC can differentiate into nucleopulpocytes (NPCytes) and produce ECM in the degenerated IVD [10–13]. So far, a variety of MSC have been used [10–13, 33, 34], but the harsh microenvironment of the degenerative IVD [35–37] result in reduced cell viability and ECM synthesis of transplanted MSC [38]. Recently, NPMSC was isolated from normal and degenerate NP tissue and displayed preferable proliferation and better ability to adapt to the harsh IVD microenvironment [39, 40]. Hence, NPMSC may have considerable potential for regenerating IDD. In the present study, the cells isolated from NP had the following characteristics: (1) presenting with spindle-shaped adherent growth and growing in colony formation, (2) higher expressions of CD73, CD90, and CD105 (>95%) and lower expressions of CD34 and CD45 (<5%), (3) higher expressions (>80%) of the NP-progenitor cell surface marker Tie2, and (4) having multilineage differentiation potential. These characteristics met the criteria stated by the ISCT for MSC. Combined with the isolated methods [41, 42], immunophenotypic characterization [9], and cellular morphology [43], the isolated cells were NPMSC indeed.

Both in vitro and in vivo animal studies have demonstrated that MSC exert its regenerative effect in the following ways: (1) differentiating into NPCytes, (2) activating endogenous cells, and (3) producing an anti-inflammatory effect [44–46]. In the present study, X-ray, MRI, and macroscopic observation results demonstrated the regenerative effectiveness of the transplanted NPMSC. The histological staining results also confirmed that IVD with transplanted NPMSC present more regular IVD structure and more ECM. The results of immunofluorescence and RT-PCR further confirmed that the expressions of collagen type II and aggrecan in the NPMSC-transplanted groups (hydrogel+cell group and cell group) were significantly higher than those in the groups without NPMSC (PBS group and hydrogel group). In addition, the transplanted NPMSC survived in the transplanted IVD for at least 30 days visualized by the IVIS system. Those results indicated that NPMSC can survive and produce regenerative effect in the transplanted degenerative IVD.

NPMSC have the potential to differentiate into NPCytes [34], but the harsh microenvironment of the degenerated IVD present a major challenge to insure the survival and function of the implanted cells. Some studies even showed

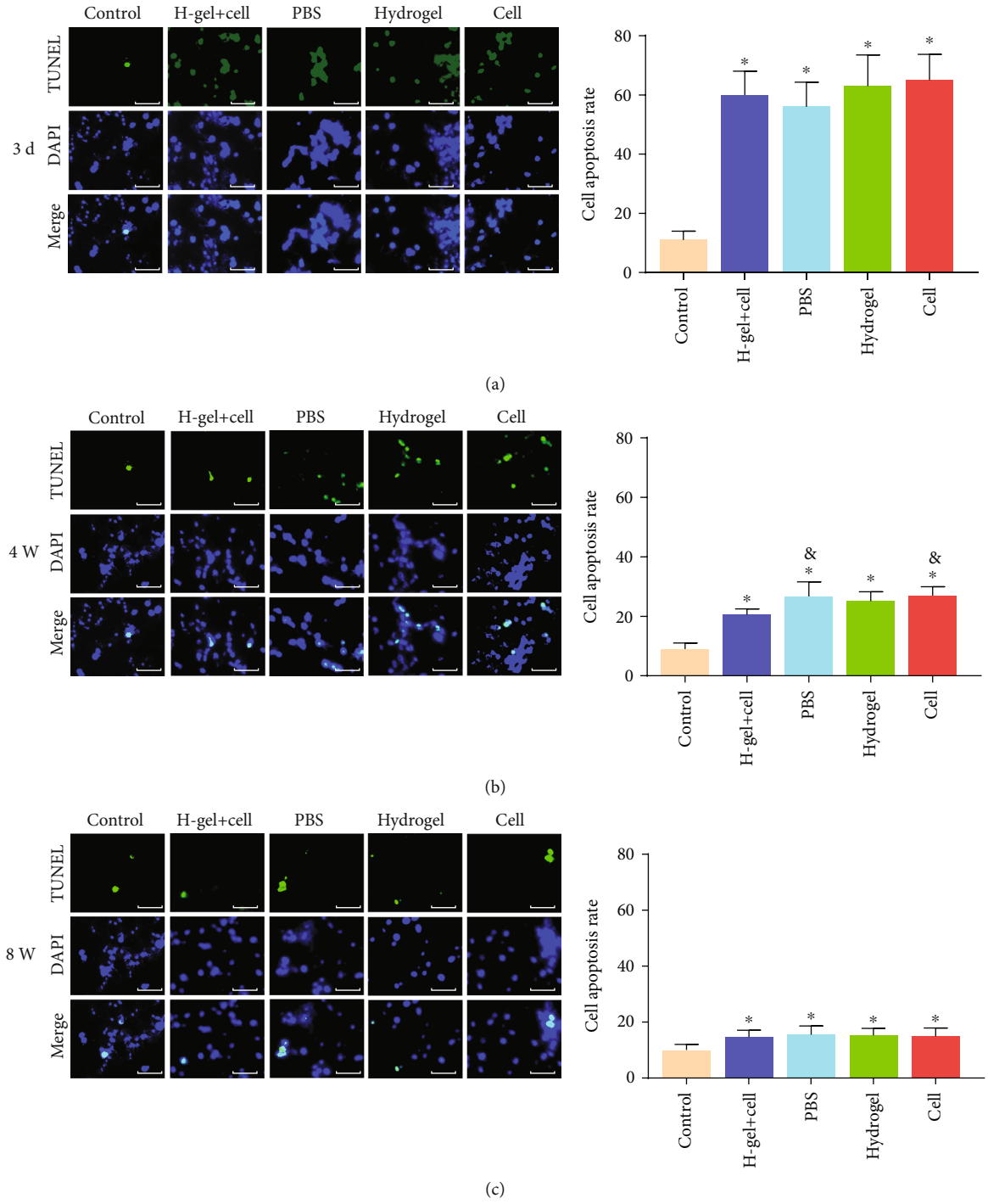

Figure 10: TUNEL staining of different groups. (a) Representative images and the percentage of TUNEL-positive cells in NP tissues at 3 days after operation. (b) Representative images and the percentage of TUNEL-positive cells in NP tissues at 4 weeks after injection. (c) Representative images and the percentage of TUNEL-positive cells in NP tissues at 8 weeks after injection. The H-gel+cell group is the hydrogel+cell group. Data represent mean ± SD; the error bars represent the standard deviation of measurements for 6 separate samples ($n = 6$); $^{*}p < 0.05$ compared with control group; $^{\&}p < 0.05$ compared with hydrogel+cell group. Scale bar = 200 μm.

that MSC injected without scaffolds had no regeneration effect [47]. Injecting NPMSC into the IVD tissue has demonstrated its ability to regenerate the degenerative IVD at some degree in the previous and present studies [34]. However, significant obstacles to successful cell therapy still remain, such as leakage of MSC into IVD surroundings, osteophyte formation, and no improvement of IVD height [48]. Therefore, a preferred option may be to encapsulate MSC into a carrier to protect cell leakage and provide a suitable environment to support MSC expansion and differentiation [49]. For this reason, hydrogels are considered an ideal and popular choice to load cells.

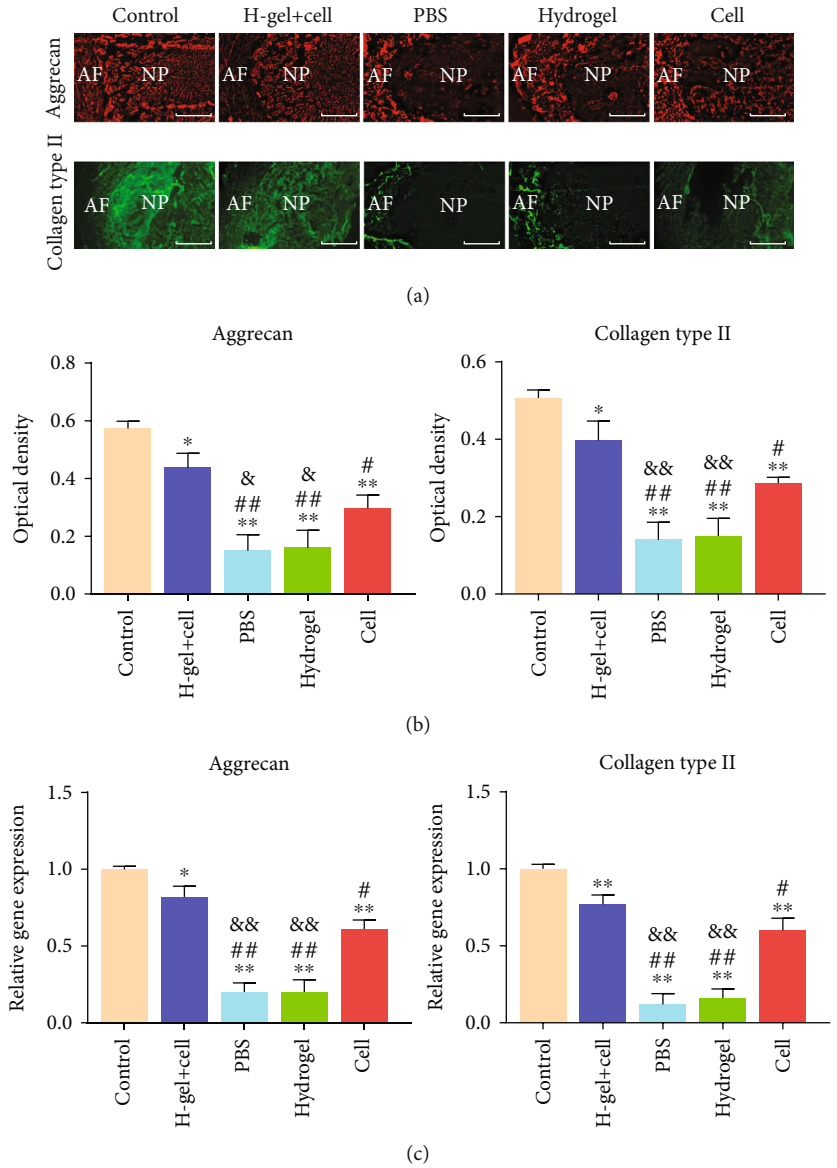

Figure 11: Immunofluorescence and RT-PCR of different groups. (a) Immunofluorescence detection of collagen type II and aggrecan of different groups at 8 weeks after injection. (b) The quantitative analysis of immunofluorescence staining. (c) Gene expression of collagen type II and aggrecan of different groups at 8 weeks after injection. Data represent mean ± SD; the error bars represent the standard deviation of measurements for 3 separate samples ($n = 3$); $^{*}p < 0.05$, $^{**}p < 0.01$ compared with control group; $^{\#}p < 0.05$, $^{\#\#}p < 0.01$ compared with hydrogel+cell group; $^{\&}p < 0.05$, $^{\&\&}p < 0.01$ compared with cell group.

Although several studies have focused on the study of IVD cells and MSC transplantation for the treatment of IDD [10, 13, 34], this study was the first to combine allogeneic NPMSC and injectable hydrogel for the treatment of IDD. Several studies have shown that a scaffold with low stiffness is more beneficial for NP-like differentiation [50]. In this study, a polysaccharide hydrogel modified with 3D RGD peptide was used, which can mimic the condition of the natural ECM of NP and provide binding sites for cells. The RGD peptide creates cell-adhesive structures in the hydrogel and greatly increases the long-term cell viability in 3D cultures [51]. The result of in vitro study showed that the hydrogel concentration of 1 : 2 *v*/*v* was most suitable for cell proliferation. This may be attributed to the fact that high crosslinking hydrogel can hinder the nutrient transport, but the low crosslinking hydrogel is less relatively rigid to provide a good scaffold for cells. Some studies found that 3D culture and spherical cell morphology could promote the viability and differentiation of loaded cells [52, 53]. The present study also demonstrated that the hydrogel can promote NPMSC proliferation and induce it to differentiate in vitro confirmed by the results of cell counting and quantified analysis of collagen type II and aggrecan. The result of cell tracking further indicated that the luminescence of ROI in the hydrogel+cell group was significantly stronger than that in the cell group, and the rate of TUNEL-positive cells in the hydrogel+cell group was lower than that in the cell group. All those results indicated that hydrogel used as a carrier in the present study

can support the long-term survival of NPMSC in vivo and induce NPMSC to differentiate into NP cells.

The amounts of ECM and hydration state of the NP are of great importance to the function of normal IVD. There were increased expressions of collagen type II and aggrecan in the hydrogel+cell group compared with the cell group. MRI index can be considered an indirect indicator to reflect the hydration state of NP tissue. There was also a significantly higher MRI index in the hydrogel+cell group compared with the cell group. However, the hydrogel alone did not regenerate the NP tissue as illustrated in the hydrogel group. Those results indicated that hydrogel can promote the regenerative effect of the transplanted NPMSC to enhance ECM synthesis, and the hydrogel used in the present study can increase the effect of the transplanted NPMSC on the hydration of degenerative IVD. In addition, being preliminary, this study still has some limitations. First, the use of a rat model of IDD cannot fully reflect the natural course of human IDD; it may be more representative to use large animals as models. Second, there is no related research on the mechanical properties of the hydrogel, which is critical for the dispersion of the IVD stress. Third, short experimental duration of this study is insufficient to reflect the complete effect of the hydrogel-loaded NPMSC transplantation on the repair of degenerative IVD; future studies should extend the experiment duration to a longer time.

5. Conclusion

This study demonstrated that the hydrogel modified with 3D RGD peptide could promote the proliferation and differentiation of NPMSC in vitro. Moreover, the hydrogel could promote NPMSC's long-term retention and survival in the degenerative IVD and ECM secretion. NPMSC-alone transplantation could repair degenerative IVD to a certain extent, but the hydrogel-loaded NPMSC offered a better effective and promising therapeutic strategy for IVD regeneration. Therefore, hydrogel combined with NPMSC has a potential therapeutic value in the regeneration of IVD.

Data Availability

The data used to support the findings of this study are available from the corresponding authors upon request.

Disclosure

No benefits in any form have been or will be received from a commercial party related directly or indirectly to the subject of this manuscript.

Conflicts of Interest

The authors declare no conflicts of interest.

Acknowledgments

Thanks are due to Clinical Medical College and Veterinary College of Yangzhou University for supporting this study. Funding for this research was provided by the National Natural Science Foundation of China (grant no. 81401830) and Young Medical Scholars Major Program of Jiangsu Province (grant number QNRC2016342).

References

[1] W. F. Stewart, J. A. Ricci, E. Chee, D. Morganstein, and R. Lipton, "Lost productive time and cost due to common pain conditions in the US workforce," *JAMA*, vol. 290, no. 18, pp. 2443–2454, 2003.

[2] D. Sakai and G. B. J. Andersson, "Stem cell therapy for intervertebral disc regeneration: obstacles and solutions," *Nature Reviews Rheumatology*, vol. 11, no. 4, pp. 243–256, 2015.

[3] J. K. Freburger, G. M. Holmes, R. P. Agans et al., "The rising prevalence of chronic low back pain," *Archives of Internal Medicine*, vol. 169, no. 3, pp. 251–258, 2009.

[4] K. M. C. Cheung, J. Karppinen, D. Chan et al., "Prevalence and pattern of lumbar magnetic resonance imaging changes in a population study of one thousand forty-three individuals," *Spine (Phila Pa 1976)*, vol. 34, no. 9, pp. 934–940, 2009.

[5] M. A. Alvi, P. Kerezoudis, W. Wahood, A. Goyal, and M. Bydon, "Operative approaches for lumbar disc herniation: a systematic review and multiple treatment meta-analysis of conventional and minimally invasive surgeries," *World Neurosurgery*, vol. 114, pp. 391–407.e2, 2018.

[6] B. L. Chen, J. B. Guo, H. W. Zhang et al., "Surgical versus nonoperative treatment for lumbar disc herniation: a systematic review and meta-analysis," *Clinical Rehabilitation*, vol. 32, no. 2, pp. 146–160, 2017.

[7] T. Lund and T. R. Oxland, "Adjacent Level Disk Disease—Is it Really a Fusion Disease?," *Orthopedic Clinics of North America*, vol. 42, no. 4, pp. 529–541, 2011.

[8] S. M. Richardson, N. Hughes, J. A. Hunt, A. J. Freemont, and J. A. Hoyland, "Human mesenchymal stem cell differentiation to NP-like cells in chitosan-glycerophosphate hydrogels," *Biomaterials*, vol. 29, no. 1, pp. 85–93, 2008.

[9] D. Sakai, Y. Nakamura, T. Nakai et al., "Exhaustion of nucleus pulposus progenitor cells with ageing and degeneration of the intervertebral disc," *Nature Communications*, vol. 3, no. 1, 2012.

[10] D. Sakai, K. Nishimura, M. Tanaka et al., "Migration of bone marrow-derived cells for endogenous repair in a new tail-looping disc degeneration model in the mouse: a pilot study," *The Spine Journal*, vol. 15, no. 6, pp. 1356–1365, 2015.

[11] X. Zhou, J. Wang, W. Fang et al., "Genipin cross-linked type II collagen/chondroitin sulfate composite hydrogel-like cell delivery system induces differentiation of adipose-derived stem cells and regenerates degenerated nucleus pulposus," *Acta Biomaterialia*, vol. 71, pp. 496–509, 2018.

[12] S. K. Leckie, G. A. Sowa, B. P. Bechara et al., "Injection of human umbilical tissue-derived cells into the nucleus pulposus alters the course of intervertebral disc degeneration in vivo," *The Spine Journal*, vol. 13, no. 3, pp. 263–272, 2013.

[13] T. Miyamoto, T. Muneta, T. Tabuchi et al., "Intradiscal transplantation of synovial mesenchymal stem cells prevents intervertebral disc degeneration through suppression of matrix metalloproteinase-related genes in nucleus pulposus cells in rabbits," *Arthritis Research & Therapy*, vol. 12, no. 6, p. R206, 2010.

[14] J. Clouet, M. Fusellier, A. Camus, C. le Visage, and J. Guicheux, "Intervertebral disc regeneration: from cell therapy to the

development of novel bioinspired endogenous repair strategies," *Advanced Drug Delivery Reviews*, 2018.

[15] F. A. N. ZHANG, X. ZHAO, H. SHEN, and C. ZHANG, "Molecular mechanisms of cell death in intervertebral disc degeneration (review)," *International Journal of Molecular Medicine*, vol. 37, no. 6, pp. 1439–1448, 2016.

[16] J. Wang, Y. Tao, X. Zhou et al., "The potential of chondrogenic pre-differentiation of adipose-derived mesenchymal stem cells for regeneration in harsh nucleus pulposus microenvironment," *Experimental Biology and Medicine (Maywood, N.J.)*, vol. 241, no. 18, pp. 2104–2111, 2016.

[17] C. L. Le Maitre, A. J. Freemont, and J. A. Hoyland, "Accelerated cellular senescence in degenerate intervertebral discs: a possible role in the pathogenesis of intervertebral disc degeneration," *Arthritis Research & Therapy*, vol. 9, no. 3, p. R45, 2007.

[18] M. V. Risbud, A. Guttapalli, T. T. Tsai et al., "Evidence for skeletal progenitor cells in the degenerate human intervertebral disc," *Spine (Phila Pa 1976)*, vol. 32, no. 23, pp. 2537–2544, 2007.

[19] H. Li, Y. Tao, C. Liang et al., "Influence of hypoxia in the intervertebral disc on the biological behaviors of rat adipose- and nucleus pulposus-derived mesenchymal stem cells," *Cells, Tissues, Organs*, vol. 198, no. 4, pp. 266–277, 2013.

[20] H. Li, J. Wang, F. Li, G. Chen, and Q. Chen, "The influence of hyperosmolarity in the intervertebral disc on the proliferation and chondrogenic differentiation of nucleus pulposus-derived mesenchymal stem cells," *Cells, Tissues, Organs*, vol. 205, no. 3, pp. 178–188, 2018.

[21] J. Liu, H. Tao, H. Wang et al., "Biological behavior of human nucleus pulposus mesenchymal stem cells in response to changes in the acidic environment during intervertebral disc degeneration," *Stem Cells and Development*, vol. 26, no. 12, pp. 901–911, 2017.

[22] D. M. O'Halloran and A. S. Pandit, "Tissue-engineering approach to regenerating the intervertebral disc," *Tissue Engineering*, vol. 13, no. 8, pp. 1927–1954, 2007.

[23] J. Silva-Correia, A. Gloria, M. B. Oliveira et al., "Rheological and mechanical properties of acellular and cell-laden methacrylated gellan gum hydrogels," *Journal of Biomedical Materials Research. Part A*, vol. 101, no. 12, pp. 3438–3446, 2013.

[24] A. S. Hoffman, "Hydrogels for biomedical applications," *Advanced Drug Delivery Reviews*, vol. 54, no. 1, pp. 3–12, 2002.

[25] T. Chen, X. Cheng, J. Wang, X. Feng, and L. Zhang, "Time-course investigation of intervertebral disc degeneration induced by different sizes of needle punctures in rat tail disc," *Medical Science Monitor*, vol. 24, pp. 6456–6465, 2018.

[26] H. J. Mao, Q. X. Chen, B. Han et al., "The effect of injection volume on disc degeneration in a rat tail model," *Spine (Phila Pa 1976)*, vol. 36, no. 16, pp. E1062–E1069, 2011.

[27] B. Han, K. Zhu, F. C. Li et al., "A simple disc degeneration model induced by percutaneous needle puncture in the rat tail," *Spine (Phila Pa 1976)*, vol. 33, no. 18, pp. 1925–1934, 2008.

[28] S. Sobajima, J. F. Kompel, J. S. Kim et al., "A slowly progressive and reproducible animal model of intervertebral disc degeneration characterized by MRI, X-ray and histology," *Spine (Phila Pa 1976)*, vol. 30, no. 1, pp. 15–24, 2005.

[29] E. Anitua and S. Padilla, "Biologic therapies to enhance intervertebral disc repair," *Regenerative Medicine*, vol. 13, no. 1, pp. 55–72, 2018.

[30] C. S. Carrier, C. M. Bono, and D. R. Lebl, "Evidence-based analysis of adjacent segment degeneration and disease after ACDF: a systematic review," *The Spine Journal*, vol. 13, no. 10, pp. 1370–1378, 2013.

[31] D. H. Rosenzweig, R. Fairag, A. P. Mathieu et al., "Thermoreversible hyaluronan-hydrogel and autologous nucleus pulposus cell delivery regenerates human intervertebral discs in an ex vivo, physiological organ culture model," *European Cells & Materials*, vol. 36, pp. 200–217, 2018.

[32] E. S. Vasiliadis, S. G. Pneumaticos, D. S. Evangelopoulos, and A. G. Papavassiliou, "Biologic treatment of mild and moderate intervertebral disc degeneration," *Molecular Medicine*, vol. 20, no. 1, pp. 400–409, 2014.

[33] C. Hohaus, T. M. Ganey, Y. Minkus, and H. J. Meisel, "Cell transplantation in lumbar spine disc degeneration disease," *European Spine Journal*, vol. 17, Suppl 4, pp. 492–503, 2008.

[34] X. Chen, L. Zhu, G. Wu, Z. Liang, L. Yang, and Z. du, "A comparison between nucleus pulposus-derived stem cell transplantation and nucleus pulposus cell transplantation for the treatment of intervertebral disc degeneration in a rabbit model," *International Journal of Surgery*, vol. 28, pp. 77–82, 2016.

[35] T. Iwashina, J. Mochida, D. Sakai et al., "Feasibility of using a human nucleus pulposus cell line as a cell source in cell transplantation therapy for intervertebral disc degeneration," *Spine (Phila Pa 1976)*, vol. 31, no. 11, pp. 1177–1186, 2006.

[36] J. P. G. Urban, "The role of the physicochemical environment in determining disc cell behaviour," *Biochemical Society Transactions*, vol. 30, no. 6, pp. 858–863, 2002, Pt 6.

[37] S. Holm and A. Nachemson, "Variations in the nutrition of the canine intervertebral disc induced by motion," *Spine (Phila Pa 1976)*, vol. 8, no. 8, pp. 866–874, 1983.

[38] C. Liang, H. Li, Y. Tao et al., "Responses of human adipose-derived mesenchymal stem cells to chemical microenvironment of the intervertebral disc," *Journal of Translational Medicine*, vol. 10, no. 1, p. 49, 2012.

[39] J. F. Blanco, I. F. Graciani, F. M. Sanchez-Guijo et al., "Isolation and characterization of mesenchymal stromal cells from human degenerated nucleus pulposus: comparison with bone marrow mesenchymal stromal cells from the same subjects," *Spine (Phila Pa 1976)*, vol. 35, no. 26, pp. 2259–2265, 2010.

[40] B. Han, H. C. Wang, H. Li et al., "Nucleus pulposus mesenchymal stem cells in acidic conditions mimicking degenerative intervertebral discs give better performance than adipose tissue-derived mesenchymal stem cells," *Cells, Tissues, Organs*, vol. 199, no. 5-6, pp. 342–352, 2014.

[41] Y. Zhao, Z. Jia, S. Huang et al., "Age-related changes in nucleus pulposus mesenchymal stem cells: an in vitro study in rats," *Stem Cells International*, vol. 2017, Article ID 6761572, 13 pages, 2017.

[42] J. Jia, S. Z. Wang, L. Y. Ma, J. B. Yu, Y. D. Guo, and C. Wang, "The differential effects of leukocyte-containing and pure platelet-rich plasma on nucleus pulposus-derived mesenchymal stem cells: implications for the clinical treatment of intervertebral disc degeneration," *Stem Cells International*, vol. 2018, 12 pages, 2018.

[43] C. J. Hunter, J. R. Matyas, and N. A. Duncan, "Cytomorphology of notochordal and chondrocytic cells from the nucleus pulposus: a species comparison," *Journal of Anatomy*, vol. 205, no. 5, pp. 357–362, 2004.

[44] B. Huang, L. T. Liu, C. Q. Li et al., "Study to determine the presence of progenitor cells in the degenerated human

cartilage endplates," *European Spine Journal*, vol. 21, no. 4, pp. 613–622, 2012.

[45] A. Hiyama, J. Mochida, T. Iwashina et al., "Transplantation of mesenchymal stem cells in a canine disc degeneration model," *Journal of Orthopaedic Research*, vol. 26, no. 5, pp. 589–600, 2008.

[46] D. Sakai, J. Mochida, T. Iwashina et al., "Differentiation of mesenchymal stem cells transplanted to a rabbit degenerative disc model: potential and limitations for stem cell therapy in disc regeneration," *Spine (Phila Pa 1976)*, vol. 30, no. 21, pp. 2379–2387, 2005.

[47] E. J. Carragee, A. S. Don, E. L. Hurwitz, J. M. Cuellar, J. Carrino, and R. Herzog, "2009 ISSLS Prize Winner: does discography cause accelerated progression of degeneration changes in the lumbar disc: a ten-year matched cohort study," *Spine (Phila Pa 1976)*, vol. 34, no. 21, pp. 2338–2345, 2009.

[48] L. Orozco, R. Soler, C. Morera, M. Alberca, A. Sánchez, and J. García-Sancho, "Intervertebral disc repair by autologous mesenchymal bone marrow cells: a pilot study," *Transplantation*, vol. 92, no. 7, pp. 822–828, 2011.

[49] S. C. W. Chan and B. Gantenbein-Ritter, "Intervertebral disc regeneration or repair with biomaterials and stem cell therapy – feasible or fiction?," *Swiss Medical Weekly*, vol. 142, p. w13598, 2012.

[50] L. E. Clarke, J. C. McConnell, M. J. Sherratt, B. Derby, S. M. Richardson, and J. A. Hoyland, "Growth differentiation factor 6 and transforming growth factor-beta differentially mediate mesenchymal stem cell differentiation, composition, and micromechanical properties of nucleus pulposus constructs," *Arthritis Research & Therapy*, vol. 16, no. 2, p. R67, 2014.

[51] H. Wang, J. Cui, Z. Zheng et al., "Assembly of RGD-modified hydrogel micromodules into permeable three-dimensional hollow microtissues mimicking in vivo tissue structures," *ACS Applied Materials & Interfaces*, vol. 9, no. 48, pp. 41669–41679, 2017.

[52] E. C. Collin, S. Grad, D. I. Zeugolis et al., "An injectable vehicle for nucleus pulposus cell-based therapy," *Biomaterials*, vol. 32, no. 11, pp. 2862–2870, 2011.

[53] G. Kumar, M. S. Waters, T. M. Farooque, M. F. Young, and C. G. Simon Jr., "Freeform fabricated scaffolds with roughened struts that enhance both stem cell proliferation and differentiation by controlling cell shape," *Biomaterials*, vol. 33, no. 16, pp. 4022–4030, 2012.

Hindawi
Stem Cells International
Volume 2019, Article ID 8636079, 9 pages
https://doi.org/10.1155/2019/8636079

Research Article

A Retrospective Study on the Use of Dermis Micrografts in Platelet-Rich Fibrin for the Resurfacing of Massive and Chronic Full-Thickness Burns

Alessandro Andreone[1] **and Daan den Hollander**[1,2]

[1]*Burns Unit, Inkosi Albert Luthuli Central Hospital, Durban, South Africa*
[2]*University of KwaZulu-Natal, Durban, South Africa*

Correspondence should be addressed to Alessandro Andreone; andreonealex@gmail.com

Received 19 April 2019; Revised 1 August 2019; Accepted 3 September 2019; Published 15 September 2019

Guest Editor: Federico Moreno

The coverage of massive burns still represents a big challenge, even if several strategies are to date available to deal with this situation. In this study, we describe the use of a combination of platelet-rich fibrin and micrograft spray-on skin in order to increase the yield of grafted cells in patients. We treated a total of five patients, of which two were affected by massive burns and three with chronic burn wounds. Briefly, autologous micrografts were obtained by Rigenera technology using a class I medical device called Rigeneracons. The micrografts were then combined with PRF and sprayed on the wound bed by a Spraypen. Before applying PRF/micrograft spray-on skin, the wound bed was covered with an Integra® dermal template, and the wounds were dressed with a layer of antimicrobial dressing applied directly over the silicone layer. When the silicone layer of the dermal template started showing signs of separation, the wound was considered ready for grafting. In all cases, we observed a fast and complete skin graft on average after 7-10 days by PRF/micrograft spray-on skin treatment. In particular, two patients with massive burns reported rapid reepithelialization, and three patients with chronic burn wounds, two of whom had failed skin grafts before the procedure, had complete wound healing within a week. In conclusion, the results showed in this study suggest that the use of PRF/micrograft spray-on skin represents a promising approach in the management of burns or chronic burn wounds.

1. Introduction

The coverage of massive burns (i.e., more than 40% TBSA) is a challenge. As about 80% of the skin can be used as possible donor sites, the area to be grafted in massive burns often exceeds the available donor skin. A number of strategies are available to deal with this situation. Reharvesting from previously used donor sites is possible but requires a regeneration period of 2-3 weeks. Wide meshing (a ratio of 1 : 4 or more) and the MEEK technique have been proposed to make better use of available skin but also require time for reepithelialization of the interstices between the grafted areas, during which time these areas need to be protected from dehydration and microbial colonization. Cultured epithelial grafts also take about 3 weeks to be cultured, and although recently an affordable technique has been developed [1], long-term results remain poor. Common to all these strategies is that complete coverage of the burn wound takes time, during which period the patient is at risk of burn wound infection, sepsis, and death. In our environment, cadaver skin is rarely offered, and the high rates of HIV/AIDS preclude the use of amniotic membrane as a temporizing dressing. Spray-on skin cells (suspended epithelial cells) are an alternative for these patients [2, 3]. Although initially cells were cultured in a medium before being sprayed on the skin, recently a new technique has been described using fresh epidermal/dermal cells in suspension, which are sprayed on immediately after harvest [4, 5]. One problem with the use of spray-on cells has been that when the cells are suspended in a low-viscosity solution such as normal saline, they tend to be

spread unevenly over the surface to be grafted, while there may be a significant graft loss, as cells float off the wound with the medium and end up on the towels. Some have combined spray-on cells with fibrin to deal with these problems [6, 7].

We recently developed a technique in which autologous micrografts are combined with platelet-rich fibrin and sprayed on the wound bed, in order to increase the yield of grafted cells. Although it is possible to use spray-on skin as the only skin cover, we have used the technique so far in combination with other grafting techniques, such as wide meshing using ratios of 3 : 1 or 6 : 1 or the MEEK technique, in accordance with the extension of the burn area requiring coverage and the available skin. The solution was first sprayed over the wound before application of the graft, followed by a second layer of solution. The spray was also applied to the donor site, which was further managed in the usual manner. A light compression bandage was used to protect the grafted areas. All grafted areas were reviewed on postoperative days 4-5 to assess graft take.

Autologous micrografts containing viable progenitor cells derived from the dermal-epidermal layer were obtained by Rigenera technology using the Rigeneracons device (Human Brain Wave, Italy), a biological tissue disruptor designed to cut tissues into small micrografts that are subsequently injected or sprayed into the desired area. This technology was originally used for the treatment of skeletal defects in orthodontic surgery [8, 9], but indications were subsequently extended to plastic surgery, in particular for the management of alopecia and chronic small wounds [10–12].

The combination of these two strategies, PRF and micrografts sprayed on the wound bed, has other potential advantages as well, related to the platelet-rich fibrin (abundance of growth factors, nutrition for developing epithelial cells), that made us explore its use in another group of patients which pose a problem in burns units, particularly under conditions of limited resources. Chronic burn wounds are the result of poor burn care, where deep burns are not excised, but the eschar is left to separate in the ward. This process can take anything between 3 and 8 weeks, at the end of which the wound is stuck in the inflammatory stage of wound healing, has very high levels of proteinases such as matrix metalloproteinases, and is often heavily colonized by microorganisms harbouring in biofilms [13]. Such wounds are characterized by epithelialization arrest and overgranulation, and sometimes a band of dark red inflamed tissue can be observed at the wound/skin interface. Such wounds have a high graft failure rate, and in the worst scenario, wound progression of the donor sites is observed, which may turn into full-thickness wounds. These wounds are a sign of poor burn care, which in a low-resource environment is often related to late referrals or to insufficient resources to timely take patients to theatre for a skin coverage procedure. The treatment of these wounds is difficult, necessitating a prolonged period of wound bed preparation before grafting can be attempted.

In this article, we describe the combined use of autologous micrografts in platelet-rich fibrin (PRF) to treat five consecutive patients affected by burns.

2. Patients and Methods

2.1. Ethics. Ethical approval for use of the Trauma/Burns database was granted by the UKZN-BREC ethics committee (Class Approval BE 207/09). Ethical approval for micrograft treatment was obtained from the Hospital Medical Human Research Ethics Committee, and all patients gave informed consent prior to the participation in this procedure.

2.2. Inclusion/Exclusion Criteria. The inclusion criteria were the following: age between 18 and 55 yrs., TBSA between 6 and 55% deep partial to full thickness with or without inhalational injury requiring split skin graft, and patients with open wounds not older than 2 months. The exclusion criteria were the following: patient younger than 17 and older than 55, wounds older than 2 months, TBSA less than 5% and more than 55%, and ventilated patient with septicaemia. A total of 12 patients were screened, and five patients were selected for the study.

2.3. Patients. We retrogradely analysed the records of patients treated with PRF/micrograft spray-on skin during the period between December 2017 and February 2018. Their clinical characteristics are reported in Table 1. All were men aged between 22 years and 46 years. Mechanism of injury was a flame burn in 4 and a hydrochloride acid burn in the fifth patient. The %TBSA burned ranged from 12% to 47%, with a mean of 22.5%.

The majority of the wounds in the patients with extensive burns were located over the torso, abdomen, neck, and face, and most of them had exposure of underlying bone structures postescharotomy. When a viable wound bed was achieved, large area wounds, including those involving the torso, the abdomen, and the neck and those involving an exposed bone (tibia), were then covered with an Integra® dermal template (Baroque, South Africa). The wounds were dressed with a layer of antimicrobial dressing (Acticoat® nanocrystalline silver dressing, Smith and Nephew) applied directly over the silicone layer followed by a nonocclusive dressing in four patients and negative wound pressure therapy in the remaining patient for 10 consecutive days. When the silicone layer of the dermal template started showing signs of separation, the wound was considered ready for grafting and taken to theatre. All the procedures performed on the patients before the PRF/micrograft spray application are indicated in Table 1.

2.4. Methods. The method used in this study involves the combination of the following two techniques: platelet-rich fibrin (PRF) and micrograft spray-on skin. The steps are summarized in Figure 1 and detailed below.

2.5. Platelet-Rich Fibrin (PRF). Vivostat® (Vivostat A/S, Lillerød, Denmark) technique [14] manufactures 5 ml of platelet-rich fibrin from 120 ml of the patient's own blood to which citrate is added to keep it in a liquid form, by ultracentrifugation for 25 minutes. The blood needs to be taken before the start of the surgery, as the resulting trauma will draw platelets to the operative site, diminishing the platelet concentration in the blood [15]. Activation of fibrin

Table 1: Clinical characteristics of five patients enrolled with the indications of previous treatments and application of PRF/micrograft spray-on skin.

Patient	Age	Case history	Previous treatment	Treatment with PRF/micrograft spray
1	39	Assault with an unknown flammable substance, resulting in 45% TBSA full-thickness burn over the anterior torso and neck and inhalational injury (Figure 2(a))	Full necrotomy by performing sharp excision and hydrosurgery with following exposure of the ribs and sternum (Figure 2(b)). Coverage of wound bed with a dermal template (Integra®) and an antimicrobial dressing (Acticoat®, S&N) (Figure 2(c))	After 10 days, the patient was taken to theatre again where the silicone layer over the chest and the flank was removed and a 4 : 1 meshed graft was placed over the neodermis. PRP/micrografts were sprayed over the wound bed and over the meshed graft. The grafted area was exposed on postoperative day 5.
2	22	Full-thickness chemical assault burn with 25% TBSA. The clinical picture suggested a hydrochloride acid burn and the areas involved were the chest, abdomen, multiple areas over the face, both arms, and both legs.	Complete excision of the burn area was performed down to the periosteum of the ribs. The wound bed was covered with an Integra® dermal template and an antimicrobial dressing (Acticoat®, S&N).	After 8 days, the silicone layer was lifted and removed, both arms and forearms were grafted with a mesh graft to a ratio of 4 : 1; PRF/micrografts were sprayed over the bed and the graft. The grafted areas were exposed on postoperative day 5.
3	43	Full-thickness poured petrol burn over both lower limb and feet with a 6.5% TBSA	Conservative treatment with silver sulfadiazine dressings on alternative days for over 3 months. Due to nonhealing wounds over the affected areas, a pus swab was done showing a wound colonization with *Pseudomonas aeruginosa*, responsive to ciprofloxacin.	After a 5-day course of antibiotics, he was taken to theatre. His wounds were debrided with hydrosurgery (Versajet®), and a combination of PRF and micrografts was sprayed over the wound bed and over the meshed graft (3 : 1).
4	45	Full-thickness flame burn with 15% TBSA treated by a traditional healer. The burn involved the left flank, part of the chest, left arm, and forearm.	Conservative treatment for 3 months before transfer to the Burn Unit where the patient was dressed with polyurethane foam (Biatain®, Coloplast)	After 4 days, wounds were debrided with the Versajet® hydrodissector and wound bed was sprayed with PRF and micrografts. Harvested skin was meshed 4 : 1 and applied, followed by a second application of PRF/micrografts. A dressing with plain petrolatum gauze was performed.
5	33	Electrical burns with 15% TBSA on both arms and both legs. He had been found unconscious after the arc of electricity hit the ladder he was holding (±66000 V).	Conservative treatment for 2 months before transfer to the Burn Unit	The wounds were cleansed with hydrosurgery (Versajet®) and then PRF/micrografts were sprayed. Ultrathin layer Integra® was then applied over the patella and the popliteal fossa on the right leg, and the areas were then covered using a modified Meek technique (Humeca®, Netherlands).

solidification does not require the addition of thrombin as in platelet-rich plasma but is simply accomplished by adding an alkaline buffer [16]. Where 120 ml of the patient's blood could not be provided, we have used banked whole blood to manufacture the PRF. The remainder of the blood can be transfused (back) into the patient. The centrifugate, consisting of platelet concentrate in polymerized fibrin, is then transferred to an application device (Spray-pen), which sprays a fine mist of PRF over the wound. It was originally designed for use in neurosurgical procedures as a hemostatic agent to decrease postsurgical leakage and has successfully been used in renal [17] and thoracic surgery [18]. It was introduced into burn surgery to aid in hemostasis producing other benefits such as better graft fixation and higher graft take.

2.6. Micrograft Spray-On Skin. Micrografts were obtained using the Rigeneracons medical device as previously described [12]. Briefly, the donor area was prepared by gently removing the top epidermal layer using the Versajet® hydrodissector until the bleeding dermis tissue is reached. Subsequently, a thin layer of skin is harvested using a Davis® dermatome, obtaining a sample of 0.2 mm (0.008 inch) deep and 4 by 2 cm^2 in size. The aim is to obtain cells from the epidermal-dermal junction [19]. This sample of the dermis is then cut with a scalpel blade into small pieces (1 to 2 mm wide) and inserted into the Rigeneracons device for mechanical disaggregation. This provides five milliliters of dermal micrograft suspension that is then transferred to a syringe provided in the Vivostat® kit. This syringe is then placed in the Vivostat® delivery unit alongside the syringe

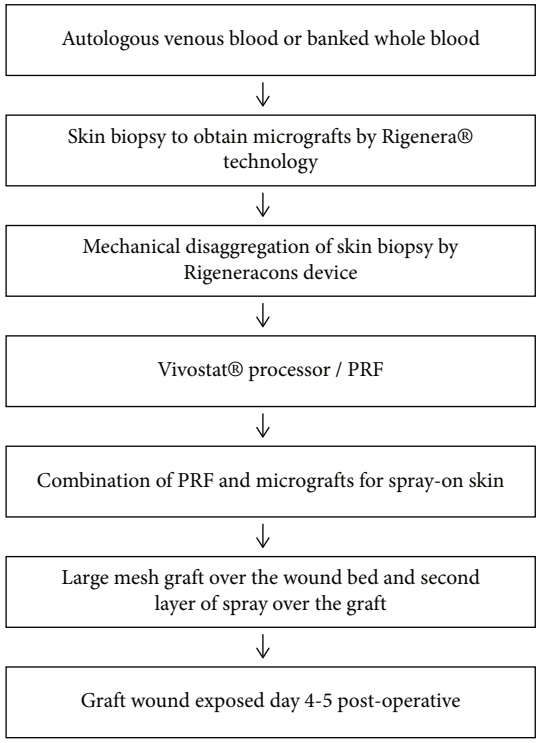

Figure 1: Sampling schedule and steps for the combined technique PRF/micrograft spray-on skin.

containing 5 ml of PRF solution. When added to the Vivostat® delivery system, both solutions are mixed immediately and are sprayed simultaneously over the wound bed using the Spraypen.

3. Results

In the first patient, the grafted area was exposed on postoperative day 5 observing a perfect adherence of the graft onto the neodermis and visible new dermal formation in the meshed areas with a complete reepithelialization on day 7 post skin graft (Figures 2(c)–2(e)). We performed the same procedure over the remaining wounds 6 and 8 weeks later. The delay between the two surgeries resulted from complications as a result of tracheostomy for difficult intubation during a routine dressing change in theatre, which was further complicated by a pneumonia with bilateral pleural effusion. The patient was discharged after a total length of stay of 15 weeks.

In the second patient affected by chemical assault burn, we observed a good adhesion of the graft to the wound bed with new skin bridging formation visible in the meshed graft. The procedure was repeated 21 days later over the chest and the abdominal wall with similar results. Small additional wounds over the lower limbs and the feet were grafted a month after admission. The patient was discharged with a completely healed wound after a total hospital stay of 14 weeks.

In the third patient, at the first dressing change on day 4 postoperatively, the grafted areas were found to be perfectly healed and dry and were dressed only with aqueous cream (Figure 3). The donor areas (sprayed with the same combination) were fully healed when first exposed on day 6 post op. The patient was discharged on day 8 postoperatively after spending 13 days in the unit.

For the fourth patient, when exposed on day 5 post skin graft, 100% skin graft take was shown. The donor areas were found to be fully reepithelialized on day 6 post harvesting. The patient was discharged 20 days after admission with fully healed wounds.

In the fifth patient, grafted and donor areas were exposed on day 7 postoperatively. The donor areas were found completely healed, with excellent graft take over the grafted areas. The patient was discharged to base hospital 5 weeks after admission to our unit. A summary of clinical outcomes is reported in Table 2.

4. Discussion

Both the use of platelet-rich plasma (PRP) and of suspended epithelial cells are strategies that already form part of the armamentarium of the burn surgeon [20–22]. PRP is plasma with a higher concentration of platelets than baseline, obtained through centrifugation of the patient's blood, after which the supernatant is siphoned off [15]. The platelets are usually concentrated 3-5 times by this method, although the process has not been standardized [20]. Immediately before application, the solution is activated by the addition of bovine thrombin. When injected into the tissues or sprayed onto a wound surface, the activated PRP immediately forms a fibrin clot (similar to fibrin glue) resulting in hemostasis and fixation of the graft to the wound bed. Harkin et al. [5], Grant et al. [23], and Mittermayr et al. [6] demonstrated this in *pig* studies using a fibrin sealant, although others failed to demonstrate a beneficial effect on graft take [7]. The latter study was, however, criticized because only small wounds were used, and the dressings used did not represent what is normally used for massive burns [16]. Although initially used as an alternative to the fibrin sealant in corneal and nerve repairs, when PRP became commercially available in the 1990s, indications rapidly expanded to include its beneficial effects on tissue healing, regeneration, and cell proliferation. However, PRP has several disadvantages, not least of which is that it requires the addition of bovine thrombin with its resultant risks such as life-threatening coagulopathies and allergic reactions [22]. This led to the development of a second generation of platelet products, of which platelet-rich fibrin is the prime representative. PRF has proven to be as effective as PRP, while avoiding the side effects.

The advantage of a platelet-derived product such as PRF over fibrin sealants is, indeed, the presence of thrombocytes. It has long been recognized that platelets have many more functions than their role in coagulation [24, 25]. Platelets play a central role in pathogen surveillance and containment, as well as in wound healing. After activation, platelets release over 300 different proteins, including coagulation factor, chemokines, proinflammatory cytokines, and over 30 different growth factors, proteases, and protease inhibitors. In addition, platelets are able to modulate inflammatory and healing processes through direct cell-to-cell contact. They contain

Figure 2: Representative images for patient 1. (a) Admission picture where a full-thickness burn over the anterior torso and neck is evidenced. (b) Post excision of burn eschar. (c) After application of Integra. (d) After application of PRF/spray-on skin; first dressing change: near-complete reepithelialization of grafted areas. (e) Results after 10 days postgrafting.

microbiocidal proteins and have been shown to engulf viruses and bacteria. The many growth factors produced by the platelet encourage multiplication as well as vascular ingrowth to provide nutrition to the seeded cells. Cell adhesion molecules released by platelets, such as fibronectin and vitronectin, enhance the migration of epithelial and vascular cells [26]. It has also been suggested that the fibrin strands may act as a template for epidermal migration [7]. Agren et al. [14] demonstrated that PRF, as obtained using the Vivostat technology, contains 3.9 times as many platelets as the baseline blood, as well increased levels of transforming growth factor-β1, platelet-derived growth factor-AB, basic fibroblast growth factor, and vascular endothelial growth factor. MMP-9 levels were reduced 139-fold. The beneficial effects of PRP on wound healing have been confirmed *in vitro* by Xian et al. [27] and in a murine study by Law et al. [28]. The effects of PRP seem to be concentration-dependent, with higher concentrations promoting inflammation and collagen deposition and lower concentrations enhancing wound remodelling [27]. A meta-analysis concluded that the application of PRP expedited the healing of wounds and in particular of chronic wounds [11]. However, a—theoretical—side effect may result from the intense inflammatory reaction caused by the increased platelet level, i.e., increased long-term scarring [29]. Venter et al. demonstrated that on its own, PRP has no benefit in full-thickness wounds. They explain this by the absence of epithelial cells ("substrate") in the full-thickness burn [26].

In addition, the plasma contains nutrients for the epithelial cells during the period before the nutrient vessels have established themselves.

The use of epidermal cell suspensions ("spray-on skin") in burn patients has been called a "common practice with no agreed protocol" with regard to indications for its use, techniques used, dressings to be used, timing of first wound review, and outcome measures [21]. In principle, two

(a) (b)

Figure 3: Representative images for patient 3. (a) Chronic burn wound with failed graft, overgranulation, and inflammatory margins. (b) Day 4 post widely meshed graft and PRF/spray-on skin where the wound is already reepithelialized.

Table 2: Clinical outcomes.

Patient	Age	Case history	Graft take	Full wound closure
1	39	Assault with an unknown flammable substance, resulting in 45% TBSA full-thickness burn over the anterior torso and neck and inhalational injury (Figure 2(a))	97%	D/C 15 weeks post grafting
2	22	Full-thickness chemical assault burn with 25% TBSA. The clinical picture suggested a hydrochloride acid burn, and the areas involved were the chest, abdomen, multiple areas over the face, both arms, and both legs.	96%	D/C 9 weeks post grafting
3	43	Full-thickness poured petrol burn over both lower limb and feet with a 6.5% TBSA	98%	D/C 22 days post grafting
4	45	Full-thickness flame burn with 15% TBSA treated by a traditional healer. The burn involved the left flank, part of the chest, left arm, and forearm.	98%	D/C 39 days post grafting
5	33	Electrical burns with 15% TBSA on both arms and both legs. He had been found unconscious after the arc of electricity hit the ladder he was holding (±66000 V).	98%	D/C 32 days post grafting

techniques are used. In cultured epidermal cell suspensions after enzymatic separation of the cells, they are brought into suspension and incubated for a minimum of 21 days to allow multiplication. The suspension is then sprayed over the wound bed or injected into the wound edges. The solution in which the keratinocytes are suspended varies from normal saline, lactate solution, hyaluronic acid matrix, to fibrin. Disadvantages of cultured epidermal cell suspensions are long delay caused by the culture, high rates of infection, and high costs and the fact that cultured cell suspensions contain only keratinocytes [30]. Long-term fragility of the new skin has also proven a problem [31]. Uncultured epidermal cell suspensions contain all types of skin cells, including keratinocytes, fibroblasts, melanocytes, and Langerhans cells and therefore should provide better long-term outcomes [4]. Wood et al. [19] analysed cell populations obtained with ReCell® and found that 75.5% of the total cell population was viable, which consisted of $64 \pm 28.8\%$ keratinocytes, 30.3 ± 14.0 fibroblasts, and 3.5 ± 0.5Y melanocytes. Separation of the skin cells may occur enzymatically (ReCell®) or mechanically (Rigenera®). No comparative studies are available to indicate which method is superior. A theoretical benefit of the Rigenera® method might be that keratinocytes and fibroblasts remain in contact, as cell-to-cell contact with fibroblasts has been suggested to be required for keratinocyte proliferation [27].

Zhao et al. [4] conducted a systematic review of the reported experience with spray-on skin in chronic wounds, including 5 studies and a total of 61 wounds. 44 (72%) of which had experienced (near) complete healing at the end of the observation period. Forty-three patients were managed with an uncultured suspension, with a good result in 30 (70%). The Medical Technologies Advisory Committee of the UK National Institute for Clinical Excellence (NICE)

[3] published a review of the use of ReCell® in the acute management of burns. The review included a total of 817 patients in 3 published studies as well as an unknown number from congress abstracts (overlap between studies could not be excluded). Of the 817 published patients, 384 received epithelial cell suspension. Two studies found that the time to healing or total hospital stay was shorter for patients treated with epithelial cell suspension [32], while in the remaining study no statistically significant difference was found. Gravante et al. [2] also found no statistically significant differences for postoperative pain and development of contracture at one-month follow-up compared to patients who had a conventional skin graft.

We report here five cases in which we used a combination of PRF and micrograft suspension in the treatment of burn wounds. The first two patients had massive, deep burns, covering more than 40% of the body surface and in both cases "fourth degree" (extending into the subcutaneous tissues, in both cases penetrating through the anterior fascia of the intercostal muscles). Both patients were admitted to our Trauma Intensive Care Unit for ventilation of an associated inhalation injury. Both underwent early total excision of the burn wound, followed by application of a dermal substitute for two principal reasons. During the early stage, the dermal matrix in combination with the overlying polyurethane film provides a low-colonized, moist wound environment, allowing the wound to enter the wound healing stage of proliferation and the ingrowth of neovasculature into the collagen matrix of the dermal template. At the end of this stage, the film will lift off, a sign that the wound is now ready to receive a graft. At this point, the patient is taken back to theatre for a widely spaced skin graft (either a widely meshed graft or by the use of the Meek technique), supplemented by the PRF and spray-on micrografts. The use of spray-on epithelial cells over an Integra® dermal template was described in a porcine model by Wood et al. [33], and although these authors used a one-stage procedure, there have been no reports in humans.

In a resource-limited environment, a significant number of patients are referred late, sometimes after a period of many months in a peripheral hospital. This situation may result when the burns centres have insufficient beds to manage all burn patients in their catchment area, while regional hospitals lack resources and manpower to surgically manage burns. Burns that are referred late (i.e., more than a month post injury) have invariably full thickness, either because the depth of the wound was underestimated on initial assessment or the wound has progressed because of the heavy contamination with bacteria that inevitably occurs in chronic burn wounds. Such burns are characterized by biofilms and high concentrations of natural proteinases, such as matrix metalloproteinases (MMPs), which lock the healing process in the inflammatory stage. Split skin grafts will often fail on such wounds, and this may be associated with progression of the donor sites to full-thickness wounds, eventually leaving a larger area to cover than before the attempted skin graft. Two of the three patients in our series had failed skin grafts before the index procedure. We currently treat these wounds with Prontosan® in combination with either nanocrystalline silver or honey-based dressings in an attempt to break down biofilms and decrease the bioburden and with topical steroids to reduce MMPs and other inflammatory mediators. This usually results in a graftable wound bed in 1-2 weeks, when the patient is taken to theatre. The three patients described underwent this regimen of wound bed preparation and were taken to theatre when the surgeon deemed the wounds ready for grafting. They were then covered with widely meshed graft and PRF/spray-on micrografts, each one with excellent results.

Although we originally thought we were the first to use this combination in humans, we have since come across a report from Birmingham, UK, where a similar protocol, but using the ReCell technique of epithelial cell preparation, was used to cover a 15% area of full-thickness burn over the back [16]. The patient had previously undergone five grafts, associated with significant graft loss. In the sixth sitting, a mixture of platelet-rich fibrin and suspended epithelial cells (processed using the ReCell® technique) was applied using the Vivostat® system. On day 7, there was excellent graft take.

Being a small retrospective evaluation, this study has several limitations. In the two patients with massive burns, although the graft take was excellent and sustained, the length of hospital stay in both patients was still longer than expected from the one day/%TBSA burnt rule, which on average applied to our patients in a previous epidemiological study [34]. The short follow-up period did not allow for assessment of long-term results, which might be adversely affected by the platelets administered to the wound as stated above. The patients in which the technique was used for the management of chronic wounds with reepithelialization arrest were subjected to a multimodal treatment, of which very few of the components have been subjected to scientific investigation. However, we feel that the results of PRF/micrograft spray-on skin are sufficiently promising to warrant setting up a randomized trial and setting one up.

5. Conclusion

The use of a micrograft suspension in platelet-rich fibrin was described. Two patients with massive burns who were subjected to wide meshing experienced rapid reepithelialization, which however was not translated to a shorter stay in the hospital. Three patients with chronic burn wounds, two of whom had failed skin grafts before the procedure, had complete wound healing within a week. Further investigation in the form of a properly executed randomized trial is warranted.

Data Availability

The data used to support the findings of this study are included within the article.

Disclosure

The results of this manuscript were presented as poster in an International Conference on Wound Care, Tissue Repair and Regenerative Medicine.

Conflicts of Interest

The authors declare that there is no conflict of interest regarding the publication of this paper.

References

[1] W. Kleintjes, G. Thomas, B. S. S. Thaele, N. Stevenson, and B. Warren, "A novel technique for composite cultured epithelial autograft in a patient with extensive burn wounds: a case report," *Clinics in Surgery*, vol. 2, p. 1579, 2017.

[2] G. Gravante, M. C. di Fede, A. Araco et al., "A randomized trial comparing ReCell® system of epidermal cells delivery versus classic skin grafts for the treatment of deep partial thickness burns," *Burns*, vol. 33, no. 8, pp. 966–972, 2007.

[3] A. Dillon, "Medical Technologies Advisory Committee. National Institute for Clinical Guidance. The ReCell spray-on skin system for treating skin los, scarring and depigmentation after burn injury," February 2017, http://nice.org.uk/.

[4] H. Zhao, Y. Chen, C. Zhang, and X. Fu, "Autologous epidermal cell suspension: a promising treatment for chronic wounds," *Journal of Tissue Viability*, vol. 25, no. 1, pp. 50–56, 2016.

[5] D. G. Harkin, R. A. Dawson, and Z. Upton, "Optimized delivery of skin keratinocytes by aerosolization and suspension in fibrin tissue adhesive," *Wound Repair and Regeneration*, vol. 14, no. 3, pp. 354–363, 2006.

[6] R. Mittermayr, E. Wassermann, M. Thurnher, M. Simunek, and H. Redl, "Skin graft fixation by slow clotting fibrin sealant applied as a thin layer," *Burns*, vol. 32, no. 3, pp. 305–311, 2006.

[7] L. J. Currie, R. Martin, J. R. Sharpe, and S. E. James, "A comparison of keratinocyte cell sprays with and without fibrin glue," *Burns*, vol. 29, no. 7, pp. 677–685, 2003.

[8] F. Carinci, A. Motroni, A. Graziano, I. Zollino, G. Brunelli, and R. D'Aquino, "Sinus lift tissue engineering using autologous pulp micro-grafts: a case report of bone density evaluation," *Journal of Indian Society of Periodontology*, vol. 17, no. 5, pp. 644–647, 2013.

[9] A. Graziano, F. Carinci, S. Scolaro, and R. D'Aquino, "Periodontal tissue generation using autologous dental ligament micro-grafts: case report with 6 months follow-up," *Annals of Oral and Maxillofacial Surgery*, vol. 1, no. 2, p. 20, 2013.

[10] P. Gentile, M. G. Scioli, A. Bielli, A. Orlandi, and V. Cervelli, "Stem cells from human hair follicles: first mechanical isolation for immediate autologous clinical use in androgenetic alopecia and hair loss," *Stem Cell Investigation*, vol. 4, no. 7, p. 58, 2017.

[11] F. Svolacchia, F. De Francesco, L. Trovato, A. Graziano, and G. A. Ferraro, "An innovative regenerative treatment of scars with dermal micrografts," *Journal of Cosmetic Dermatology*, vol. 15, no. 3, pp. 245–253, 2016.

[12] M. Marcarelli, L. Trovato, E. Novarese, M. Riccio, and A. Graziano, "Rigenera protocol in the treatment of surgical wound dehiscence," *International Wound Journal*, vol. 14, no. 1, pp. 277–281, 2017.

[13] A. D. Widgerow, "Nanocrystalline silver, gelatinases and the clinical implications," *Burns*, vol. 36, no. 7, pp. 965–974, 2010.

[14] M. S. Ågren, K. Rasmussen, B. Pakkenberg, and B. Jørgensen, "Growth factor and proteinase profile of Vivostat® platelet-rich fibrin linked to tissue repair," *Vox Sanguinis*, vol. 107, no. 1, pp. 37–43, 2014.

[15] S. Mehta and J. T. Watson, "Platelet Rich Concentrate: Basic Science and Current Clinical Applications," *Journal of Orthopaedic Trauma*, vol. 22, no. 6, pp. 432–438, 2008.

[16] P. Johnstone, J. S. S. Kwei, G. Filobbos, D. Lewis, and S. Jeffery, "Successful application of keratinocyte suspension using autologous fibrin spray," *Burns*, vol. 43, no. 3, pp. e27–e30, 2017.

[17] M. Hevia, J. M. Abascal-Junquera, R. Sacristán et al., "Haemostasis control during laparoscopic partial nephrectomy without parenchymal renorrhaphy: The Vivostat® experience," *Actas Urológicas Españolas (English Edition)*, vol. 37, no. 1, pp. 47–53, 2013.

[18] E. Belcher, M. Dusmet, S. Jordan, G. Ladas, E. Lim, and P. Goldstraw, "A prospective, randomized trial comparing BioGlue and Vivostat for the control of alveolar air leak," *The Journal of Thoracic and Cardiovascular Surgery*, vol. 140, no. 1, pp. 32–38, 2010.

[19] F. M. Wood, N. Giles, A. Stevenson, S. Rea, and M. Fear, "Characterisation of the cell suspension harvested from the dermal epidermal junction using a ReCell® kit," *Burns*, vol. 38, no. 1, pp. 44–51, 2012.

[20] N. Pallua, T. Wolter, and M. Markowicz, "Platelet-rich plasma in burns," *Burns*, vol. 36, no. 1, pp. 4–8, 2010.

[21] A. Allouni, R. Papini, and D. Lewis, "Spray-on-skin cells in burns: A common practice with no agreed protocol," *Burns*, vol. 39, no. 7, pp. 1391–1394, 2013.

[22] S. Nanditha, B. Chandrasekaran, S. Muthusamy, and K. Muthu, "Apprising the diverse facets of platelet-rich fibrin in surgery through a systematic review," *International Journal of Surgery*, vol. 46, pp. 186–194, 2017.

[23] I. Grant, K. Warwick, J. Marshall, C. Green, and R. Martin, "The co-application of sprayed cultured autologous keratinocytes and autologous fibrin sealant in a porcine wound model," *British Journal of Plastic Surgery*, vol. 55, no. 3, pp. 219–227, 2002.

[24] E. M. Golebiewska and A. W. Poole, "Platelet secretion: from haemostasis to wound healing and beyond," *Blood Reviews*, vol. 29, no. 3, pp. 153–162, 2015.

[25] J. D. McFadyen and Z. S. Kaplan, "Platelets are not just for clots," *Transfusion Medicine Reviews*, vol. 29, no. 2, pp. 110–119, 2015.

[26] N. G. Venter, R. G. Marques, J. S. Santos, and A. Monte-Alto-Costa, "Use of platelet-rich plasma in deep second- and third-degree burns," *Burns*, vol. 42, no. 4, pp. 807–814, 2016.

[27] L. J. Xian, S. Roy Chowdhury, A. Bin Saim, and R. Bt Hj Idrus, "Concentration-dependent effect of platelet-rich plasma on keratinocyte and fibroblast wound healing," *Cytotherapy*, vol. 17, no. 3, pp. 293–300, 2015.

[28] J. X. Law, S. R. Chowdhury, A. B. Saim, and R. B. H. Idrus, "Platelet-rich plasma with keratinocytes and fibroblasts enhance healing of full-thickness wounds," *Journal of Tissue Viability*, vol. 26, no. 3, pp. 208–215, 2017.

[29] M. J. Carter, C. P. Fylling, and L. K. S. Parnel, "Use of Platelet Rich Plasma Gel on Wound Healing: A Systematic Review and Meta-Analysis," *Eplasty*, vol. 11, article e38, 2011.

[30] R. E. Marck, E. Middelkoop, and R. S. Breederveld, "Considerations on the Use of Platelet-Rich Plasma, Specifically for Burn Treatment," *Journal of Burn Care & Research*, vol. 35, no. 3, pp. 219–227, 2014.

[31] M. H. Desai, J. M. Mlakar, R. L. McCauley et al., "Lack of Long-Term Durability of Cultured Keratinocyte Burn-Wound Coverage," *Journal of Burn Care & Rehabilitation*, vol. 12, no. 6, pp. 540–545, 1991.

[32] F. Wood, L. Martin, D. Lewis et al., "A prospective randomised clinical pilot study to compare the effectiveness of Biobrane® synthetic wound dressing, with or without autologous cell suspension, to the local standard treatment regimen in paediatric scald injuries," *Burns*, vol. 38, no. 6, pp. 830–839, 2012.

[33] F. M. Wood, M. L. Stoner, B. V. Fowler, and M. W. Fear, "The use of a non-cultured autologous cell suspension and Integra® dermal regeneration template to repair full-thickness skin wounds in a porcine model: A one-step process," *Burns*, vol. 33, no. 6, pp. 693–700, 2007.

[34] D. den Hollander, M. Albert, A. Strand, and T. C. Hardcastle, "Epidemiology and referral patterns of burns admitted to the Burns Centre at Inkosi Albert Luthuli Central Hospital, Durban," *Burns*, vol. 40, no. 6, pp. 1201–1208, 2014.

Hindawi
Stem Cells International
Volume 2019, Article ID 2168709, 13 pages
https://doi.org/10.1155/2019/2168709

Research Article

Transplantation of Human Urine-Derived Stem Cells Ameliorates Erectile Function and Cavernosal Endothelial Function by Promoting Autophagy of Corpus Cavernosal Endothelial Cells in Diabetic Erectile Dysfunction Rats

Chi Zhang,[1,2] **Daosheng Luo**,[3] **Tingting Li**,[2] **Qiyun Yang**,[1] **Yun Xie**,[1,4] **Haicheng Chen**,[1] **Linyan Lv**,[2] **Jiahui Yao**,[1,2] **Cuncan Deng**,[2] **Xiaoyan Liang**,[2] **Rongpei Wu**,[5] **Xiangzhou Sun**,[1] **Yuanyuan Zhang**,[6] **Chunhua Deng**,[1] **and Guihua Liu**[2]

[1]*Department of Andrology, The First Affiliated Hospital of Sun Yat-sen University, Guangzhou, China*
[2]*Reproductive Medicine Research Center, The Sixth Affiliated Hospital of Sun Yat-sen University, Guangzhou 510000, China*
[3]*Department of Urology, Dongguan People's Hospital, Dongguan 523000, China*
[4]*Guangdong Provincial Key Laboratory of Orthopedics and Traumatology, Guangzhou 510000, China*
[5]*Department of Urology, The First Affiliated Hospital of Sun Yat-sen University, Guangzhou 510000, China*
[6]*Wake Forest Institute for Regenerative Medicine, Wake Forest University, Winston-Salem, NC 27101, USA*

Correspondence should be addressed to Yuanyuan Zhang; yzhang@wakehealth.edu, Chunhua Deng; dch0313@163.com, and Guihua Liu; liuguihua@mail.sysu.edu.cn

Received 17 February 2019; Revised 3 July 2019; Accepted 8 August 2019; Published 9 September 2019

Guest Editor: Letizia Trovato

Aims. Cavernosal endothelial dysfunction is one of the factors in developing diabetic erectile dysfunction (DED), but the mechanism of cavernosal endothelial dysfunction is unclear. The present study is aimed at determining the contribution of autophagy in cavernosal endothelial dysfunction of DED rats and explaining the therapeutic effect of urine-derived stem cells (USCs). *Methods*. After rat corpus cavernosal vascular endothelial cells (CCECs) were isolated and cultured *in vitro*, CCECs were treated with advanced glycation end products (AGEs) to mimic the diabetic situation. Autophagy flux, proliferation, and apoptosis of CCECs were determined by mRFP-GFP-LC3 adenovirus infection combined with fluorescence observation and western blot analysis. USCs were isolated from the urine of six healthy male donors, and coculture systems of USCs and CCECs were developed to assess the protective effect of USCs for CCECs *in vitro*. The contribution of autophagy to the cellular damage in CCECs was evaluated by the autophagic inhibitor, 3-methyladenine (3-MA). Then, DED rats were induced by streptozotocin (50 mg/kg) and screened by apomorphine test (100 μg/kg). In DED rats, USCs or PBS as vehicle was administrated by intracavernous injection ($n = 15$ per group), and another 15 normal rats served as normal controls. Four weeks after injection, erectile function was evaluated by measuring the intracavernosal pressure (ICP) and mean arterial pressure (MAP). Cavernosal endothelial function and autophagic activity were examined by western blot, immunofluorescence, and transmission electron microscopy. *Results*. *In vitro*, AGE-treated CCECs displayed fewer LC3 puncta formation and expressed less LC3-II, Beclin1, and PCNA but expressed more p62 and cleaved-caspase3 than controls ($p < 0.05$). Coculture of USCs with CCECs demonstrated that USCs were able to protect CCECs from AGE-induced autophagic dysfunction and cellular damage, which could be abolished by 3-MA ($p < 0.05$). DED rats showed lower ratio of ICP/MAP, reduced expression of endothelial markers, and fewer autophagic vacuoles in the cavernosal endothelium when compared with normal rats ($p < 0.05$). Intracavernous injection of USCs improved erectile function and cavernosal endothelial function of DED rats ($p < 0.05$). Most importantly, our data showed that the repaired erectile function and cavernosal endothelial function were the result of restored autophagic activity of the cavernosal endothelium in DED rats ($p < 0.05$). *Conclusions*. Impaired autophagy is involved in the cavernosal endothelial dysfunction and erectile dysfunction of DED rats. Intracavernous injection of USCs upregulates autophagic activity in the cavernosal endothelium, contributing to ameliorating cavernosal endothelial dysfunction and finally improving the erectile dysfunction induced by diabetes.

1. Introduction

Erectile dysfunction (ED) is a common complication of diabetes, affecting 35% to 90% of male patients [1]. Diabetic ED (DED) has an earlier onset and is more severe, and its incidence increases with disease duration [1–3]. The core pathogenesis of DED is cavernosal smooth muscle relaxation disorder and corporal fibrosis, leading to corporal veno-occlusive dysfunction [4–7]. Cavernosal endothelial dysfunction is currently suggested as an initiating factor in developing DED, and it is in the upstream of smooth muscle relaxation disorder and corporal fibrosis [8–10]. Cavernosal endothelial dysfunction can be promoted by hyperglycemia-induced formation of advanced glycation end products (AGEs) or increased oxidative stress [9, 11]. But the mechanism of cavernosal endothelial dysfunction remains to be elucidated.

Autophagy is an evolutionarily conserved cellular catabolic process, in which cytoplasmic materials are encased in intracellular vesicles and then delivered to lysosome for degradation [12, 13]. In most cells, a basal level of autophagy is occurring constantly and is essential to maintain the cellular homeostasis by eliminating damaged organelles, protein aggregates, and invading pathogens [14]. Numerous studies have indicated that autophagy plays critical and complex roles in diabetes and its complications [15–17]. Autophagy defect induced by mTORC1 upregulation was found in podocytes of both animal models and humans with diabetic nephropathy [18]. And it is reported that histone HIST1H1C regulates autophagy in the development of diabetic retinopathy [19]. However, limited studies have addressed the relationship between autophagy and DED.

Owing to the complex pathogenesis, DED does not respond well to phosphodiesterase type 5 inhibitors which are currently the first-line treatment for ED [20–22]. Consequentially, it is urgent to develop new therapies targeting DED. Recently, stem cell therapy has become a novel choice for ED treatment [23]. Several types of stem cells, such as bone marrow-derived mesenchymal stem cells and adipose tissue-derived stem cells, have been proven to be effective for the treatment of DED [24–26]. Urine-derived stem cells (USCs) are a new subpopulation of stem cells isolated from human urine. Our previous study and unpublished data revealed that USCs originate from parietal epithelium cells of the renal capsule [27]. They can be easily isolated and expanded by noninvasive method *in vitro*, possess multipotential differentiation capacity, and share similar characteristics of mesenchymal stem cells (MSCs) [28–30]. We have previously demonstrated that both USCs and USCs genetically modified with bFGF could improve erectile function and repair cavernosal endothelial structure in DED rat models [31]. The exact mechanisms of USCs' repair effect on cavernosal endothelial dysfunction and whether USCs take effect via regulating autophagic activity are unclear.

Based on the above evidence, in this study, we have focused on endothelial dysfunction in DED, and thus on the autophagic changes of cavernosal endothelial cells in a diabetic state *in vitro* and *in vivo*, and whether USCs restored erectile function and cavernosal endothelial function via the regulation of autophagy.

2. Materials and Methods

2.1. Isolation, Culture, and Identification of USCs. A total of 18 sterile voided urine samples (300-400 ml) from 6 healthy male volunteers (24-28 years old) were collected. The protocol to use human urine samples conforms to the ethical guidelines of Helsinki Declaration and was approved by the Institutional Review Board of the First Affiliated Hospital of Sun Yat-sen University. Written informed consent was obtained from every urine donor. The USCs were isolated and cultured as reported previously [28]. Briefly, fresh mid- and last-stream urine samples were centrifuged at 500 × g at room temperature for 10 minutes, and the cell pellet was gently suspended with mixed medium composed of keratinocyte serum-free medium and progenitor cell medium in a 1 : 1 ratio. The cell suspension was plated in 24-well plates and incubated at 37°C in a humidified atmosphere with 5% CO_2. The culture medium was refreshed every other day. Colonies that derived from single cells were marked and passaged using 0.25% trypsin when they reached approximately 80% confluence. USCs at passage 3–4 were used for the following study.

The USCs were identified according to our previously described methods [31]. The osteogenic and adipogenic differentiation of the USCs were assessed by Alizarin red S (Santa Cruz Biotechnology, Santa Cruz, CA, USA) or Oil red O staining (Abcam, Cambridge, UK), respectively. Cell surface markers of USCs were measured with flow cytometry analysis (S3e™ Cell Sorter, Bio-Rad Laboratories, USA) by using fluorochrome-conjugated antibodies including CD24-FITC (20 μl/test; 560992, BD Biosciences, USA), CD31-FITC (20 μl/test; 560984, BD Biosciences), CD34-FITC (20 μl/test; 560942, BD Biosciences), CD44-PE (20 μl/test; 561858, BD Biosciences), CD45-PE (20 μl/test; 561866, BD Biosciences), CD73-PE (20 μl/test; 561014, BD Biosciences), CD90-APC (5 μl/test; 561971, BD Biosciences), and CD105-PE (5 μl/test; 560839, BD Biosciences).

2.2. Culture and Characterization of CCECs. The primary cultured rat corpus cavernosal vascular endothelial cells (CCECs) were purchased from Procell Life Science & Technology Co. Ltd. (Wuhan, China). CCECs were cultured in endothelial cell growth media (EGM-2; Lonza, Switzerland) at 37°C in a humidified atmosphere containing 5% CO_2. The cells were passaged using 0.25% trypsin when they reached approximately 80% confluence. Passage 2 was used for the present study. The CCECs were identified by immunofluorescent staining of cell surface-bound CD31, as described previously [32].

2.3. Treatment of CCECs. CCECs at passage 2 were randomly divided into five groups: (1) control (homoculture of CCECs only); (2) bovine serum albumin (BSA; Abcam, USA); (3) AGE-BSA (AGEs; Abcam); (4) AGEs+USCs; and (5) AGEs +USCs+3-methyladenine (3-MA; Selleckchem, USA).

The coculture was performed in a Transwell unit (Costar 3413, Corning, USA). Cell suspensions of CCECs or USCs were prepared in endothelial cell growth media, respectively, at the concentration of 1×10^5 cells/ml. CCECs (600 μl) were

cultured in the lower chamber, and USCs (100 μl) were cultured in the upper chamber separately. After being incubated overnight, CCECs were infected with mRFP-GFP-LC3 adenovirus (HanBio Technology, Shanghai, China) according to the instructions. After 2 h, CCECs were changed with complete medium, and BSA/AGEs was added into the culture medium according to the grouping for 72 h. For groups (4) and (5), the upper chambers with USCs were placed above the lower CCEC chambers. For group (5), 3-MA was added into the lower chambers for 24 h. All experiments were performed in triplicate. The concentration of AGEs (200 μg/ml) and 3-MA (2 mM) used in the present study was referred to previous studies [33–35].

2.4. Western Blot Analysis for Autophagy, Proliferation, and Apoptosis of CCECs after Treatment In Vitro. The autophagy, proliferation, and apoptosis of CCECs after treatment were analyzed by western blot as described previously [36]. Briefly, all the CCECs were harvested from each lower chamber, and proteins were extracted using RIPA lysis buffer (Cwbiotech, China) containing proteinase inhibitor cocktail (Cwbiotech) and phosphatase inhibitor cocktail (Cwbiotech). The primary antibodies included anti-PCNA (1 : 1000; 200947-2E1, ZenBio, China), anti-cleaved-caspase3 (1 : 1000; 9661, Cell Signaling Technology, USA), anti-LC3 A/B (1 : 1000; 4108, Cell Signaling Technology), anti-p62 (1 : 1000; ab56416, Abcam), anti-Beclin1 (1 : 2000; ab207612, Abcam), and anti-GAPDH (1 : 2000; Affinity Biosciences, USA) antibodies. PCNA is an indicator of cell proliferation and cleaved-caspase3 is an indicator of cell apoptosis. LC3, p62, and Beclin1 are autophagic markers. GAPDH was used as loading control.

2.5. Autophagic Flux Assay of CCECs after Treatment In Vitro via Confocal Microscopy. The fluorescent signal of GFP could be quenched under the acidic condition, but the mRFP fluorescent signal has no significant change. The neutral autophagosomes are shown as yellow puncta (RFP+GFP+), and acidic autolysosomes are shown as red puncta (RFP+ GFP-) [37]. The mRFP-GFP-LC3 adenovirus makes it possible to monitor the progression of autophagic flux.

The LC3 puncta were examined with a confocal microscope (TSC-SP8, Leica, Germany). For each group, ten independent images were randomly selected to count the number of LC3 puncta.

2.6. Establishment of a DED Rat Model and USC Implantation In Vivo. Sixty-five male Sprague-Dawley rats (8–10 weeks old) were used in this study. The animal procedures were approved by the Institutional Animal Care and Use Committee of Sun Yat-sen University. Diabetes was induced by intraperitoneal (ip) injection of streptozotocin (STZ; 50 mg/kg; Sigma-Aldrich, USA) dissolved in pH 4.5 citric acid buffer. Diabetes was defined as a random blood glucose level higher than 300 mg/dl for three consecutive days after 72 hours of STZ injection. Eight weeks after STZ injection, an apomorphine (Sigma-Aldrich) test (100 μg/kg) was performed to confirm DED rats according to Heaton's method [38].

After being anesthetized with pentobarbital sodium (50 mg/kg, ip), the DED rats received bilateral intracavernous injection of a total of 1×10^6 USCs in 200 μl phosphate-buffered saline (USC-treated group) or just 200 μl PBS (DED group) ($n = 15$ per group), as our previous study described [24]. Another 15 normal rats served as the control group.

2.7. Erectile Function Evaluation. Erectile function was evaluated via intracavernosal pressure (ICP) and the ratio of ICP to mean arterial pressure (MAP) at four weeks after intracavernous injection, as previously described [39]. Briefly, rats were anesthetized with pentobarbital sodium (50 mg/kg, ip). The left carotid artery was cannulated with a PE-50 catheter filled with heparinized saline (250 IU/ml) to monitor the MAP. A 25-gauge needle filled with heparin (250 IU/ml) was inserted into the penile crus and connected to another pressure transducer. The cavernosal nerve was isolated and hooked by a bipolar electrode 3–4 mm distal to the major pelvic ganglion. Monophasic rectangular pulses (stimulus parameter settings of 2 ms width, 5 V voltage, 25 Hz frequency, and 60 s duration) were delivered from the stimulator (BL-420F, Taimeng, China). Three electrostimulations were replicated at intervals of 10 minutes. MAP and ICP were recorded and analyzed with BL New Century 2.1 software (Taimeng). The erectile function was evaluated as the ratio of ICP/MAP to normalize for variations in systemic blood pressure. The penis was then harvested for histological and western blot analysis.

2.8. Western Blot Analysis for Endothelial Function and Autophagy in Corpus Cavernosum Tissues. The corpus cavernosum tissues were lysed, and western blot analysis was performed as described previously [36]. The primary antibodies included anti-CD31 (1 : 2000; ab222783, Abcam), anti-eNOS (1 : 500; ab76198, Abcam), anti-phosphor-eNOS (S1177) (1 : 1000; 9571, Cell Signaling Technology), anti-VEGFRA (1 : 200; ab1316, Abcam), anti-VEGFR2 (1 : 1000; 9698, Cell Signaling Technology), anti-LC3 A/B (1 : 1000; 4108, Cell Signaling Technology), anti-p62 (1 : 1000; ab56416, Abcam), anti-Beclin1 (1 : 2000; ab207612, Abcam), and anti-GAPDH (1 : 2000; Affinity Biosciences, USA) antibodies. CD31, eNOS, phosphor-eNOS (S1177), VEGFRA, and VEGFR2 are indicators of endothelial function.

2.9. Immunofluorescent Staining Analysis for Endothelial Marker in Corpus Cavernosum Tissues. The corpus cavernosum tissues were fixed in 4% paraformaldehyde overnight. Paraffin-embedded tissue specimens were routinely prepared, sectioned at 5 μm thickness. To visualize the tissular expression of endothelial marker, an anti-CD31 antibody (1 : 100; ab222783, Abcam) was used for immunofluorescent staining, as described previously [36]. Images were captured with a confocal microscope (TSC-SP8, Leica).

2.10. Autophagic Vacuole Observations via Transmission Electron Microscopy. Specimens of the corpus cavernosum were fixed in a fixative for TEM (Servicebio, China) at 4°C for 2-4 h and then postfixed in osmium tetroxide and embedded in EMBed 812 (SPI, USA). The specimens were cut into 0.1 μm sections, stained with uranyl acetate/lead citrate, and

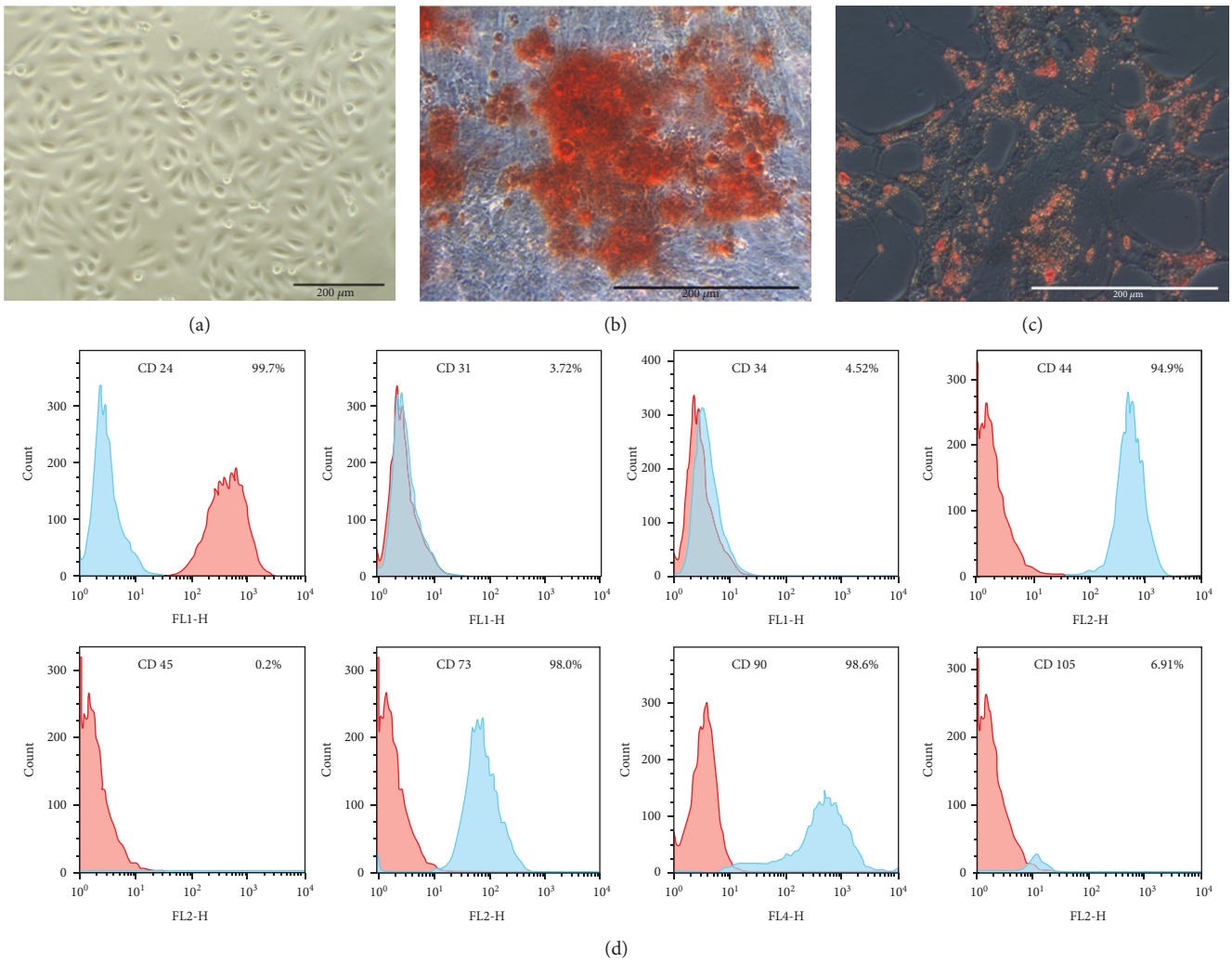

Figure 1: Characterization of urine-derived stem cells (USCs). (a) The typical rice-shaped appearance of USCs (p1). (b) Osteogenic- and (c) adipogenic-induced USCs with Alizarin red S staining or Oil red O staining, respectively. (d) Flow cytometry analysis showed that USCs (p3) were strongly positive for mesenchymal stem cell markers (CD24, CD44, CD73, and CD90), weakly positive for CD105, and negative for hematopoietic stem cell markers (CD31, CD34, and CD45).

viewed with a transmission electron microscope (TEM; HT7700, Hitachi, Japan). The tissues obtained from three rats in each group were examined. For each specimen, ten cavernosal endothelial cells were randomly selected, and the average number of autophagic vacuoles (including autophagosomes and autolysosomes) was compared between the samples collected from each group.

2.11. Statistical Analyses. Continuous values were expressed as mean ± standard deviation. One-way analysis of variance followed by a Student-Newman-Keuls post hoc test for multiple comparisons was used when appropriate. A two-tailed $p < 0.05$ was considered as statistically significant. Statistical analysis was performed with IBM SPSS Statistics 23.0 (IBM, USA).

3. Results

3.1. Characterization of USCs. USCs exhibited typical rice-shaped appearance (Figure 1(a)). The osteogenic- and adipogenic-induced USCs (stained with Alizarin red S or Oil red O, respectively) confirmed the multipotential differentiation capacity of USCs (Figures 1(b) and 1(c)). Flow cytometry analysis showed that USCs were strongly positive for MSCs markers (CD24, CD44, CD73, and CD90), weakly positive for CD105, and negative for hematopoietic stem cell markers (CD31, CD34, and CD45) (Figure 1(d)).

3.2. Characterization of CCECs. CCECs exhibited typical cobblestone-like appearance (Figure 2(a)), whose morphology and growth features were similar to previous reports [40, 41]. Immunofluorescent staining was performed to analyze the expression of endothelial marker (CD31), and more than 90% of CCECs stained positive for CD31 (Figure 2(b)).

3.3. AGEs Induce Autophagic Dysfunction and Cellular Damage in CCECs In Vitro. Western blot analysis was performed to assess autophagic markers in protein levels. Compared with blank controls, AGE treatment significantly reduced the ratio of LC3-II/LC3-I and the expression of

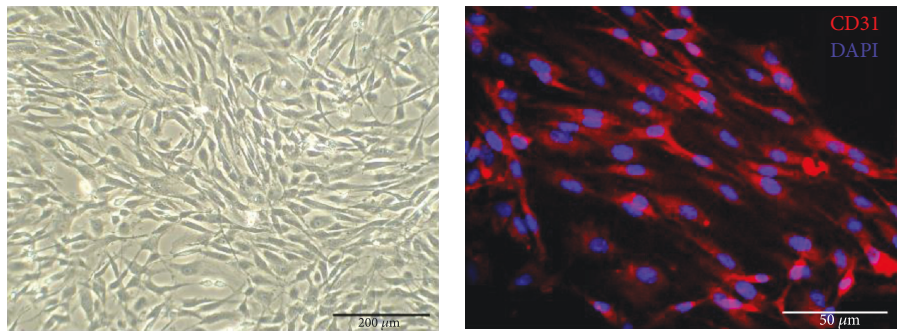

(a) (b)

Figure 2: Characterization of corpus cavernosal vascular endothelial cells (CCECs). (a) The typical cobblestone-like appearance of CCECs (p1). (b) Immunofluorescent staining showed that more than 90% of CCECs (p2) were positive for endothelial markers (CD31, red fluorescence).

Beclin1 in CCECs and simultaneously increased the level of autophagic substrate (p62) ($p < 0.05$) (Figures 3(a)–3(d)). To further confirm the effect of AGEs on autophagic flux, we examined the mRFP-GFP-LC3 puncta formation with a confocal fluorescence microscope. Consistently, CCECs treated with AGEs displayed significantly reduced number of both autophagosomes (yellow puncta) and autolysosomes (red puncta) ($p < 0.05$) (Figures 3(e)–3(g)).

Cellular viability and apoptosis of CCECs were determined via western blot analysis. As shown in Figures 4(a)–4(c), AGEs significantly decreased the expression of proliferation-related protein PCNA and increased the expression of apoptosis-related protein cleaved-caspase3 ($p < 0.05$), which indicated that AGEs induced cellular damage in CCECs.

Compared with the control group, none of the above changes was observed following BSA treatment ($p > 0.05$), indicating that BSA was not cytotoxic to CCECs (Figures 3(a)–3(g) and 4(a)–4(c)).

3.4. USCs Protect CCECs from AGE-Induced Autophagic Dysfunction and Cellular Damage In Vitro. Compared with the AGE-treated group, the ratio of LC3-II/LC3-I was higher, the expression of Beclin1 was increased, and the protein levels of p62 were reduced in the USC coculture group demonstrated by western blot analysis ($p < 0.05$) (Figures 3(a)–3(d)). Moreover, autophagic flux detection via mRFP-GFP-LC3 adenovirus showed that USCs markedly increased the number of autophagosomes in AGE-treated CCECs ($p < 0.05$). Interestingly, the autolysosomes displayed an increasing tendency, but it was not statistically significant ($p > 0.05$) (Figures 3(e)–3(g)).

Importantly, when cocultured with USCs, the expression of PCNA was significantly reduced and the expression of cleaved-caspase3 was increased in AGE-treated CCECs ($p < 0.05$) (Figures 4(a)–4(c)). These data indicated that the USCs could protect CCECs from AGE-induced autophagic dysfunction and cellular damage.

In order to further confirm the protective effect of USCs, specific autophagy inhibitor (3-MA) was added in the medium of CCECs. Our data showed that the inhibition of autophagy by 3-MA could abolish the protective effect of USCs (Figures 3(a)–3(g) and 4(a)–4(c)).

3.5. Autophagic Activity Is Decreased in Cavernosal Endothelium of DED Rats. Importantly, significantly lower ratio of LC3-II/LC3-I and expression of Beclin1 and higher levels of p62 were found in corpus cavernosum tissues of the DED group than in the normal control group by western blot analysis ($p < 0.05$) (Figures 5(a) and 5(b)). To further investigate the exact autophagic activity in the cavernosal endothelium, autophagic vacuoles were directly observed via TEM. The number of autophagic vacuoles in DED rats' cavernosal endothelial cells was significantly smaller than that in the normal control group ($p < 0.05$) (Figures 5(c) and 5(d)).

3.6. USCs Improve Erectile Function and Cavernosal Endothelial Function in DED Rats. As shown in Figures 6(a)–6(c), four weeks after USC intracavernous injection, the ICP and ICP/MAP ratio of the USC-treated group reached up to 67.6 ± 7.6 mmHg and $60.1 \pm 8.3\%$, respectively, which were significantly higher than those of the DED group (44.5 ± 3.0 mmHg and $39.8 \pm 3.4\%$) ($p < 0.05$), representing an improved erectile function. But the values were still lower than those in the normal control group (97.7 ± 5.3 mmHg and $85.7 \pm 5.4\%$) ($p < 0.05$).

A series of endothelial markers were assessed by western blot analysis (Figures 6(d) and 6(e)). The results showed a large decrease in CD31, eNOS, phospho-eNOS, VEGFRA, and VEGFR2 expression in DED rats compared with the normal control group ($p < 0.05$). Intracavernous injection of USCs partially restored the endothelial content in DED rats' penile tissues ($p < 0.05$). Similarly, the expression of CD31 decreased in DED rats' penile tissues and increased in USC treatment confirmed by immunofluorescent staining analysis (Figure 6(f)).

3.7. USCs Restore Autophagic Activity of Cavernosal Endothelium in DED Rats. Compared with the DED group, the USC-treated group exhibited significantly higher ratio of LC3-II/LC3-I, higher levels of Beclin1 in the cavernous tissue, and lower levels of p62 ($p < 0.05$) (Figures 5(a) and 5(b)). Correspondingly, more autophagic vacuoles were observed via TEM in DED rats' cavernosal endothelium after USC injection than in the DED group ($p < 0.05$) (Figures 5(c) and 5(d)). Taken together, these observations indicated that

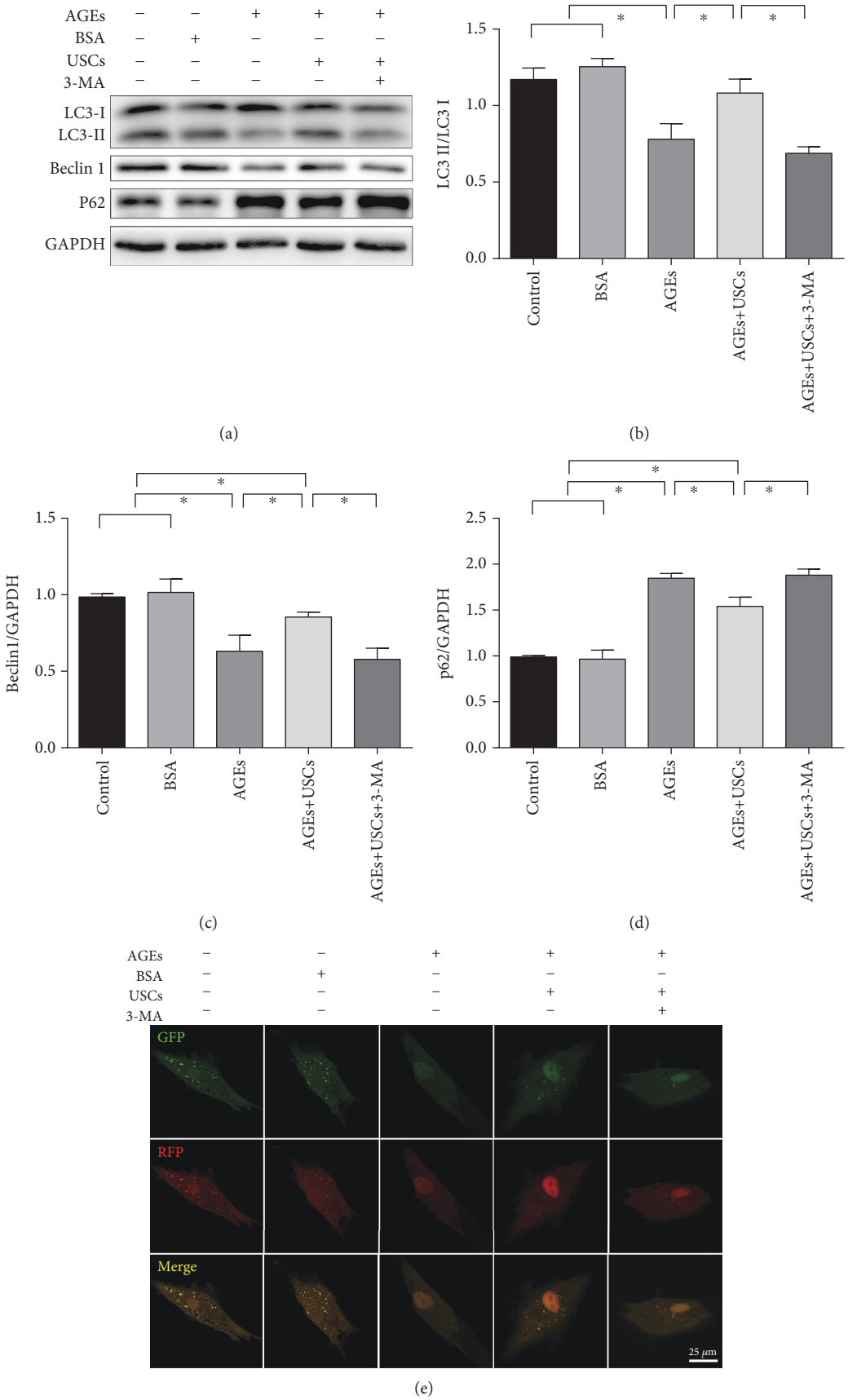

Figure 3: Continued.

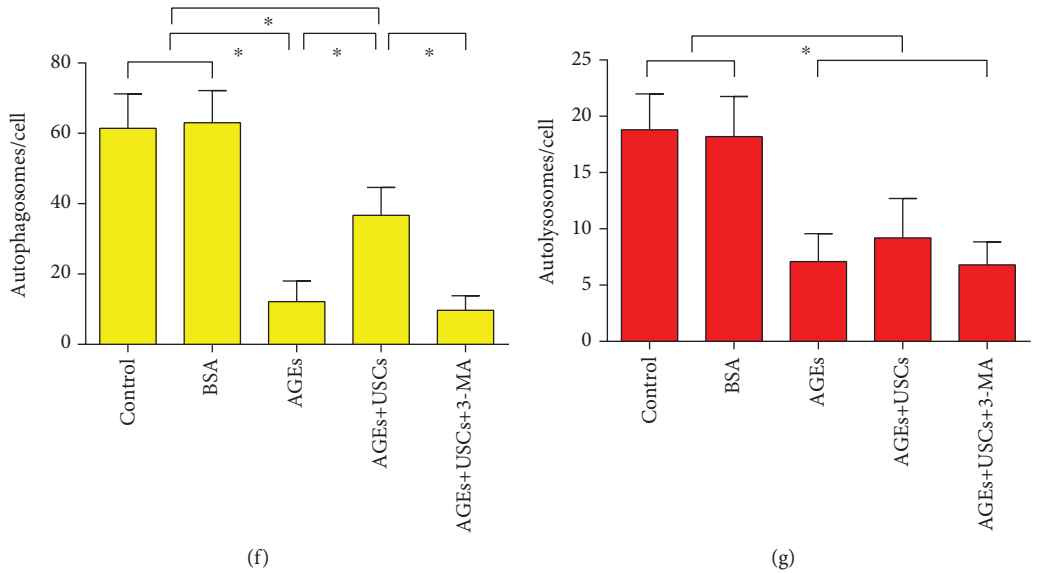

Figure 3: USCs protected CCECs from AGE-induced autophagic dysfunction in vitro and inhibition of autophagy attenuated the protective effect of USCs. (a) Western blot and (b–d) quantification for western blot of autophagy positive-related proteins (LC3 and Beclin1) and autophagy negative-related proteins (p62) in CCECs for each group. (e) Representative images of LC3 staining in CCECs for each group after infection with mRFP-GFP-LC3 adenovirus. Autophagosomes were shown as yellow puncta (RFP+GFP+), and autolysosomes were shown as red puncta (RFP+GFP-). (f, g) Quantification for autophagosome and autolysosome formation representing puncta staining sites per cell of 30 cells from each group. Treatment groups: control, BSA, AGEs, AGEs+USCs, and AGEs+USCs+3-MA. The concentration of BSA or AGEs was 200 μg/ml. The concentration of 3-MA was 2 mM, and the treat time was 24 h. $n = 3$. $^*p < 0.05$. C-caspase3: cleaved-caspase3; BSA: bovine serum albumin; AGEs: advanced glycation end products; 3-MA: 3-methyladenine.

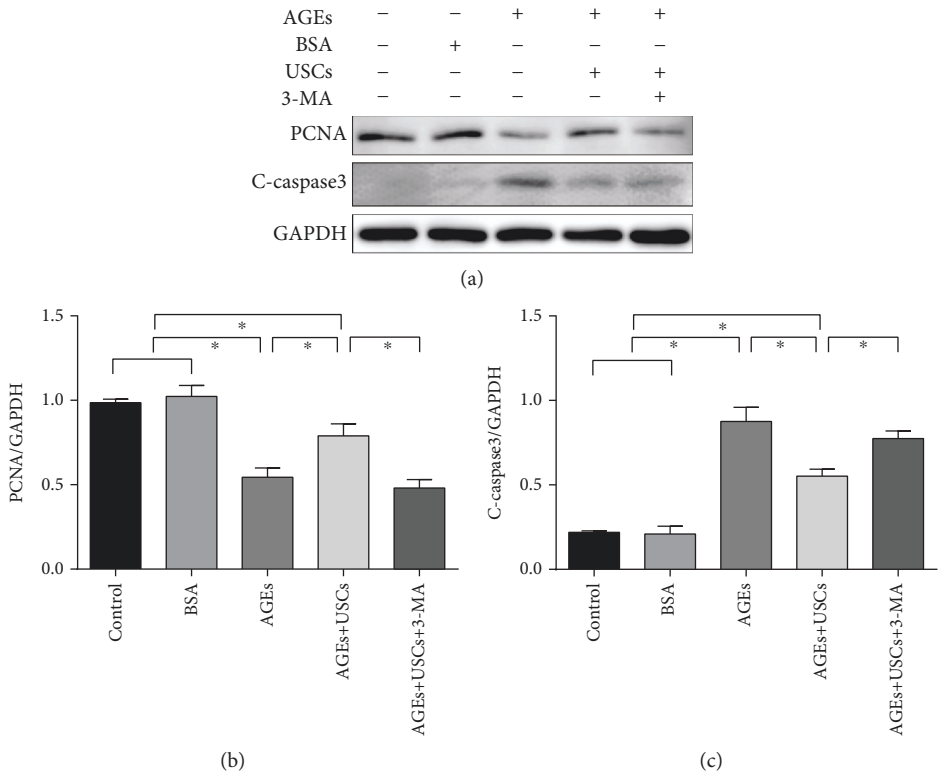

Figure 4: USCs protected CCECs from AGE-induced cellular damage in vitro and inhibition of autophagy attenuated the protective effect of USCs. (a) Western blot and (b, c) quantification for western blot of proliferation-related protein (PCNA) and apoptosis-related protein (C-caspase3) in CCECs for each group. Treatment groups: control, BSA, AGEs, AGEs+USCs, and AGEs+USCs+3-MA. The concentration of BSA or AGEs was 200 μg/ml. The concentration of 3-MA was 2 mM, and the treat time was 24 h. $n = 3$. $^*p < 0.05$. C-caspase3: cleaved-caspase3; BSA: bovine serum albumin; AGEs: advanced glycation end products; 3-MA: 3-methyladenine.

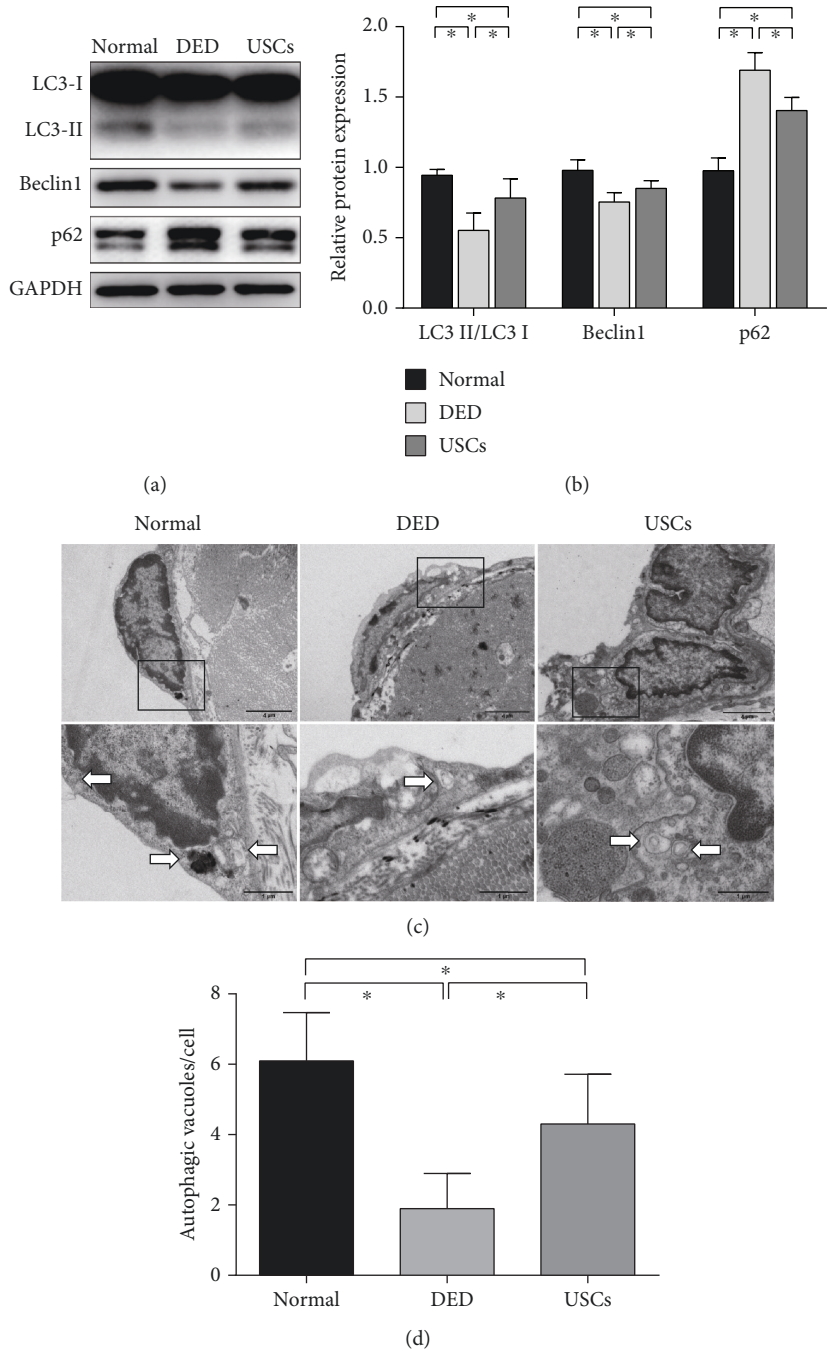

Figure 5: USCs restored autophagic activity of the cavernosal endothelium in DED rats. (a) Western blot and (b) quantification for western blot of autophagy positive-related proteins (LC3 and Beclin1) and autophagy negative-related proteins (p62) in cavernous tissue of normal rats and DED rats 4 weeks after intracavernous injection of PBS or USCs ($n = 6$ per group). (c) Representative TEM images of autophagic vacuoles (arrows) in cavernosal endothelial cells for each group. (d) Quantification for average autophagic vacuoles in 10 cells randomly selected from every specimen in each group ($n = 3$ per group). $^*p < 0.05$. TEM: transmission electron microscopy.

USCs could restore autophagic activity in the cavernosal endothelium of DED rats.

4. Discussion

The present study demonstrated that AGEs could inhibit the autophagic flux in CCECs and consequently lead to cellular damage *in vitro*. After being cocultured with USCs, the autophagic activity of CCECs was restored and cellular damage was alleviated. In further experiment, we found that suppressed autophagic activity was involved in the dysfunction of cavernosal endothelial cells in DED models. Intracavernous injection of USCs led to a significant increase of autophagic activity in the cavernosal endothelium, which coincided with improved cavernosal endothelial function and erectile function.

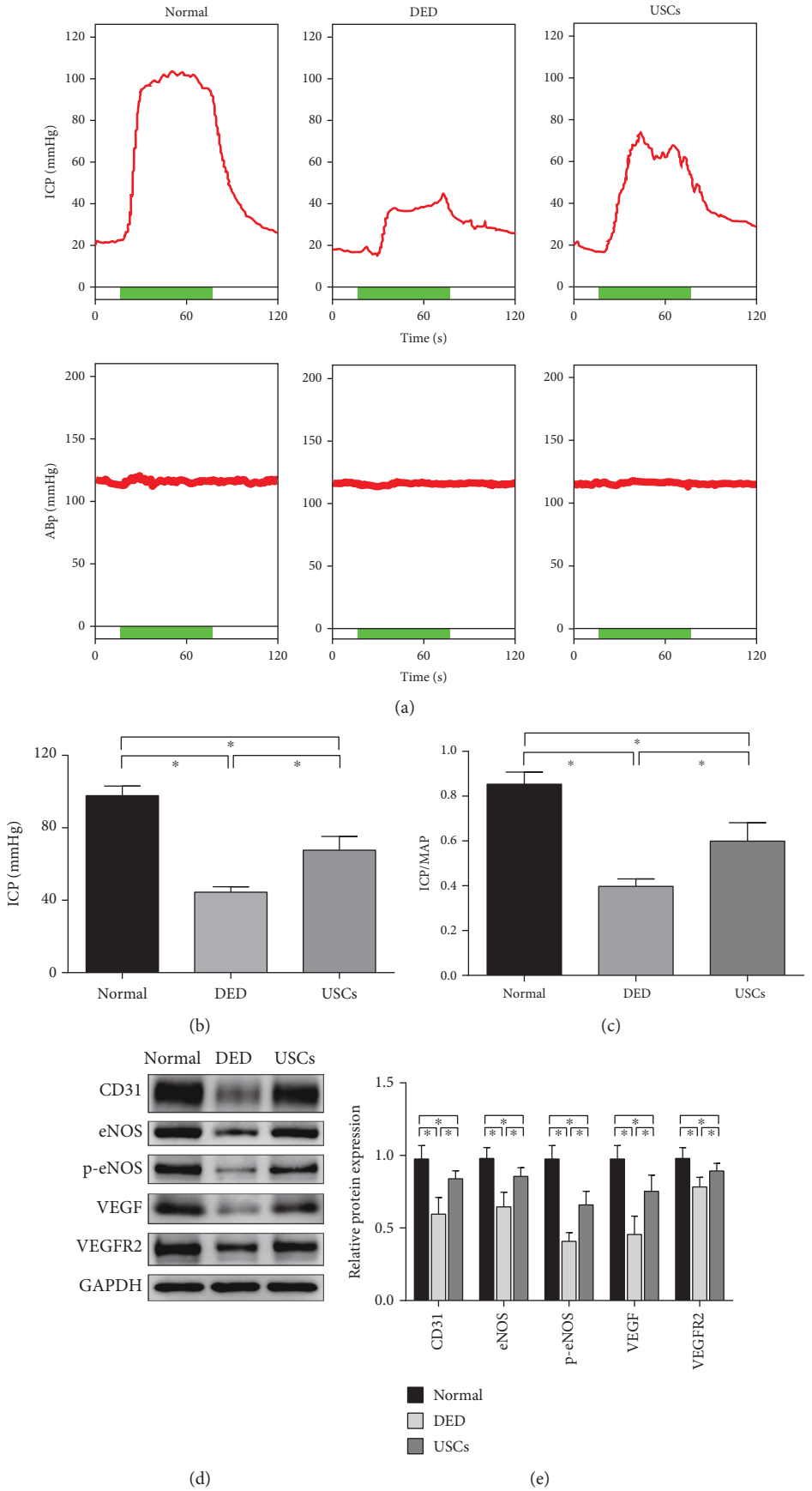

Figure 6: Continued.

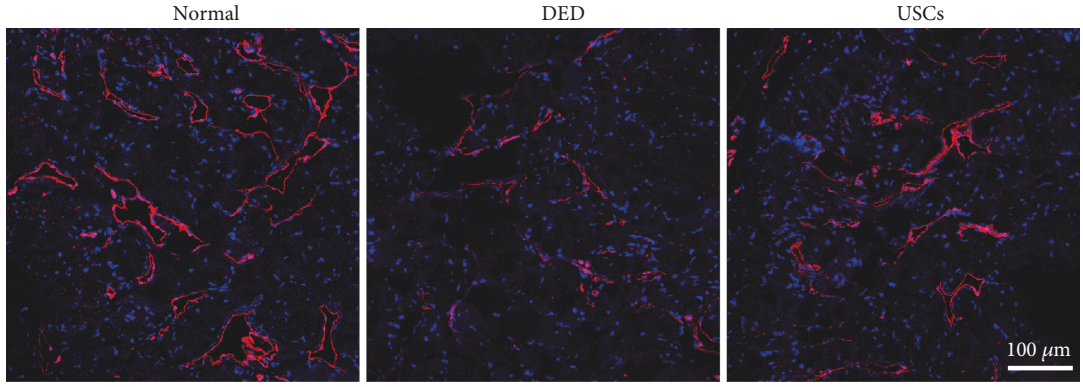

(f)

Figure 6: USCs improved erectile function and cavernosal endothelial function in diabetic erectile dysfunction (DED) rats. (a) Representative ICP tracing response to the stimulation of cavernous nerve (2 ms, 5 V, 25 Hz, and duration of 60 s) in normal rats and DED rats 4 weeks after intracavernous injection of PBS or USCs. (b) The USC injection increased ICP of DED rats, and (c) the ratio of ICP to MAP was calculated for each group ($n = 8$ per group). (d) Western blot and (e) quantification for western blot revealed that CD31, eNOS, p-eNOS, VEGFRA, and VEGFR2 expressions were all increased in the USC-treated group 4 weeks after cell transplantation ($n = 6$ per group). (f) Immunofluorescent staining confirmed the significantly higher expression of CD31 in cavernous tissue. $^*p < 0.05$. ICP: intracavernous pressure; MAP: mean arterial pressure; p-eNOS: phospho-eNOS.

AGEs are a group of heterogeneous compounds continuously formed under hyperglycemic conditions [42]. Increased levels of AGEs have been found in both diabetic human beings and rodents [34, 43]. There is evidence that the accumulation of AGEs is associated with diabetic complications [11] and is responsible for cavernosal endothelial dysfunction in DED [9, 11]. AGEs have been adopted in some previous studies [32–34] to investigate the cellular effects of chronic hyperglycemia, as a more appropriate treatment factor in *in vitro* experiment than just high glucose level. Our data showed that, after treatment with AGEs, CCECs displayed reduced number of autophagosomes and autolysosomes, reduced expression of autophagy positive-related proteins (LC3 and Beclin1), and increased expression of autophagy negative-related protein (p62), indicating a blocked autophagic flux. At the same time, the cellular viability was decreased and apoptosis was increased, revealing the AGE-induced autophagic dysfunction was relevant to cellular damage. Similar outcomes were reported in the AGE-treated podocytes and chondrocytes from previous studies [33, 34].

However, in some other studies, AGEs induced cellular autophagy, which is contrary to our results [32, 44]. There are likely several explanations for this contradiction. On the one hand, different types of cells have different sensibility and different autophagic response to AGEs. On the other hand, the concentration of AGEs and exposure time determine the treatment effects. Short exposure to AGEs causes the cells to be in a state of acute stress, which is a common trigger of autophagy, activating the cellular self-protection program [12]. But a high concentration of AGEs and long exposure time tend to cause cellular decompensation, when autophagic dysfunction and cellular damage are observed. These concentration-dependent and time-dependent effects have already been demonstrated in previous study [33, 34].

Then, we established a DED rat model to further confirm the above phenomenon *in vivo*. Besides a lower ratio of ICP/-MAP and decreased expression of a series of endothelial function-related proteins in DED rats, levels of autophagic protein markers (LC3, p62, and Beclin1) in corpus cavernosum tissues of DED rats indicate a reduced autophagic activity, which is in accordance with other studies [45]. But these results only represented the autophagic change in the whole corpus cavernosum, and the endothelium only accounts for a small proportion of penile tissue. To detect the autophagic activity exactly in the endothelium, we used TEM to observe the autophagic vacuoles in endothelial cells. We found that the number of autophagic vacuoles in DED rats' cavernosal endothelial cells was significantly fewer than that in the normal control group. Taking all the data of *in vitro* and *in vivo* experiments into consideration, we have sufficient reasons to speculate that long-standing diabetes induces autophagic dysfunction in cavernosal endothelial cells, eventually leading to endothelial dysfunction and erectile dysfunction in DED rat. In addition, it is likely that the autophagy in the cavernosal smooth muscle also plays a significant role in the condition of DED, and more studies are needed to examine its relative impact vis-à-vis the endothelium.

As we have revealed the autophagic disorder in the cavernosal endothelium of DED rats, the regulation of autophagy may be a new therapeutic target for reversing DED. It has been reported that rapamycin can ameliorate erectile function via inducing autophagy in DED rats [46]. Nevertheless, autophagy possesses organ specificity, tissue specificity, and even cell specificity, that is, a different body part has different autophagic changes in the same disease. Moreover, excessively activated autophagy would lead to negative impacts [47]. Therefore, systemic administration of autophagy-regulated agents is inappropriate. In recent years, stem cell therapy emerges as a promising strategy in treating chronic diseases [48, 49]. Stem cells can help repair

damaged tissues or structures towards the normal state, and numerous studies have demonstrated that stem cells take effect via restoring autophagy homeostasis [50, 51]. Several types of MSCs, such as bone marrow-derived mesenchymal stem cells and adipose tissue-derived stem cells, have been utilized to treat DED via intracavernous injection and shown positive effects [24, 25]. However, these stem cells must be obtained by invasive methods, thus limiting their use in clinical practice. USCs may be a better cell candidate as they can be obtained through a safe, simple, low-cost, and noninvasive procedure.

In this study, we utilized a coculture system to investigate the effects of USCs on CCECs. We found that USCs could partly correct the autophagic disorder of AGE-treated CCECs and reduce cellular damage *in vitro*, and these protective effects could be abolished by autophagy inhibitors. Furthermore, we found that intracavernous injection restored autophagic activity in cavernosal endothelial cells of DED rats, as well as the cavernosal endothelial function and erectile function. These outcomes contribute to a better understanding of the mechanism of USCs in the treatment of DED. Our previous outcomes showed that rare labeled USCs could be tracked in the penile tissue since day 7 after cell transplantation, which was similar to most studies that utilized other MSCs to treat ED rat models [31]. Thus, we speculate that it was the paracrine effect of USCs that regulated autophagic balance due to USCs were able to secrete lots of paracrine factors [30], and further studies are needed to verify this hypothesis. It is reported that VEGF expressed by MSCs can take part in autophagy via triggering the PI3K/AKT/mTOR signaling pathway and consequently ameliorate DED in rats [45]. Maybe USCs regulate autophagy via the same signaling pathway, as we have demonstrated that VEGF is one of the growth factors that USCs secrete [31].

Due to the fact that human cells were injected into immunocompetent rats, the issue of immune tolerance is very important. As a type of MSCs, USCs possess the same immunomodulatory and immunosuppressive property, which permits their allogeneic or even xenogeneic transplantation into immunocompetent recipients in the absence of immunosuppressants [52]. Our previous studies have proven that neither immune reaction nor inflammatory response occurred within the injected sites of rats' penile tissue after injection of USCs [31, 36]. As for the limitation of USCs, their therapeutic effect may be influenced by changes in the biochemical composition of urine. Thus, for patients with urological diseases, such as urinary infection and renal or other urologic neoplasms, their USCs do not appear to be suitable for autologous cell transplantation.

Inevitably, some limitations existed in our study. First, the exact autophagic pathway that is abnormal in DED and by which USCs restore autophagic activity of the cavernosal endothelium needs to be clarified in further studies. Second, no attempt was done to assess changes in the functions of cavernosal smooth muscle, fibroblasts, or peripheral nerve after endothelial dysfunction was alleviated. Third, the effects of USCs are complicated, and it is unclear how long the USCs persist, when the paracrine effects occur, and how long the effects last.

5. Conclusion

Our study suggests that impaired autophagy is involved in the cavernosal endothelial dysfunction and erectile dysfunction of DED rats. Intracavernous injection of USCs upregulates autophagic activity in the cavernosal endothelium, contributing to ameliorating cavernosal endothelial dysfunction and finally improving the erectile dysfunction induced by diabetes. These findings provide a basis for the future use of USCs as a new biological therapeutic approach for DED.

Data Availability

The data are available by contacting the corresponding authors.

Conflicts of Interest

The authors declare that there is no duality of interest associated with this manuscript.

Authors' Contributions

Chi Zhang, Daosheng Luo, and Tingting Li contributed equally to this work.

Acknowledgments

This work was supported by the National Natural Science Foundation of China (grant numbers 81671449, 81671834, 81571489, and 81871110); the Frontier and Key Technology Innovation Special Foundation of Guangdong Province, China (grant number 2016B030230001); the Natural Science Foundation of Guangdong Province, China (grant numbers 2015A030313013, 2016A030313229, and 2018A030310286); the Health Care Collaborative Innovation Foundation Major Projects of Guangzhou City, Guangdong Province, China (grant number 201604020189); and the Youth Teacher Training Project of Sun Yat-sen University (grant numbers 17ykpy68 and 18ykpy09).

References

[1] L. S. Malavige and J. C. Levy, "Erectile Dysfunction in Diabetes Mellitus," *The Journal of Sexual Medicine*, vol. 6, no. 5, pp. 1232–1247, 2009.

[2] V. S. Thorve, A. D. Kshirsagar, N. S. Vyawahare, V. S. Joshi, K. G. Ingale, and R. J. Mohite, "Diabetes-induced erectile dysfunction: epidemiology, pathophysiology and management," *Journal of Diabetes and its Complications*, vol. 25, no. 2, pp. 129–136, 2011.

[3] D. F. Penson, D. M. Latini, D. P. Lubeck, K. L. Wallace, J. M. Henning, and T. F. Lue, "Do impotent men with diabetes have more severe erectile dysfunction and worse quality of life than the general population of impotent patients? Results from the Exploratory Comprehensive Evaluation of Erectile Dysfunction (ExCEED) database," *Diabetes Care*, vol. 26, no. 4, pp. 1093–1099, 2003.

[4] I. S. De Tejada, J. Angulo, S. Cellek et al., "Pathophysiology of Erectile Dysfunction," *The Journal of Sexual Medicine*, vol. 2, no. 1, pp. 26–39, 2005.

[5] J. Hidalgo-Tamola and K. Chitaley, "Type 2 Diabetes Mellitus and Erectile Dysfunction," *The Journal of Sexual Medicine*, vol. 6, no. 4, pp. 916–926, 2009.

[6] I. Kovanecz, G. Nolazco, M. G. Ferrini et al., "Early onset of fibrosis within the arterial media in a rat model of type 2 diabetes mellitus with erectile dysfunction," *BJU International*, vol. 103, no. 10, pp. 1396–1404, 2009.

[7] W. J. Li, M. Xu, M. Gu et al., "Losartan preserves erectile function by suppression of apoptosis and fibrosis of corpus cavernosum and corporal veno-occlusive dysfunction in diabetic rats," *Cellular Physiology and Biochemistry*, vol. 42, no. 1, pp. 333–345, 2017.

[8] Z. A. Kamenov, "A comprehensive review of erectile dysfunction in men with diabetes," *Experimental and Clinical Endocrinology & Diabetes*, vol. 123, no. 3, pp. 141–158, 2015.

[9] A. Castela and C. Costa, "Molecular mechanisms associated with diabetic endothelial-erectile dysfunction," *Nature Reviews. Urology*, vol. 13, no. 5, pp. 266–274, 2016.

[10] B. Musicki and A. L. Burnett, "Endothelial dysfunction in diabetic erectile dysfunction," *International Journal of Impotence Research*, vol. 19, no. 2, pp. 129–138, 2007.

[11] N. Ahmed, "Advanced glycation endproducts–role in pathology of diabetic complications," *Diabetes Research and Clinical Practice*, vol. 67, no. 1, pp. 3–21, 2005.

[12] N. Mizushima and M. Komatsu, "Autophagy: renovation of cells and tissues," *Cell*, vol. 147, no. 4, pp. 728–741, 2011.

[13] N. Mizushima, B. Levine, A. M. Cuervo, and D. J. Klionsky, "Autophagy fights disease through cellular self-digestion," *Nature*, vol. 451, no. 7182, pp. 1069–1075, 2008.

[14] C. He and D. J. Klionsky, "Regulation mechanisms and signaling pathways of autophagy," *Annual Review of Genetics*, vol. 43, no. 1, pp. 67–93, 2009.

[15] Y. Riahi, J. D. Wikstrom, E. Bachar-Wikstrom et al., "Autophagy is a major regulator of beta cell insulin homeostasis," *Diabetologia*, vol. 59, no. 7, pp. 1480–1491, 2016.

[16] Z. F. Chen, Y. B. Li, J. Y. Han et al., "The double-edged effect of autophagy in pancreatic beta cells and diabetes," *Autophagy*, vol. 7, no. 1, pp. 12–16, 2011.

[17] D. Bhattacharya, M. Mukhopadhyay, M. Bhattacharyya, and P. Karmakar, "Is autophagy associated with diabetes mellitus and its complications? A review," *EXCLI Journal*, vol. 17, pp. 709–720, 2018.

[18] T. B. Huber, C. L. Edelstein, B. Hartleben et al., "Emerging role of autophagy in kidney function, diseases and aging," *Autophagy*, vol. 8, no. 7, pp. 1009–1031, 2012.

[19] W. Wang, Q. Wang, D. Wan et al., "Histone HIST1H1C/H1.2 regulates autophagy in the development of diabetic retinopathy," *Autophagy*, vol. 13, no. 5, pp. 941–954, 2017.

[20] B. G. A. Stuckey, M. N. Jadzinsky, L. J. Murphy et al., "Sildenafil citrate for treatment of erectile dysfunction in men with type 1 diabetes: results of a randomized controlled trial," *Diabetes Care*, vol. 26, no. 2, pp. 279–284, 2003.

[21] I. Goldstein, J. M. Young, J. Fischer et al., "Vardenafil, a new phosphodiesterase type 5 inhibitor, in the treatment of erectile dysfunction in men with diabetes: a multicenter double-blind placebo-controlled fixed-dose study," *Diabetes Care*, vol. 26, no. 3, pp. 777–783, 2003.

[22] Y. Vardi, "Microvascular complications in diabetic erectile dysfunction: do we need other alternatives?," *Diabetes Care*, vol. 32, suppl_2, pp. S420–S422, 2009.

[23] A. Alwaal, U. B. Zaid, C. S. Lin, and T. F. Lue, "Stem cell treatment of erectile dysfunction," *Advanced Drug Delivery Reviews*, vol. 82-83, pp. 137–144, 2015.

[24] G. Liu, X. Sun, J. Bian et al., "Correction of diabetic erectile dysfunction with adipose derived stem cells modified with the vascular endothelial growth factor gene in a rodent diabetic model," *PLoS One*, vol. 8, no. 8, p. e72790, 2013.

[25] Y. He, W. He, G. Qin, J. Luo, and M. Xiao, "Transplantation KCNMA1 modified bone marrow-mesenchymal stem cell therapy for diabetes mellitus-induced erectile dysfunction," *Andrologia*, vol. 46, no. 5, pp. 479–486, 2014.

[26] M. Li, H. Li, Y. Ruan, T. Wang, and J. Liu, "Stem cell therapy for diabetic erectile dysfunction in rats: a meta-analysis," *PLoS One*, vol. 11, no. 4, p. e0154341, 2016.

[27] S. Bharadwaj, G. Liu, Y. Shi et al., "Multipotential differentiation of human urine-derived stem cells: potential for therapeutic applications in urology," *Stem Cells*, vol. 31, no. 9, pp. 1840–1856, 2013.

[28] Y. Zhang, E. McNeill, H. Tian et al., "Urine derived cells are a potential source for urological tissue reconstruction," *The Journal of Urology*, vol. 180, no. 5, pp. 2226–2233, 2008.

[29] G. Liu, X. Wang, X. Sun, C. Deng, A. Atala, and Y. Zhang, "The effect of urine-derived stem cells expressing VEGF loaded in collagen hydrogels on myogenesis and innervation following after subcutaneous implantation in nude mice," *Biomaterials*, vol. 34, no. 34, pp. 8617–8629, 2013.

[30] G. Liu, R. Wu, B. Yang et al., "Human urine-derived stem cell differentiation to endothelial cells with barrier function and nitric oxide production," *Stem Cells Translational Medicine*, vol. 7, no. 9, pp. 686–698, 2018.

[31] B. Ouyang, X. Sun, D. Han et al., "Human urine-derived stem cells alone or genetically-modified with FGF2 Improve type 2 diabetic erectile dysfunction in a rat model," *PLoS One*, vol. 9, no. 3, p. e92825, 2014.

[32] H. Jin, Z. Zhang, C. Wang et al., "Melatonin protects endothelial progenitor cells against AGE-induced apoptosis via autophagy flux stimulation and promotes wound healing in diabetic mice," *Experimental & Molecular Medicine*, vol. 50, no. 11, p. 154, 2018.

[33] Z. J. Wang, H. B. Zhang, C. Chen, H. Huang, and J. X. Liang, "Effect of PPARG on AGEs-induced AKT/MTOR signaling-associated human chondrocytes autophagy," *Cell Biology International*, vol. 42, no. 7, pp. 841–848, 2018.

[34] X. Zhao, Y. Chen, X. Tan et al., "Advanced glycation endproducts suppress autophagic flux in podocytes by activating mammalian target of rapamycin and inhibiting nuclear translocation of transcription factor EB," *The Journal of Pathology*, vol. 245, no. 2, pp. 235–248, 2018.

[35] Y. Wang, Z. Hu, Z. Liu et al., "MTOR inhibition attenuates DNA damage and apoptosis through autophagy-mediated suppression of CREB1," *Autophagy*, vol. 9, no. 12, pp. 2069–2086, 2013.

[36] Q. Yang, X. Chen, T. Zheng et al., "Transplantation of human urine-derived stem cells transfected with pigment epithelium-derived factor to protect erectile function in a rat model of cavernous nerve injury," *Cell Transplantation*, vol. 25, no. 11, pp. 1987–2001, 2016.

[37] D. J. Klionsky, K. Abdelmohsen, A. Abe et al., "Guidelines for the use and interpretation of assays for monitoring autophagy (3rd edition)," *Autophagy*, vol. 12, no. 1, pp. 1–222, 2016.

[38] J. P. W. Heaton, S. J. Varrin, and A. Morales, "The characterization of a bio-assay of erectile function in a rat model," *The Journal of Urology*, vol. 145, no. 5, pp. 1099–1102, 1991.

[39] G. Liu, X. Sun, Y. Dai et al., "Chronic administration of sildenafil modified the impaired VEGF system and improved the erectile function in rats with diabetic erectile dysfunction," *The Journal of Sexual Medicine*, vol. 7, no. 12, pp. 3868–3878, 2010.

[40] J. Chen, C. L. Sun, Z. Chen et al., "Separation, culture and identification of SD rat corpus cavernosal endothelial cells," *Andrologia*, vol. 44, no. 4, pp. 250–255, 2012.

[41] Z. Zhang, H. Y. Zhang, Y. Zhang, and H. Li, "Inactivation of the Ras/MAPK/PPARγ signaling axis alleviates diabetic mellitus-induced erectile dysfunction through suppression of corpus cavernosal endothelial cell apoptosis by inhibiting HMGCS2 expression," *Endocrine*, vol. 63, no. 3, pp. 615–631, 2019.

[42] K. Nowotny, T. Jung, A. Hohn, D. Weber, and T. Grune, "Advanced glycation end products and oxidative stress in type 2 diabetes mellitus," *Biomolecules*, vol. 5, no. 1, pp. 194–222, 2015.

[43] B. K. Kilhovd, T. J. Berg, K. I. Birkeland, P. Thorsby, and K. F. Hanssen, "Serum levels of advanced glycation end products are increased in patients with type 2 diabetes and coronary heart disease," *Diabetes Care*, vol. 22, no. 9, pp. 1543–1548, 1999.

[44] X. Hou, Z. Hu, H. Xu et al., "Advanced glycation endproducts trigger autophagy in cadiomyocyte via RAGE/PI3K/AKT/mTOR pathway," *Cardiovascular Diabetology*, vol. 13, no. 1, p. 78, 2014.

[45] G. Q. Zhu, S. H. Jeon, W. J. Bae et al., "Efficient promotion of autophagy and angiogenesis using mesenchymal stem cell therapy enhanced by the low-energy shock waves in the treatment of erectile dysfunction," *Stem Cells International*, vol. 2018, 14 pages, 2018.

[46] H. Lin, T. Wang, Y. Ruan et al., "Rapamycin supplementation may ameliorate erectile function in rats with streptozotocin-induced type 1 diabetes by inducing autophagy and inhibiting apoptosis, endothelial dysfunction, and corporal fibrosis," *The Journal of Sexual Medicine*, vol. 15, no. 9, pp. 1246–1259, 2018.

[47] G. Das, B. V. Shravage, and E. H. Baehrecke, "Regulation and function of autophagy during cell survival and cell death," *Cold Spring Harbor Perspectives in Biology*, vol. 4, no. 6, p. a008813, 2012.

[48] M. F. Wang, Y. B. Li, X. J. Gao, H. Y. Zhang, S. Lin, and Y. Y. Zhu, "Efficacy and safety of autologous stem cell transplantation for decompensated liver cirrhosis: a retrospective cohort study," *World Journal of Stem Cells*, vol. 10, no. 10, pp. 138–145, 2018.

[49] E. Favaro, A. Carpanetto, S. Lamorte et al., "Human mesenchymal stem cell-derived microvesicles modulate T cell response to islet antigen glutamic acid decarboxylase in patients with type 1 diabetes," *Diabetologia*, vol. 57, no. 8, pp. 1664–1673, 2014.

[50] H. He, Q. Zeng, G. Huang et al., "Bone marrow mesenchymal stem cell transplantation exerts neuroprotective effects following cerebral ischemia/reperfusion injury by inhibiting autophagy via the PI3K/Akt pathway," *Brain Research*, vol. 1707, pp. 124–132, 2019.

[51] B. P. Woodall and A. B. Gustafsson, "Mesenchymal stem cell-mediated autophagy inhibition," *Circulation Research*, vol. 123, no. 5, pp. 518–520, 2018.

[52] C. S. Lin, G. Lin, and T. F. Lue, "Allogeneic and xenogeneic transplantation of adipose-derived stem cells in immunocompetent recipients without immunosuppressants," *Stem Cells and Development*, vol. 21, no. 15, pp. 2770–2778, 2012.

Hindawi
Stem Cells International
Volume 2019, Article ID 9843407, 8 pages
https://doi.org/10.1155/2019/9843407

Clinical Study

The Role of Autologous Dermal Micrografts in Regenerative Surgery: A Clinical Experimental Study

Marco Mario Tresoldi,[1,2] **Antonio Graziano**,[3,4] **Alberto Malovini**,[5] **Angela Faga**,[6] **and Giovanni Nicoletti**[1,2,6]

[1]*Plastic and Reconstructive Surgery, Department of Clinical Surgical, Diagnostic and Pediatric Sciences, University of Pavia, Viale Brambilla, 74 Pavia, Italy*
[2]*Plastic and Reconstructive Surgery Unit, Department of Surgery, Istituti Clinici Scientifici Maugeri, Via Salvatore Maugeri, 10 Pavia, Italy*
[3]*Department of Public Health, Experimental and Forensic Medicine, University of Pavia, Via Forlanini 6, Pavia, Italy*
[4]*Sbarro Health Research Organization (SHRO), Temple University, 1900 N 12th St., Philadelphia, PA 19122, USA*
[5]*Laboratory of Informatics and Systems Engineering for Clinical Research, Istituti Clinici Scientifici Maugeri, Via Salvatore Maugeri, 10 Pavia, Italy*
[6]*Advanced Technologies for Regenerative Medicine and Inductive Surgery Research Center, University of Pavia, Viale Brambilla, 74 Pavia, Italy*

Correspondence should be addressed to Marco Mario Tresoldi; marcomario.tresoldi@unipv.it

Received 26 March 2019; Revised 3 July 2019; Accepted 4 August 2019; Published 8 September 2019

Guest Editor: Fabio Naro

The aim of the study was the objective assessment of the effectiveness of a microfragmented dermal extract obtained with Rigenera™ technology in promoting the wound healing process in an *in vivo* homogeneous experimental human acute surgical wound model. The study included 20 patients with 24 acute postsurgical soft tissue loss and a planned sequential two-stage repair with a dermal substitute and an autologous split-thickness skin graft. Each acute postsurgical soft tissue loss was randomized to be treated either with an Integra® dermal substitute enriched with the autologous dermal micrografts obtained with Rigenera™ technology (group A—Rigenera™ protocol) or with an Integra® dermal substitute only (group B—control). The reepithelialization rate in the wounds was assessed in both groups at 4 weeks through digital photography with the software "ImageJ." The dermal cell suspension enrichment with the Rigenera™ technology was considered effective if the reepithelialized area was higher than 25% of the total wound surface as this threshold was considered far beyond the expected spontaneous reepithelialization rate. In the Rigenera™ protocol group, the statistical analysis failed to demonstrate any significant difference vs. the controls. The old age of the patients likely influenced the outcome as the stem cell regenerative potential is reduced in the elderly. A further explanation for the unsatisfying results of our trial might be the inadequate amount of dermal stem cells used to enrich the dermal substitutes. In our study, we used a 1 : 200 donor/recipient site ratio to minimize donor site morbidity. The gross dimensional disparity between the donor and recipient sites and the low concentration of dermal mesenchymal stromal stem cells might explain the poor epithelial proliferative boost observed in our study. A potential option in the future might be preconditioning of the dermal stem cell harvest with senolytic active principles that would fully enhance their regenerative potential. This trial is registered with trial protocol number NCT03912675.

1. Introduction

The dermal extracellular matrix plays a relevant both structural and functional role in signalling cell proliferation, development, shaping, function, and migration. The dermis is provided with a relevant both mesenchymal and adnexa-related stem cell pool. Such properties support the use of dermis-derived extracts to stimulate tissue

regeneration [1–3]. Currently, many technologies are available to separate and expand dermis-derived cells to obtain injectable autologous cell suspensions for regenerative purposes [4, 5]. Recently, in the European Union area, cell manipulation underwent restricting regulations that significantly reduced the availability of cell expansion technology. According to current regulations, any cell manipulation involving enzymatic treatment and cell culture expansion is allowed in Cell Factories only, with a relevant increase of time and cost burden [6].

Recently, the development of an innovative technology for dermal mechanical microfragmentation named Rigenera™ allowed the harvest of a filtered available cell pool without any enzymatic manipulation. Such a cell fraction, rich in progenitor cells, was successfully used in the treatment of difficult-to-heal wound [3, 7–9]. The advantage of this innovative technology is its unrestricted use in any clinical context and setting.

Nevertheless, such an evidence was demonstrated within the frame of pathologies with heterogeneous aetiology. The aim of the study was the objective assessment of the effectiveness of such a microfragmented dermal extract in promoting the wound healing process in an *in vivo* homogeneous experimental human acute surgical wound model.

2. Materials and Methods

2.1. Study Design. A prospective randomized controlled open clinical trial was carried out at the Plastic and Reconstructive Surgery Unit of the Istituti Clinici Scientifici Maugeri. Twenty patients (4 females and 16 males), with an age range of 53-93 years (mean 77.80, median 79), were enrolled in the trial over a period of 15 months, from September 2017 to December 2018. The exclusion criteria were wound infection, chemotherapy in the last 6 months, use of corticosteroids or immunosuppressive treatment, and metabolic, endocrine, autoimmune, and collagen diseases. The study included patients with a postsurgical defect in any site of the body with a size range of 4-400 cm^2. The surgical defect followed an immediate excision of 22 skin cancers, 1 ulcerated actinic keratosis, and 1 chronic difficult-to-heal wound (Table 1). A sequential two-stage repair with a dermal substitute and an autologous split-thickness skin graft was planned. The acute postsurgical soft tissue loss was considered the experimental unit of the study irrespective of the number of wounds per patient. Twenty-four experimental units were enrolled in the trial. Each unit, which fulfilled the entry criteria, was randomized to be treated either with an Integra® dermal substitute enriched with the autologous dermal micrografts obtained with Rigenera™ protocol (group A—Rigenera™ protocol) or with an Integra® dermal substitute only (group B—control). Each group included 12 experimental units. All of the wounds were planned for a sequential second-stage repair with a split-thickness skin graft at the time of complete engraftment of the Integra® dermal substitute. According to our clinical experience, the time lag between the first and the second surgical stages was around 4 weeks. The expected endpoint was a spontaneous reepithelialization higher than 25% of the total wound area in the group treated with Rigenera™ protocol at 4 weeks that would contraindicate the second staged cover with a split-thickness skin graft. The secondary endpoint was the comparison of the reepithelialization rate at 4 weeks after the first surgical stage between the group treated with Rigenera™ protocol and the controls.

Table 1: Cohort's characteristics. Categorical variables' distribution is described by counts and relative frequencies (%); continuous variables' distribution by median (25^{th}–75^{th} percentiles).

Variable	Distribution
Age (years)	78.0 (74.5-84.0)
Gender	
Females	4 (17.39%)
Males	16 (82.61%)
Localization	
Limbs	7 (30.43%)
Scalp	1 (4.35%)
Face	15 (65.22%)
Protocol	
A	11 (47.83%)
B	12 (52.17%)
Cause	
BCC	16 (69.57%)
SCC	4 (17.39%)
Other	3 (13.09%)
T1 area (cm^2)	9.26 (7.06-12.54)
Reepithelialization (%)	13.94 (11.96-20.85)
≥25%	3 (13.04%)
<25%	20 (86.96%)

The reepithelialization rate in the wounds was assessed at each time point of the study through digital photography with the software "ImageJ" (Figure 1). As a wound spontaneously reduces in size, due to a physiologic shrinkage process, the measurement of the reepithelialization rate was referred to the actual total wound size at each time point.

A formal informed written consent was obtained from all of the patients, and the study conformed to the Declaration of Helsinki. The trial was approved by the Ethical Committee (protocol number 2142) of the Istituti Clinici Scientifici Maugeri SB SpA IRCCS of Pavia.

2.2. Materials and Methods. The micrografts were obtained by Rigeneracons, a single-use sterile CE-certified Class I medical device able to mechanically disaggregate tissues into micrografts that are immediately available for transfer in the clinical practice [10]. It is made of a plastic container provided with an openable lid divided into two chambers by a stationary stainless steel grid with 100 hexagonal holes. Around each hole, 6 microblades are designed for efficient cutting of hard and soft tissues allowing a filtration cut-off of about 80 μm. The upper chamber is provided with a rotating helix forcing the tissue fragments through the grid towards the bottom chamber. The rotation of Rigeneracons

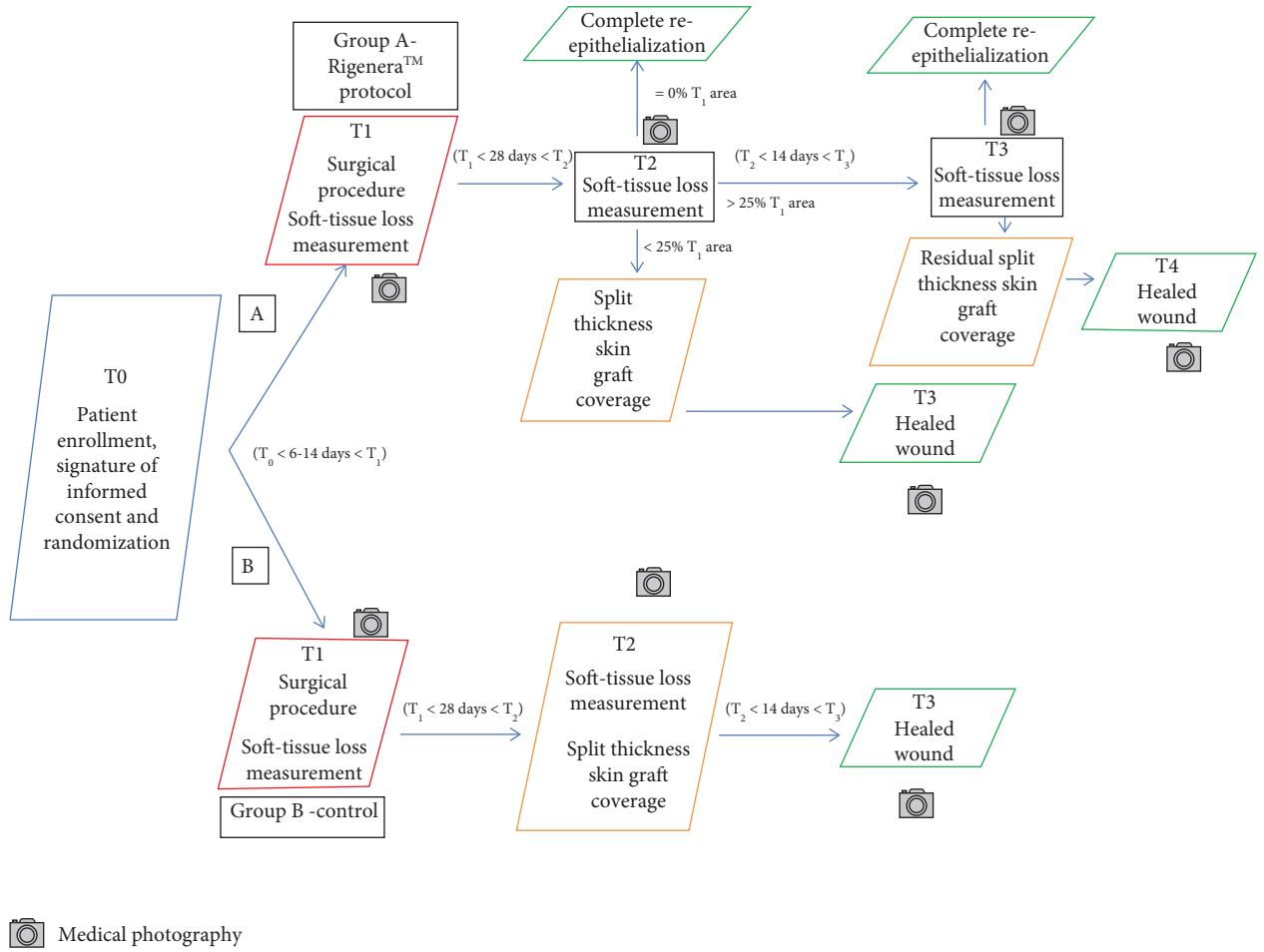

Figure 1: Scheme of the overall study structure.

is activated by a Rigenera OR-PRO machine (Esacrom, Italy) using a connection adaptor (Adacons Max).

2.3. The Operative Protocol. The operative protocol consists of different steps:

(a) Choice of the micrograft donor site with preference of the retroauricular region

(b) Gentle blade shaving of the donor site to remove the epidermis and obtain a bare papillary dermis

(c) Harvest of the adequate number of 3 mm punch biopsies from the previously deepithelialized skin; the number of dermal punch biopsies calculated according to the size of the wound, considering that 1 mm^2 of the dermal graft was expected to regenerate an epithelial cover up to 2 cm^2 (Figure 2)

(d) Loading the disposable Rigeneracons with a maximum of 3 dermal samples at a time and addition of 2.5 ml of saline solution (Figures 3 and 4)

(e) Device connection to the rotating machine, operating at 80 rpm for 90 seconds, that provides a mechanical disaggregation of the dermal sample into a suspension containing autologous dermal micrografts (Figure 5)

(f) Aspiration of the micrografts containing saline solution with a sterile syringe (Figure 6)

(g) Cover of the postsurgical soft tissue loss with Integra® dermal substitute (Figure 7)

(h) Fixation of the dermal substitute with stitches and gentle imbibition with the saline micrograft suspension (Figure 8)

(i) Infiltration of the micrograft suspension in the perilesional tissues

2.4. The Treatment. The time points of the study were designed as follows:

(i) T_0: starting time includes patient enrollment, signature of informed consent, and randomization.

(ii) T_1: the first-stage was characterized by surgical procedure of skin lesion excision, digital medical photographs, and soft-tissue loss measurement were obtained with the use of the "ImageJ" program. Soft tissue loss was covered with an Integra® dermal

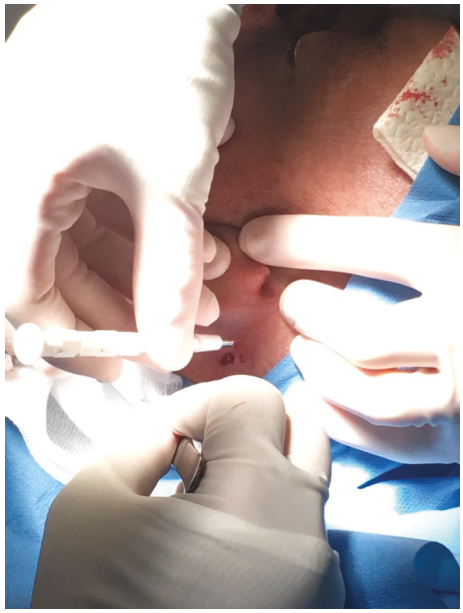

Figure 2: Harvest of the 3 mm punch biopsies from the previously deepithelialized skin.

Figure 3: The harvested skin punch biopsy.

substitute alone (group B—controls) or enriched with the autologous dermal micrografts (group A—Rigenera™ protocol).

(iii) T_2: 4 weeks after the first surgical stage, digital medical photographs and residual soft-tissue loss measurement were obtained with the use of the software "ImageJ." In the Rigenera™ protocol group, if the deepithelialized area in the wound was the same as at T_1, a split-thickness skin graft was planned; if the reepithelialized area was >25% than the one at T_1, a follow-up was planned in 2 weeks' time (T_3); if reepithelialization was complete, the wound was considered healed and the patient was discharged from the study. In the control group, a split-thickness skin graft cover was carried out.

(iv) T_3: digital photographs and residual soft-tissue loss measurement were obtained with the use of the software "ImageJ" in the Rigenera™ protocol group; in the latter group, whatever the extension of the residual deepithelialized area, a split-thickness skin graft was planned at this time; if reepithelialization was complete, the wound was considered healed and the patient was discharged from the study.

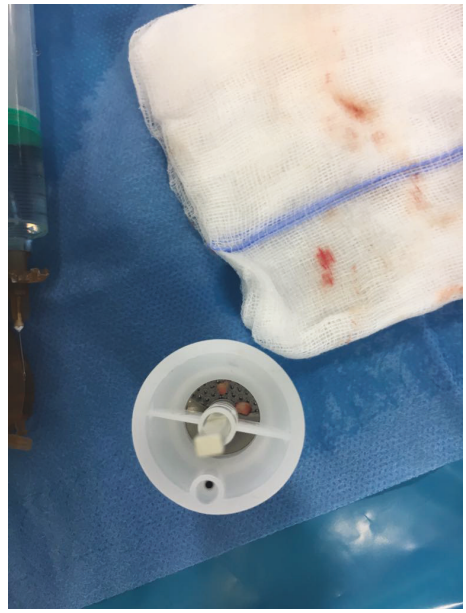

Figure 4: The disposable Rigeneracons loaded with a maximum of 3 dermal samples.

(v) T_4: there was complete reepithelialization 1 week after the split-thickness skin graft cover at T_3 in the Rigenera™ protocol group.

2.5. Statistical Methods. The deviation of continuous variable distribution from the normal distribution was assessed by visual inspection of quantile-quantile plots and by the Shapiro test. T1 and final area distribution was normalized by natural logarithm transformation. Continuous variable distribution is described by median and 25^{th}–75^{th} percentiles; categorical variable distribution is described by counts and frequencies (%). The Fisher exact test and the Wilcoxon rank-sum test were applied to compare the categorical and quantitative variables' distribution between protocols. The Spearman test allowed quantifying the strength of the correlation between continuous variables (rho). Statistical procedures were performed by the R statistical software (http://www.r-project.org.)

3. Results

One male patient out of 20 with surgical excision of a squamous cell carcinoma of the scalp dropped out of the study due to postoperative wound infection. An overall of 23 experimental units (12 in the control group and 11 in the Rigenera™ protocol group) completed the trial.

At T_2, 4 weeks after the first surgical step, the reepithelialization rate was 12.98% (10.40-17.61) in the control group and 15.14% (12.42-22.03) in the Rigenera™ protocol group

Figure 5: Connection of the disposable Rigeneracons to the Rigenera OR-PRO rotating machine.

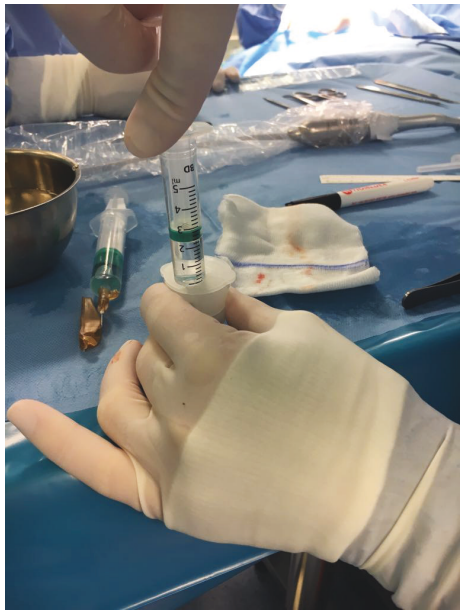

Figure 6: Aspiration of the micrografts containing saline solution with a sterile syringe.

Figure 7: Cover of the postsurgical soft tissue loss with Integra® dermal substitute.

Figure 8: Imbibition of the dermal substitute with the saline micrograft suspension.

($p = 0.607$). In the latter group, only one wound out of 11 (9.09%) demonstrated a reepithelialization > 25% of the total wound area, while in the control group, such an outcome was observed in 2 wounds out of 12 (16.67%) ($p = 1$).

4. Discussion

It is a common knowledge that the human dermis is a source of stem cells with demonstrated regenerative properties [11–16]. The dermal mesenchymal stromal stem cells display adhesion properties, fibroblast morphology, and osteogenic and adipocyte differentiation. Typically, they express both mesenchymal (α-SMA) and neural (Nestin and βIII-tubulin) cell membrane markers and lack the haematopoietic and endothelial ones (CD31) [13]. Recently, the dermal mesenchymal stromal stem cells were demonstrated to express also the CD105, CD73, and CD90 markers that specifically regulate regeneration in the wound healing process. These cells enhance cell survival and proliferation in the wound site through a fine modulation of the immune and inflammatory response, operated by a finely tuned cascade of local mediators. They definitely play a relevant active

role along the inflammatory, proliferative, and remodeling phases allowing an eventual favorable outcome in the wound healing process.

The hair follicle matrix has been demonstrated to host cells that are capable of self-renewal and produce epithelial transient progenitors, thus having attributes of stem cells, too. Stem cells are multipotent, capable of giving rise not only to all the cell types of the hair but also to the epidermis and the sebaceous gland. These cells display a highly sophisticated organization and carry out several functions controlling the shape of the hair follicle. The inner structures are each produced by a distinct, restricted set of precursors occupying a specific position along the proximodistal axis of the matrix. The matrix seems to be organized by two systems working in orthogonal dimensions and controlling two key operations of hair follicle morphogenesis, notably cell diversification and cell behavior [17]. The bulge cell progeny located in the upper follicle has been demonstrated to emigrate into the epidermis and to proliferate, thus contributing to the long-term maintenance of the epidermis [18, 19]. Based on these observations, it has been proposed that the bulge is a major repository of skin keratinocyte stem cells, which may thus be regarded as the ultimate epidermal stem cell [20, 21]. Since stem cells are known to be involved in skin tumor formation [22–27], the coincidence of greater tumor susceptibility with the transient proliferation of the bulge cells is consistent with the hypothesis that the bulge cells are stem cells and indicates that follicular stem cells can give rise to experimentally induced skin cancers [22–25]. Taken together, these data suggest that the bulge is the site of follicular stem cells.

The Rigenera™ method allows the harvesting of a dermis-derived autologous cell suspension including a stem cell fraction, ready for use without any cell manipulation process [28]. Several clinical studies demonstrated the effectiveness of the Rigenera™ cell harvesting method in the management of complex wounds with complete obliteration and reepithelialization of deep soft tissue loss [1–3, 7–9].

In order to objectively assess the effectiveness of the Rigenera™ method, we established a homogeneous experimental fresh surgical wound model providing measurable data that excluded gross experimental bias and fit a rigorous statistical analysis.

Rigenera™ provides a fluid cell suspension that may be both injected in deep spaces and applied on superficial soft tissue loss in combination with a dermal substitute [29].

According to our current clinical practice, we deliberately enrolled patients with a planned two-stage soft tissue loss repair using a dermal substitute followed 4 weeks later by a split-thickness skin graft. The enrichment of a dermal substitute with an autologous cell suspension graft was considered a minimal modification of a current and well-established clinical protocol involving a negligible donor site morbidity and, therefore, allowed approval of the trial by the Ethical Committee.

Considering our long-term clinical experience in the field [30], the dermal substitute of choice for the study was Integra® as it was demonstrated to provide an in vitro favorable environment for dermal stromal mesenchymal stem cell engraftment and replication as early as 7 days [29]. The peculiar three-dimensional structure of Integra®, with a controlled 80 μm porous structure, allows a physiological cell adhesion, infiltration, distribution, and proliferation with the preservation of the typical mesenchymal fibroblast morphology.

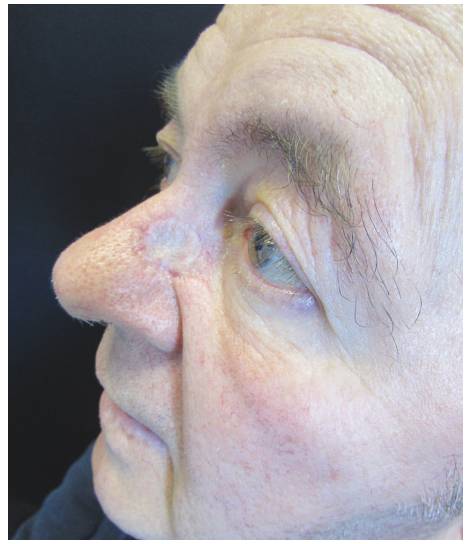

Figure 9: Complete healing of the defect after STSG in group A.

In our study, the treatment with the dermal cell suspension prepared with the Rigenera™ technology was considered effective if the reepithelialized area was higher than the 25% of the total wound surface as the latter threshold was considered far beyond the expected spontaneous reepithelialization rate.

Nevertheless, in the Rigenera™ protocol group, the statistical analysis did not demonstrate any significant difference vs. the controls.

The old age of the patients likely influenced the outcome.

Indeed, our experimental plan, designed as a two-stage procedure, had to meet ethical requirements, too. Currently, such a procedure is the gold standard in frail elderly patients that often come to observation for advanced skin cancers, requiring extensive demolitions but that are unfit for complex reconstructive procedures [31]. The use of a sequential two-stage reconstructive procedure with a dermal substitute and a split-thickness skin graft in these cases allows for a better functional and cosmetic outcome than a simple one-staged skin graft [32–34] (Figure 9).

Undoubtedly, the stem cell regenerative potential is reduced in the elderly. Recent literature reports demonstrate an antiapoptotic action of the senescent cells that prevents the full expression of the regenerative potential in the stem cell pool [35]. In our opinion, a sample pretreatment with specific active principles targeting the senescent cells might be suggested to increase the regenerative potential in the dermal stromal mesenchymal stem cell transfer [36]. The latter specific pretreatment might enhance the full regenerative potential of a minimally invasive cell transfer, making it a specifically convenient procedure for the frail critical patient.

Therefore, reepithelialization of large skin loss in the elderly patient drawing on a minimal dermal fragment might be a realistic option.

A further explanation for the unsatisfying results of our experimental trial might be the inadequate amount of dermal stem cells used to enrich the dermal substitutes. Actually, in our study, we used a 1 : 200 donor/recipient site ratio in order to minimize donor site morbidity. The gross dimensional disparity between the donor and recipient sites and the low concentration of dermal mesenchymal stromal stem cells might explain the poor epithelial proliferative boost observed in our study. Unpublished data from animal experimental trials by our research partner staff would suggest that the optimal donor/recipient site ratio is 1 : 20. Nevertheless, such a ratio would not make the dermal cell suspension transfer a convenient procedure in terms of donor site morbidity vs. a traditional large meshed split-thickness skin graft [37].

Actually, in previous literature reports, the Rigenera™ dermal cell transfer proved to be effective in the difficult-to-heal wound where a split-thickness skin graft was not indicated. Therefore, we suppose that the reported favorable outcome might have been related to an overall change of the wound environment, where a spontaneous reepithelialization might have been related to a nonspecific boost of a torpid wound bed from mesenchymal dermal and epithelial stem cells and matrix-derived factors. Instead, in our opinion, in an acute fresh wound, all of the factors involved in the wound healing process display a maximal expression, thus shading the supposed contribution of the dermal extract as a whole. Indeed, a preconditioning of the dermal cells with a treatment enhancing their regenerative potential might yield a better outcome.

5. Conclusions

The role of the human dermal stem cell regenerative pool in enhancing the wound healing process is a well-established knowledge and is leading to an increasing number of promising clinical applications. The Rigenera™ technology might promote a spontaneous reepithelialization; nevertheless, even if proved to be effective in stimulating a difficult-to-heal wound by turning a torpid chronic process into an active one, in our experience, it could not demonstrate any improvement in the reepithelialization process of a fresh surgical wound. A potential option in the future might be a preconditioning of the dermal stem cell harvest with senolytic active principles that would fully enhance their regenerative potential. Such a treatment might extend the clinical indications of this minimally invasive, standardized, operator-independent, and easy procedure, specifically suitable for the management of complex and critical cases.

Data Availability

The data used to support the findings of this study are restricted by the Ethical Committee (protocol number 2142) of the Istituti Clinici Scientifici Maugeri SB SpA IRCCS of Pavia in order to protect patient privacy. Data are available for researchers who meet the criteria for access to confidential data from the corresponding author upon request.

Conflicts of Interest

The author Antonio Graziano is a member of the Scientific Division of Human Brain Wave, the company owner of Rigenera™ Technology. The other authors have no conflict of interests to declare.

Acknowledgments

The experiments were supported by the Human Brain Wave srl supplying Rigeneracons medical devices.

References

[1] F. Svolacchia, F. De Francesco, L. Trovato, A. Graziano, and G. A. Ferraro, "An innovative regenerative treatment of scars with dermal micrografts," *Journal of Cosmetic Dermatology*, vol. 15, no. 3, pp. 245–253, 2016.

[2] E. Baglioni, L. Trovato, M. Marcarelli, A. Frenello, and M. A. Bocchiotti, "Treatment of oncological post-surgical wound dehiscence with autologous skin micrografts," *Anticancer Research*, vol. 36, no. 3, pp. 975–979, 2016.

[3] F. De Francesco, A. Graziano, L. Trovato et al., "A Regenerative Approach with Dermal Micrografts in the Treatment of Chronic Ulcers," *Stem Cell Reviews and Reports*, vol. 13, no. 1, pp. 139–148, 2017.

[4] W. K. Boss, H. Usal, P. B. Fodor, and G. Chernoff, "Autologous Cultured Fibroblasts: A Protein Repair System," *Annals of Plastic Surgery*, vol. 44, no. 5, pp. 536–542, 2000.

[5] S. Maxson, E. A. Lopez, D. Yoo, A. Danilkovitch-Miagkova, and M. A. Leroux, "Concise review: role of mesenchymal stem cells in wound repair," *Stem Cells Translational Medicine*, vol. 1, no. 2, pp. 142–149, 2012.

[6] European Commission, *Guidelines on Good Manufacturing Practice specific to Advanced Therapy Medicinal Products*, 2017.

[7] M. Giaccone, M. Brunetti, M. Camandona, L. Trovato, and A. Graziano, "A new medical device, based on Rigenera protocol, in the management of complex wounds," *Journal of Stem Cell Reviews and Reports*, vol. 1, no. 3, p. 3, 2014.

[8] L. Trovato, G. Failla, S. Serantoni, and F. P. Palumbo, "Regenerative Surgery in the Management of the Leg Ulcers," *Journal of Cell Science & Therapy*, vol. 7, no. 2, 2016.

[9] M. Marcarelli, L. Trovato, E. Novarese, M. Riccio, and A. Graziano, "Rigenera protocol in the treatment of surgical wound dehiscence," *International Wound Journal*, vol. 14, no. 1, pp. 277–281, 2017.

[10] L. Trovato, M. Monti, C. del Fante et al., "A new medical device Rigeneracons allows to obtain viable micro-grafts from mechanical disaggregation of human tissues," *Journal of Cellular Physiology*, vol. 230, no. 10, pp. 2299–2303, 2015.

[11] K. Takahashi, K. Tanabe, M. Ohnuki et al., "Induction of pluripotent stem cells from adult human fibroblasts by defined factors," *Cell*, vol. 131, no. 5, pp. 861–872, 2007.

[12] R. Vishnubalaji, M. Al-Nbaheen, B. Kadalmani, A. Aldahmash, and T. Ramesh, "Skin-derived multipotent stromal cells–an archrival for mesenchymal stem cells," *Cell and Tissue Research*, vol. 350, no. 1, pp. 1–12, 2012.

[13] M. Dominici, K. le Blanc, I. Mueller et al., "Minimal criteria for defining multipotent mesenchymal stromal cells. The International Society for Cellular Therapy position statement," *Cytotherapy*, vol. 8, no. 4, pp. 315–317, 2006.

[14] B. Coulomb, L. Friteau, J. Baruch et al., "Advantage of the presence of living dermal fibroblasts within in vitro reconstructed skin for grafting in humans," *Plastic and Reconstructive Surgery*, vol. 101, no. 7, pp. 1891–1903, 1998.

[15] F. M. Wood, N. Giles, A. Stevenson, S. Rea, and M. Fear, "Characterisation of the cell suspension harvested from the dermal epidermal junction using a ReCell® kit," *Burns*, vol. 38, no. 1, pp. 44–51, 2012.

[16] R. I. Sharma and J. G. Snedeker, "Paracrine interactions between mesenchymal stem cells affect substrate driven differentiation toward tendon and bone phenotypes," *PLoS One*, vol. 7, no. 2, article e31504, 2012.

[17] E. Legué and J. F. Nicolas, "Hair follicle renewal: organization of stem cells in the matrix and the role of stereotyped lineages and behaviors," *Development*, vol. 132, no. 18, pp. 4143–4154, 2005.

[18] G. Cotsarelis, T.-T. Sun, and R. M. Lavker, "Label-retaining cells reside in the bulge area of pilosebaceous unit: implications for follicular stem cells, hair cycle, and skin carcinogenesis," *Cell*, vol. 61, no. 7, pp. 1329–1337, 1990.

[19] R. M. Lavker, S. Miller, C. Wilson et al., "Hair follicle stem cells. Their location, role in hair cycle, and involvement in skin tumor formation," *Journal of Investigative Dermatology*, vol. 101, no. 1, pp. S16–S26, 1993.

[20] R. M. Lavker, T.-T. Sun, H. Oshima et al., "Hair follicle stem cells," *The Journal of Investigative Dermatology*, vol. 8, no. 1, pp. 28–38, 2003.

[21] G. Taylor, M. S. Lehrer, P. J. Jensen, T.-T. Sun, and R. M. Lavker, "Involvement of follicular stem cells in forming not only the follicle but also the epidermis," *Cell*, vol. 102, no. 4, pp. 451–461, 2000.

[22] R. J. Morris, S. M. Fischer, and T. J. Slaga, "Evidence that a slowly cycling subpopulation of adult murine epidermal cells retains carcinogen," *Cancer Research*, vol. 46, no. 6, pp. 3061–3066, 1986.

[23] S. J. Miller, Z. G. Wei, C. Wilson, L. Dzubow, T. T. Sun, and R. M. Lavker, "Mouse skin is particularly susceptible to tumor initiation during early anagen of the hair cycle: possible involvement of hair follicle stem cells," *The Journal of Investigative Dermatology*, vol. 101, no. 4, pp. 591–594, 1993.

[24] R. J. Morris, K. Coulter, K. Tryson, and S. R. Steinberg, "Evidence that cutaneous carcinogen-initiated epithelial cells from mice are quiescent rather than actively cycling," *Cancer Research*, vol. 57, no. 16, pp. 3436–3443, 1997.

[25] R. J. Morris, K. A. Tryson, and K. Q. Wu, "Evidence that the epidermal targets of carcinogen action are found in the interfollicular epidermis or infundibulum as well as in the hair follicles," *Cancer Research*, vol. 60, no. 2, pp. 226–229, 2000.

[26] G. Nicoletti, F. Brenta, A. Malovini, O. Jaber, and A. Faga, "Sites of basal cell carcinomas and head and neck congenital clefts: topographic correlation," *Plastic and Reconstructive Surgery Global Open*, vol. 2, no. 6, article e164, 2014.

[27] G. Nicoletti, M. M. Tresoldi, A. Malovini, S. Prigent, M. Agozzino, and A. Faga, "Correlation between the sites of onset of basal cell carcinoma and the embryonic fusion planes in the auricle," *Clinical Medicine Insights: Oncology*, vol. 12, pp. 1–5, 2018.

[28] V. Purpura, E. Bondioli, A. Graziano et al., "Tissue Characterization after a New Disaggregation Method for Skin Micro-Grafts Generation," *Journal of Visualized Experiments*, vol. 109, no. 109, 2016.

[29] T. da Silva Jeremias, R. G. Machado, S. B. C. Visoni, M. J. Pereima, D. F. Leonardi, and A. G. Trentin, "Dermal substitutes support the growth of human skin-derived mesenchymal stromal cells: potential tool for skin regeneration," *PLoS One*, vol. 9, no. 2, article e89542, 2014.

[30] G. Nicoletti, M. M. Tresoldi, A. Malovini, M. Visaggio, A. Faga, and S. Scevola, "Versatile use of dermal substitutes: a retrospective survey of 127 consecutive cases," *Indian Journal of Plastic Surgery*, vol. 51, no. 1, pp. 46–53, 2018.

[31] S. Scevola, M. M. Tresoldi, and A. Faga, "Rigenerazione e riabilitazione: esperienza di chirurgia plastica in un centro di riabilitazione," *Giornale Italiano di Medicina del Lavoro ed Ergonomia*, vol. 40, no. 2, pp. 97–105, 2018.

[32] G. Nicoletti, S. Scevola, and A. Faga, "Bioengineered Skin for Aesthetic Reconstruction of the Tip of the Nose," *Dermatologic Surgery*, vol. 34, no. 9, pp. 1283–1287, 2008.

[33] A. Faga, G. Nicoletti, F. Brenta, S. Scevola, G. Abatangelo, and P. Brun, "Hyaluronic acid three-dimensional scaffold for surgical revision of retracting scars: a human experimental study," *International Wound Journal*, vol. 10, no. 3, pp. 329–335, 2013.

[34] G. Nicoletti, F. Brenta, M. Bleve et al., "Long-termin vivoassessment of bioengineered skin substitutes: a clinical study," *Journal of Tissue Engineering and Regenerative Medicine*, vol. 9, no. 4, pp. 460–468, 2015.

[35] M. V. Blagosklonny, "Paradoxes of senolytics," *Aging*, vol. 10, no. 12, pp. 4289–4293, 2018.

[36] J. L. Kirkland, T. Tchkonia, Y. Zhu, L. J. Niedernhofer, and P. D. Robbins, "The clinical potential of senolytic drugs," *Journal of the American Geriatrics Society*, vol. 65, no. 10, pp. 2297–2301, 2017.

[37] R. Cuomo, L. Grimaldi, B. Cesare, G. Nisi, and C. D'Aniello, "Skin graft donor site: a procedure for a faster healing," *Acta Biomedica*, vol. 88, no. 3, pp. 310–314, 2017.